Understanding The Mechanisms By Which Molybdenum-Containing Additives Reduce Friction in Tribological Contacts

How Tribological, Tribofilm and Formulation Properties Affect Molybdenum Friction Modifier Performance



Aaron Lynford Barnes

Submitted in accordance with the requirements for the degree of

Doctor of Philosophy

EPSRC Centre for Doctoral Training in Integrated Tribology

School of Mechanical Engineering

The University of Leeds

June, 2021

The candidate confirms that the work submitted is his own and that appropriate credit has been given where reference has been made to the work of others.

This copy has been supplied on the understanding that it is copyright material and that no quotation from the thesis may be published without proper acknowledgement.

The right of Aaron Lynford Barnes to be identified as Author of this work has been asserted by him in accordance with the Copyright, Designs and Patents Act 1988.

© 2021 The University of Leeds and Aaron Lynford Barnes

Acknowledgements

I would first like to thank my academic supervisors for this project, Professors Ardian Morina and Anne Neville whose advice and support have been so critical to the completion of this project. I would like to thank Prof. Morina for his support, incisive questioning and critical analysis of my work that made my analyses, results, and experimental plans more robust. I would like to thank Prof. Neville for her constant supply of enthusiasm and new ideas when work felt like it had hit a wall. I would also like to thank my Industrial supervisor at Infineum, Dr. Rhiann Andrew, whose support and guidance have ensured that the results of this project bear practical fruit as well as new knowledge, as well as Infineum more generally for sponsoring this work. I thank you all, I could not wish for a better supervisory team.

I'd like to thank all of the technical & research support staff in the School of Mechanical Engineering for their practical assistance, as well as training and access to key technical equipment. Special thanks go to Mr. Jordan Thomas for tribology support, Dr. Andrew Brittain for XPS help, Dr. Chun Wang for Raman and the staff at LEMAS for their microscopy expertise.

I would like to thank my colleagues and staff at the Centre for Doctoral Training in Integrated Tribology and IFS for their insight and productive conversations, as well as my CDT cohort (Matty, Emily, Simon, Chris, Rosie and Pravin) and office mates in 3.32a for their support.

Finally, I would like to thank my parents, Lynford and Angela. Without whose relentless self-sacrifice for the sake of my education, none of this would have been possible.

Abstract

Molybdenum additives are commonly used as friction modifiers in automotive lubricants. Molybdenum additives reduce friction by forming molybdenum disulfide (MoS_2) *in-situ*.

In this work, the structure-activity relationships of a variety of molybdenum additive structures are investigated in a range of pure sliding tribological contact conditions, both unidirectional and reciprocating. The additives investigated included a range of molybdenum dialkyldithiocarbamate (MoDTC) dimer and trimers, as well as a sulfur-free molybdate ester.

Tribological characterisation showed that additives are not interchangeable and that they behave differently in similar contact conditions. The driving tribological factors for friction responses in all cases was the roughness of the contacting surfaces and the temperature of the lubricant oil bath.

The tribofilm surfaces were analysed chemically by Raman, XPS and FIB-TEM. It was observed that all of the additive systems were able to reduce friction through the formation of MoS_2. The final friction coefficient was not found to be dependent on the MoS_2 surface coverage, rather, it appears likely that film crystallinity is the main driver of low friction. The MoDTC trimer monoblend structure produced a thicker, more amorphous film under the conditions studied which afforded it a greater degree of friction durability, but a higher coefficient of sliding friction.

The sulfur-dependence of a sulfur-free molybdate ester was investigated and it was found that reductions in the additive sulfur supply affected friction performance quickly. The role of amines was investigated and it was observed that amines can reduce the friction coefficient of molybdate ester systems by inhibiting the formation of an anti-wear ZDDP tribofilm.

Table of Contents

Acknowledgements ..... **i**
Abstract ..... **ii**
Table of Contents ..... **iii**
List of Tables ..... **ix**
List of Equations ..... **xi**
List of Figures ..... **xii**
Nomenclature ..... **xx**
Abbreviations ..... **xxii**
Chapter 1: Introduction **1**
1.1 The importance of friction to automotive engine performance 1
1.2 Friction modifiers 2
1.2.1 Introduction to friction modifiers 2
1.2.2 Organic friction modifiers 2
1.2.3 Inorganic friction modifiers 4
1.3 The environmental impact of sulfur-containing additives 5
1.4 Aims of this work 6
1.4.1 Rationale 6
1.4.2 Study objectives 7
1.5 Thesis outline 8
Chapter 2: Tribology & Lubricants **10**
2.1 Introduction to tribology 10
2.2 Friction 10
2.3 Wear 14
2.4 Lubrication 14
2.4.1 Hydrodynamic lubrication 16
2.4.2 Elastohydrodynamic lubrication 16
2.4.3 Mixed lubrication 18
2.4.3 Boundary lubrication 18
2.5 Lubricants 18
2.5.1 Viscosity 18
2.5.2 Lubricant base stocks 19
2.5.3 Lubricant additive packages 21

2.6 The nature of real surfaces 22
2.7 Contact between surfaces 24
2.9 Tribochemistry 27
Chapter 3: Literature Review 29
3.1 Molybdenum disulfide (MoS_2) 29
3.1.1 Molybdenum disulfide structure 29
3.1.2 Factors affecting the mechanical properties of bulk MoS_2 30
3.1.3 Raman spectroscopic studies of MoS_2 31
3.1.3.1. First order MoS_2 Raman peaks 32
3.1.3.1.1. Effect of film thickness 35
3.1.3.1.2. Effect of temperature 35
3.1.3.1.3. Effect of pressure 36
3.1.3.2. Resonant Raman peaks of MoS_2 37
3.2 Molybdenum DialkyldiThioCarbamate (MoDTC) 39
3.2.1 Structure and synthesis of MoDTC 39
3.2.2 Thermal decomposition of MoDTC 40
3.2.2.1. Anaerobic decomposition 40
3.2.2.2. Aerobic decomposition 40
3.2.2.3. Oil-based thermal decomposition 41
3.2.3 The friction-reducing performance of MoDTC 44
3.2.3.1. MoDTC Friction profile and durability 44
3.2.3.2. Effect of MoDTC concentration 45
3.2.3.3. Effect of temperature 46
3.2.3.4. Effect of contact conditions 47
3.2.3.5. Effect of MoS_2 surface coverage 50
3.2.3.6. TEM of MoS_2 films 51
3.2.4 Tribological mechanism of MoDTC decomposition 54
3.2.4.1. The role of iron in MoDTC decomposition 58
3.3 Molybdenum trimer 60
3.3.1 Synthesis of Mo-trimer 60
3.3.2 Friction reduction of Mo-trimer 62
3.4 Molybdate ester 62
3.4.1 Synthesis of molybdate ester 63
3.4.2 Mode of action of molybdate ester 64

3.4.3 Friction-reducing performance of molybdate ester 66
3.4.4 Decomposition via MoS_3 68
3.5 Zinc dialkyldithiophosphate (ZDDP) 71
3.5.1 Nature of ZDDP tribofilms 72
3.5.1.1. Chemical nature of ZDDP films 72
3.5.1.2. Mechanical properties of ZDDP films 74
3.5.2 ZDDP-dispersant antagonism 75
3.5.3 Decomposition of ZDDP 76
3.6 Summary 77
3.6.1 Main points of current knowledge 77
3.6.2 Current unknowns 78
3.6.2.1. Tribological activation 79
3.6.2.2. The nature of MoS_2 films derived from differing molybdenum additives 79
3.6.2.3. Molybdate ester-additive interactions 80
3.6.2.4. Decomposition intermediates of molybdenum additives 80
Chapter 4: Methodology 82
4.1 Materials and lubricants 82
4.1.1 Dry chemicals 82
4.1.2 Lubricants and additives 82
4.2 Surface Roughness Characterisation 85
4.3 TE77 reciprocating pin-on-plate tribometer 87
4.3.1 Set-up and function of tribometer 87
4.3.2 TE77 tribotesting 90
4.3.2.1. Conditions for additive friction performance characterisation 90
4.3.2.2. Tribofilm formation for chemical analysis 94
4.3.2.3. Molybdate ester Mo:S ratio testing 95
4.3.2.4. Molybdate mechanism testing 96
4.4 High speed pin-on-disc tribometer 97
4.4.1 High speed pin-on-disc setup 97
4.4.2 High speed pin-on-disc tribotesting 100
4.5 Viscosity determination 101
4.6 Raman surface analysis 102
4.7 X-Ray Photoelectron Spectroscopy (XPS) 106

4.8 Scanning electron microscopy (SEM-EDX) 109
4.9 X-ray diffraction (XRD) 110
4.10 Transmission electron microscopy (TEM) 112
4.11 Thermogravimetric analysis (TGA) of $(NH_4)_2MoS_4$ 115
4.12 Optical microscopy 116
Chapter 5: Activation Of Molybdenum-Containing Additive Friction Reduction 118
5.1 Introduction 118
5.2 Response of molybdenum additives to contact conditions 118
5.2.1 Effect of load 118
5.2.2 Effect of surface roughness 124
5.2.2.1. Reciprocating contact surface roughness 124
5.2.2.2. Simulation of asperity contact pressures 131
5.2.3 Effect of changing lambda ratio 134
5.2.4 Effect of lubricant temperature 140
5.2.5 Thermal formation of MoS_2 147
5.2.6 Effect of Hertzian contact area in reciprocating contact 148
5.3 Summary 152
Chapter 6: Differences In Tribofilm Structures Derived From Varying Molybdenum-Sulfur Chemistries 154
6.1 Introduction 154
6.2 Tribofilm formation 155
6.3 Raman analysis of tribofilm wear scars 158
6.4 XPS characterisation of tribofilms 165
6.5 Nanoscale tribofilms 170
6.6 Tribofilm durability 173
6.7 Amorphous molybdenum sulfides as a decomposition intermediate 174
6.8 Summary 179
Chapter 7: The Behaviour Of Sulfur-Starved Molybdate Ester Formulations 181
7.1 Introduction 181
7.2 Friction performance of molybdate ester systems 182
7.2.1 Fully-formulated systems 183
7.2.2 Binary systems 185
7.2.2.1. Binary systems – smooth surfaces 185
7.2.2.2. Binary systems – rough plates 187

7.2.3 Temperature dependence of molybdate ester systems.... 191
7.3 Fatty amine booster effect 194
7.4 Role of friction-reducing precipitate in molybdate ester binary mixture friction performance 197
7.4.1 Role of precipitate in friction 197
7.4.2 Chemical identification of friction-reducing precipitate..... 199
7.4.2.1. SEM-EDX characterisation..... 199
7.4.2.2. Raman characterisation 200
7.4.2.3. X-Ray diffraction..... 202
7.5 Effect of a ZDDP film and additive interactions on the friction performance of molybdate ester formulations 203
7.5.1 Basic nature of amines..... 204
7.5.2 Oil ageing and removal of ZDDP thermally 207
7.5.3 Investigation of molybdate ester mechanism 209
7.5.3.1. Friction testing..... 210
7.5.3.2. Raman analysis..... 213
7.6 Summary..... 215
Chapter 8: Discussion..... 218
8.1 Introduction 218
8.2 The relative importance of contact parameters to the decomposition of molybdenum additives 219
8.2.1 Flash temperatures 220
8.2.2 Role of surface roughness 221
8.2.3 Contact pin radius of curvature 223
8.2.4 Temperature of the bulk lubricant & Triboactivation 226
8.2.4.1. Mechanical component of tribochemical reaction rate 227
8.2.4.2. The role of thermal energy in the tribochemical reaction rate 229
8.2.5 Interactions between the additive and surface chemistry..... 230
8.3 MoS_3 as a decomposition intermediate 232
8.3.1 MoDTC trimer's increased ability to form MoS_3..... 234
8.3.2 MoS_3 vs MoS_2 formation 234
8.4 Idealised properties of molybdenum sulfide tribofilms 235
8.4.1 Friction performance 235
8.4.1.1. MoS_2 surface coverage 236

8.4.1.1.1. Film crystallinity 236
8.4.1.1.2. Raman MoS_2 surface coverage as an analysis technique 237
8.4.2 Tribofilm durability 238
8.4.2.1. Monoblend tribofilms 238
8.4.2.2. Fully-formulated tribofilms 239
8.4.2.3. An ideal MoS_2 film 240
8.5 The formulation dependence of molybdate ester additive systems 241
8.5.1 Dependence on sulfur supply in fully-formulated conditions 241
8.5.2 The relative difficulty in activation of molybdate ester friction response 243
8.5.3 The effect of amines/dispersants on the activity of molybdate ester formulations 245
Chapter 9: Conclusions & Future Work 247
9.1 Conclusions 247
9.1.1 Contact conditions for activation of Molybdenum additive friction responses 247
9.1.2 Molybdenum additive structure-activity relationships 247
9.1.3 MoS_2 tribofilm properties 248
9.1.4 Molybdate Ester behaviour 249
9.2 Future Work 250
9.2.1 The kinetic behaviour of the MoDTC dimer induction period 250
9.2.2 Quantitative XPS for determination of Mo/S ratio in MoS_x species 251
9.2.3 Harsh conditions and the role of iron molybdates 251
9.2.4 Molybdates with non-film-forming sulfur sources 252
9.2.5 Tungstates as DLC-friendly molybdate analogues 252
9.2.6 Quantitative nanoscale dispersant antagonisms 253
List of References 255
Appendix A: TE77 Waveforms for high and low friction sections of the molybdenum additive tests 266
Appendix B: Overlaid friction profiles of TE77 friction characterisation tests 269

List of Tables

Table 1: Base oil group types 21

Table 2: Equations for Hertzian contact analysis of a point contact 26

Table 3: Phonon frequency of Raman-active and longitudinal acoustic modes at different Brillouin zone points of MoS_2 38

Table 4 Depletion of inorganic sulfur-containing additives at 140°C 42

Table 5: Oil additive systems used in this study 83

Table 6: Organic groups of MoDTC dimer additives used in this study 83

Table 7: Mo:S ratio oils used in this study 85

Table 8: TE77 additive performance characterisation 100 N rough plate 91

Table 9: TE77 additive performance characterisation 25 N rough plate 92

Table 10: TE77 additive performance characterisation 25 N smooth plate 93

Table 11: TE77 additive performance characterisation 300 N smooth plate 94

Table 12 Contact conditions for production of MoS_2 films for chemical analysis 95

Table 13: Contact conditions for molybdate ester tribotesting 96

Table 14: Contact conditions for molybdate ester mechanism testing 97

Table 15: High speed pin-on-disc contact conditions 101

Table 16: Standard Raman spectral acquisition parameters 105

Table 17: Contact conditions for changing load of TE77 119

Table 18: Hertzian contact conditions for investigation of lambda ratio in reciprocating contact 128

Table 19: Hertzian contact areas with various pin radii 149

Table 20: XPS peak information for the fully-formulated oil tribofilms 167

Table 21: XPS peak information for the monoblend oil tribofilms 169

Table 22: Hertzian contact pressures and predicted flash temperatures for tribological tests with 100 mm radius TE77 pins outlined in chapter 5 at 40°C 221

Table 23: Effect of asperity contact pressures and surface roughness on predicted flash temperatures at constant Hertzian pressure of 200 MPa 222

Table 24: Hertzian contact areas and predicted flash temperatures for tribological tests with 100 N load TE77 tests outlined in chapter 5 at 40°C 224

Table 25: Unit cell sizes of MoDTC Dimer and MoDTC Trimer (R = ethyl)..... 228

List of Equations

Equation 1 Basic expression for coefficient of friction 11
Equation 2 Bowden-Tabor real area of contact 13
Equation 3 Bowden-Tabor frictional force 13
Equation 4 Bowden-Tabor friction coefficient 14
Equation 5 Archard's wear law 14
Equation 6 Film thickness of an EHD contact 17
Equation 7 Lubricant entrainment speed 17
Equation 8 Ellipticity parameter 18
Equation 9 Definition of absolute viscosity 19
Equation 10 Centre-line average roughness (R_a) 23
Equation 11 Root mean square surface roughness 23
Equation 12 Radius of contact area 26
Equation 13 Effective radius of curvature 26
Equation 14 Reduced Young's modulus 26
Equation 15 Maximum Hertzian contact pressure 26
Equation 16 Mean Hertzian contact pressure 26
Equation 17 Tribologically-modified Arrhenius equation 28
Equation 18 Irreducible representation of bulk 2H-MoS_2 32
Equation 19 Synthesis of MoDTC 40
Equation 20 Bragg's Law 110
Equation 21 Thermal decomposition of ammonium tetrathiomolybdate $(NH_4)_2MoS_4$ 176
Equation 22 Blok frictional flash temperature rise 220
Equation 23 Peclet frictional flash temperature rise [233] 220
Equation 24 Thermal rate constant Arrhenius behaviour 226
Equation 25 Tribological-thermal rate relationship [191,245] 227

List of Figures

Figure 1.1 Passenger car fuel energy breakdown [1] **1**
Figure 1.2 Typical organic friction modifier structures **3**
Figure 1.3 Organic friction modifier structural units **3**
Figure 1.4 Organic friction modifier tribofilm **4**
Figure 1.5 General MoDTC structure **5**
Figure 1.6 Action of a catalytic converter **6**
Figure 2.1 Determination of friction coefficient **11**
Figure 2.2 General Stribeck curve of a lubricated contact **15**
Figure 2.3 Hydrodynamic lubrication of a journal bearing **16**
Figure 2.4 Dynamic viscosity determination between two parallel plates **19**
Figure 2.5 Example of a surface roughness profile [27] **24**
Figure 2.6 Representation of a point contact of two radii **25**
Figure 2.7 Ball-on-plate contact Hertzian contact geometry **27**
Figure 3.1 Coordination spheres of the three MoS_2 Polymorphs [31] **29**
Figure 3.2 2H-MoS_2 layer structure **30**
Figure 3.3 Effect of humidity on friction performance of MoS_2 in air [32] **31**
Figure 3.4 Multilayer structure of MoS_2 [40] **32**
Figure 3.5 Vibrational modes of bulk MoS_2 [45] **33**
Figure 3.6 Orientation dependence of E_{1g} MoS_2 peak [49] **34**
Figure 3.7: Migration of $E2g1$ and $A1g$ peaks with MoS_2 layer thickness [53] **35**
Figure 3.8 Migration of MoS_2 Raman peaks with temperature [56] **36**
Figure 3.9 Response of MoS_2 Raman spectrum to pressure [60] **37**
Figure 3.10 Comparison of non-resonant and resonant MoS_2 Raman spectra [61] **38**
Figure 3.11 MoDTC general structure **39**
Figure 3.12 Curly arrow mechanism for formation of dithiocarbamate ligands **39**
Figure 3.13 Thermo-oxidative MoDTC degradation mechanism [69] **43**
Figure 3.14 MoDTC friction response **44**
Figure 3.15 Friction response of MoDTC film when switched for different oils mid-test [73] **45**

Figure 3.16 Effect of MoDTC concentration upon friction [76] **46**

Figure 3.17 Temperature dependence of MoDTC friction performance [79] **47**

Figure 3.18 Effect of slide-to-roll ratio (SRR) on MoDTC friction performance [80] **48**

Figure 3.19 Raman intensity distribution of MoS_2 across a wear scar [76] **49**

Figure 3.20 Time-resolved MoS_2 spatial distribution intensity within small wear scar area [84] **51**

Figure 3.21 MoS_2 wear debris TEM [85] **52**

Figure 3.22 TEM sections of high friction (left) and low friction (right) tribofilms [87] **53**

Figure 3.23 TEM sections of tribofilms formed at different temperatures [88] **53**

Figure 3.24 Fully-formulated oil tribofilm [89] **54**

Figure 3.25 Mo region XPS spectrum of MoDTC tribofilm and molybdenum standard compounds [85] **55**

Figure 3.26 Grossiord MoDTC decomposition mechanism **56**

Figure 3.27 Khaemba MoDTC decomposition mechanism [98] **57**

Figure 3.28 Friction performance of MoDTC-containing oils with mileage [119] **60**

Figure 3.29 Mo-trimer structure **61**

Figure 3.30 Mo-trimer molybdenum-sulfur cores **61**

Figure 3.31 Original molybdate ester structures **63**

Figure 3.32 Synthesis of amide/ester molybdate **64**

Figure 3.33 The tetrathiomolybdate anion **65**

Figure 3.34 Molybdate ester MoS_2 formation mechanism **65**

Figure 3.35 Friction performance of molybdenum additives [143] **67**

Figure 3.36 Proposed mechanism of fatty amine booster effect [143] **67**

Figure 3.37 Evolution of molybdate ester tribofilm Raman spectra with contact condition severity [102] **68**

Figure 3.38 Evolution of Raman spectra of decomposed ammonium tetrathiomolybdate [102] **69**

Figure 3.39 Initially proposed chain structure of MoS_3 [150] **70**

Figure 3.40 Cluster structure of MoS_3 [152] **70**

Figure 3.41 Front and side views of amorphous MoS_3 [154] **71**

Figure 3.42 Structure of monomeric ZDDP **71**

Figure 3.43 Development of ZDDP phosphate crystallinity with Tribofilm depth [166] **73**

Figure 3.44 Formation of polyphosphates from thiophosphorylates[159] **76**

Figure 3.45 Schematic outlining current knowledge gaps regarding the action of molybdenum additives **81**

Figure 4.1 Molybdenum additive structures used in this study **84**

Figure 4.2 Surface roughness profile determination scheme for TE77 plates **85**

Figure 4.3 Surface roughness profile determination scheme for High-Speed Pin-on-Disc discs **86**

Figure 4.4 TE77 reciprocating pin-on-plate tribometer **87**

Figure 4.5 TE77 schematic **88**

Figure 4.6 TE77 friction coefficient determination flowchart **89**

Figure 4.7 High speed pin-on-disc schematic **98**

Figure 4.8 High speed pin-on-disc tribometer **98**

Figure 4.9 High speed pin-on-disc detailed disc view **99**

Figure 4.10 High speed pin-on-disc in usage configuration **99**

Figure 4.11 High speed pin-on-disc contact zone in usage configuration **100**

Figure 4.12 Malvern rotational rheometer **102**

Figure 4.13 Renishaw Raman Microscope **103**

Figure 4.14 Raman backscattering optics configuration **104**

Figure 4.15 TE77 plate wear scar with highlighted Raman mapping area **106**

Figure 4.16 a) X-ray photoelectron spectrometer main component schematic. b) X-ray absorption leading to ejection of photoelectrons **107**

Figure 4.17 UHV XPS Spectrometer **108**

Figure 4.18 SEM Principle of operation **109**

Figure 4.19 EVO MA15 scanning electron microscope **110**

Figure 4.20 X-ray diffraction principle of operation **111**

Figure 4.21 Bruker D8 X-ray diffractometer [197] **112**

Figure 4.22 FIB milling method to prepare cross-sections of specific sites for TEM analysis[199] **113**

Figure 4.23 FEI Helios G4 CX DualBeam FIB-SEM used to prepare tribofilm cross-sections **114**

Figure 4.24 FEI Titan3 TEM used to analyse tribofilm cross-sections **115**

Figure 4.25 Shimadzu TGA50 Thermogravimetric analyser[200] **116**

Figure 4.26 Leica DM6000 optical microscope[201] **117**

Figure 5.1 Individual friction profiles of molybdenum additives at 100 N **120**

Figure 5.2 TE77 load cell waveforms in late and early stages of tribological testing for 100 N tests **122**

Figure 5.3 Individual friction profiles of molybdenum additives at 25 N **123**

Figure 5.4 Individual smooth plate friction profiles of molybdenum additives at 25 N **125**

Figure 5.5 TE77 plate representative wear scar raman spectra **127**

Figure 5.6 300N smooth plate individual friction profiles **129**

Figure 5.7 Elastic asperity pressure Distribution for a) 50 nm R_a and b) 500 nm R_a at 200 MPa **132**

Figure 5.8 Elastic-plastic asperity pressure Distribution for a) 50 nm Ra and b) 500 nm Ra at 200 MPa **133**

Figure 5.9 Comparison of asperity pressure distributions between elastic and plastic analysis **134**

Figure 5.10 Friction response of MoDTC Dimer (Oil 1) with sliding speed and lambda ratio **135**

Figure 5.11 Friction response of MoDTC trimer (Oil 2) with sliding speed and lambda ratio **136**

Figure 5.12 Oil 1 (MoDTC Dimer) wear scar Raman spectra for various sliding speeds **137**

Figure 5.13 Oil 2 wear scar Raman spectra for various sliding speeds **138**

Figure 5.14: MoDTC dimer friction performance with changing lambda ratio in unidirectional sliding at 40°C **139**

Figure 5.15 Temperature-viscosity profiles of base stocks **141**

Figure 5.16 Friction response of MoDTC dimer (Oil 1) with temperature **142**

Figure 5.17 Friction response of MoDTC trimer (Oil 2) with temperature **143**

Figure 5.18 Additive friction response in low viscosity oil at 40°C **144**

Figure 5.19 Additive friction response in medium viscosity oil at 80°C **144**

Figure 5.20 Additive friction response in high viscosity oil at 120°C **145**

Figure 5.21 Representative wear scar Raman spectra for oils 1 and 2 with temperature **147**

Figure 5.22 Raman spectra of discs heated to 120°C in molybdenum additive-containing oil after tribological formation of surface iron oxides 148

Figure 5.23 Effect of pin radius of curvature on Oil 1 (MoDTC Dimer)..... 150

Figure 5.24 Effect of pin radius of curvature on Oil 2 (MoDTC Trimer)..... 151

Figure 6.1 Molybdenum additives subjected to tribofilm characterisation 155

Figure 6.2 Friction profiles of molybdenum additive tribofilms..... 156

Figure 6.3 Friction profiles for molybdenum additive fully-formulated systems 157

Figure 6.4 Final friction performance of molybdenum oil systems 158

Figure 6.5 MoS_2 410 cm^{-1} surface distribution in fully-formulated oil systems. Pink lines show the outer bounds of the wear scar area. 159

Figure 6.6 MoS_2 410 cm^{-1} surface distribution in monoblend systems. Pink lines show the outer bounds of the wear scar area..... 160

Figure 6.7 Mean Raman spectra derived from Raman mapping data of fully-formulated and monoblend additive tribofilms..... 161

Figure 6.8 Binary MoS_2 distribution in fully-formulated oils 162

Figure 6.9 Binary MoS_2 distribution in monoblend oils 162

Figure 6.10 Raman surface coverage maps superimposed upon friction performance 163

Figure 6.11 Friction performance of additive systems with MoS_2 Raman surface coverage..... 163

Figure 6.12 Representative MoDTC trimer Raman spectrum 164

Figure 6.13 Relative peak intensity of MoS_3 scattering peaks to the 291 cm^{-1} Fe_2O_3 peak 165

Figure 6.14 Wear scar XPS of fully-formulated Mo 3d and S 2p environments..... 166

Figure 6.15 wear scar XPS of monoblend Mo 3d and S 2p environments..... 168

Figure 6.16 MoDTC trimer tribofilm crystallinity..... 171

Figure 6.17 FIB-TEM cross-section of MoDTC trimer tribofilm 171

Figure 6.18 FIB-TEM cross-section of MoDTC dimer tribofilm..... 172

Figure 6.19 Fully-formulated tribofilm durability test friction profile.. 173

Figure 6.20 Monoblend tribofilm durability test friction profile..... 174

Figure 6.21 Structure of MoDTC trimer and MoS_3 175

Figure 6.22 Thermogravimetric profile of MoS_3 preparation from ammonium tetrathiomolybdate 176

Figure 6.23 XPS spectrum of MoS_3 sample Mo 3d region 177

Figure 6.24 XPS spectrum of MoS_3 sample Mo S 2p region 177

Figure 6.25 Raman spectrum of MoS_3 sample 179

Figure 7.1 Molybdate ester structure mixture 181

Figure 7.2 Proposed molybdate ester MoS_2 formation mechanism ... 182

Figure 7.3 Individual friction profiles of molybdate ester FFO Mo:S ratio oils under smooth plate conditions 183

Figure 7.4 Raman surface coverage maps of 410 cm^{-1} $A1g$ vibration for Mo:S ratio FFO oils 184

Figure 7.5 Individual profiles of molybdate ester binary Mo:S ratio oils under smooth plate conditions 185

Figure 7.6 Raman surface coverage maps of 410 cm^{-1} $A1g$ vibration for Mo:S ratio binary oils in smooth plate conditions . 186

Figure 7.7 Raman surface coverage of binary and FFO Mo:S ratio oil systems with friction 187

Figure 7.8 Fully-formulated Mo:S ratio oils with rough plates 188

Figure 7.9 Individual profiles of binary molybdate ester Mo:S ratio oils under rough plate conditions 189

Figure 7.10 Raman surface coverage maps of 410 cm^{-1} $A1g$ vibration for Mo:S ratio binary oils in rough plate conditions 190

Figure 7.11 Friction performance of binary and FFO oils as a function of Mo:S ratio 191

Figure 7.12 Friction performance of Mo:S ratio FFOs with lubricant bath temperature 192

Figure 7.13 Friction performance of Mo:S ratio binary oils with lubricant bath temperature 193

Figure 7.14 Structure of Triameen “fatty amine” 194

Figure 7.15 Response of 1:2 Mo:S ternary Oil with fatty amine dispersant 195

Figure 7.16 Friction response of Triameen blended in ZDDP-only oil 196

Figure 7.17 Comparision of binary mixture and MoS_2 dispersed in oil 197

Figure 7.18 Precipitate settling in oil 198

Figure 7.19 Friction response of binary mixture with and without precipitate 199

Figure 7.20 SEM characterisation of friction-reducing precipitate 200

Figure 7.21 Raman characterisation of precipitate under higher laser powers 201

Figure 7.22 Low laser power Raman spectrum of precipitate 202

Figure 7.23 X-Ray diffractogram of friction reducing precipitate..... 202

Figure 7.24 Optical microscope images of 1:2 Mo:S TE77 pin wear scars derived from a range of conditions 204

Figure 7.25 Formation of basic ZDDP through action of amines 205

Figure 7.26 Structure of diisopropylethylamine (DIPEA) 205

Figure 7.27 Friction profile of binary mixture with DIPEA 206

Figure 7.28 Ageing of binary oil 207

Figure 7.29 Friction profile of nitrogen aged binary oil..... 208

Figure 7.30 TE77 pin wear scar of nitrogen aged binary oil 209

Figure 7.31 Molybdate mechanism testing friction profiles 100°C 211

Figure 7.32 Molybdate mechanism testing friction profiles 40°C 212

Figure 7.33 Raman spectra of molybdate mechanism testing wear scars for 100°C tests..... 214

Figure 7.34 Raman spectra of ammonium tetrathiomolybdate wear scar after rubbing at 40°C in PAO base oil 215

Figure 8.1 Computational model response to increasing applied Hertzian contact pressure 225

Figure 8.2 Adsorption behaviour of MoDTCs on an iron surface [249] **..... 231**

Figure 8.3 Structure of MoS_3 [216]**..... 233**

Figure 8.4 Structural relation between MoDTC trimer and MoS_3..... 234

Figure 8.5 Effect of tribofilm nature on the durability of friction performance 240

Figure 8.6 Molybdate ester sulfur transfer mechanism 242

Figure A0.1 TE77 Load Cell response of rough plate 100 N friction test of Oil 1: MoDTC Dimer monoblend..... 266

Figure A0.2 TE77 Load Cell response of rough plate 100 N friction test of Oil 2: MoDTC Trimer monoblend..... 266

Figure A0.3 TE77 Load Cell response of rough plate 100 N friction test of Oil 3: MoDTC Dimer (C8-C14) monoblend 267

Figure A0.4 TE77 Load Cell response of rough plate 100 N friction test of Oil 3: MoDTC Dimer (Branched) monoblend..... 267

Figure A0.5 TE77 Load Cell response of rough plate 100 N friction test of Oil 5: Molybdate Ester monoblend..... 268

Figure A0.6 TE77 Load Cell response of rough plate 100 N friction test of Polyalpha olefin base oil..... 268

Figure B0.1 Overlaid 100 N friction profiles 269
Figure B0.2 Overlaid 25 N friction profiles 269
Figure B0.3 300 N smooth plate overlaid friction profiles 270
Figure B0.4 Overlaid 25 N smooth plate friction profiles 270
Figure B0.5 Overlaid friction profiles of 10 mm radius pin tests 271
Figure B0.6 Overlaid friction profiles of 40 mm radius pin tests 271
Figure B0.7 Overlaid friction profiles of 100 mm radius pin tests 272
Figure B0.8 Overlaid friction profiles of pin radius testing for Oil 1 (MoDTC Dimer) 272
Figure B0.9 Overlaid friction profiles of pin radius testing for Oil 2 (MoDTC Trimer) 273
Figure B0.10 Overlaid profiles of molybdate ester FFO Mo:S ratio friction performance at 100°C and 100 N, smooth plate conditions 273
Figure B0.11 Overlaid friction profiles of binary molybdate ester Mo:S ratio oils under smooth plate conditions 274
Figure B0.12 Overlaid friction profiles of binary molybdate ester Mo:S ratio oils under rough plate conditions 274
Figure B0.13 Overlaid friction profiles of binary molybdate ester Mo:S ratio oils under rough plate conditions 275

Nomenclature

Term	Definition	Units
μ	Coefficient of friction	None
F	Friction force	N
W	Applied load	N
A	Contact area	m^2
ξ	Yield pressure	Pa
$\hbar$	Junction shear strength	Pa
ω	Material Loss	mm^3
K	Archard wear constant	None
H	Material hardness	GPa
h_{min}	Minimum film thickness	m
R	Contact radius	m
U	Entrainment velocity	ms^{-1}
η_0	Ambient lubricant viscosity	Pa.s
E^*	Effective elastic modulus	Pa
α	Pressure-viscosity coefficient	m^2N^{-1}
k	Ellipticity parameter	None
τ	Shear stress	Pa
γ	Shear rate	s^{-1}
R_a	Centre-line average roughness	nm
R_q	Root-mean-square roughness	nm

P	Contact pressure	Pa
E_a	Activation energy	$kJmol^{-1}$
k_B	Boltzmann constant	JK^{-1}
T	Absolute Temperature	K
V	Activation volume	$Å^3$
a	Contact area width	m
C_p	Specific heat capacity	$JK^{-1}kg^{-1}$
κ	Thermal conductivity	$Wm^{-1}K^{-1}$
ρ	Density	kgm^{-3}
$\boldsymbol{R}$	Ideal gas constant	$JK^{-1}mol^{-1}$
d	Crystal layer spacing	m
λ	Wavelength	m

Abbreviations

Abbreviation	Definition
MoDTC	Molybdenum dialkyldithiocarbamate
ZDDP	Zinc dialkyldithiophosphate
DLC	Diamond-like carbon
XPS	X-ray photoelectron spectroscopy
XRD	X-ray diffraction
EDX	Energy dispersive X-ray analysis
SEM	Scanning electron microscopy
TEM	Transmission electron microscopy
FTIR	Fourier transform infra-red spectroscopy
HSPOD	High-speed pin-on-disc
MTM	Mini traction machine
SLIM	Spacer layer imaging
AFM	Atomic force microscopy
PAO	Poly-alpha-olefin
BO	Base oil
FFO	Fully-formulated oil
SRR	Slide-roll ratio
AES	Auger electron spectroscopy
FIB	Focussed ion beam

Chapter 1: Introduction

1.1 The importance of friction to automotive engine performance

Automotive engines are composed of many moving parts. Each of these moving components experiences frictional resistance as they move relative to other surfaces. When the cumulative effect of friction is considered for all the components of the combustion chamber, crankshaft, drive train, as well as all of the engine's bearings, the energy lost to friction is found to be quite significant. In fact, automotive engines spend one third of their fuel energy input overcoming friction in one form or another, with 16.5% of fuel energy wasted as friction in the engine. This proportion of wasted energy is greater than that of all aerodynamic losses [1].

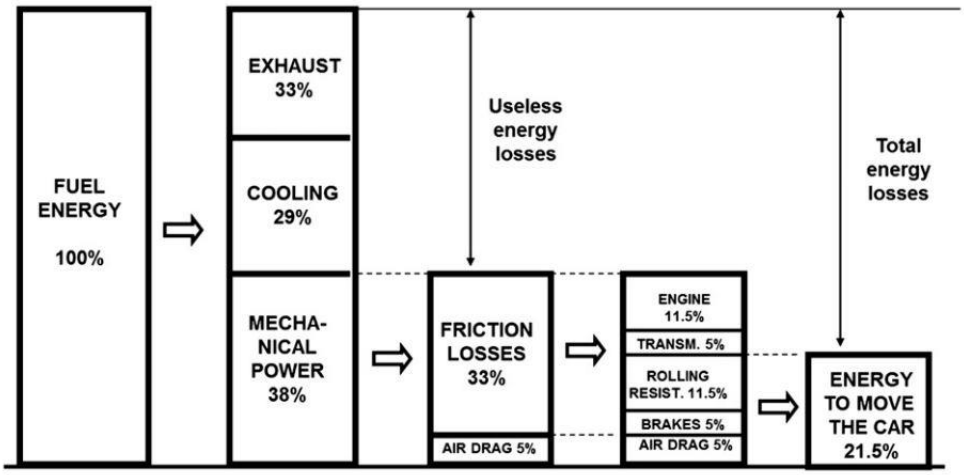


Figure 1.1 Passenger car fuel energy breakdown [1]

In order to increase the fuel efficiency of automotive engines, reducing frictional energy losses is an attractive target. The role of achieving this goal falls to all parties in the design process, from effective design of components to reduce friction, the implementation of new materials, surface technologies and lubricants. Of these technologies, the improvement of lubricants is the cheapest per percentage point increase in fuel efficiency. Lubricant technology has improved fuel economy in recent years with the employment

of low-viscosity base oils, which reduce the energy required to pump the lubricant around the engine. This drop in viscosity has led to an increase in the amount of direct boundary surface contact in the engine, which in turn increases the demands placed upon the lubricant's additive package. The chemical species in a lubricant additive package tasked with reducing boundary friction are known as friction modifiers.

1.2 Friction modifiers

1.2.1 Introduction to friction modifiers

Friction modifiers are chemical species added to lubricant formulations with the intention of reducing friction in the boundary lubrication regime (where direct surface-surface contact occurs). These species perform this function by forming sacrificial surface layers which prevent the asperities of the contacting surfaces from touching, either by forming low-friction protective layers or easily sheared solid intermediate layers. Friction modifiers are broadly defined into two types, organic and inorganic.

1.2.2 Organic friction modifiers

Organic friction modifiers have similar structures which consist of two distinct parts. Firstly, there is a surface-active ligating group on one end of the molecule. These are often polar groups such as carboxy, diol, dithionate and amine groups that are electronically attracted to the surfaces of metals. The rest of the molecule is usually a hydrophobic long alkyl tail which is soluble in mineral oil lubricants with little branching in the chains in order to maximise the density of the friction modifier monolayer on the metal surface. This style of structure has historically been the most investigated due to the discovery of the effectiveness of fatty acids as lubricants in the early 20^{th} century [2,3]. Improved molecular design of organic friction modifiers has led to improved performance by increasing the strength of the interaction between the polar head and the contacting surfaces and selecting a nonpolar tail length appropriate to the contact conditions in which the lubricant will be utilised.

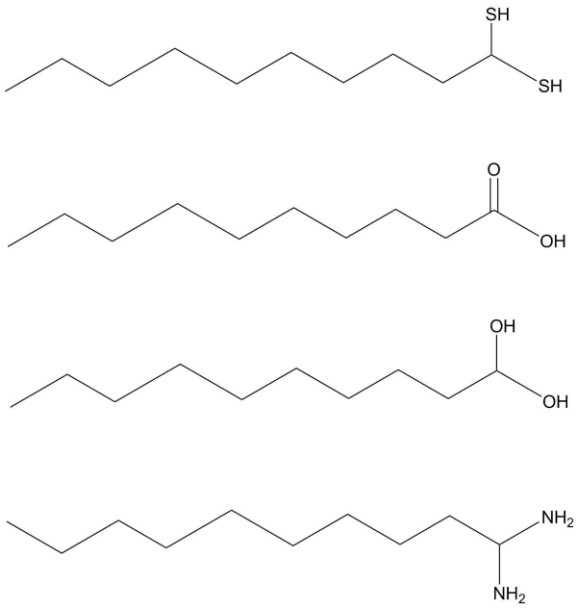


Figure 1.2 Typical organic friction modifier structures

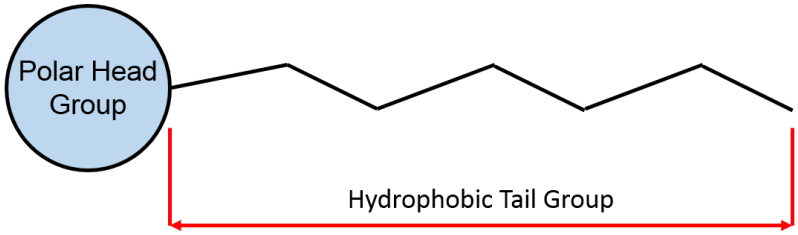


Figure 1.3 Organic friction modifier structural units

Organic friction modifiers act by chemisorption of the polar group onto the metal surface [2]. This leaves the linear alkyl chain pointing upwards from the surface into the lubricant in a contact. It is thought that if the concentration of organic friction modifiers is sufficient, this occurs across the whole of both contacting surfaces to create a monolayer of friction-modifying polymers [4,5]. Some friction modifiers appear to work by forming thicker films than monolayers under certain conditions. Organic friction modifiers with carboxylate head groups have been found by X-ray diffraction and ultra-thin film interferometry to create tribofilms that are more than 100 nm thick in a viscous layer [6,7]. It has been proposed that this is due to the formation of metal carboxylate soaps from strongly ligating carboxylate groups in these molecules under acidic conditions [8]. In both mechanistic cases the end

result is that the long alkyl chains resist compression in the contact and prevent interacting surfaces from touching [9,10]. This action both lowers the friction coefficient of a contact and reduces wear by preventing hard asperities from meeting in boundary contact conditions.

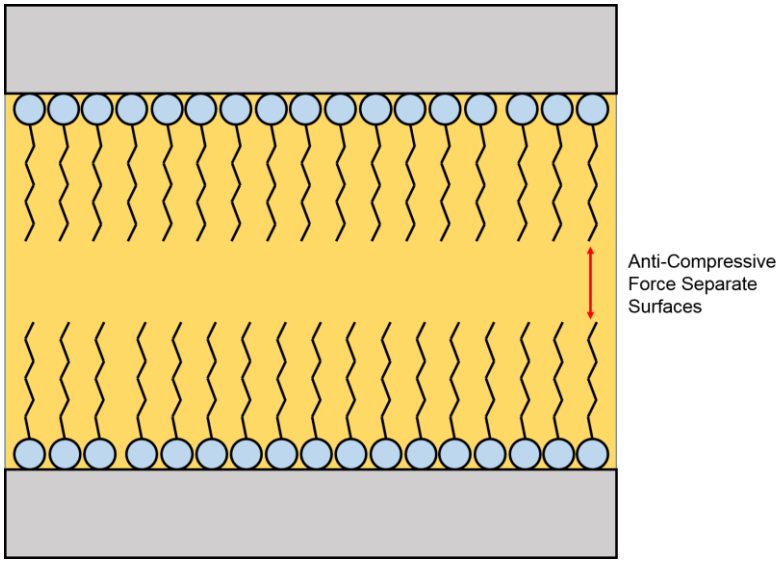


Figure 1.4 Organic friction modifier tribofilm

1.2.3 Inorganic friction modifiers

Inorganic friction modifiers represent all friction modifiers whose structure is not based around molecular carbon chains. As such, there is a wider range of chemistry on display for these additives. Inorganic friction modifiers reduce friction by forming low shear lattice structures *in-situ* within a tribological contact. This lattice structure can be pre-made, as is the case with graphite and sputtered molybdenum disulfide (MoS_2) films, or the tribofilm can be made tribochemically *in-situ*, as is the case for molybdenum dialkyldithiocarbamates (MoDTCs) and organic borate species, or can be mechanically exfoliated from nanoparticles suspended in a lubricant solution [11,12].

Graphite consists of hexagonal layers of carbon atoms with weak bonding between the carbon layers. Under shear, the layers slide over one another to achieve a low coefficient of friction [13]. Graphite is not soluble in base oil so is often utilised as a solid lubricant. The insolubility of graphite makes it unsuitable as a friction modifier to be formed *in-situ*, as it must be applied to

surfaces prior to the commencement of rubbing to be effective. There is also no practical way to replenish the supply of graphite in a contact.

In order to ensure a constant supply of friction modifier to a contact, friction modifiers which can be made from oil-soluble molecular species are preferred. Molybdenum disulfide (MoS_2) is the most well-known friction modifier species which can be applied to a surface, forming a layered structure which can easily shear. This species can be deposited on a surface using oil-soluble molybdenum-sulfur additives. The most well-known of this class of additives are the molybdenum dialkyldithiocarbamates (MoDTCs).

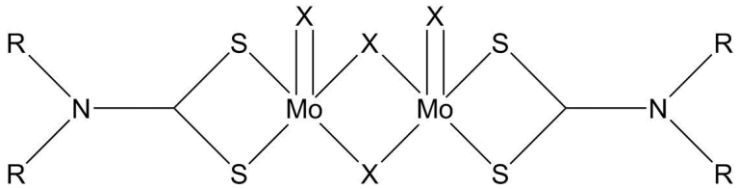


Figure 1.5 General MoDTC structure

X = O or S

In these molecules MoS_2 is derived from the molybdenum oxy-sulfur core whilst oil-solubility is provided by organic 'R' groups typically of C5-C14 length. MoDTCs are able to effectively form MoS_2 on contact surfaces and reduce friction, as such they have served as a workhorse of the lubricant industry for decades. However, the sulfur-rich nature of the additive has meant that the role of this additive is being re-examined, as lubricant formulators seek low-sulfur additive solutions to meet increasingly stringent environmental regulations.

1.3 The environmental impact of sulfur-containing additives

Some of the products of gasoline and diesel combustion, including unburnt hydrocarbons, carbon monoxide and oxides of nitrogen (NO_x) are harmful pollutants [14,15]. The emission of these pollutants from an engine is reduced by passing exhaust gas through a catalytic converter. These devices use finely dispersed platinum and palladium surfaces of extremely high surface area to convert harmful emissions into less harmful carbon dioxide,

nitrogen gas and water. In order to function effectively, as much platinum and palladium surface is exposed as possible [16].

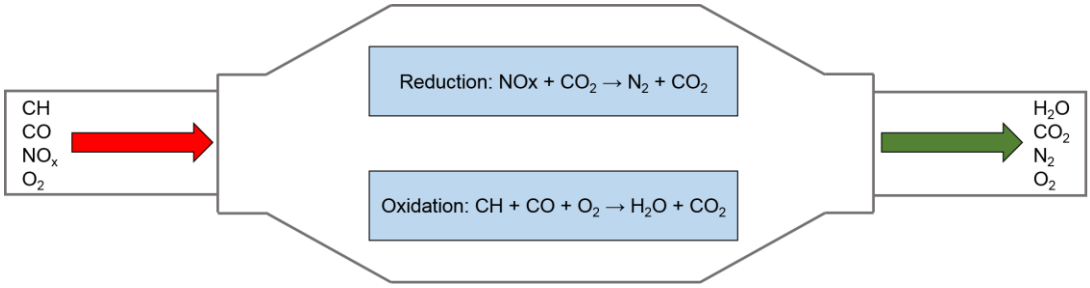


Figure 1.6 Action of a catalytic converter

The action of catalytic converters can be inhibited or 'poisoned' by some strongly binding surface species. Poisoning of the catalytic converters leads to increased emissions of unburnt hydrocarbons, CO and NO_x. The most famous catalyst poisoning element is lead, which requires all cars equipped with catalytic converters to run on unleaded fuel. Other poisoning elements include sulfur, phosphorus, zinc, and manganese. Sulfur, phosphorus and zinc poisoning components can be all derived from combustion of the additive package of lubricants [17]. Volatile combustion products of the lubricant additive package can pass into the exhaust gas when oil is burnt with fuel in the engine's combustion chambers. These components then travel down the exhaust and poison the catalytic converter, inhibiting its ability to reduce harmful emissions.

1.4 Aims of this work

1.4.1 Rationale

In order to reduce levels of harmful pollutants, the sulfur content of the lubricant additive package must be reduced. In order to do this, development low-sulfur and sulfur-free additives is required, as well as better understanding of the action mechanisms of the additives which are currently employed. An understanding of the mechanisms and relative tribological performance of different molybdenum additive structures will be critical in the design of the next generation of additives.

1.4.2 Study objectives

In this work, the tribological performance and decomposition of a series molybdenum-based additives are investigated and compared. The resulting tribofilms derived from varying contact conditions are characterised chemically and mechanically to determine their respective tribofilm properties. This information is then related back to the molecular additive structures. The mechanism of decomposition of a molybdate ester is studied and its dependence upon formulation is investigated. The objectives of this study are as follows:

1. **Understand the interfacial processes during tribological testing with molybdenum-based additives**

    - To investigate the influence of contact parameters of different molybdenum additives and their respective friction responses.

    - Using this information, identify the differences in required breakdown energies between additives and identify the key contact parameters necessary for MoS_2 formation from each system.

2. **Investigate the nature of tribofilms derived from different molybdenum additives**

    - Study the chemical composition of tribofilms derived from the molybdenum additives, identifying their respective decomposition products.

    - Study the physical nature of the films in terms of tribofilm thickness, surface coverage and durability and then relate these factors to the chemistry of the additive used to create the films.

3. **Investigate the formulation dependence of the molybdate ester**

- To investigate the limits of a molybdate ester additive's sulfur dependence and use this reaction dependence upon sulfur to make mechanistic inferences regarding the action of this additive.

1.5 Thesis outline

- **Chapter 2:** Overviews the fundamental theory of tribology, lubrication, and lubricant chemistry relevant to this study.

- **Chapter 3:** Review of the current literature in the field of molybdenum friction modifiers, their chemistry, tribology, and mechanisms.

- **Chapter 4:** Outlines the equipment, materials, techniques, and experimental procedures utilised in this study.

- **Chapter 5:** Tribological results comparing the relative friction-reducing and MoS_2 activation properties of a series of molybdenum additives.

- **Chapter 6:** Results of the chemical characterisation of the tribofilms derived from MoDTC dimer, molybdate ester and Mo-trimer, with relation to their friction performance and film properties.

- **Chapter 7:** The formulation dependence of the molybdate ester additive is investigated. The limits of the sulfur transfer with ZDDP are tested, followed by mechanistic testing wherein the rate-limiting step of molybdate ester decomposition is studied.

- **Chapter 8:** The results are discussed and compared with the current working knowledge of the field literature.

- **Chapter 9:** The conclusions of the work are presented and suggestions for appropriate future work and advancement in this area of tribochemical understanding are provided.

Chapter 2: Tribology & Lubricants

2.1 Introduction to tribology

The nature of the surfaces of mechanical components is a critical factor in their employment within moving systems. The effective use and design of surfaces, both in terms of operational lifetimes of components and their energy efficiency is a vital part of the design process. Tribology is a truly ancient subject as humanity has utilised an understanding of friction and wear to improve lives since the mastery of fire and the invention of the wheel [18]. However, as a science the scope of Tribology was first defined in the 1960s, upon the publication of the UK government's Jost Report, which aimed to quantify the cost of friction and wear to the UK economy [19]. The scientists and engineers involved in the Jost report laid the foundations for tribology as a science and introduced the term "tribology" to the world.

Tribology, from the Greek "τρί́βω – tribos", meaning "to rub" is the science of interacting surfaces in relative motion, along with associated technologies. This broad definition is generally broken down into three main themes: friction, material wear and lubrication.

1. Friction is the resistance to tangential motion of a surface as it is moved across another.

2. Wear is the destructive loss of material from a body as a result of another body sliding against it.

3. Lubrication is the use of an imposing layer of solid, liquid or gaseous material between two surfaces to reduce friction and wear between them.

Each of these topics has been covered in this work and some of the fundamental concepts are outlined below.

2.2 Friction

Friction is the resistance to relative tangential motion of a surface as it is moved across another. Frictional forces apply to all mechanically interacting

surfaces, be they solid or fluid. The counterface with which they interact can be solid, liquid or gaseous in nature.

When two dry surfaces are rubbed together, the resulting frictional force in known as *dry* friction. This system is the most familiar frictional system in everyday life and therefore the most useful with which to illustrate relevant frictional concepts.

The coefficient of friction, often denoted by the letter μ, is the ratio of the tangential frictional force between two surfaces (F) and the magnitude of the normal force compressing those same surfaces together (W).

$$\mu = \frac{F}{W}$$

Equation 1 Basic expression for coefficient of friction

The magnitude of this quantity varies most strongly with the nature of the contacting materials. For example, most people are familiar that steel will slide easily over ice in the form of ice skates, but that rubbing two pieces of vulcanised rubber together requires a great deal more energy expenditure.

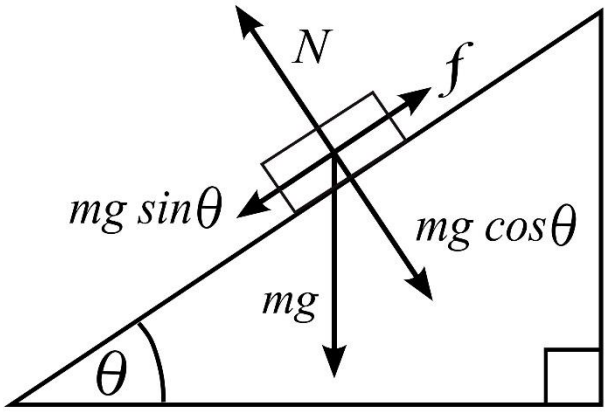


Figure 2.1 Determination of friction coefficient

A common method of determining the coefficient of friction between materials, often encountered in high school physics courses. A block is placed upon an inclined plane, held against gravity by friction. As the block begins to slide $\boldsymbol{\mu = \tan\theta}$

The coefficient of friction for a given system is now known to be a complex product of the mechanical contact parameters and the chemistry of the materials in the system. However, some basic laws of friction can be defined for simple, unlubricated systems. There are three such “laws of friction” determined from the work of Amontons and Coulomb in the 17th and 18th centuries respectively. The laws are:

1. The lateral friction force experienced by an object is linearly proportional to the applied load. (Equation 2.1)

2. The frictional force is independent of the nominal area of contact between the contacting surfaces.

3. The kinetic friction force is independent of the sliding velocity between the contacting surfaces.

The consequence of the first law is that the harder that two surfaces are pressed against one another, the greater the magnitude of the frictional force. This is familiar to those who have moved heavy bookshelves along a floor by sliding. It is significantly easier to slide the surfaces against one another if the weight of the books is removed from the bookshelf first.

The third law is the least strongly held of the three as certain materials, particularly those which can flow, have speed dependent friction performance at high sliding speeds. Broadly speaking however, this law also holds for most common engineering bearing materials.

The second law teaches that the friction coefficient is independent of the apparent contact area between surfaces. The consequence of this is that if one is attempting to slide a cuboid box across a surface, the magnitude of the friction force is independent of the orientation of the cuboid. This is often a surprising finding to lay readers but is caused by the fact that the **real** area

of contact between two surfaces is often much less than the **nominal** contact area.

This difference between the nominal and real areas of contact can be understood using an adhesive friction model initially proposed by Desaguliers and developed by Bowden and Tabor [18,20]. In a contact, the load between the surfaces is not shared by the apparent contact area but is instead held only by a discrete number of spots defined by the asperities. The localised pressures in these contacts are sufficient to induce plastic deformation of the asperities. The plastic deformation leads to the formation of junctions which must be broken by shear forces in order for sliding motion to occur [21,22]. This cumulative force required to break these junctions is the friction force.

The true area of contact (A) is related to the load (W) by a parameter representing the yield pressure of the softer surface (ξ).

$$A \approx \frac{W}{\xi}$$

Equation 2 Bowden-Tabor real area of contact

The friction force (F) is then made from the product of the mean shear strength of the junctions ($\hbar$) and the real contact area (A).

$$F = A \times \hbar$$

Equation 3 Bowden-Tabor frictional force

As the frictional force is linearly proportional to the applied load, this leads to an expression of the friction coefficient which satisfies the first and second laws of friction, yielding a friction coefficient that is independent of load and apparent contact area.

$$\mu = \frac{F}{W} = \frac{\hbar}{\xi}$$

Equation 4 Bowden-Tabor friction coefficient

2.3 Wear

Wear is the progressive damage and material loss of a surface as a result of motion relative to other surfaces. Wear occurs by a variety of mechanisms, depending on the contact conditions and material characteristics. Wear can be either chemically induced, as in the case of corrosion or mechanically in the case of ploughing or adhesive wear. In addition, the wear particles from other wear processes can then act as third bodies to accelerate wear.

Wear is often measured by the volume or mass loss of material and as such can be quantified. Like friction, there are laws associated with wear. First among these is the Archard wear law outlined below:

$$\omega = K\frac{W}{\mathrm{H}}$$

Equation 5 Archard's wear law

Where ω is the material loss in mm^3, *W* is the applied load in N and H is the material hardness. *K* is a dimensionless constant known as the wear coefficient, it is usually quoted in $mm^3\,N^{-1}\,m^{-1}$ and represents the wear volume per unit sliding distance, per unit normal load.

2.4 Lubrication

Lubrication is the attempt to reduce friction and wear in a contact by the application of an interposing layer between two solid surfaces. Although the

lubricants with which most people are familiar will be fluids; solids and greases can also be used to lubricate contacts.

In fluid lubrication there are four main mechanisms known as lubrication regimes. These lubrication regimes were determined by the German engineer Richard Stribeck at the beginning of the 20th century and the resulting plot which describes them, the Stribeck curve, bears his name. The four lubrication regimes are:

1. Hydrodynamic Lubrication
2. Elastohydrodynamic Lubrication
3. Mixed Lubrication
4. Boundary Lubrication

The four lubrication regimes are determined through a parameter known as the lambda ratio (λ). The lambda value of a lubricated system is the ratio of the protective lubricant film thickness to the combined roughness of the contact surfaces. The result of changing lambda ratio upon friction is outlined qualitatively in the Stribeck Curve, wherein lubricant film thickness is steadily increased by increasing the lubricant entrainment velocity.

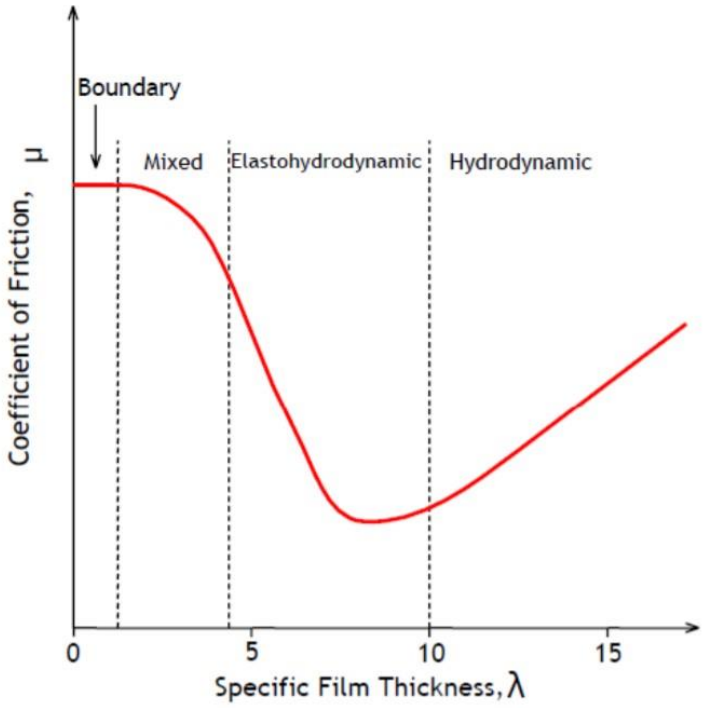


Figure 2.2 General Stribeck curve of a lubricated contact

2.4.1 Hydrodynamic lubrication

In hydrodynamic lubrication, the interacting mechanical surfaces are separated fully by an interposing layer of fluid lubricant. In this instance there is no solid-solid contact and the friction coefficient is primarily determined by the viscosity of the interposing fluid. In these systems, the thickness of the interposing lubricant film is > 1 µm, more than sufficient to separate the asperities of most rough engineering surfaces. A common example of a hydrodynamically lubricated system is a journal bearing, wherein a shaft rotates within a sleeve, dragging its own protective lubricant film as it rotates. The hydrodynamic lubricant film thickness in Figure 2.3 is exaggerated for clarity.

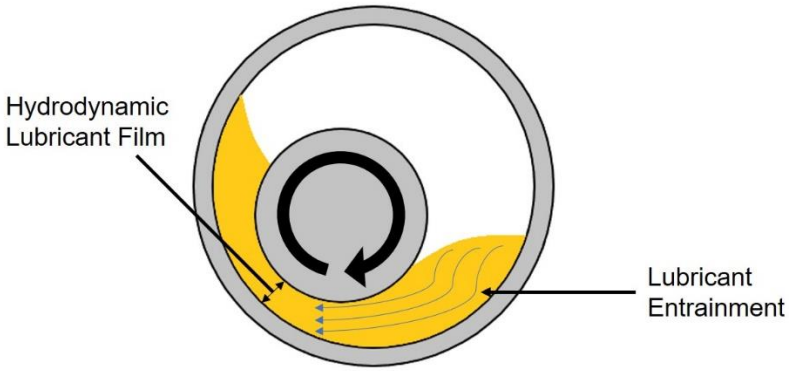


Figure 2.3 Hydrodynamic lubrication of a journal bearing

2.4.2 Elastohydrodynamic lubrication

Elastohydrodynamic (EHD) lubrication occurs in highly loaded, non-conformal contact such as gear teeth and cam-follower systems. In elastohydrodynamic lubrication the increased pressure acting on the contact leads to two effects occurring:

1. There is a pressure-induced increase in the viscosity of the lubricant.

2. Pressure induced elastic deformation of the surfaces occurs, reducing surface roughness.

The combination of these effects leads to maintenance of low-friction hydrodynamic friction coefficients under conditions where extensive surface contact would be expected to occur.

In an elastohydrodynamically lubricated contact, the lubricant film thickness is given by the following equation, known as the Dowson-Hamrock equation for a point contact [23–26]:

$$\frac{h_{min}}{R_x} = 3.63\left(\frac{U\eta_0}{E^* {R_x}^2}\right)^{0.68}(\alpha E^*)^{0.49}\left(\frac{W}{E^* {R_x}^2}\right)^{-0.073}(1 - e^{-0.68k})$$

Equation 6 Film thickness of an EHD contact

Where R_x is the radius of curvature of the contact in the x-direction (m), U is the lubricant entrainment speed in (ms^{-1}), E^* is the reduced Young's modulus (Pa), η_0 is the ambient dynamic viscosity of the lubricant, α is the pressure-viscosity coefficient of the lubricant in (Pa^{-1}) and W is the applied load (N). The entrainment velocity, U is given by the average velocity of the two surfaces in the contact:

$$U = \frac{(U_1 + U_2)}{2}$$

Equation 7 Lubricant entrainment speed

k is the ellipticity parameter of the contact in question. This is a function of the relative curvature of the contact, from 1 in a ball-on-plate contact to 8 in a line contact. k is given by the equation below [24,25]:

$$k = 1.03\left(\frac{R_y}{R_x}\right)^{0.64}$$

Equation 8 Ellipticity parameter

2.4.3 Mixed lubrication

In mixed systems, load is held by a mixture of a thin lubricant film and direct contact between surface asperities. The mixed regime spans a range of degrees of surface contact, from primarily lubricant held loads to almost boundary conditions.

2.4.3 Boundary lubrication

Boundary lubricated contacts experience the highest friction coefficients of lubricated systems. As a result, they are often deemed to be undesirable as they lead to both frictional energy wastage and an increased likelihood of severe wear. In the boundary regime the load is held by the surface asperities and a monomolecular layer of lubricant molecules. In this regime there is extensive deformation of the contact surfaces, greater lubricant shear rates and higher contact temperatures that allow tribochemical reactions to occur with additives in the lubricant.

2.5 Lubricants

2.5.1 Viscosity

The most important property of a fluid lubricant fluid from a mechanical perspective is its viscosity. This property defines the resistance of a fluid to shear and hence its likely ability to support an applied load. Absolute viscosity (η) is determined by the shearing force in the direction of flow between two parallel plates of unit size per unit velocity gradient between them.

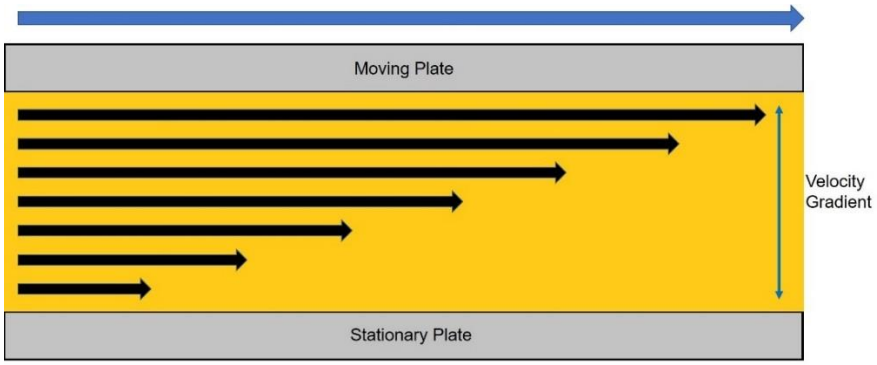


Figure 2.4 Dynamic viscosity determination between two parallel plates

The shear force per unit area gives a shear stress (τ) and the velocity gradient is the same as the local shear strain rate (γ). Therefore, the absolute viscosity is defined by:

$$\eta = \frac{\tau}{\gamma}$$

Equation 9 Definition of absolute viscosity

In addition to the absolute value of the viscosity in Pa.s, this parameter is also often quoted as the kinematic viscosity, which is determined simply by division of the absolute viscosity by the fluid density. The kinematic viscosity is often used in preference to the absolute viscosity as gravity-fed viscometers which determine kinematic viscosity are cheaper than their rotational counterparts.

2.5.2 Lubricant base stocks

For the majority of human history lubricants have been composed primarily of animal fats and plants oils [18]. Since the late 19th century exploitation of crude oil, the overwhelming majority of lubricants have been derived from heavier fractions of refined oil. The chemical composition and mechanical properties of these fractions are dependent on the source of the crude oil from which they are refined. As such some categorisation of oil base

stocks is required. The hydrocarbon base stocks which compose the bulk of mineral-derived base oils are divided into three categories:

1. Paraffins: These are primarily long chain hydrocarbons with some small degree of branching, but not ring structures. The hydrocarbons are saturated and as such, these oils are the most oxidatively stable.

2. Naphthenes: These oils are formed of ring-containing saturated hydrocarbons. These are less oxidatively stable than paraffins and have inferior temperature-viscosity behaviour.

3. Aromatics: Aromatic oils contain a greater proportion of unsaturated ring structures. These ring structures are not oxidatively stable and as such these oils degrade the fastest of the three main base stock types.

In addition to these mineral-derived oils, synthetic oils also exist that are man-made. The most common of these “synthetic” base stocks are the poly-alpha-olefins (PAOs). This base stock is highly paraffinic, containing very few ring structures, aromatics or heteroatom impurities. As a result, these base oils are more stable to oxidation and have superior temperature-viscosity characteristics, however, they are also more expensive.

For purchasing purposes oils are divided into four groups depending on their naphthene, aromatic and sulfur contents. These are useful to both consumers and researchers in order to gain an idea of the expected performance of a lubricant.

Table 1: Base oil group types

Base Oil Category	Sulfur (%)	Saturates (%)	Viscosity Index
Group I	>0.03	<90	80-120
Group II	<0.03	>90	80-120
Group III	<0.03	>90	>120
Group IV	PAO Synthetic Lubricants		
Group V	All base oils not included in Groups I-IV		

2.5.3 Lubricant additive packages

The base oils by themselves are unable to provide the lubricating performance demanded of them by consumers. In order to improve the performance of lubricants to meet consumers demands, an additive package of complex chemicals is dissolved into the base stock. The additive package of a lubricant composes about 25% of the overall lubricant system and contains a variety of different chemical structures to fulfil specific roles. Some of these additive classes are outlined below:

1. Anti-wear additives: These additives form protective layers upon boundary-lubricated surfaces to reduce deleterious wear.

2. Friction modifiers: Friction-reducing species which form a sacrificial layer with a lower coefficient of friction than the substrate on which they sit.

3. Detergents: Species with a basic pH which are used to neutralise excess acid which results from oxidation of oil and to maintain engine cleanliness by removing sludge.

4. Dispersants: Aid in the solubility of additives and help to solubilise small particulates of soot which can cause third-body abrasive wear.

5. Anti-foaming additives: Reduce the tendency of a base stock to form air bubbles in order to maintain favourable mechanical properties.

6. Viscosity modifiers: Polymeric species which maintain the viscosity of an oil over a wider temperature range in order to improve its viscosity index.

7. Pour-point depressants: Base oils form waxes at low temperatures that inhibit their performance. These chemicals reduce the temperature at which waxes form so that lubricants can operate in colder environments.

2.6 The nature of real surfaces

Outside of a few specific contexts, no real engineering surfaces is truly flat on the atomic scale, even those polished down to what are deemed “mirror finishes”. In truth, every surface has an associated roughness determined by its surface asperities.

Whilst this may seem like a simple concept, it is quite challenging to quantify, as the behaviour of a surface depends not just on the magnitude of its surface roughness but also the distribution of that roughness and the sharpness of the asperities.

The most basic (and most common) parameter used to describe surface roughness is the centre line average roughness of a surface (R_a). This is defined by the equation below:

$$R_a = \frac{1}{L}\int_0^L |z| dx$$

Equation 10 Centre-line average roughness (R_a)

Where z is the height of the surface measured above the mean. The centre-line is defined as the z value at which the areas above and below it are equal.

One issue with the (R_a) parameter is that it fails to distinguish between the sharpness of asperities. A surface of gently undulating asperities can have the same R_a value as one with sharp peaks and valleys. To distinguish between such surfaces the root mean square roughness (R_q) is used, as a squared term amplifies the contribution of sharper surface topography variations.

$$R_q = \sqrt{\frac{1}{L}\int z^2 dx}$$

Equation 11 Root mean square surface roughness

The roughness of a surface has an effect on the wear processes of a tribological contact. For example, smooth surfaces tend towards adhesive wear whilst rougher surfaces are more likely to plough and undergo scratching processes. The sharpness of asperities will also affect the pressure-distribution of a surface and the resulting thermal and shear forces caused by boundary friction.

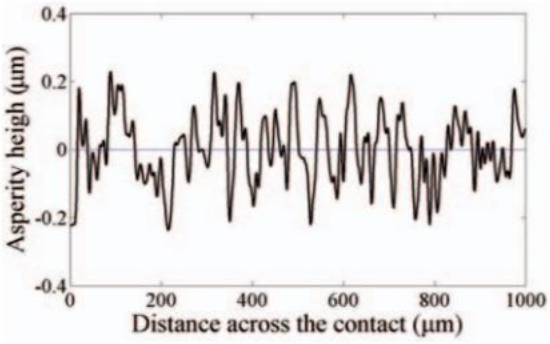


Figure 2.5 Example of a surface roughness profile [27]

2.7 Contact between surfaces

Surfaces have nominal shapes but under load these will deform depending on the magnitude of the load and the properties of the materials in question. Upon deformation, the contact area will change and so will the resulting calculated pressure. This problem was addressed in the 19th century by Hertz, who developed a theoretical framework of contact deformation analysis when studying the effect of deformation upon the action of lenses.

For the purposes of Hertzian contact analysis, the approach taken depends upon the geometry of the contact. For example, if the contact is a ball-on-plate, ball-on-ball, cylinder-on-cylinder etc. In this work all of the contacts are ball-on-plate geometry point contacts, so this analysis will be covered here.

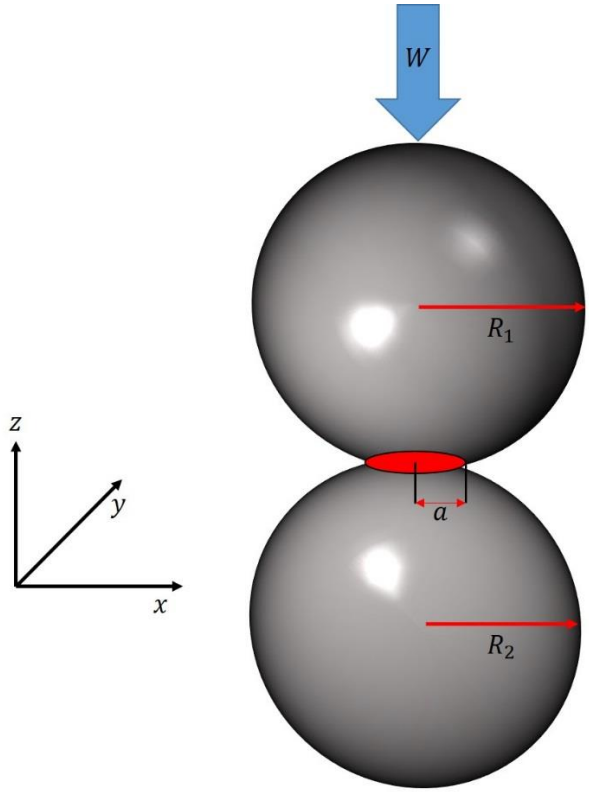


Figure 2.6 Representation of a point contact of two radii

A ball-on-plate contact is modelled by a perfectly smooth sphere of defined radius indenting into a smooth, infinitely large plane. As the ball presses into the plane, the two surfaces deform elastically and the surface area of the contact increases, changing the pressure distribution of the contact. Contact parameters of interest can be calculated from the equations in the table below:

Table 2: Equations for Hertzian contact analysis of a point contact

$a = \left(\frac{3WR^*}{4E^*}\right)^{\frac{1}{3}}$	**Equation 12 Radius of contact area**
$R^* = \left(\frac{1}{R_1} + \frac{1}{R_2}\right)^{-1}$	**Equation 13 Effective radius of curvature**
$E^* = \frac{2E_1E_2}{(1-{v_1}^2)E_2 + (1-{v_2}^2)E_1}$	**Equation 14 Reduced Young's modulus**
$P_{max} = \frac{1}{2\pi}\left(\frac{3WE^{*2}}{R^{*2}}\right)^{\frac{1}{3}}$	**Equation 15 Maximum Hertzian contact pressure**
$P_{mean} = \frac{2}{3}P_{max}$	**Equation 16 Mean Hertzian contact pressure**

Where a is the contact area, W is the applied load in (N), R^* is the effective radius of the two contacting surfaces in (m), R_n is the radius of curvature of radius number n in (m). E^* is the reduced Young's modulus in (Pa), E_n is the Young's modulus of the bulk of surface n in (Pa). v_n is the Poisson's ratio of the bulk material of surface n. p is the contact pressure in (Pa).

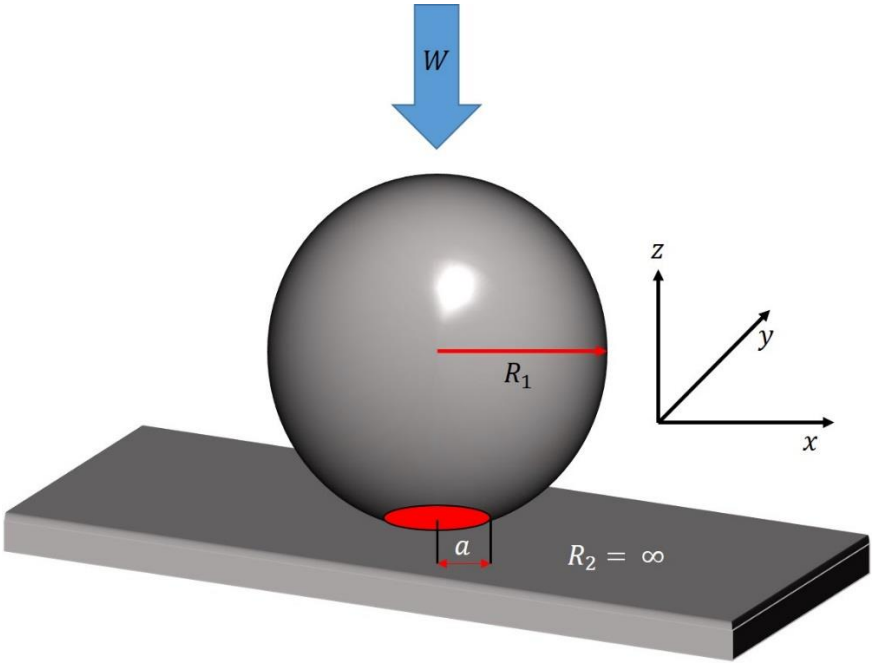


Figure 2.7 Ball-on-plate contact Hertzian contact geometry

Hertzian contact analysis assumes that the surfaces involved are perfectly smooth, as such the quoted pressures are averaged over the entire contact area. In reality, the contact load will be held primarily by the surface asperities, which will observe greater contact pressures than those predicted by Hertzian analysis. It is predicted that the real area of contact for ambient air surfaces can be as little as 1% of the apparent area. An understanding of the pressures in a contact is important for the prediction of flash temperatures and shear stress which drive the tribochemical processes in additive film formation.

2.9 Tribochemistry

Tribochemistry is the name given to those chemical process which occur as a result of mechanical action caused by friction. The chemical reactions are driven by shear stress, frictional flash temperatures and wear processes.

Tribochemical reactions are observed primarily in the boundary regime where frictional flash temperatures and contact stresses are the greatest. Some tribological reactions, including the critical decomposition of zinc

dialkydithiophosphates (ZDDPs) and MoDTCs are shown to occur at lower temperatures in tribological contact than their thermal decomposition would suggest. As a result of these findings it has been proposed that shear stress in the tribocontact can reduce the activation energy of tribochemical reactions. This behaviour is modelled by a modified Arrhenius kinetic rate mechanism.

$$k_{tribo} = A_0 e^{\left(-\frac{E_a - \tau V}{k_b T}\right)}$$

Equation 17 Tribologically-modified Arrhenius equation

A_0 is a pre-exponential factor, τ is the shear stress to which a the chemical bonds are subjected, V is a constant of mechanical cross section, E_a is the thermal activation energy, k_b is the Boltzmann constant and T is the absolute temperature.

As the shear stress increases, the reaction rate is expected to increase to the point where an appreciable amount of reaction product is created relative to the thermal reaction alone. The resulting tribochemically created products can then alter the friction and wear behaviour of the contact.

Chapter 3: Literature Review

3.1 Molybdenum disulfide (MoS_2)

3.1.1 Molybdenum disulfide structure

In lubricant formulations, molybdenum-based friction modifiers are added to create MoS_2 on contact surfaces. Molybdenum disulfide is a member of a class of inorganic compounds known as transition metal dichalcogenides [28,29]. These compounds have the general formula MX_2, where M is a transition metal and X is a chalcogen (an element from group 16 of the periodic table). MoS_2 is composed of covalently bonded Mo-S units, with the sulfur atoms placed in layers above and below a layer of Mo atoms. The MoS covalently-bonded units are coordinated in a trigonal prismatic coordination sphere with sulfur atom sharing. The trigonal prismatic coordination spheres pack in a hexagonally close packed geometry, giving the most common polymorph of MoS_2 the title “hexagonal MoS_2”, also known as 2H-MoS_2 [30]. Two other polymorphs of MoS_2 are known, a rhombohedral form known as 3R-MoS_2 and a metastable tetragonal phase 1T-MoS_2.

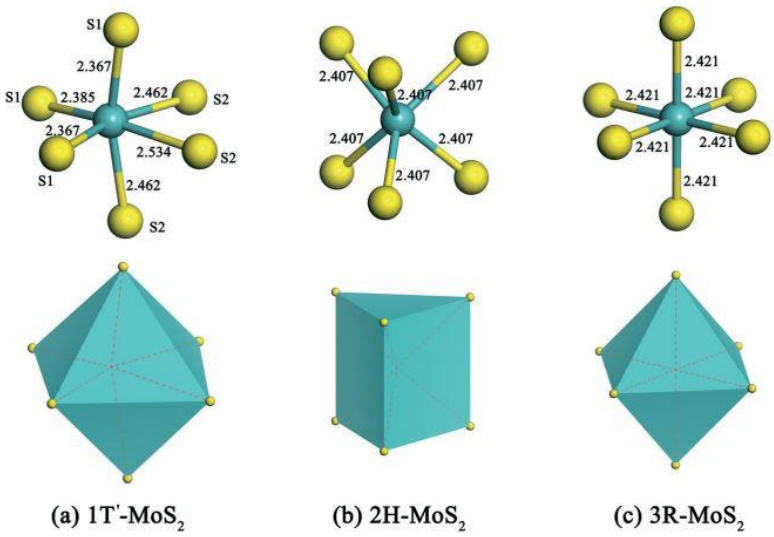


Figure 3.1 Coordination spheres of the three MoS_2 Polymorphs [31]

The two-dimensional 2H-MoS_2 covalent layers can stack upon each other to create multiply layered MoS_2. In the multi-layered compound the covalent sheets are bound to one another only by weak Van der Waals forces. The result of this is that the bonds within MoS_2 layers are strong, but the interlayer bonds are weak, allowing MoS_2 sheets to easily shear over one another. It is this ease of interlayer shearing which makes MoS_2 an effective friction-reducing species.

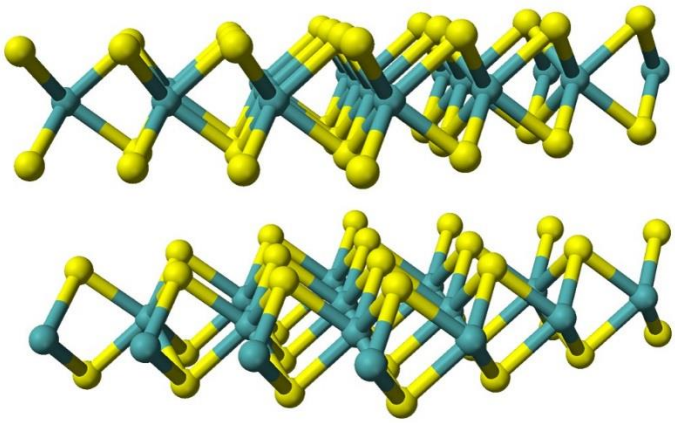


Figure 3.2 2H-MoS_2 layer structure
Molybdenum atoms in turquoise, sulfur atoms in yellow

3.1.2 Factors affecting the mechanical properties of bulk MoS_2

The friction-reducing performance of MoS_2 is dependent upon the contact conditions and local chemistry. In oxygenated and humid environments, the low-friction performance of MoS_2 breaks down as it oxidises to form MoO_2 and MoO_3. These chemical transformations break up the MoS_2 sheets and prevent the layers from sliding easily over one another [32–35].

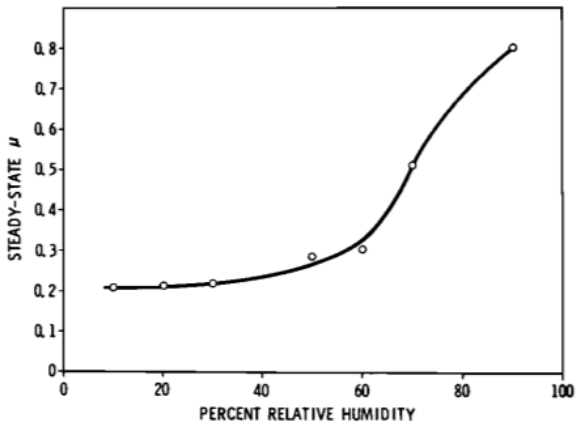


Figure 3.3 Effect of humidity on friction performance of MoS_2 in air [32]

In order for bulk oxidation to occur, both oxygen and water are water are needed. In dry air the friction performance of MoS_2 films is comparable to that of MoS_2 in nitrogen [34]. Oxidation occurs preferentially at the edge sites of MoS_2 sheets which interrupt the layer structure [36].

Even in the absence of bulk oxidation of the additive, contamination by water is thought to inhibit the performance of MoS_2. Water is able to intercalate the layers of MoS_2 and “pucker” the sheets so that they are unable to slide over each other in a linear manner [37,38].

The friction performance of MoS_2 is best under ultra-high vacuum conditions, where interlayer spacing can be maximised, weakening the Van Der Waals forces holding the sheets together [39].

3.1.3 Raman spectroscopic studies of MoS_2

Molybdenum disulfide has been extensively studied using Raman spectroscopy. This is a useful technique for characterisation of MoS_2 thin films as it can be performed on surfaces, needs only small amounts of MoS_2 and a good deal of chemical information can be derived from it.

3.1.3.1. First order MoS_2 Raman peaks

The Raman spectrum of MoS_2 is a product of its chemical structure and symmetry. In MoS_2 molybdenum atoms are sandwiched between sulfur atoms in a trigonal prismatic coordination sphere, a two-dimensional sheet of these units is formed by sulfur atom sharing. The covalently-bonded Molybdenum-sulfur coordination units are stacked in layers, bonded together by weak Van der Waals interactions.

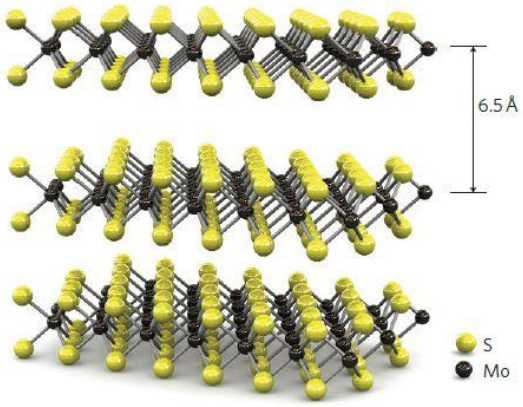


Figure 3.4 Multilayer structure of MoS_2 [40]

The structure of bulk MoS_2 puts molybdenum disulfide in the D_{6h} space group. The symmetry around the Mo centre is D_{3h} and that around the sulfur atoms is C_{3v} [41,42]. The structure of bulk MoS_2 has normal vibrational modes with the irreducible representations:

$$\Gamma = A_{1g} \times 2A_{2u} \times B_{1u} \times E_{1g} \times 2E_{1u} \times 2E_{2g} \times E_{2u}$$

Equation 18 Irreducible representation of bulk 2H-MoS_2

Of these modes, two are translational acoustic modes (A_{2u}, E_{1u}) and the $2B_{2g}, B_{1u}, E_{2u}$ modes are spectroscopically inactive. The other vibrational modes are all observable spectroscopically, with the remaining A_{2u} and E_{1u} modes being IR-active, leaving the $E_{2g}^2, E_{1g}, E_{2g}^1$ and A_{1g} as the Raman-active vibrations [31,43,44].

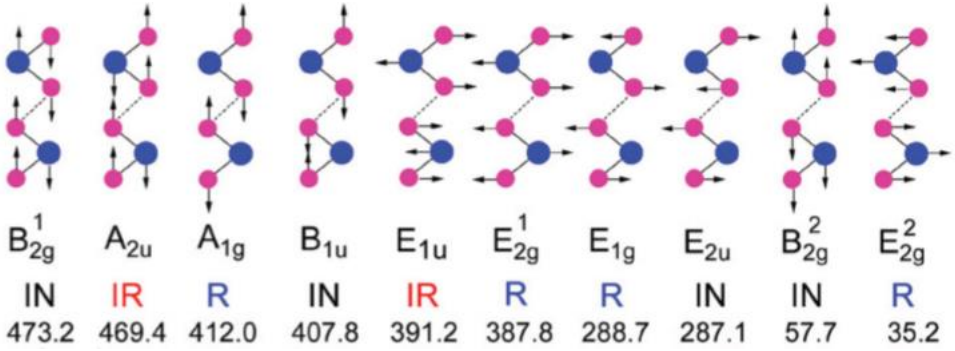


Figure 3.5 Vibrational modes of bulk MoS_2 [45]

Of the four Raman modes three are in-plane vibrations ($E_{2g}^2, E_{1g}, E_{2g}^1$) and the A_{1g} is an out-of-plane vibration [46].

The E_{2g}^2 mode found at 35 cm^{-1} is a low-frequency interlayer breathing mode. This mode is hardly observed with most typical Raman scattering equipment as it is often overshadowed by the much stronger Rayleigh scattering at low wavenumbers. The mode has been observed experimentally by Verble and Wietling through the use of very well filtered light [47,48]. The E_{2g}^2 mode is the only vibration involving multiple MoS_2 layers, the other three are intra-layer vibrations.

The E_{1g} mode is found at 289 cm^{-1}. Like the E_{2g}^2 mode, this vibration is rarely seen in the Raman spectra of MoS_2, but for different reasons. The intensity of the E_{1g} vibration is highly dependent upon the MoS_2 crystal orientation and the polarisation of the scattered light. Wietling performed Raman analysis on MoS_2 crystals cleaved along their basal and c-axis planes respectively. The crystals oriented on a surface by their basal planes showed no E_{1g} scattering, while those oriented on their c-axis displayed a notable E_{1g} peak intensity [49]. This behaviour was later confirmed by Chen who found that the peak has a very intense polarisation dependence, being more intense in p-polarised light, and absent in s-polarised light [47]. As the majority of MoS_2 sputtered films are basally oriented, it is commonly expressed that this vibration is forbidden in a backscattering geometry [50,51]. However, its presence in a spectrum is a more complex result of the applied crystal orientation and optical configuration of the spectrometer.

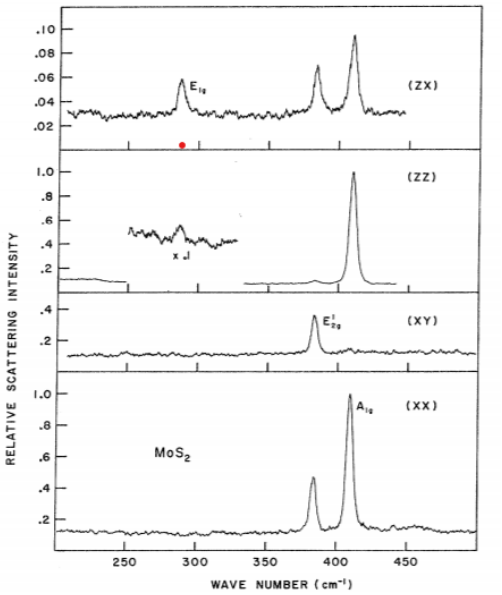


Figure 3.6 Orientation dependence of E_{1g} MoS_2 peak [49]
c-axis oriented crystals (top two spectra) and basally oriented MoS_2 crystals (bottom two spectra)

As a result of the limitations on the E_{2g}^2 and E_{1g} vibrations, the Raman spectra of MoS_2 are dominated by the E_{2g}^1 and A_{1g} peaks at 380 cm^{-1} and 408 cm^{-1} respectively. Due to their intense scattering these peaks have been studied in greater detail than the others to examine the nature of MoS_2 samples.

The relative intensity of the two peaks is found to depend upon the collection angle of the scattered light. Wang observed that the A_{1g} peak intensity is maximised at 180° in a backscattering configuration, reaching a minimum when scattering light was collected orthogonally to the incident beam. The E_{2g}^1 peak intensity was found to be independent of collection angle [52].

Like the E_{1g} mode, the E_{2g}^1 and A_{1g} peaks are sensitive to the polarisation of the laser light and crystal orientation. Chen observed that the E_{2g}^1 mode shows reduced intensity under s-polarised light [47]. In addition, in the crystal orientation studies of Wietling [49] c-axis oriented crystals under z-coordinate polarised light, the intensity of the E_{2g}^1 was reduced. The A_{1g} peak of basally oriented crystals had reduced intensity under xy polarisation, such that the

normally weaker E_{2g}^1 became the primary peak in the spectrum. This is shown above in Figure 3.6.

3.1.3.1.1. Effect of film thickness

The E_{2g}^1 and A_{1g} vibrations have been used to characterise the thickness of MoS_2 samples. In few-layer MoS_2 samples the two peaks migrate such that the gap between them decreases with decreasing numbers of MoS_2 layers [50,53].

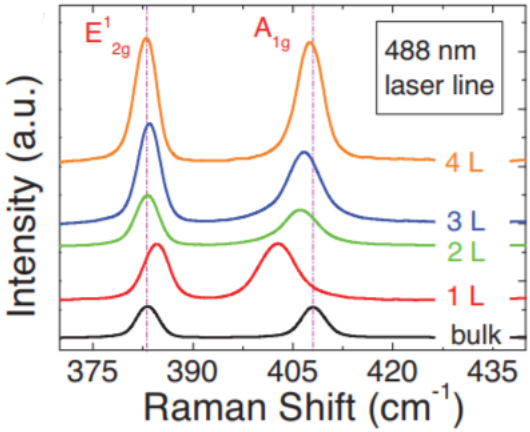


Figure 3.7: Migration of E_{2g}^1 and A_{1g} peaks with MoS_2 layer thickness [53]

This effect is believed to be due to the increasing strength of interlayer restoring forces when more MoS_2 layers are present [54]. This view is supported by the largest migration of peaks occurring between monolayer and bilayer MoS_2. In the monolayer there are no interlayer restoring forces, but when these are introduced the E_{2g}^1 peak moves from 386 cm^{-1} to 383 cm^{-1} and the A_{1g} peak migrates from 405 cm^{-1} to 408 cm^{-1} [55].

3.1.3.1.2. Effect of temperature

In addition to the migration of the E_{2g}^1 and A_{1g} with film thickness, these two peaks, as well as the E_{1g} peak red-shift with increasing temperature. With increasing temperatures the width of the scattering peaks also increases [56].

The migration of the peaks and of the linewidth are found to be linear relationships [57].

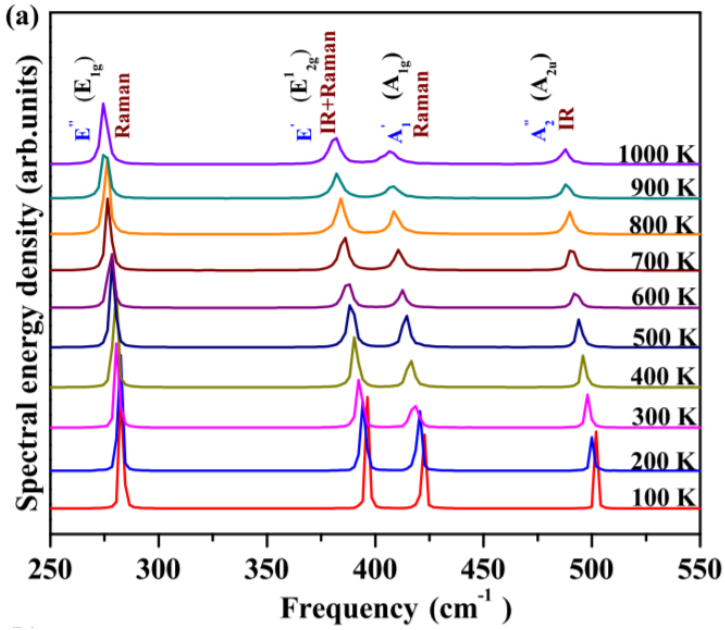


Figure 3.8 Migration of MoS_2 Raman peaks with temperature [56]

3.1.3.1.3. Effect of pressure

In contrast to the effect of temperature on the Raman spectrum, the spectrum of MoS_2 blue-shifts under applied pressure. When strain is applied to an MoS_2 crystal, the Raman spectrum migrates to higher wavenumber at a rate of 3.7 $cm^{-1}GPa^{-1}$ for the A_{1g} peak and 1.8 $cm^{-1}GPa^{-1}$ for the E^1_{2g} peak. At pressures in excess of 25 GPa, the E^1_{2g} peak disappears almost entirely [58,59].

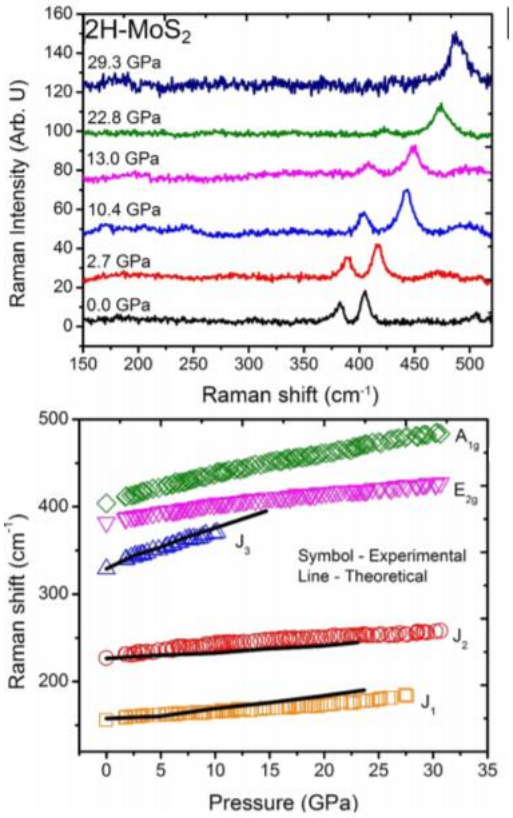


Figure 3.9 Response of MoS_2 Raman spectrum to pressure [60]

3.1.3.2. Resonant Raman peaks of MoS_2

When the energy of the incoming laser light matches that of an electronic transition within the molecule under study, an electronic transition can occur which alters the symmetry properties of the molecule. The result of this is the creation of new Raman peaks which are not present in the non-resonant spectrum. MoS_2 has two electronic transitions which can be stimulated by laser light at 1.9 eV and 2.1 eV. In order to excite these transitions, a He-Ne 632.8 nm laser is used as it falls between both absorption bands [46]. Most of the new peaks observed are due to difference procedures between the Raman vibrational modes and longitudinal acoustic phonon modes [41,47]. The resonant Raman peaks result from second order processes from the Brillouin zone.

Table 3: Phonon frequency of Raman-active and longitudinal acoustic modes at different Brillouin zone points of MoS_2

Phonon Frequency (cm^{-1})				
	Γ	M	M	K
A_{1g}	409	397	412	408
E^1_{2g}	383	373	370	345
E_{1g}	287	294	330 309	336
E^2_{2g}	34	-	233 (LA) 160 (ZA)	241 (LA) 192 (ZA)
LA	-	234	235	241

Of the new resonant Raman peaks, the most obvious in the spectrum is a combination mode at 468 cm^{-1} assigned as the 2LA(M) acoustic phonon.

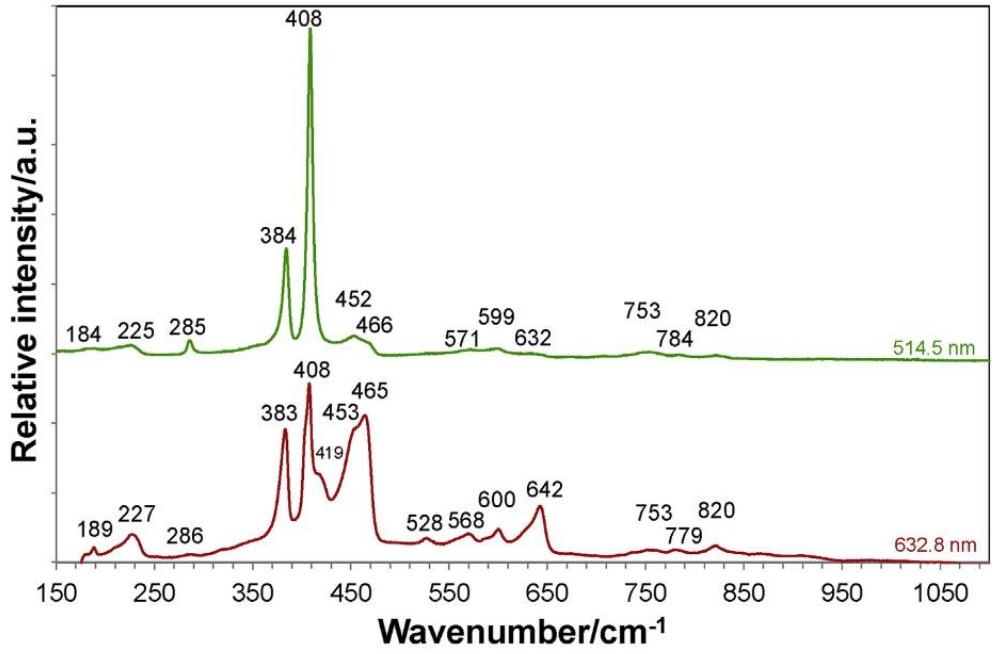


Figure 3.10 Comparison of non-resonant and resonant MoS_2 Raman spectra [61]

Top: Non-resonant MoS_2 Raman spectrum taken with 514.5 nm laser. Bottom: Resonant Raman spectrum of MoS_2 using 632.8 nm laser, displaying high intensity 2LA(M) mode at 465 cm^{-1}

3.2 Molybdenum DialkyldiThioCarbamate (MoDTC)

3.2.1 Structure and synthesis of MoDTC

In lubricant formulations the most commonly used molybdenum-based friction modifiers are molybdenum dialkyldithiocarbamates. These compounds consist of a molybdenum oxy-sulfur core solubilised in oil by the addition of organic groups. Whilst MoDTC is often quoted as being a single structure, it actually exists with a range of levels of sulfidation dependent upon its synthesis and the degree of age-related oxidation.

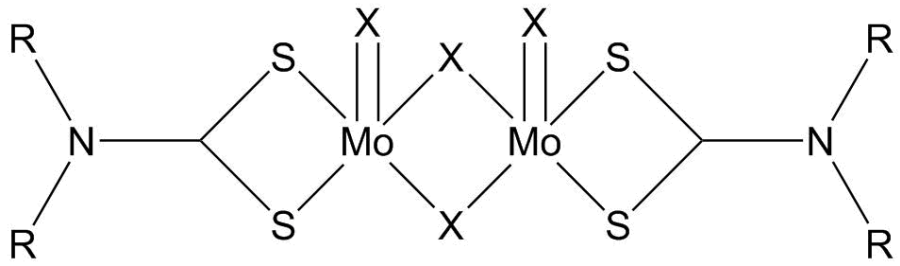


Figure 3.11 MoDTC general structure

Any of the X atoms can be either O or S

Molybdenum dialkyldithiocarbamates were first synthesised in the 1950s[62,63]. The dithiocarbamate ligands were prepared from nucleophilic attack of secondary amines on carbon disulfide in basic solution.

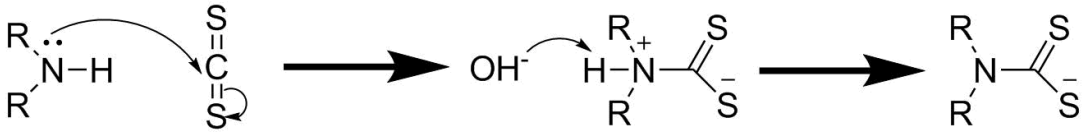
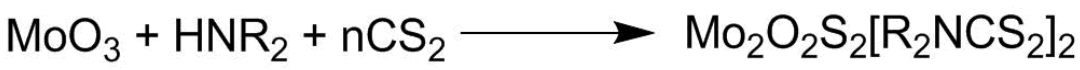


Figure 3.12 Curly arrow mechanism for formation of dithiocarbamate ligands

The dithiocarbamate ligands are reacted with molybdenum trioxide (MoO_3) to yield molybdenum dialkyldithiocarbamate as a yellow powder, according to Equation 19 [64,65].



$$MoO_3 + HNR_2 + nCS_2 \longrightarrow Mo_2O_2S_2[R_2NCS_2]_2$$

Equation 19 Synthesis of MoDTC

3.2.2 Thermal decomposition of MoDTC

3.2.2.1. Anaerobic decomposition

Molybdenum dialkyldithiocarbamates are thermally stable within the standard bulk oil operating temperatures within an engine. They undergo thermal decomposition at temperatures greater than 300°C. The thermal decomposition of molybdenum dithiocarbamates has been studied by Lozano [66] and Sakurai [64] using thermogravimetric analysis (TGA), who found that MoDTCs decompose under nitrogen to form MoS_2, with release of H_2S and C_4H_4S at 295°C [67].

There are some variations in the actual temperatures of this decomposition stage depending on the nature of the alkyl groups. Sakurai found that branching of the alkyl groups increased the temperature at which the formation of MoS_2 occurred [64]. In addition, this group found that increasing alkyl chain length also increased the onset temperature of MoS_2 formation [64].

3.2.2.2. Aerobic decomposition

Molybdenum dialkyldithiocarbamates are able to react with oxygen in an aerobic environment. There are differences in the thermal decomposition mechanism relative to nitrogen environments. As car engines are aerobic environments it is these decomposition processes which primarily affect the performance and oxidation stability of MoDTCs in practical use. For the dry powders of MoDTC, the additives now show two step decompositions by TGA.

The first is the formation of MoS_2 discussed in the previous section and the second is oxidation of the resulting MoS_2 to form MoO_3 at ca. 400-450°C [64,67,68]. Undergoing oxidation in the presence of air leads to a drop in the onset temperature for MoS_2 formation by 10-20°C, depending on the alkyl groups of the dithiocarbamates [64].

3.2.2.3. Oil-based thermal decomposition

Whilst it is useful to understand the thermal decomposition properties of purified MoDTC samples as dry powders, it is of more practical use to understand the thermal behaviour of MoDTC when it is dissolved in a lubricant oil.

Martin et al. [69] studied the depletion of MoDTC by High performance liquid chromatography (HPLC) in an oxidative oil bath held at 140°C. The group found that the concentration of the additive was depleted after just 4 hours, with no detectable MoDTC present in the oil after 16 hours.

Table 4 Depletion of inorganic sulfur-containing additives at 140°C

Atomic percentage concentration					
Additive (mass %)	Fresh Oil	Oxidised 4 hours	Oxidised 8 hours	Oxidised 12 hours	Oxidised 16 hours
ZDDP	1.45	1.15	0.74	0.32	0.04
ZDDP as [P]	0.10	0.08	0.04	0.01	0.00
MoDTC	1.6	1.1	0.5	0.3	0.2
MoDTC as [Mo]	0.077	0.052	0.018	0.003	0.000

This depletion of MoDTC occurs at much lower temperatures in an oil than would be expected from the TGA data of the pure compounds. Therefore, it stands to reason that a different chemical decomposition pathway is at play in oils. The chemistry of this oxidative pathway was studied by De Feo et al [70,71]. This group oxidised oil samples at 160°C for a period between 0 and 8 hours and analysed the resulting oxidation products by HPLC and mass spectrometry (MS). From the time-resolved evolution of the mass spectra, an oxidative decomposition pathway was proposed.

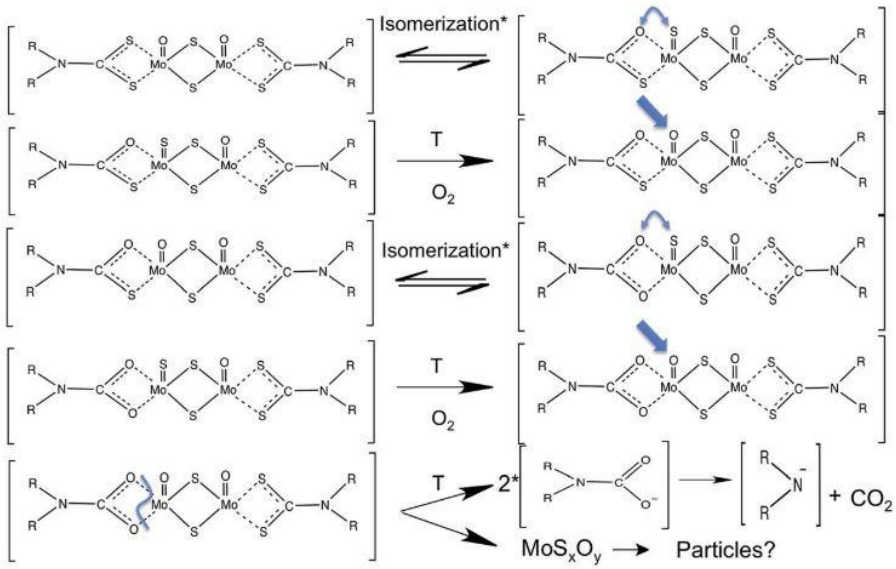


Figure 3.13 Thermo-oxidative MoDTC degradation mechanism [69]

Unlike the thermal decomposition of the pure MoDTC powders, this oxidative decomposition does not lead to the formation of MoS_2. As such, this oxidative decomposition of MoDTC is detrimental to its performance as a friction modifier. When this oxidative process occurs, after 8-12 hours of aging, there is no drop in friction from using MODTC relative to base oil alone [69,70].

The influence of oxidative species on the performance of MoDTC was also studied by Ponjavic et al. [72]. From previous studies it was unclear whether oxidation of MoDTC was caused by NO_x or by molecular oxygen, so this group tested the performance of MoDTCs subjected to differing oxidising gas compositions at a range of temperatures. The group found that at 160°C, molecular oxygen in air would rapidly oxidise MoDTC to the point of no friction reduction within 1 hour of aging, with NO_x content having little effect on the performance. At 100°C, the oxidation process was primarily NO_x driven. The group also confirmed the oxidative nature of the decomposition pathway, observing no detriment to friction performance when MoDTC was aged in argon at 160°C.

3.2.3 The friction-reducing performance of MoDTC

The effectiveness with which MoDTC acts as friction modifier depends upon a variety of factors. The friction performance which can be gained from MoDTC is a complex product of the level of decomposition, the amount and quality of MoS_2 formed from the additive, and the contact conditions to which the resulting MoS_2 is exposed.

3.2.3.1. MoDTC Friction profile and durability

Whilst the final friction results may vary, the overall profile of friction reduction by MoDTC follows a consistent pattern. At the beginning of MoDTC supply to the contact, a high friction period is observed (known as the induction period). This induction period is then followed by a rapid drop in friction as MoDTC decomposes, which maintains a low friction value for as long as the MoDTC supply is maintained.

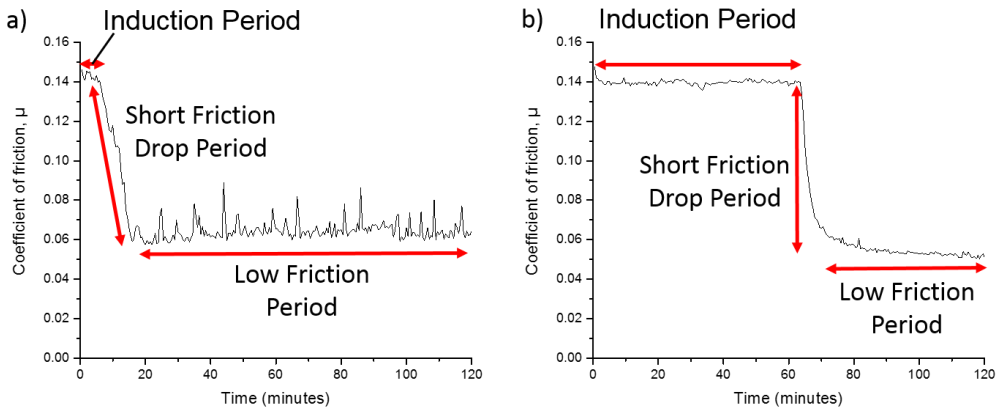


Figure 3.14 MoDTC friction response

a) Typical friction profile of an MoDTC-containing lubricant, b) friction profile of an MoDTC lubricant with extended induction time for clarity.

If the supply of MoDTC is removed, or replaced with a non-MoDTC containing oil, the friction coefficient will rapidly increase to the value associated with the base oil. Morina and Neville [73] ran tribological sliding tests with a MoDTC-containing oil, then removed this oil and replaced it with

other oils containing different additives [74]. They found that if the replacement oil contained anything other than MoDTC, the friction coefficient would rise almost instantly [74][75]. This suggests that the tribofilm formed from MoDTC is not durable and that the friction-reducing species (MoS_2) is being constantly formed and removed from the contact, the tribofilm is being sacrificed as sliding contact occurs.

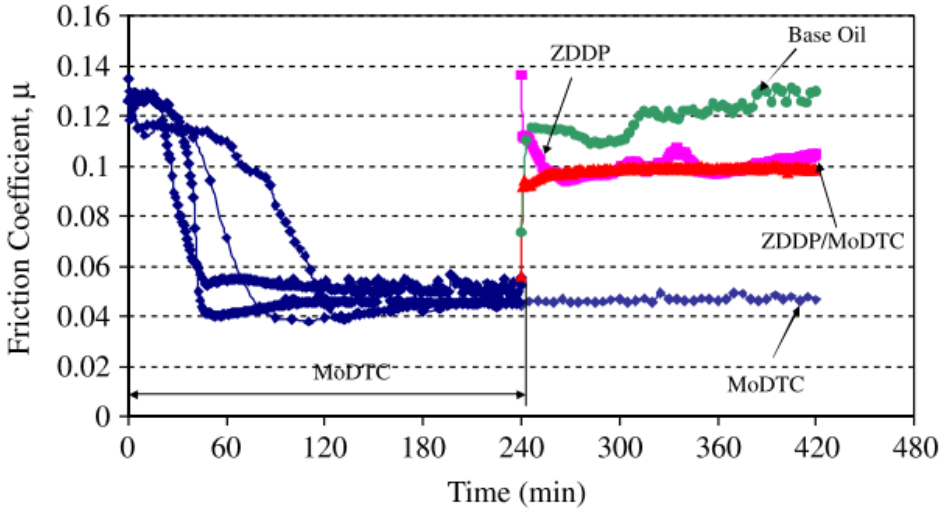


Figure 3.15 Friction response of MoDTC film when switched for different oils mid-test [73]

3.2.3.2. Effect of MoDTC concentration

The friction response of an MoDTC-containing lubricant is dependent upon the concentration of MoDTC in the oil. Miklozic et al. [76] found that at 0.05 wt% MoDTC, there was no reduction in friction relative to base oil. Upon increase of the MoDTC concentration to 0.125 wt% the friction coefficient was halved from $\mu = 0.15$ to $\mu = 0.075$. Yamamoto [77] observed an increase in the XPS peaks intensity of MoS_2 in oils with higher MoDTC concentration, while no MoS_2 peaks were observed with low concentration MoDTC oils. This MoS_2 peak intensity also correlated well with the observed reduction in friction [77].

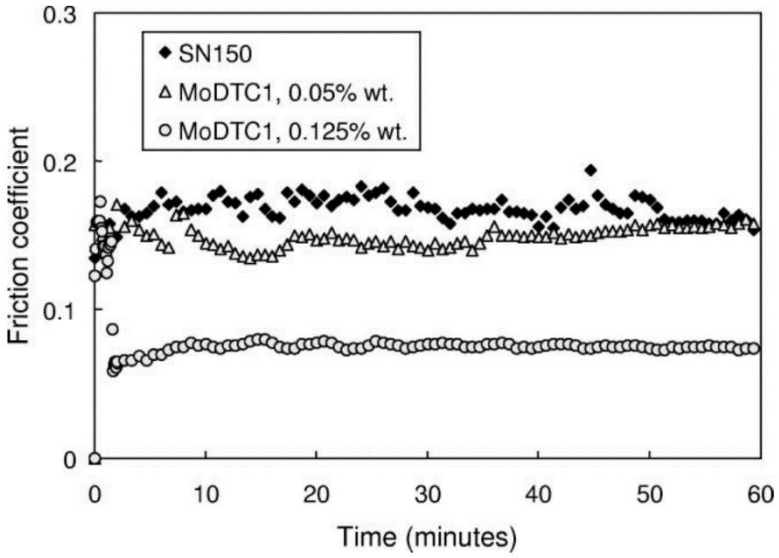


Figure 3.16 Effect of MoDTC concentration upon friction [76]

Induction times are also shortened by increases in MoDTC concentration. With higher loadings of MoDTC, MoS_2 can be detected by XPS within the first minute of contact, whereas in lower concentrations where friction reduction was still observed, MoS_2 was only detected after 4 minutes of contact [77,78].

3.2.3.3. Effect of temperature

The most obvious physical parameter which affects the friction performance of MoDTC lubricants is the temperature of the oil. In addition to providing more thermal energy for MoDTC decomposition, high temperatures increase the spacing of MoS_2 layers as the available thermal energy is greater relative to the Van Der Waals forces between the layers. This makes shearing layers relative to one another less energetically demanding and the overall friction coefficient decreases [79]. It is difficult to decouple the effect of lubricant temperature from other contact parameters. For example, increasing the temperature of a lubricant will reduce the viscosity of the oil and reduce the ability of the lubricant to support a load, thus lowering the lambda ratio (the ratio of the lubricant thickness to the combined roughness of the surfaces).

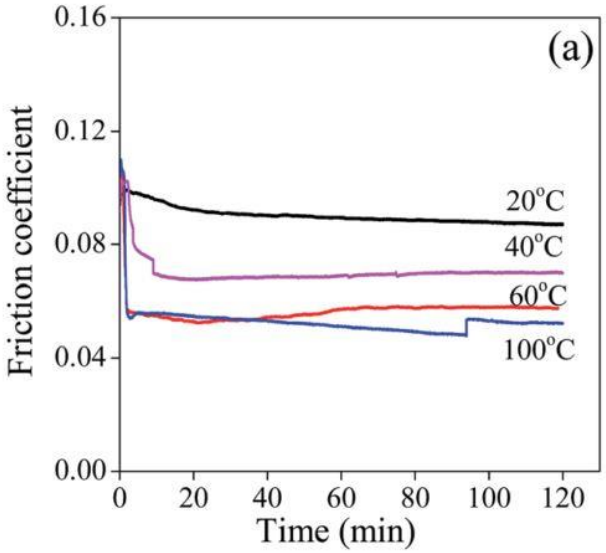


Figure 3.17 Temperature dependence of MoDTC friction performance [79]

3.2.3.4. Effect of contact conditions

The nature of the sliding contact under study is an important factor and the relative amounts of rolling and sliding contact, along with the unidirectional or reciprocating nature of the sliding contact, have a marked effect on the frictional performance of MoDTCs.

Graham et al. [78] studied the effect of surface roughness on friction reduction by MoDTC. Two surface roughnesses were used in the tests, with rough plates of R_a = 150-200 nm and smooth plates of R_a = 10 nm. The smooth discs did not lead to any friction reduction and no MoS_2 was observed on the surfaces, whereas the rougher surfaces underwent facile friction reduction with only a brief induction period. The absence of MoS_2 in the smooth plate tests was confirmed with Raman spectroscopy.

Expanding on this work, Khaemba et al. studied the effect of slide-roll ratio (SRR) and surface roughness on the friction behaviour of MoDTCs [80]. It was observed that the friction behaviour of MoDTC followed the standard friction pattern at all SRR values for surface roughnesses of R_a = 150 nm. When the surface roughnesses were reduced to 10 nm there was a difference in behaviour with SRR. Tests at an SRR of 100 % showed a standard MoDTC

response but when the sliding component of the contact was increased to SRR = 200 % the friction coefficient rapidly increased, prior to dropping and then oscillating around a value of μ = 0.06. Raman surface analysis of the tribofilms displayed formation of MoS_2 under all conditions along with $FeMoO_4$. MoS_2 was formed in the higher friction tests despite not displaying the effective friction performance of the other tests.

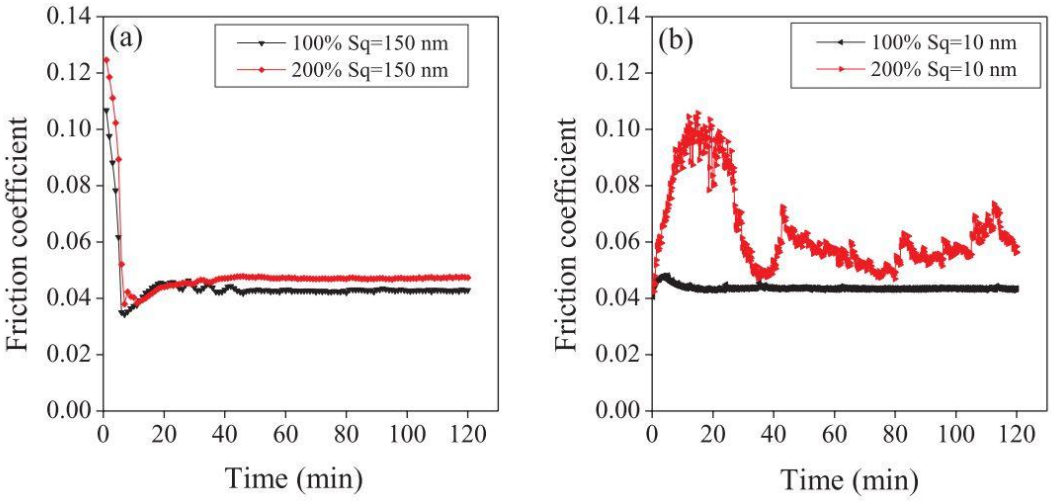


Figure 3.18 Effect of slide-to-roll ratio (SRR) on MoDTC friction performance [80]

Wu et al. [81,82] investigated the effect of SRR and of unidirectional vs reciprocating sliding upon the lubrication efficiency of MoS_2 nanoparticles in oil. Tests were run in unidirectional and reciprocating sliding contact under the same load, temperature and surface chemistry. The group analysed the flow pattern of MoS_2 nanoparticles and found that the reciprocating contact displayed a lower coefficient of friction than unidirectional sliding. The unidirectional sliding tests did not show any difference in friction performance relative to base oil while reciprocating sliding showed a coefficient of friction drop down to μ = 0.075. This behaviour was ascribed to MoS_2 nanoparticles blocking the inlet to the contact in unidirectional sliding conditions and starving the contact of friction modifying species, whilst the reciprocating contact prevented the flow of nanoparticles from ever becoming so great as to block the contact. This observed behaviour may not be applicable to *in-situ* MoS_2 formation as the MoS_2 nanoparticles used are much larger than the MoDTC molecule. It is likely that MoDTC will be able to enter the contact more easily

than MoS_2 nanoparticles and will reduce friction in unidirectional sliding conditions more effectively.

Graham et al [83] studied the effect of various contact parameters on the frictional performance of MoDTC in a reciprocating contact and found that the friction coefficient decreased with increasing sliding speed for a given stroke length. This finding is consistent with there being more energy available for the MoDTC decomposition reaction and greater shear stress in a contact. Graham et al. [78] also investigated the distribution of MoS_2 across the sample surface of a reciprocating contact using Raman spectroscopy and found that the regions of highest MoS_2 intensity were at the edges of the contact and the contact's centre. It is known that the MoDTC tribofilm is not durable and is easily removed from the contact. Therefore, it is likely that that the high MoS_2 concentration observed at the edges of the contact is due to the tribofilm being pushed out of the contact. At the centre of the contact the sliding speed is at its greatest; this is also the point in the stroke at which the lubricant film is thickest. The higher intensity of MoS_2 observed in the centre of the wear scar may be due to reduced surface contact and hence a lesser rate of MoS_2 removal from the contact.

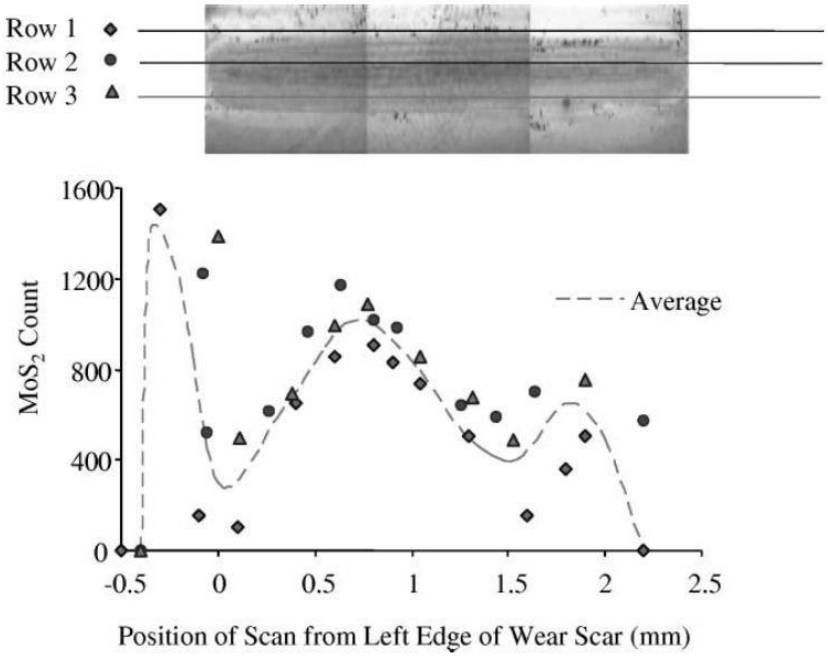


Figure 3.19 Raman intensity distribution of MoS_2 across a wear scar [76]

3.2.3.5. Effect of MoS_2 surface coverage

The action of MoDTC in a lubricant follows a well prescribed friction trace, beginning with a high friction induction period followed by a drop to low friction upon the formation of MoS_2. As we know that chemical transformation is an important part of the action of MoDTC it stands to reason that following the development of the surface chemistry as a function of time will allow some insight to be gained regarding the friction performance of these additives. Rai et al. [84] studied the development of MoS_2 *in-situ* with a specialised Raman spectroscopy-connected tribometer. This allowed for *in-lubro* but out of contact chemical analysis of the wear scar to be performed. Rai found that in the high friction induction period, the only species present on the surface were iron oxides formed from the contact. At higher temperatures iron molybdate Raman scattering was observed even during the high friction period but no MoS_2 peaks. Molybdenum disulfide was only observed during the low friction section of the MoDTC friction profile.

In addition to point Raman, Rai created maps of MoS_2 concentration by analysing the spatial distribution of the MoS_2 with increasing rubbing time. Rai found that MoS_2 concentration increased with rubbing time in a patchy manner. He also noted that upon repeated examination of the same area, the relative distribution of peak intensities was not the same. These findings support the view from previous literature by Grossiord et al. [85] that the formation of MoS_2 occurs in a patchy fashion, and that the tribofilm is not durable and is being moved by the contact. Xu et al. [86] utilised a similar time-resolved Raman tribometer to create a model of MoS_2 coverage and its relation to friction performance.

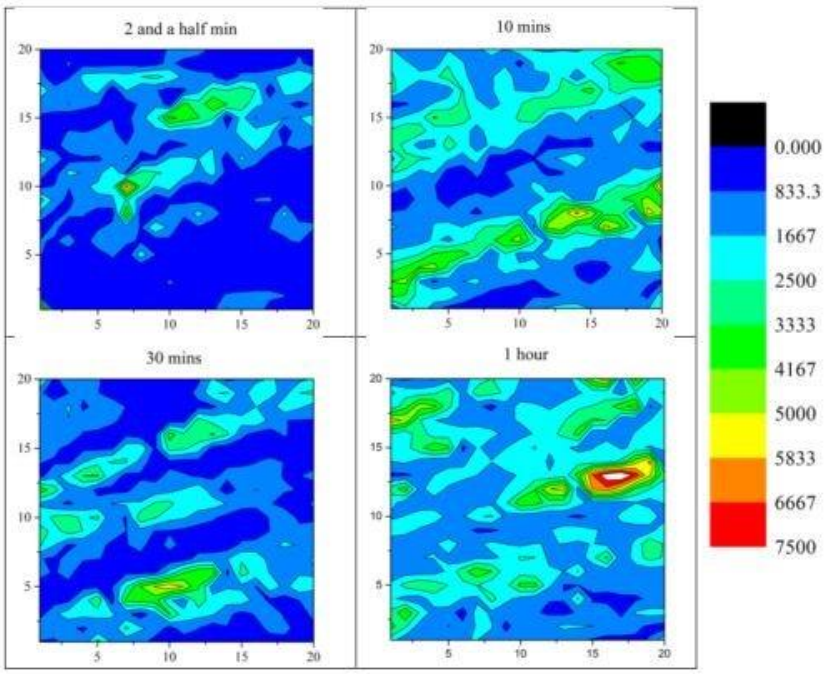


Figure 3.20 Time-resolved MoS_2 spatial distribution intensity within small wear scar area [84]

3.2.3.6. TEM of MoS_2 films

MoS_2 tribofilms derived from MoDTC have been studied on the nanoscale using transmission electron microscopy (TEM). Grossiord et al. [85] studied the wear debris from contact with MoDTC lubricant and found the debris to be covered in short MoS_2 chains.

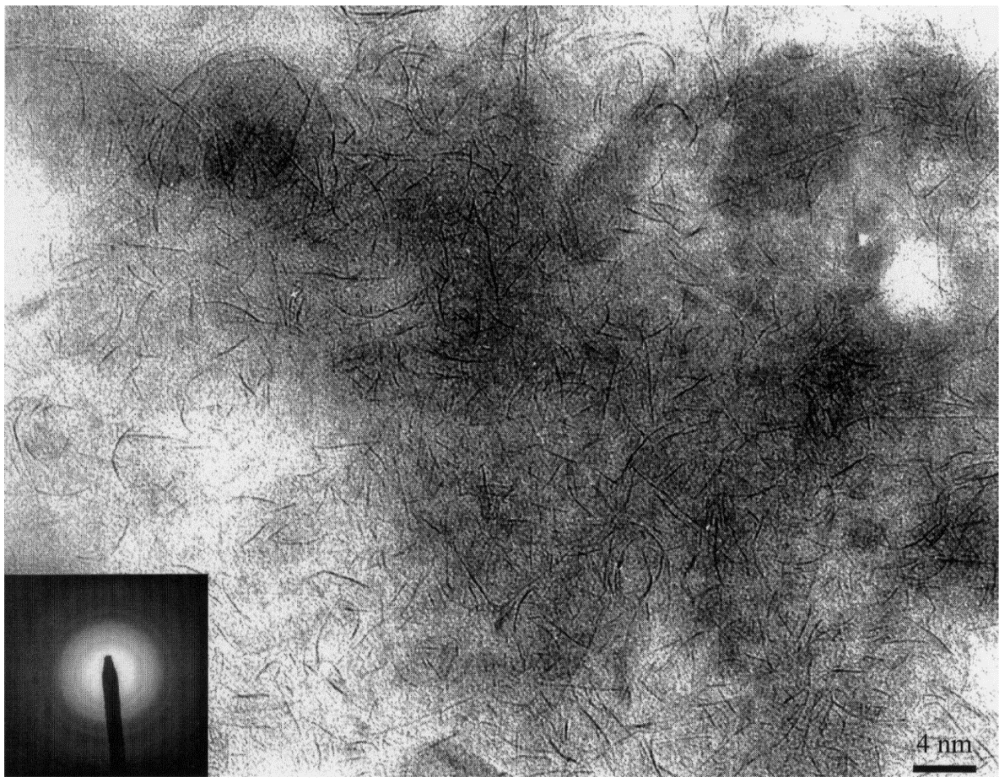


Figure 3.21 MoS_2 wear debris TEM [85]
In this micrograph, MoS_2 can be seen as randomly oriented dark lines

In monoblend MoDTC systems, MoDTC-derived MoS_2 films have been studied by Rai and Komaba [87,88]. In these tests the tribofilms were formed in a unidirectional contact under Hertzian contact pressures of 1.9 GPa and 1.4 GPa respectively. From 2.5 minutes in contact at 100°C, before a friction drop had occurred, Rai found tribofilms of 20-40 nm thickness that were amorphous in nature but was unable to see this as MoS_2 through Raman spectroscopy. After an hour in contact MoS_2 crystalline sheets oriented in the sliding direction of the contact were observed [87].

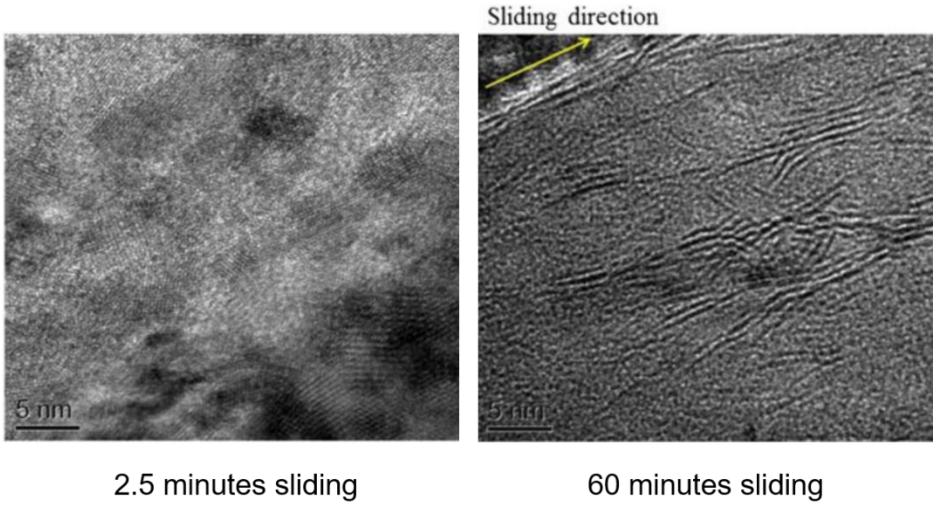


Figure 3.22 TEM sections of high friction (left) and low friction (right) tribofilms [87]

Komaba et al. [88] observed 10 nm films after 1 hour of contact under the lower 1.4 GPa contact pressure. Komaba et al. took TEM cross-sections formed at different contact temperatures and found that the film thickness appeared to be independent of contact temperature.

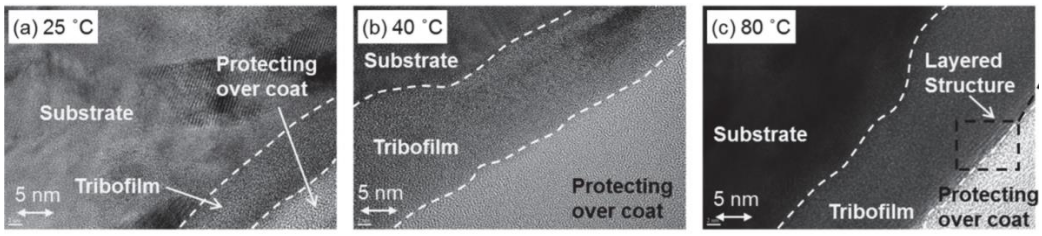


Figure 3.23 TEM sections of tribofilms formed at different temperatures [88]

In fully-formulated systems MoS_2 tribofilms consist of a few layers of MoS_2, oriented in the sliding direction of the contact. Unlike in monoblend systems the MoS_2 is not directly bound to the surface, but instead sits atop the thick ZDDP tribofilm.

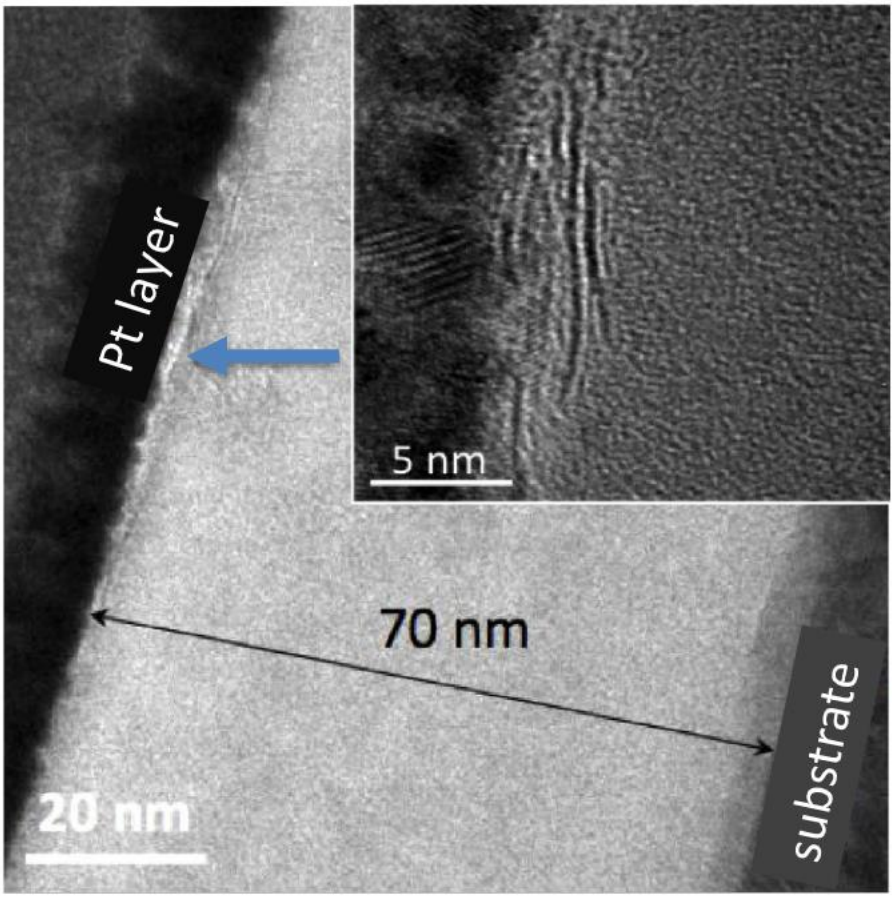


Figure 3.24 Fully-formulated oil tribofilm [89]

In fully-formulated systems the MoS_2 layer is very thin and the tribofilm is dominated by the ZDDP phosphate film.

3.2.4 Tribological mechanism of MoDTC decomposition

MoDTC is added to lubricant formulations because it leads to lower friction than can be provided by the base oil. In tribological contacts, MoDTC is known to be able to form MoS_2 at temperatures as low as 30°C [90]. It was initially considered that the frictional flash temperatures were sufficient to lead to the decomposition of the additives. However, in the majority of lubricated tribological contacts, the frictional temperature rise is predicted to be of the order of 5-20K, far below that required for MoDTC thermal decomposition [91–94].

As a result of this inconsistency, it is believed that mechanical force is able to tribochemically decompose MoDTC to form MoS_2 by a

mechanochemical mechanism. Various attempts have been made to unravel this mechanism.

The mechanism which has received the most attention was proposed by Grossiord et al. [95]. This mechanism involves the homolytic cleavage of a Mo-S bond to form two dithiocarbamate radicals and a molybdenum oxysulfide core. It is proposed that the dithiocarbamate radicals recombine to form thiuram disulfide whilst the metal centre decomposes to form MoS_2 and oxides of molybdenum. One intermediate in this decomposition mechanism is a mixed Molybdenum-oxo-sulfide species $MoS_{2-x}O_x$. The existence of this intermediate has been suggested as its loss as a stable fragment in mass spectrometric studies of MoDTCs [71]. The intermediates determined through his mechanism were suggested due to interpretation of XPS analysis of the tribofilm. XPS of lubricant-derived MoS_2 films shows a mixture of molybdenum (IV),(V) and (VI) oxidation states. The (IV) oxidation state is consistent with that of MoS_2 [96,97]. The Mo (V) oxidation state was believed to be the native MoDTC molybdenum centre, while the Mo (VI) state observed was assigned as a mixture of MoO_3 and the mixed oxysulfide intermediate.

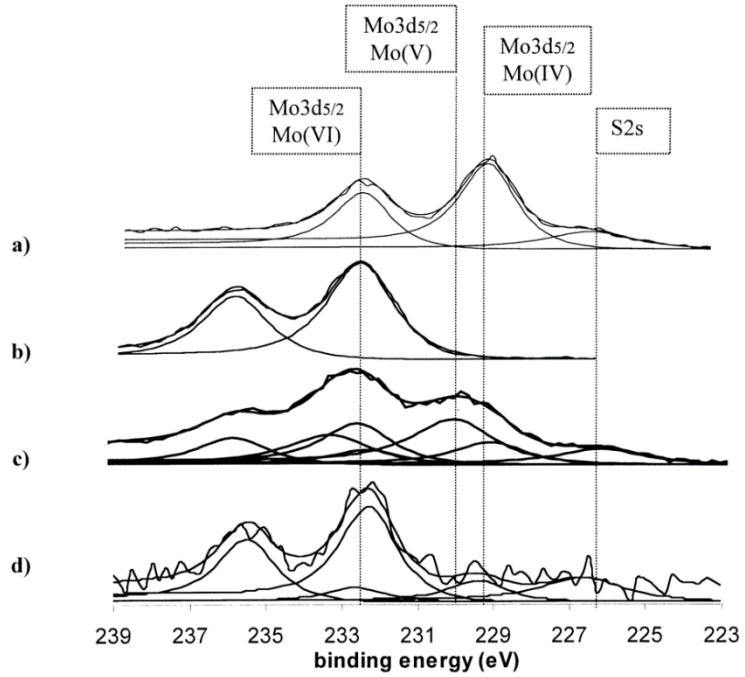


Figure 3.25 Mo region XPS spectrum of MoDTC tribofilm and molybdenum standard compounds [85]

a) MoS_2, b) MoO_3, c) MoDTC tribofilms, d) MoDTC molecule

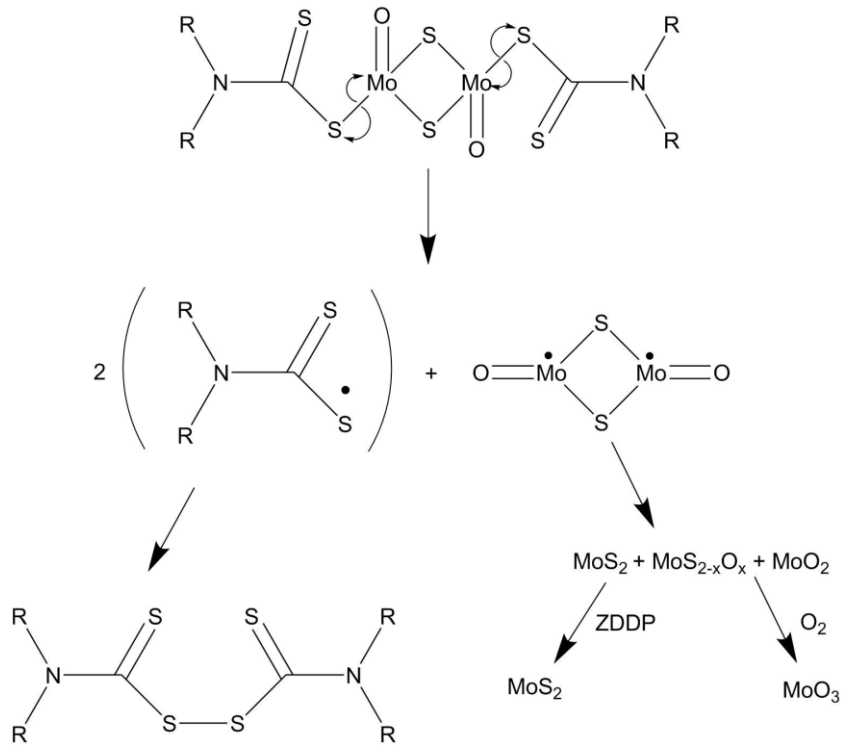


Figure 3.26 Grossiord MoDTC decomposition mechanism

Chemical characterisation with XPS is difficult. A great deal of care must be taken to fit peaks correctly. Even when correctly performed it is possible for multiple different species to give very similar signals. In order to overcome this and identify the chemical nature of the MoS_2 film, other, more definitive surface spectroscopies were performed. When Raman spectroscopy was used to study an MoDTC tribofilm it was found that the expected absorption peaks for MoO_3 and MoO_2 were absent, casting doubt on the Grossiord mechanism [76,98,99]. Molybdenum oxides are known to develop from hydrolysis of MoDTCs and MoS_2 in highly water contaminated lubricant solutions, but this was unlikely to be the case in the newly formulated lubricants that Grossiord et al. [85] tested [38]. To account for the lack of oxymolybdenum species Khaemba proposed a new mechanism for MoDTC decomposition in ferrous contacts, involving the formation of a mixed stoichiometry molybdenum-sulfur species MoS_x and the development of Iron molybdate ($FeMoO_4$), which is observed in the Raman spectra of MoDTC tribofilms [98][100].

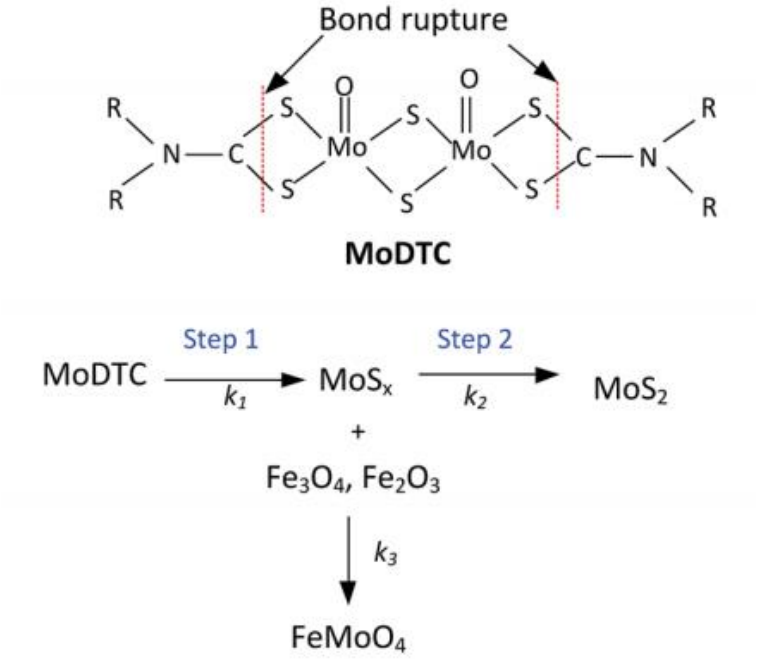


Figure 3.27 Khaemba MoDTC decomposition mechanism [98]

In this mechanism it is proposed that the initial reaction k_1 from the MoDTC to the mixed stoichiometry MoS_x species is mechanically driven by shear stress, and that the second reaction to form molybdenum disulfide k_2 is driven by a mixture of mechanical stress and thermal action. The Khaemba mechanism has several advantages over the Grossiord mechanism. Firstly, it removes the need for the formation of oxo-molybdenum species which are not observed in Raman studies. The mechanism also displays the weakest bonds (C-S) bonds breaking as a result of mechanical action but it does not account for what happens to the strong molybdenum oxygen double bond which is unlikely to be easily cleaved due to its high bond strength [101]. Neither of the above decomposition mechanisms account for the lability of the dialkyldithiocarbamate ligands in mixed zinc dialkyldithiophosphate (ZDDP) and MoDTC systems. It is known that in solution dialkyldithiocarbamate ligands are readily exchangeable with dialkyldithiophosphate ligands of zinc dialkyldithiophosphate (ZDDP) [75].

The amorphous MoS_x species proposed by Khaemba has also been proposed as a decomposition intermediate by Oumahi et al. [102]. This group studied the tribofilm formation of another molybdenum additive which showed Raman peaks consistent with MoS_x upon decomposition and proposed that

due to its mechanistic similarities with MoDTC, that it is likely that MoDTC also forms this species. Amorphous MoS_x species are known to decompose into MoS_2 upon electrical, thermal or mechanical loading. MoS_x, in the form of MoS_3 is a decomposition product of ammonium tetrathiomolybdate (ATTM) $(NH_4)_2MoS_4$ [103–105]. In the field of hydrogen evolution catalysis ATTM is decomposed to create films of amorphous MoS_x in preference to MoS_2 for its superior electrocatalytic properties [106–108].

3.2.4.1. The role of iron in MoDTC decomposition

An important aspect of any tribological contact is the chemical properties of the contacting surfaces. In most tribological research regarding MoDTCs the contacting surfaces are ferrous in nature. When attempting to determine the mechanism of MoDTC decomposition it is important to account for the chemical activity of the surfaces.

On the top of ferrous surfaces there exists a layer of iron oxides (Fe_2O_3 and Fe_3O_4) which can be removed by sliding to reveal the nascent iron surface beneath [109]. In steels there exists a variety of alloying elements such as chromium, manganese, vanadium and carbon. MoS_2 is formed from MoDTCs under normal ferrous-ferrous contact.

Haque et al. [110] have studied the action of MoDTC using contacting surfaces of cast iron against a counter face with a diamond-like carbon (DLC) coating [110,111]. The Haque group found that the friction drop associated with MoDTC still occurred using these surfaces but the use of MoDTC led to greater wear relative to base oil. This suggests that MoDTC interacts chemically with the DLC coating or the iron surface. Okubo and Sasaki [112,113] ran a series of experiments where both contacting surfaces were DLC coated and noted the absence of friction reduction from MoDTC relative to the normal DLC on DLC friction coefficient. This group also found that when using two DLC surfaces there was no wear acceleration of the DLC coating when lubricated with MoDTC-containing oil, indicating that the presence of an iron surface is an important feature in MoDTC decomposition. However, the

contact conditions of DLC-DLC contact and Iron-DLC contact are not directly comparable as DLC has different elastic behaviour to cast iron and steel.

The lack of MoDTC decomposition observed in systems where both faces are DLC coated could be ascribed to the milder contact conditions associated with the coated surfaces. Kosarieh [114] tested DLC against a non-ferrous, ceramic material and found no friction reduction resulting from MoDTC lubrication [115]. This result further supports the view that the presence of iron is necessary for the decomposition of MoDTC.

To investigate the effect of iron oxides Khaemba tested the thermal breakdown of MoDTC in the presence of iron oxides [99]. Fe_3O_4 was suspended as a precipitate in a MoDTC-containing polyalpha olefin base stock and the mixture was heated to 100 °C for 1 hour. Raman analysis of the solid Fe_3O_4 particles showed the characteristic Raman peaks of MoS_2 at 380 cm^{-1} and 410 cm^{-1}. This testing temperature is well below the 300 °C needed for MoDTC to degrade thermally of its own accord. This suggests that iron oxides are capable of acting as a catalyst for MoDTC decomposition, despite the MoS_2 product being of a lower level of crystallinity than would be expected from its tribochemical formation. It would be of interest to future researchers to test non-ferrous metallic materials for their effect upon the formation of molybdenum disulfide. If MoS_2 is present in an alumina-alumina contact for example this information could be used to exclude the catalytic action of iron oxides as part of the decomposition mechanism.

Thermal tests of MoDTC containing oils have been conducted on steel surfaces in the absence of contact. When a steel disc was heated for 3 hours at 100 ˚C in a MoDTC oil there were no MoS_2 peaks found by Raman spectroscopy [98]. This suggests that the nascent, high-energy iron surfaces exposed through wear may be necessary to the formation of MoS_2 thermally.

If MoDTC does indeed interact with iron as part of its decomposition mechanism then the scope of chemical investigation of decomposition intermediates may well have to increase, as molybdenum and sulfur have a rich variety of chemistries with iron, which opens many possibilities for possible surface species [116–118].

3.3 Molybdenum trimer

3.3.1 Synthesis of Mo-trimer

The oil-based oxidative degradation of MoDTC discussed above leads to a reduction in the effectiveness of the additive, especially in the longer term, requiring increased frequency of oil changes [119]. In order to improve long-term friction reduction, a new molybdenum additive was developed with the aim of providing greater thermal oxidative stability than MoDTC.

To fulfil this need a molybdenum trimeric structure was developed by Exxon [120].

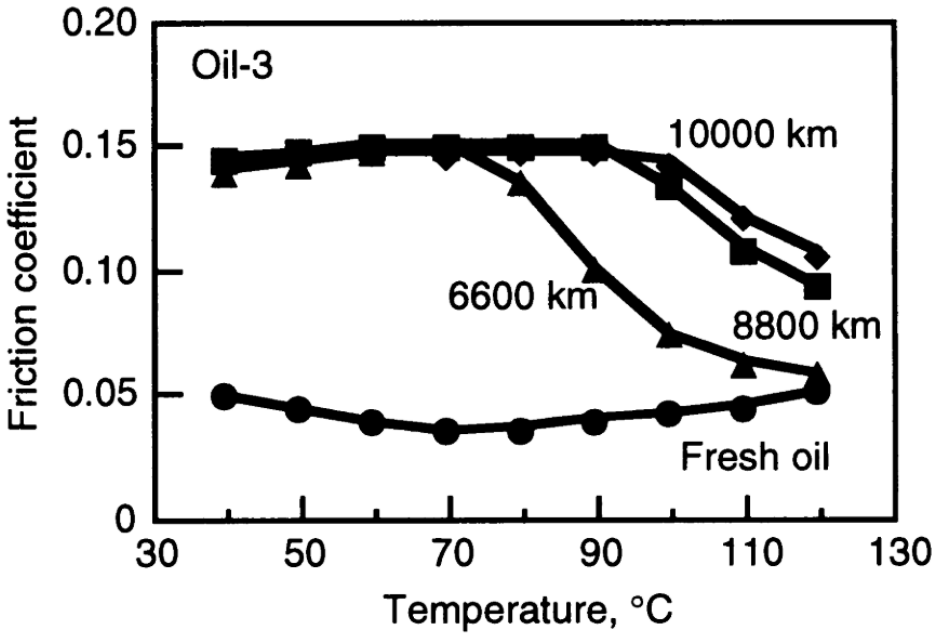


Figure 3.28 Friction performance of MoDTC-containing oils with mileage [119]

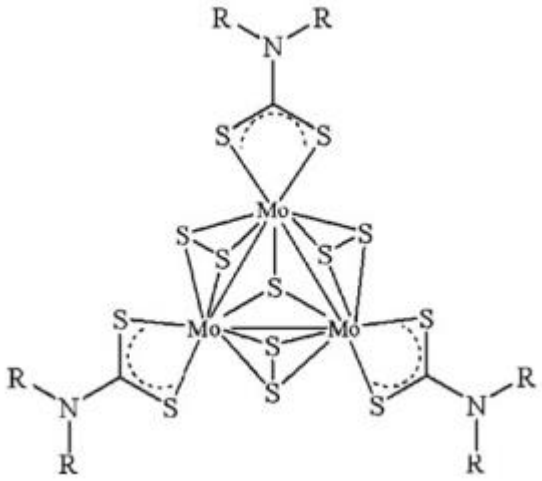


Figure 3.29 Mo-trimer structure

The additive exists as a mixture of Mo_3S_7 and Mo_3S_4 cores, coordinated by dithiocarbamate ligands. Each of the three Mo centres is in a Mo(IV) oxidation state. The Mo centres are coordinated by two either bridging sulfide or μ_2-sulfido ligands, each of which provide a single negative charge to the metal centre. At the outside of the molecule the Mo centres are co-ordinated to a dithiocarbamate ligand with alkyl groups to aid in oil solubility. In the centre of the core is a μ_3 apical sulfide bonded to all of the Mo centres. This leaves the core with a (+1) net charge which is balanced in the salt form with another dithiocarbamate ligand.

The structures are synthesised by reaction of ammonium thiomolybdate with tetraalkylthiuram disulfide, or by reaction of a molybdenum-sulfur halide salt with dithiocarbamates [120,121]. The compounds can be purified but are usually used as crude product.

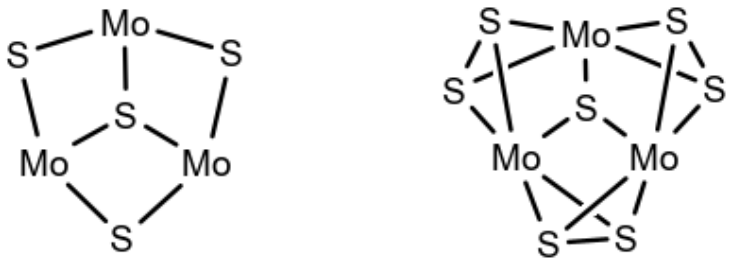


Figure 3.30 Mo-trimer molybdenum-sulfur cores

3.3.2 Friction reduction of Mo-trimer

Molybdenum trimer additives were developed to be added to oil compositions that already contained dimeric MoDTC, in order to provide longer term friction-reduction performance and in long-term tribological tests they proved successful, effectively maintaining low-friction beyond the expected period of MoDTC alone [120–122]. The overall principle is the same as with MoDTC, the Mo-trimer structure decomposes under tribological contact to form MoS_2.

In academic tribology studies this additive is often subjected to tribotesting in order to compare its friction performance to MoDTC as a benchmark. Numerous groups have investigated the performance of this additive in tandem with MoDTC and have found that under a range of contact conditions the friction performance is comparable. Some groups have found that the performance of Mo-trimer relative to MoDTC is dependent on the surface chemistry and the contact conditions. For example, De Barros Bouchet et al. [123] found Mo-trimer had a lower friction coefficient than MoDTC in reciprocating contact in both steel-on-steel and steel-on-nanocrystalline diamond systems [89]. Haque et al also found that the friction coefficient of Mo-trimer was lower than MoDTC dimer in reciprocating contact for DLC/steel and steel/steel contacts [124,125]. However, using Chromium nitride coatings against cast iron, the friction performance was slightly inferior to that of MoDTC dimer [110,124,125].

3.4 Molybdate ester

Due to a desire to reduce the sulfur content of lubricating formulations, there has been renewed interest in the development of low-sulfur friction modifier additives [126–128]. Among these low-sulfur additives has been extensive interest in OFM and borate ester systems [3,129–131]. Within the field of molybdenum-based friction modifiers, there has been a re-emergence of studies on a sulfur-free molybdenum additive developed during the 1960's often termed "organic molybdate" or "molybdate ester" [132–135]. This

additive is an organic oxo-molybdenum species that can reduce the usually high sulfur loadings imparted by other additives such as MoDTC.

3.4.1 Synthesis of molybdate ester

This additive class was originally prepared by reaction of alkane diols with molybdenum trioxide or ammonium molybdate in xylene under reflux to yield the structures below, depending on the diols used [134].

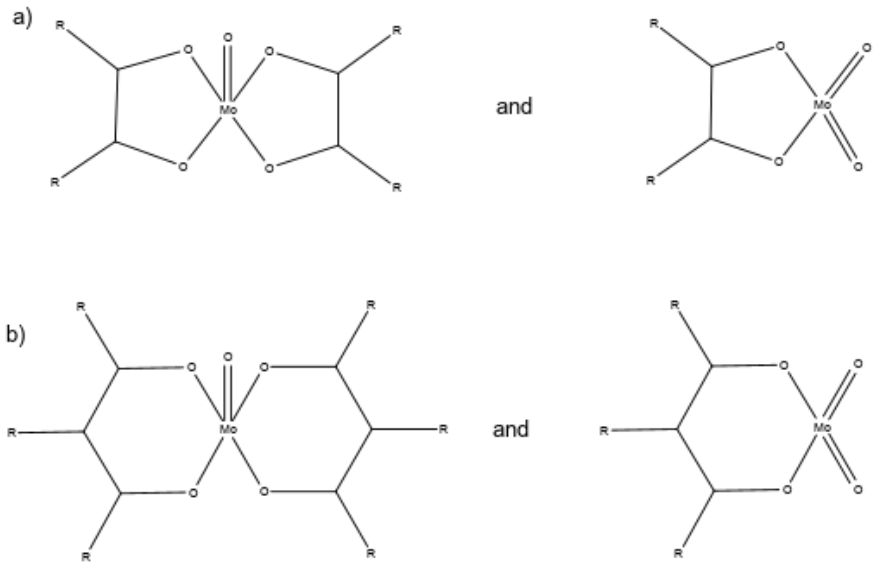


Figure 3.31 Original molybdate ester structures

The structure of the molybdate ester derived from the initial synthesis technique is dependent upon the diol used. Diols with an alpha relationship lead to the structures in a) whereas beta diols yield b) structures

The solubility of this additive was later improved with a new synthesis. Instead of using long chain diols, the ligating part of the organic structure was synthesised by reaction of glycerol ester with diethanolamine, prior to the addition of the molybdenum source [133,135]. The result of this was a change to the organic structure of the molecule, adding an amide or ester to what was previously just an alkyl chain [136]. The modern additive is supplied as a mixture of molybdate amide and ester. A major advantage of this synthetic method is the low-cost of the glycerol ester feedstock, which can be derived from cheap plant oils.

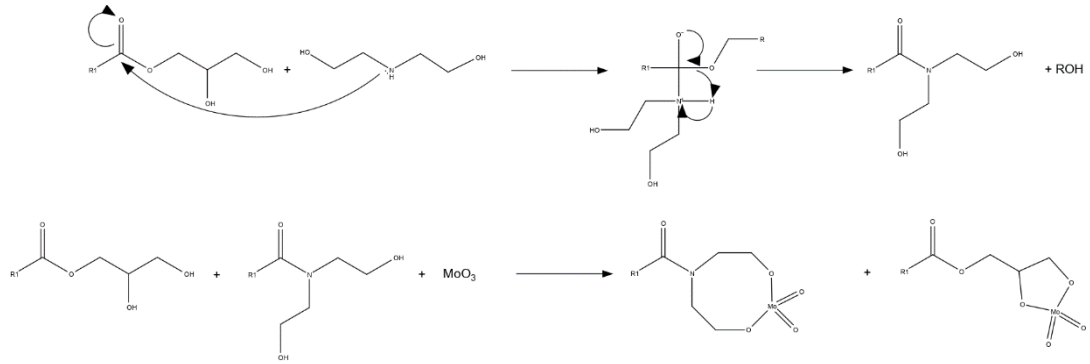


Figure 3.32 Synthesis of amide/ester molybdate

Prior to reaction with molybdenum trioxide, the glycerol ester is substituted with ethanolamine to create an amide. The mixture of amide and ester then produce the additive structure with molybdenum.

3.4.2 Mode of action of molybdate ester

Like MoDTC and Mo-trimer, the molybdate ester reduces friction by the formation of MoS_2 in a contact. However, unlike MoDTC and Mo-trimer, this additive is unable to form MoS_2 through self-decomposition as it has no sulfur in its structure. As a result, monoblend formulations containing just the additive alone are ineffective at reducing friction [137].

In order to effectively form MoS_2, molybdate esters must interact with other additives in a formulation. Molybdate esters reduce friction effectively in the presence of other sulfur-containing additives, which leads in turn to the formation of MoS_2. Appropriate sulfur additives which fulfil this purpose include organic polysulfides, thiophosphoric acids and thioacetates [134]. However, by far the most practical sulfur source for lubricant formulations is the ubiquitous sulfur-containing anti-wear additive Zinc DialkylDithioPhosphate (ZDDP).

Molybdate ester is thought to create MoS_2 through the development of sulfur-containing molybdenum intermediates which result from sulfur transfer reactions between the molybdate ester and ZDDP. It is well known that tetrathiomolybdates (MoS_4^{2-}), which bear some structural similarities to the molybdate ester, can act as friction modifiers in aqueous solutions [138,139].

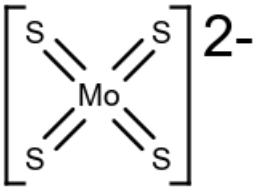


Figure 3.33 The tetrathiomolybdate anion

Like the molybdate ester molecular structure, tetrathiomolybdates have Mo in a (VI) oxidation state. However, compared to the oxo ligands in the molybdate ester, there is a much greater degree of covalency in the bonding of the tetrathiomolybdate, similar to that of MoS_2 [140–142]. Thiomolybdates have been investigated as species for friction reduction, Chinas-Castillo et al. [138] observed friction reduction by both thiomolybdates and thiotungstenates in aqueous solution under unidirectional contact, confirming the presence of MoS_2 with Raman spectroscopy. Unfortunately, thiomolybdates in their native form are not suitable for oil-based lubrication due to their low solubility. However, this does not preclude their transient formation near polar surfaces which may allow them to act as friction modifiers.

De Barros Bouchet et al. [143] proposed a mechanism by which successive transfer of sulfur from ZDDP to the molybdate ester is responsible for the formation of MoS_2 from molybdate ester. The mechanism is summarised below in three steps:

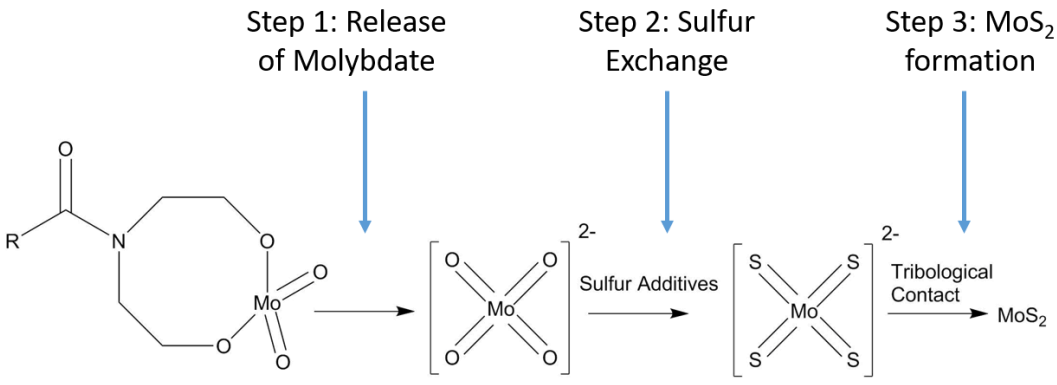


Figure 3.34 Molybdate ester MoS_2 formation mechanism

The mechanism is believed to proceed through step-wise exchange of oxygens by sulfur. All of the intermediate molybdates of the form MoO_xS_y (x +y = 4) have previously been observed in aqueous solutions [144,145]. This mechanism appears a reasonable first estimate as some degree of sulfur exchange must occur, as well as removal of the organic component in order to form MoS_2 sheets.

3.4.3 Friction-reducing performance of molybdate ester

Wu et al. [146] studied the effect of changing ZDDP and Molybdate concentration on the friction performance of molybdate ester lubricants in a 4-ball wear testing tribometer. The group found that in the absence of ZDDP, the molybdate ester performed no better than base oil. As the ZDDP concentration was increased from 0 to 0.5 wt% ZDDP the friction coefficient dropped from $\mu = 0.09$ to $\mu = 0.07$, but not dropping further with increasing ZDDP concentration. Similar tests were also performed by Hu, who found friction dropping to $\mu = 0.06$ upon addition of 1.0 wt% of ZDDP to the additive mixture [137]. These values showed some degree of friction reduction with the molybdate ester, but not the low coefficients of friction (μ=0.04) that are typically associated with additives such as MoDTC and Mo-trimer.

More thorough friction testing of the molybdate ester was undertaken by Oumahi et al. and De Barros Bouchet et al. [102,143]. Oumahi et al. [147] found that in reciprocating contact at lambda ratios of $\lambda < 0.04$ the molybdate ester/ZDDP mixture could reduce friction to $\mu = 0.04$ [102]. In the same tribometer De Barros Bouchet et al. [143] found the performance of molybdate ester/ZDDP to be superior to that of both the Mo-trimer and MoDTC. These results are supported by those of Gorbatchev et al. [89] who also found molybdate ester to have lower friction than MoDTC dimer and trimer in steel/steel contact.

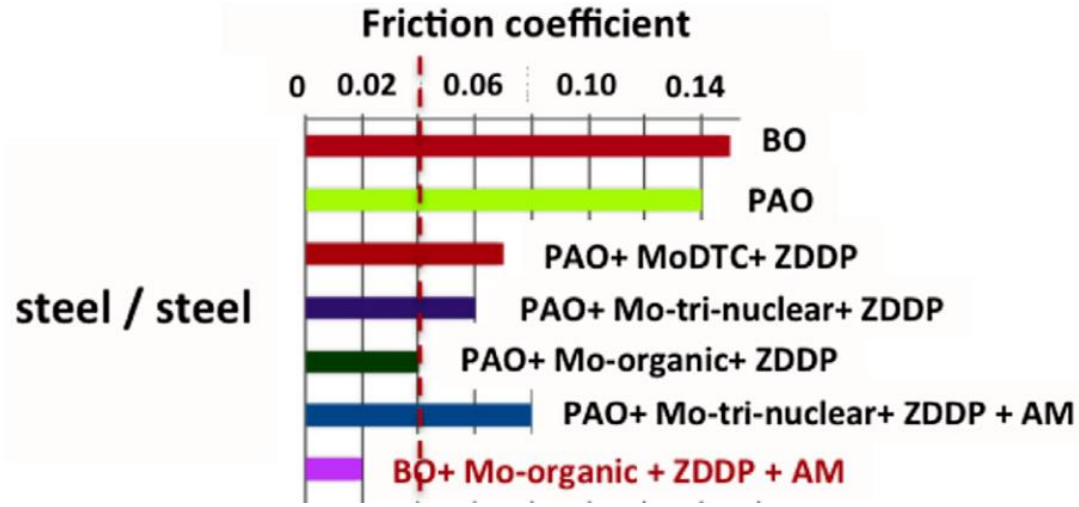


Figure 3.35 Friction performance of molybdenum additives [143]

De Barros Bouchet et al. [143] observed a further improvement in the low-friction performance of molybdate ester in the presence of long chain polyamines, reducing the observed friction coefficient to μ = 0.02. This phenomenon, termed the “fatty amine booster effect” was proposed to be due to the increased formation of MoS_2 caused by stabilisation of the oxymolybdate intermediate by the polar amines. According to the proposed mechanism, the molybdate ester is hydrolysed in the oil, to form an amine salt of the molybdate ion, which promotes the sulfur transfer reaction with ZDDP.

$$R_2(MoO_4) + 2\ R'(NH_2) + 2H_2O \rightarrow 3\ (RNH_3)_2MoO_4 + 2ROH''$$

$$(RNH_3)_2MoO_4 + 4\ S^{2-} \rightarrow (RNH_3)_2MoS_4 + 4\ O^{2-}$$

$$(RNH_3)_2MoS_4 \rightarrow MoS_3 + 2\ RNH_2 + 2H_2S \text{ by thermal decomposition}$$

$$MoS_3 \rightarrow MoS_2 + S \text{ under friction}$$

Figure 3.36 Proposed mechanism of fatty amine booster effect [143]

This friction-reducing effect of fatty amines is not specific to the molybdate ester however, friction reducing synergies between molybdenum and long chain amines have also been observed for MoDTC. The groups of Miklozic [148] and Lundgren [149] have found that the boosting effect of amines also improves the performance of MoDTC, so this effect may be a

more general interaction with MoS_2 or of additive dispersibility, rather than an interaction with the molybdate ester specifically.

3.4.4 Decomposition via MoS_3

One of the intermediates proposed by De Barros Bouchet et al. [143] to explain the fatty amine booster effect, and the performance of the molybdate ester more generally, is the species molybdenum trisulfide MoS_3. The role of this intermediate was investigated in more depth by Oumahi et al. [147] who prepared a sample of MoS_3 via the thermal decomposition of ammonium tetrathiomolybdate to compare to molybdate ester tribofilms. Under mild contact conditions, both MoS_3 and MoS_2 were observed in the Raman spectrum of molybdate ester tribofilms. Under harsher contact conditions, only MoS_2 was observed, either due to removal of MoS_3, or the MoS_2 signal drowning out that of MoS_3. Comparison between the mild tribofilms (Figure 3.37) and the thermally produced MoS_3 (Figure 3.38) showed similar broad peaks.

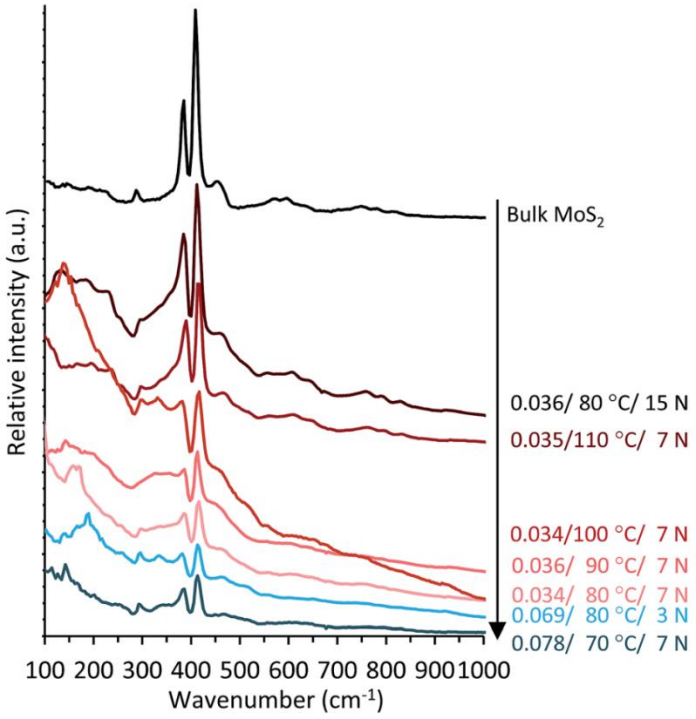


Figure 3.37 Evolution of molybdate ester tribofilm Raman spectra with contact condition severity [102]

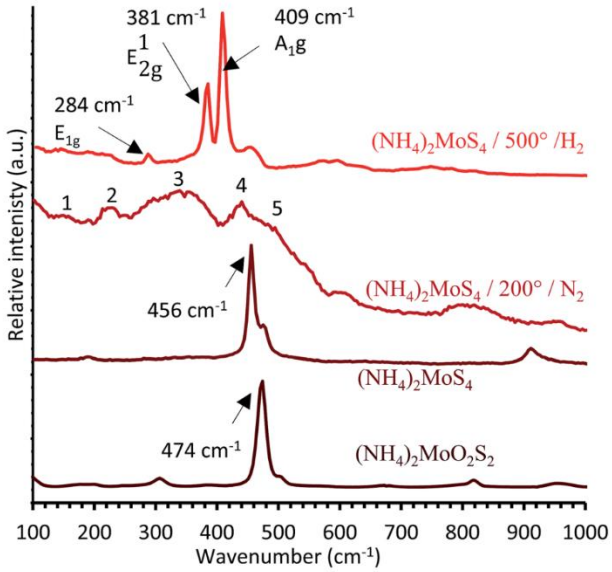


Figure 3.38 Evolution of Raman spectra of decomposed ammonium tetrathiomolybdate [102]

From these results it was proposed that MoS_3 is a possible intermediate of all molybdenum-based friction modifier additives.

MoS_3 is an amorphous structure which itself thermally decomposes in a broad range above 300°C to form crystalline MoS_2 [103,140]. Like MoS_2, the molybdenum centres are in a (IV) oxidation state, but the structure of the compound is poorly defined due to its amorphous nature. It is believed to consist of molybdenum centres sharing bridging sulfide and μ_2-sulfido bridging ligands. It was initially believed that the structure was that of chains of Molybdenum centres with a degree of Mo-Mo bonding [150]. This structure was found to be consistent with modelling studies to fit know neutron diffraction studies of thermally prepared MoS_3 [151].

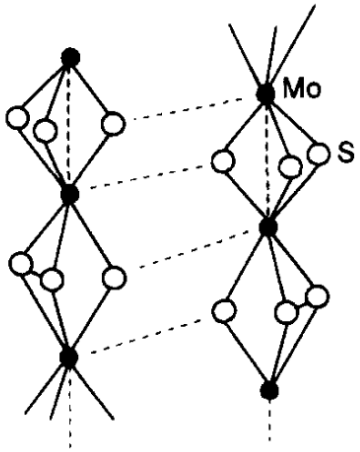


Figure 3.39 Initially proposed chain structure of MoS_3 [150]

MoS_3 is a desirable compound to prepare in the field of hydrogen evolution catalysis. Its many edge sites relative to MoS_2 make the amorphous structure a superior catalyst to the crystalline form. As such, there has been great interest in the understanding the structure of MoS_3 in this field. In recent years there has been a view towards MoS_3 being composed of Mo_3S_{13} interlinked cores bridged by sulfido ligands [152,153].

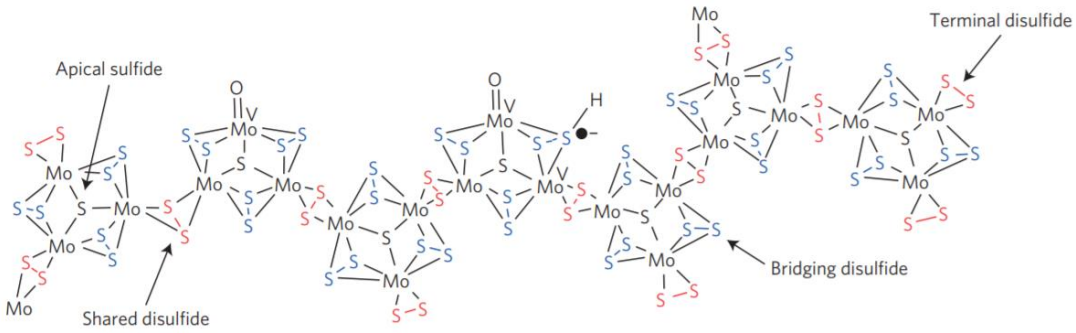


Figure 3.40 Cluster structure of MoS_3 [152]

Molybdenum-Oxygen bonds form due to surface oxidation of unsaturated molybdenum edge sites

Whether MoS_3 is ultimately composed of clusters or chains is not currently clear, and it may well be a mixture of the two, or dependent upon the processing techniques used to form MoS_3, be they thermal or electrochemical. A cluster structure when viewed side-on is very similar to that of chains, so it may be the case that MoS_3 does have a chain structure, but that the chains are interlinked in three dimensions.

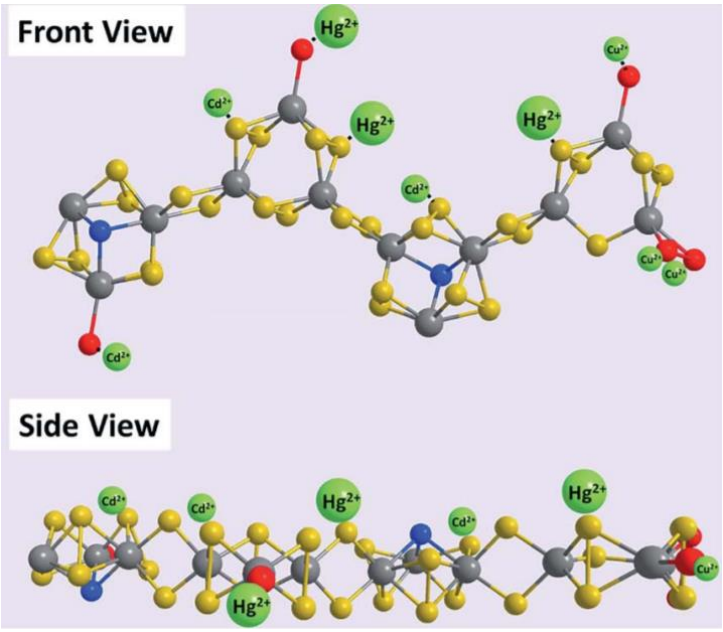


Figure 3.41 Front and side views of amorphous MoS_3 [154]

Blue: Apical Sulfur, Red: Terminal sulfur, Yellow: Bridging sulfur, Grey: Molybdenum

3.5 Zinc dialkyldithiophosphate (ZDDP)

As ZDDP is a critical component in the friction-reducing ability of the molybdate ester, the action and nature of ZDDP will be briefly covered to aid in understanding of the action of the molybdate ester.

ZDDP is an anti-wear additive which forms a protective film on boundary-lubricated surfaces. Initially developed in the 1940's, ZDDPs are now used in practically all automotive lubricant formulations [155–158].

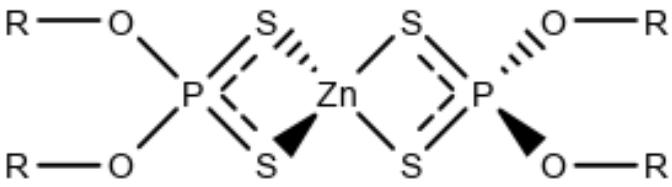


Figure 3.42 Structure of monomeric ZDDP

3.5.1 Nature of ZDDP tribofilms

3.5.1.1. Chemical nature of ZDDP films

ZDDP breaks down in contact to form a glassy phosphate film, dispersed in concentrated pads over a surface, rather than a continuous surface coverage [159]. The interposition of this glassy film between the contacting surfaces reduces the wear which occurs between them.

ZDDP tribofilms build up in thickness with increasing rubbing time. Initiation of film growth occurs in tribological contact in ferrous-ferrous contact, which nucleates the formation of ZDDP pad structures. As rubbing continues, these pads grow and coalesce, spreading and thickening the film [160,161]. Tribologically derived films tend to grow up to a maximum of 150 nm in thickness.

The nature of these films has been the subject of extensive study. ZDDP tribofilms are believed to be bonded to the ferrous surface with a thin layer of iron sulfides [162]. Atop this initial layer is a layer of 50-150 nm thickness composed of a mixture of phosphates. The composition of this film varies throughout the depth of the film. It is observed by X-Ray Absorption Near Edge Structure (XANES) that the bottom part of the film is composed of short-chain phosphates whereas the topmost region of the film has much longer, polyphosphate chains [163,164]. It was observed by Parsaeian et al. [165] that the relative abundance of these two kinds of phosphate could be controlled with the humidity of the contact. Analysis of the bonding and non-bonding oxygen environments by XPS showed that in humid environments, thinner films were formed with a greater proportion of short chain polyphosphates. Subsequent investigations of the durability of the resulting films observed that the chains composed of shorter chain phosphates were more durable than those of longer polyphosphates [165,166].

Recently, the amorphous nature of the ZDDP film has been revisited. Ueda et al. [166] performed FIB-TEM analysis of ZDDP tribofilms at various time intervals in the development of the ZDDP film. The group found that the phosphate film closest to the bonded iron surface wasn’t amorphous but was

in fact nanocrystalline. As the distance from the surface increased the level of crystallinity decreased, with the topmost sections of the film being amorphous. Durability testing of the film was then performed, in which the formulated lubricant was swapped for base oil during rubbing. The resulting surface was again studied by FIB-TEM and it was found that the amorphous section of the film had been removed, leaving the more durable nanocrystalline region. This behaviour is likely due to the protection from pressure that the lower film experiences at the expense of the upper film. Gauvin et al. [167] observed that zinc phosphates can be amorphized by applied pressure, so it is possible that increased ZDDP film build-up may protect the lower film from amorphisation long enough for the lower phosphates to crystallise into a more durable film.

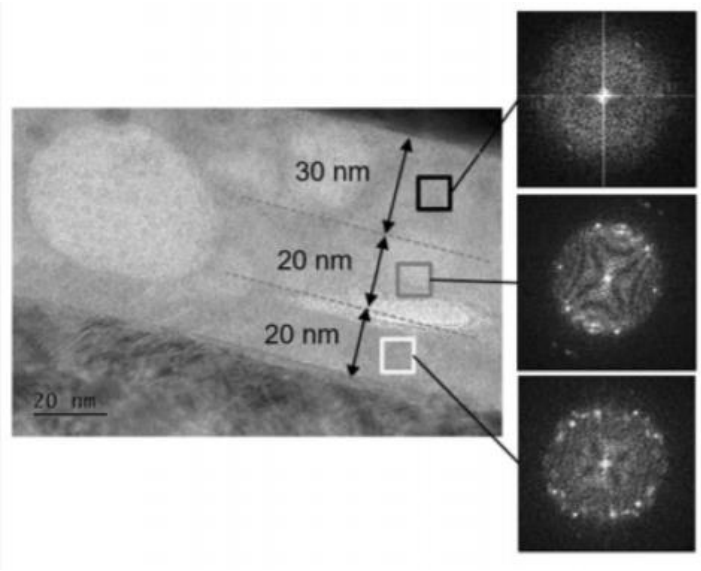


Figure 3.43 Development of ZDDP phosphate crystallinity with Tribofilm depth [166]

It is worthy of note that ZDDP tribofilms are known the digest iron particles which can be seen on tribofilm cross-sections by EDX [168,169]. The work discussed in the above section did not specify the crystal structures observed, so it is possible that the reduction in crystallisation may be due to the lower concentration of digested iron oxide particles as one moves further away from the contact surfaces which determine the nanocrystallinity observed in the film.

3.5.1.2. Mechanical properties of ZDDP films

The interposition of a ZDDP film between two contacting steel surfaces changes the mechanical nature of the surface contact, as the surface mechanical properties of one or both of the surfaces become dominated by the properties of the ZDDP films. The nanomechanical properties of tribologically-derived ZDDP films were determined by Aktary [170]. The elastic modulus of the ZDDP films were found to be dependent on the rubbing time, varying from 88.5 GPa after 5 minutes rubbing, up to 96.1 GPa after two hours of rubbing. The hardness of the film (as determined with the use of a cube-corner indenter) was mostly invariable at 3.5 GPa. These results agree well with those of Graham et al. [171] who performed similar nanoindentation experiments on ZDDP films. This shows that the ZDDP film has a much lower elastic modulus than the stainless steel (210 GPa) to which it usually binds. This allows the film to absorb dissipate energy through plastic deformation, whilst preserving the steel surface beneath.

Ye et al. [172] investigated the mechanical properties of ZDDP films as a function of depth. The group found that the hardness and elastic modulus of the ZDDP film increased with increasing tribofilm depth. This correlates well with the proposed increase in crystallinity observed by Ueda et al. [166]. Ye proposed that the top layer of the ZDDP film is able to plastically flow under pressure while the lower layer remains more rigid. The ability of ZDDP films to flow was later confirmed by Dorgham et al. [173,174], who printed zig-zags patterns of ZDDP films formed from an AFM tip and observed the films bleeding into one another under pressure. This effect was more pronounced at long rubbing times, where a fluid film of longer chain polyphosphates was formed.

ZDDP tribofilms are known on the macroscale to lead to higher friction than base oil and MoS_2-lubricated contacts [175–177]. On the macroscale, the overall friction coefficient is the product of the friction forces from the entire surface, including those regions not covered by the ZDDP film, which is known to be patchy in nature. In order to determine the relative friction performance of the ZDDP film specifically, Ye et al. [178] studied the nanofrictional

properties of ZDDP films using an AFM/LFM. Ye found that the frictional resistance in ZDDP films, MoDTC films and base oil systems varied in a ratio of 1.5:0.7:1.0 respectively. It was proposed that the friction-enhancing effect was due to increased surface roughness created by the build-up of ZDDP films. However, Taylor et al. [175,176] observed that in full-additive systems ZDDP pads are smoother than the underlying surface and proposed instead that inhibition of elastohydrodynamic lubricant entrainment is the cause of higher ZDDP film friction.

3.5.2 ZDDP-dispersant antagonism

The thickness of the ZDDP film is dependent upon the chemical formulation of the lubricating oil. ZDDP films created from lubricants containing amine dispersants are thinner than those made from oils without dispersants [179]. Zhang et al. [180,181] studied the chemical interactions between ZDDP and succinimide dispersants and found that the onset reaction temperature for ZDDP decomposition was reduced from 175°C to 150°C in the presence of dispersants. This reduction in ZDDP breakdown temperature was assigned to formation of amino zinc complex in solution [182]. Shiomi et al. [183] determined that this complex had lower surface affinity for steel than free ZDDP did. The effect of dispersant to ZDDP ratio was investigated by Zhang [180], who observed a consistent decrease in ZDDP film thickness using MTM-SLIM in the presence of dispersants. At high dispersant concentrations, there was no ZDDP film formation at all. The group also found that the thickness of the film could not be restored through the addition of more ZDDP to the formulation. In addition to chemical interactions, amines are able to act as organic friction modifiers and can compete for surface sites that would otherwise be critical for the deposition of a ZDDP tribofilm [184–186]. This competition for active sites, combined with chemical interaction display a dual antagonism towards ZDDP tribofilm development.

3.5.3 Decomposition of ZDDP

Much like MoDTC, ZDDP tribofilms are formed in contacts under much lower temperatures than their thermal decomposition studies would suggest. ZDDP films can be formed at lubricant bath temperatures as low as 25°C [187]. In purely thermal conditions ZDDPs decompose at temperatures between 130°C and 250°C, depending on the nature of the alkyl groups, with secondary alkyl ZDDPs being less thermally stable than primary ones [188,189]. The thermal decomposition products of ZDDP are thiophosphorylates, alkenes, hydrogen disulfide and thiophosphorylates, which are believed to polymerise to form the polyphosphate film [159].

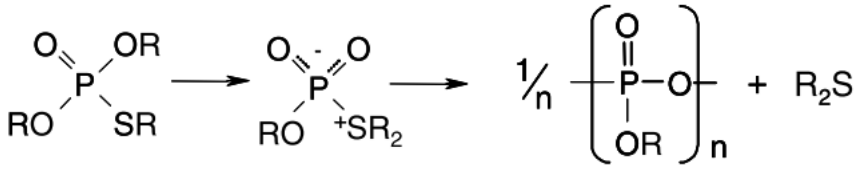


Figure 3.44 Formation of polyphosphates from thiophosphorylates[159]

The rate of tribochemical decomposition and hence film formation from ZDDP is dependent on both the contact temperature and the applied shear stress in the contact. Gosvami et al. [190] grew ZDDP films using *in-situ* AFM as a single asperity contact to develop a tribofilm growth model accounting for both temperature and contact stress. The group determined that the tribofilm growth rate was exponentially dependent upon a stress altered activation energy with Arrhenius-like behaviour, dependent on the stress and activation volume of the bonds to be broken.

On a larger scale, a similar model has been used by Zhang [161] to explain the formation of ZDDP films in contacts nominally in the elastohydrodynamic regime which should not have asperity contact [161]. This model has been expanded upon extensively by Tysoe and Konda, and has gained traction as a tool to explain the low reaction temperatures of chemistry in mechanical systems [191–194].

Even in normal lubricant operating temperatures, the thiophosphate ligands of ZDDP are known to be labile, undergoing exchange with the dithiocarbamates ligands of MoDTC. It has been shown by Sarpal et al. [195] that in solution ZDDP and MoDTC undergo facile ligand exchange. They did this using time resolved ^{31}P nuclear magnetic resonance spectroscopy and have found the movement of the expected phosphorus signals for both the MoDTC and ZDDP molecules. This result has important consequences regarding the ease of the sulfur transfer reaction with both MoDTC and molybdate ester.

3.6 Summary

3.6.1 Main points of current knowledge

From the studies thus far performed we have gained a good understanding of the tribological behaviour of molybdenum additives. The following list provides a summary of subjects about which the scientific community has a good understanding.

- The structures and syntheses of the Mo additive structures in their solid and solutions states, at least as monoblends.

- It is well established that the decomposition product responsible for friction reduction for all of the additives discussed is MoS_2.

- The Mo-trimer and Molybdate ester are able to achieve friction performance similar to that of MoDTC under harsh contact conditions.

- Post-mortem surface analysis has provided a good understanding that the positioning and coverage of MoS_2 on a surface seem to be important to overall friction performance. Raman analysis has shown that iron oxides of various kinds also compose parts of the MoS_2 tribofilm. Raman spectroscopy has confirmed that molybdenum oxides are not formed in the tribofilm in a crystalline form.

- XPS analysis has shown that the top section of the MoS_2 tribofilm is composed of at least two different molybdenum environments, depending upon how the peaks are fit. There is a Mo (IV) environment fit to MoS_2 and a Mo (VI) environment, often fit to MoO_3 oxidation on the very top layer of MoS_2, or some other Mo (VI) decomposition product.
- The activation parameters of MoDTC dimer which lead to friction drops have been well defined in terms of contact conditions and formulation dependence, including surface roughness, concentration and temperature

- That molybdenum additives undergo interactions with ZDDP and other additives in a formulation that alter the frictional properties of the additives. The most notable of these is the interaction of molybdate ester with sulfur sources necessary to produce MoS_2.

From these known facts and observations of the post-contact surface chemistry, a number of mechanistic steps and chemical species have been proposed including the formation of mixed oxysulfide species, thiuram disulfide, molybdenum oxides amorphous molybdenum sulfides, iron molybdates. It is difficult without *in-lubro* spectroscopy to know whether these species are part of the decomposition process as intermediates or if they are formed as side products of the MoS_2 formation mechanism.

3.6.2 Current unknowns

There are a series of knowledge gaps which still blur understanding of the activity and mechanisms of molybdenum-based friction modifiers. In addition to these, there are a few assumptions that automatically regard the different molybdenum species as equivalent. The gaps in current understanding addressed in this work are discussed here.

3.6.2.1. Tribological activation

The contact conditions under which MoDTC is able to form MoS_2 and effectively reduce friction are well documented in terms of temperature, surface roughness and sliding speed. However, work by Khaemba et al. [80] has taught that the contact conditions required for friction reduction may be a more complex topic than previously thought.

Although there has been extensive study of the tribological activation parameters of MoDTC, far less work has been done regarding if the Mo-trimer or molybdate ester respond to contact conditions in the same manner as MoDTC. Tribological studies which aim to characterise surface chemistry often utilise harsh contact conditions in order to form MoS_2 films, which will activate MoS_2 formation from all additives. However, due to their different chemistries, Mo-trimer and molybdate ester may respond very differently to mechanical contact when compared to MoDTC. In order to understand if a molybdenum additive will be an effective friction modifier in a particular engine contact, we need to understand their relative mechanical activation points of MoS_2 formation. In this work the tribological environmental parameters for the molybdate ester and Mo-trimer are compared with MoDTC to determine their relative MoS_2 formation.

3.6.2.2. The nature of MoS_2 films derived from differing molybdenum additives

It is known that MoS_2 is the cause of low friction in molybdenum-lubricated contacts. However, there are a range of degrees of friction reduction which can be obtained from lubricant-derived MoS_2 films, all of which display MoS_2 on the surface. Therefore, the mere presence of MoS_2 is insufficient to provide optimal friction performance. In order to understand how to obtain ideal friction performance from additive films there needs to be an understanding about what properties of an MoS_2 tribofilm are key to friction reduction, be it surface coverage, crystallinity, bulk amount of MoS_2 etc.

In addition, the differences in the performance of other molybdenum additives will depend upon the nature of MoS_2 tribofilms they form. It is worth

investigating if there are differences in the nature of MoS_2 tribofilms which are derived from different additive chemistries, along with how these differences affect the mechanical performance of these films. Subsequent relation of the formed tribofilms to the molecular structures of the molybdenum additives can inform future synthesis in order to provide MoS_2 tribofilms with favourable properties.

3.6.2.3. Molybdate ester-additive interactions

The molybdate ester forms MoS_2 through a sulfur-exchange reaction with other additives in formulations. The kinetics and formulation dependence of this reaction are currently unknown, as are the subsequent effects on friction performance. In order to understand the limitations of MoS_2 formation in a bimolecular fashion, as well as the mechanism by which molybdate ester forms MoS_2, an understanding of the MoS_2 formation reaction kinetics is needed.

3.6.2.4. Decomposition intermediates of molybdenum additives

Although much work has been done to try and understand the decomposition mechanism of MoDTC, no definitive answer has been found as options for *in-lubro* chemical analysis are limited. In order to determine decomposition intermediates for molybdenum additives, time-resolved spectroscopic techniques are required which can analyse the surface chemistry *in-situ*. It would be of interest to determine the relative tribological decomposition pathways for differing molybdenum additives. If it can be determined that different additives decompose via unique pathways, or via a common intermediate, then this information can be fed back into molecular design to create species with more facile decomposition to MoS_2.

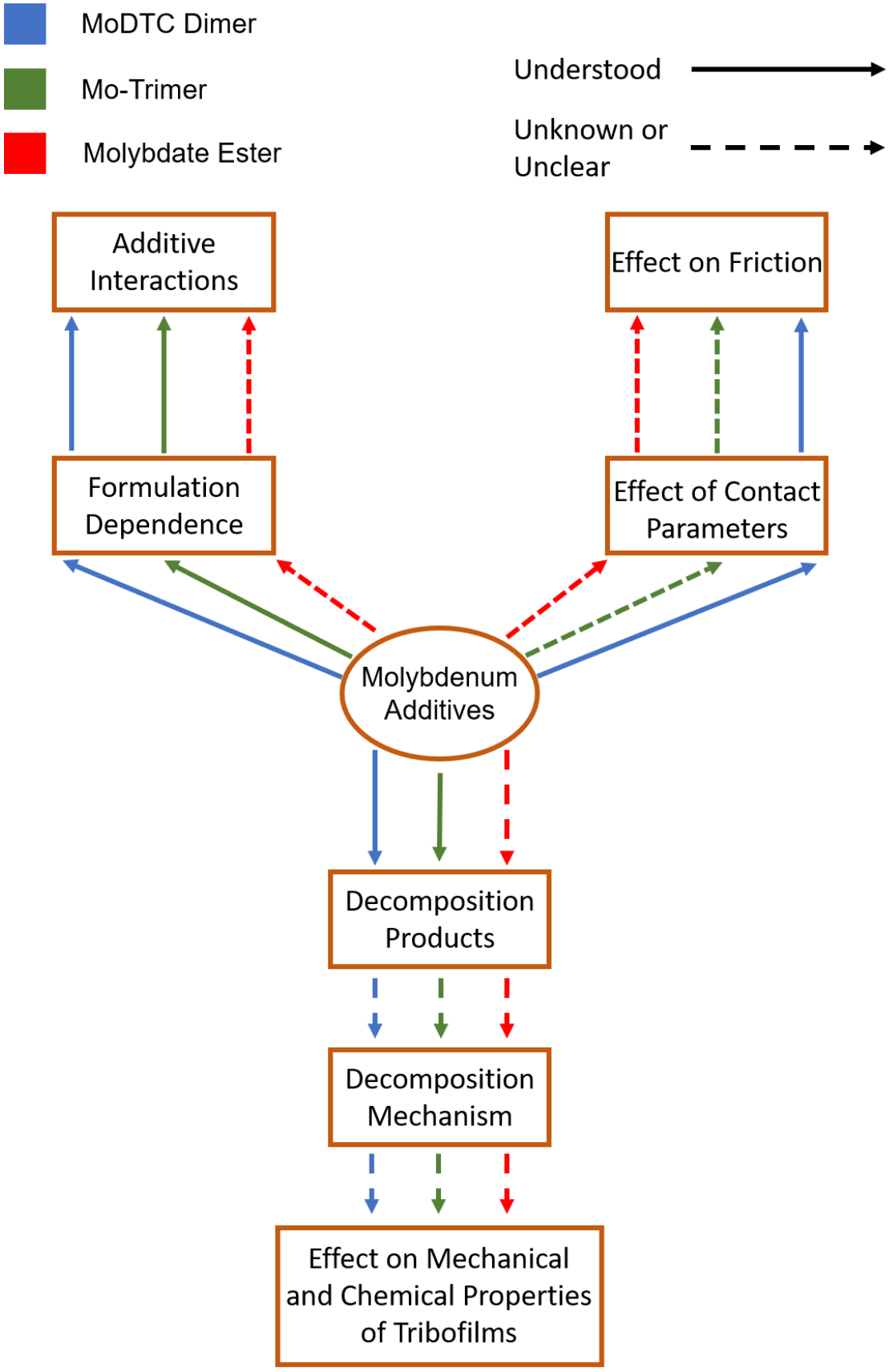


Figure 3.45 Schematic outlining current knowledge gaps regarding the action of molybdenum additives

Chapter 4: Methodology

4.1 Materials and lubricants

4.1.1 Dry chemicals

Pure powders of MoS_2, Fe_3O_4, Fe_2O_3, $(NH_4)_2MoO_4$ and $(NH_4)_2MoS_4$ were sourced from Sigma-Aldrich and Alfa Aesar. These species were used as references for Raman analysis and as model compounds for the tribological investigation of the molybdate ester mechanism.

The diisopropyl ethylamine used for the investigation of the fatty amine booster effect was sourced from Alfa Aesar. The polyamine described as “Triameen” was sourced from AkzoNobel.

4.1.2 Lubricants and additives

All base oils, and any oil systems with the additives ZDDP, MoDTC, Mo-trimer and molybdate ester within them were provided by Infineum UK Ltd. Blending of these oils took place in the Blending Centre of Excellence (BCoE) at Infineum’s UK Milton Hill site. The concentrations of [Mo] and [Zn], [P] and [S] were determined through on-site ICP analysis. Base oils were Group IV PAOs and Group II mineral oils. Unless otherwise stated, the Group IV PAO was used. Oils were provided as monoblend systems, with the additive alone dissolved in base oil. Later studies of selected oils utilised fully-formulated systems with a full additive package including anti-wear additives, dispersants, detergents and viscosity modifiers.

A series of different molybdenum additives and MoDTC structures were used in this work. The oil additive systems described in this study are outlined in Table 5 below:

Table 5: Oil additive systems used in this study

Oil	Molybdenum Species (500 ppm by [Mo])
1	MoDTC Dimer
2	MoDTC Trimer
3	MoDTC Dimer (C8-C14)
4	MoDTC Dimer (branched)
5	Mo ester and amido ester mixture

The MoDTC dimer additives (Oils 1, 3 and 4) have a structure similar to most commercial MoDTCs. The additives differ from one another by the length and coordination nature of their ‘R’ groups.

Table 6: Organic groups of MoDTC dimer additives used in this study

Oil	R-groups
1	2-ethylhexyl
3	Linear C8-C14 length
4	Branched C8-C14 length

The MoDTC trimer additive has a tri-nuclear structure with a mixture of two different core structures shown in Figure 3.30. The ‘R’ groups for the MoDTC trimer are 2-ethylhexyl groups.

The sulfur-free molybdate ester, Oil 5, is supplied as a mixture of a glyceryl ester and an amido ester. The structures of the different molybdenum core structures are presented below in Figure 4.1.

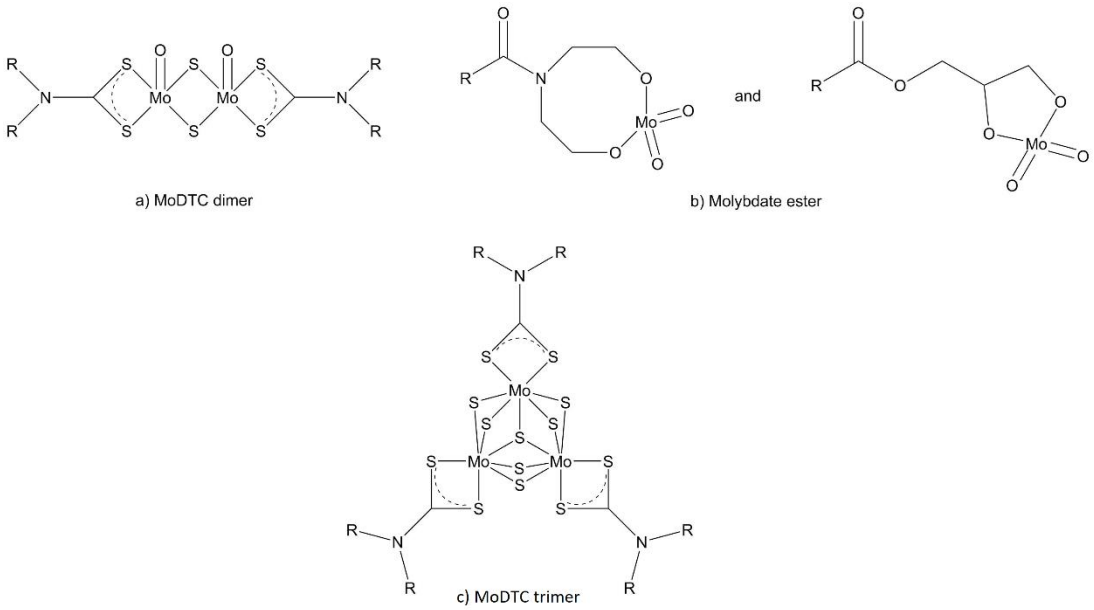


Figure 4.1 Molybdenum additive structures used in this study

a) MoDTC dimer (Oils 1, 3 and 4), b) Molybdate ester (Oil 5), c) MoDTC trimer (Oil 2)

In Chapter 7, the dependence of the molybdate ester upon sulfur supply is investigated. In order to perform these tests, lubricant mixtures of molybdate ester with primary ZDDP were formulated and supplied by Infineum UK with a variety of formulated molybdenum to sulfur ratios (Mo:S). The Mo:S ratio of the formulations was controlled by maintaining a constant molybdenum concentration of 400 ppm and altering the ZDDP concentration. The oils were supplied as both binary mixtures of molybdate ester and ZDDP in base oil, and as fully-formulated systems with dispersants, detergents and viscosity modifiers. The Mo:S ratio oil systems provided are shown in Table 7 below:

Table 7: Mo:S ratio oils used in this study

Mo:S Ratio	Binary Molybdate Ester + ZDDP Oil	Fully-formulated Oil
1:2	✓	✓
1:1.5	✓	✗
1:1	✓	✓
2:1	✓	✓

4.2 Surface Roughness Characterisation

Two types of plate counterfaces were used in this work, TE77 plates for reciprocating sliding tests and discs for unidirectional sliding tests on the High-Speed Pin-on-Disc tribometer. Surface roughnesses (measured as centre-line surface roughness R_a) of these surfaces were determined using a Taylor-Hobson Talysurf stylus profilometer.

The surface roughness of the TE77 plates was determined by calculating the mean surface roughness of four, 7 mm long lines in the linear sliding direction of the expected contact.

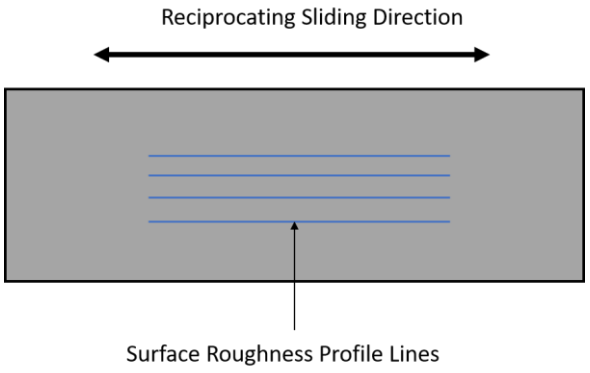


Figure 4.2 Surface roughness profile determination scheme for TE77 plates

For the unidirectional sliding disks, the surface roughness was determined by taking 7 mm straight line profiles along the wear scar at 90 degree intervals similar to the manner for the TE77 plates.

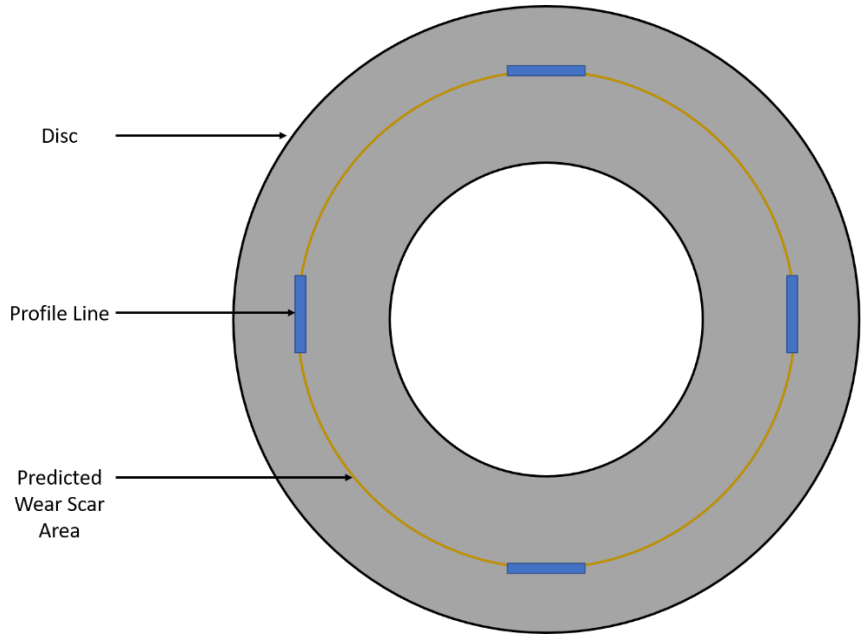


Figure 4.3 Surface roughness profile determination scheme for High-Speed Pin-on-Disc discs

For the TE77 plates, all the surface roughnesses determined from the surface profilometer were very similar between the four lines tested on the testing samples. In the sliding direction, the surface roughness was consistent in the area of the predicted wear scar. As the sliding in this contact occurs in one axis only, surface anisotropy effects will be negligible.

For the pin-on-disc surface profiles, each of the surface roughness profiles displayed comparable R_a values, despite being oriented at 90° intervals. This is suggestive of a lack of anisotropy in the final surface finish. The final processing step for these discs prior to use was manual polishing with sandpaper on a rotating stage. During this process the disc would be subjected to polishing under all orientations with the same piece of sandpaper, so each profiling line was subjected to the same final finishing procedure. From the profilometry, it was concluded that samples prepared in this way did not display surface anisotropy to a degree which would be expected to affect the expected asperity contact conditions to a significant degree.

4.3 TE77 reciprocating pin-on-plate tribometer

4.3.1 Set-up and function of tribometer

In the reciprocating tribological tests performed in this work, both to measure the coefficient of friction of additive systems and to form the tribofilms for chemical analysis, a Cameron-Plint TE77 reciprocating pin-on-plate tribometer was used.

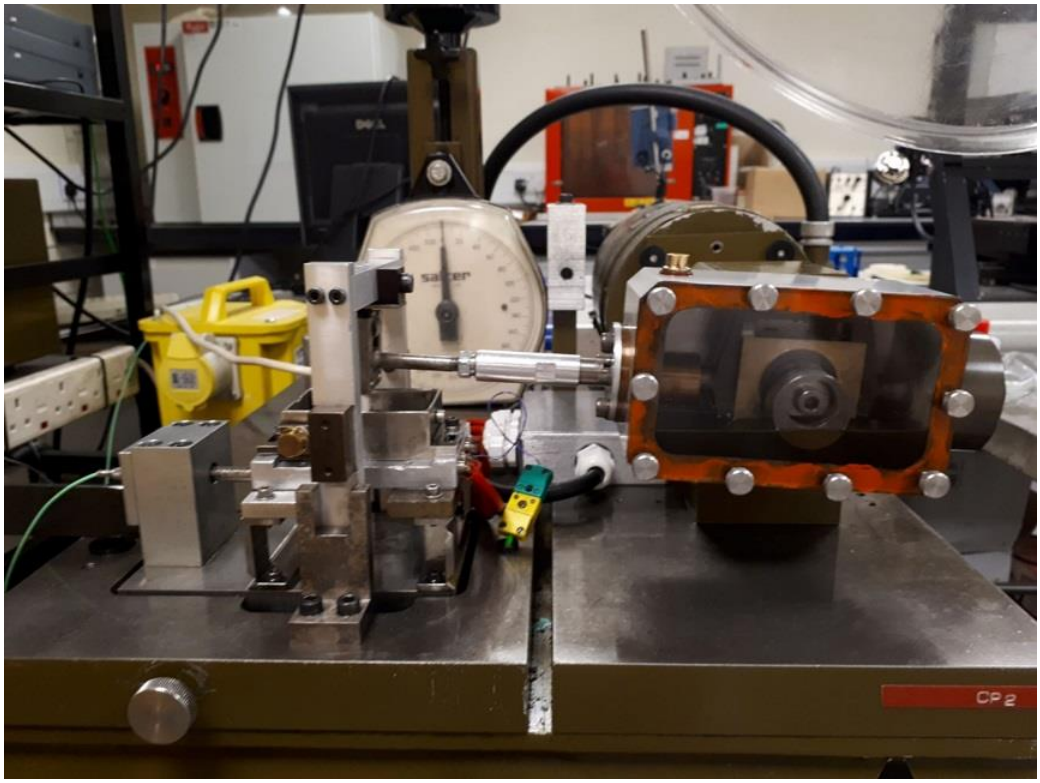


Figure 4.4 TE77 reciprocating pin-on-plate tribometer

The tribometer consists of a fixed oil bath that remains stationary throughout the friction test. The contact surface plate is held within the oil bath, immersed in 10ml of lubricant. The pin is the component in the tribometer which moves. The pin, which is held by a reciprocating arm has a normal load applied by a winding mechanism. The reciprocating motion of the pin arm is provided by a Scotch-Yoke mechanism which allows for alteration of the

desired stroke length. A schematic of the major components is presented in Figure 4.5.

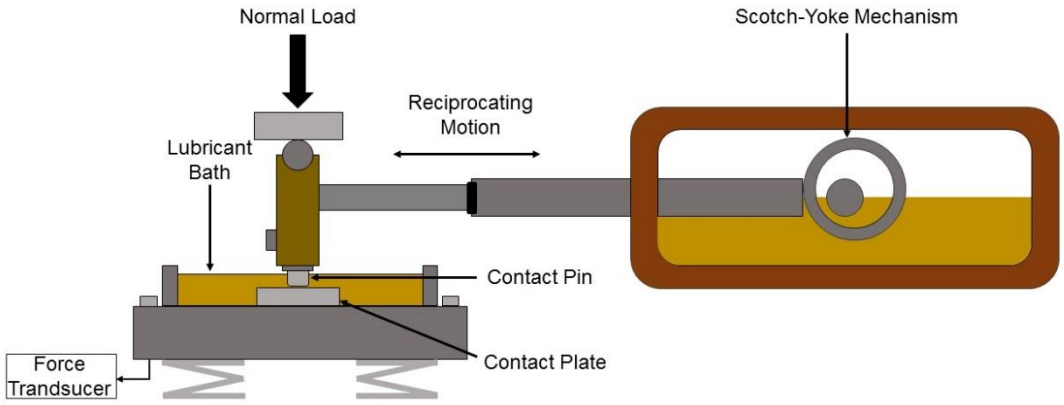


Figure 4.5 TE77 schematic

This tribometer determines friction coefficient by measuring the mechanical force applied to a load cell. The process by which friction coefficients are determined is outlined in Figure 4.6. As the reciprocating arm moves backwards and forwards, the frictional resistance of the oil bath provides a mechanical force that is registered by the load cell. The reciprocating profile of the frictional force creates a square wave voltage in the load cell. The root mean square of the voltage wave amplitude is then taken to find a single value for the load cell voltage. This voltage value is then compared to a calibration curve of the load cell's response to known mechanical forces in order to determine the magnitude of the frictional resistance. Finally, the force value is divided by the known normal load to yield a friction coefficient. The load cell reads a voltage value every millisecond for 1 second to produce a single friction coefficient point. Friction coefficient points are taken at user-defined intervals, depending upon the desired data resolution.

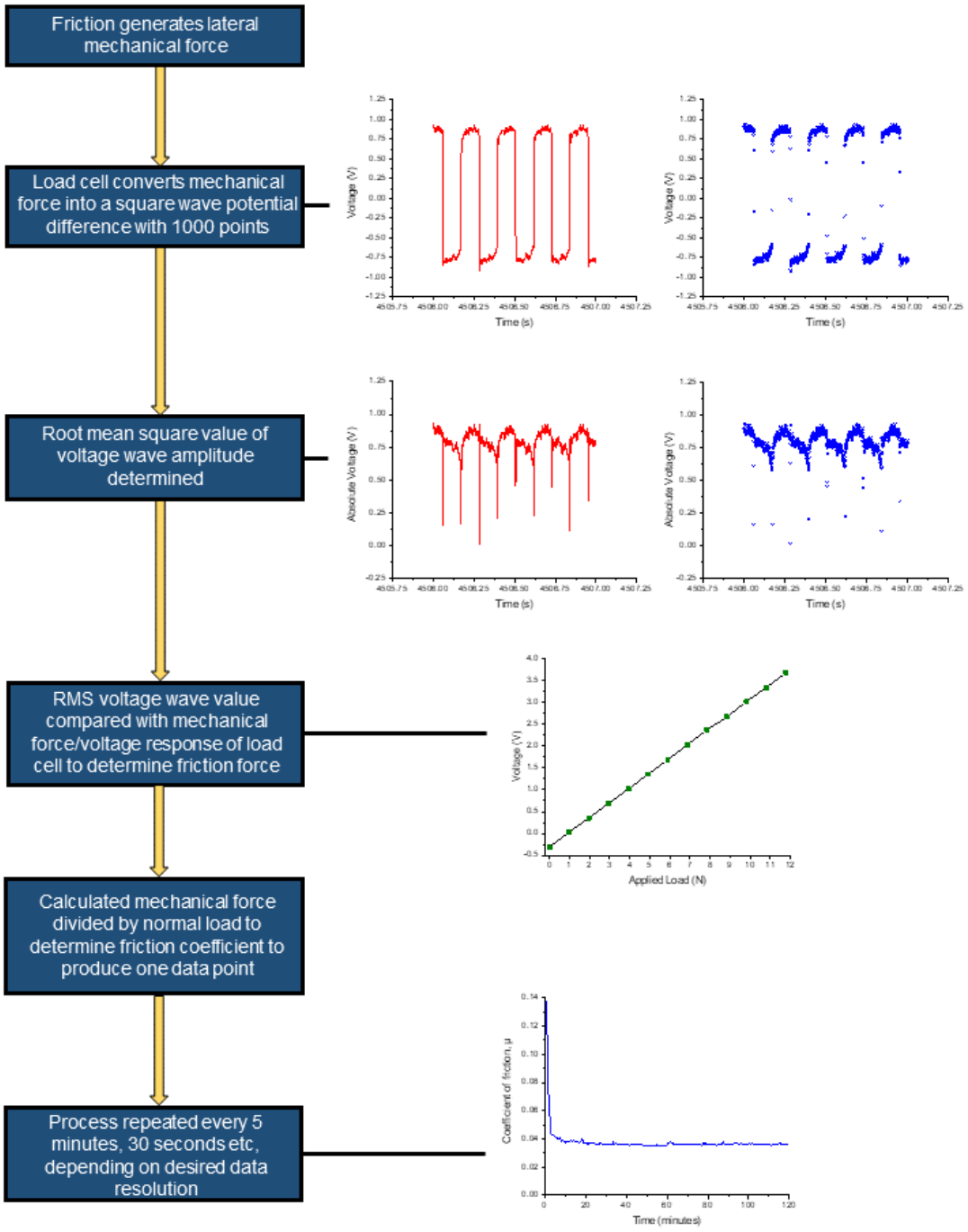


Figure 4.6 TE77 friction coefficient determination flowchart

4.3.2 TE77 tribotesting

Prior to tribotesting, the contacting surfaces, both pin and plate were ultrasonically cleaned in heptane for 10 minutes. The surfaces were then allowed to dry, contact side upwards for 5 minutes before being placed into the dry oil bath. The pin and plate were then aligned and fixed into position. The lubricant was then added to the oil bath and the oil bath was allowed to reach the desired temperature and left to equilibrate for 10 minutes.

Upon completion of the test, the reciprocating contact was stopped and the oil bath allowed to cool to room temperature. The contacting surfaces were then removed from the tribometer before being ultrasonically rinsed in heptane for 10 minutes. The samples were then allowed to air dry on a piece of blue roll for 5 minutes in order to remove residual heptane. TE77 samples were then wrapped in aluminium foil to prevent damage.

The conditions utilised in the study are outlined below:

4.3.2.1. Conditions for additive friction performance characterisation

For initial investigation of the response of the series of molybdenum additive outline in Chapter 5, the oil formulations were subjected to the contact conditions outlined in Table 8. Contact pressures were determined through Hertzian contact analysis using Equation 15 and Equation 16. Lambda Ratio was calculated using the minimum EHD film thickness calculated from the Dowson-Hamrock equation (Equation 6). It is worth noting that in a reciprocating contact there is a constant variation in the sliding speed from stationary at the turning points to a maximum value at the centre of the reciprocating stroke. Due to this variation in speed, the sliding speeds for this tribometer are expressed as a range.

Table 8: TE77 additive performance characterisation 100 N rough plate

Contact Parameter	Value
Contact Materials	AISI 52100 Bearing Steel
Pin Radius of Curvature	100 mm
Stroke Length	7 mm
Lubricant Bath Temperature	40°C
Load	100 N
Maximum Contact Pressure	186 MPa
Mean Contact Pressure	124 MPa
Maximum Lambda Ratio	0.04
Test Duration	2 hours
Sliding Distance	508 m
Reciprocating Frequency	5 Hz
Sliding Speed	0-0.11 ms^{-1}
Plate Surface Roughness (R_a)	0.5 µm
Pin surface roughness (R_a)	50 nm

In addition to the 100 N tests for additive performance characterisation, tests were also performed with a reduced load of 25 N in 5.2.1, keeping all of the other conditions the same as those above in Table 8. This led to an alteration in the contact forces and pressures outlined in Table 9.

Table 9: TE77 additive performance characterisation 25 N rough plate

Contact Parameter	Value
Contact Materials	AISI 52100 Bearing Steel
Pin Radius of Curvature	100 mm
Stroke Length	7 mm
Lubricant Bath Temperature	40°C
Load	100 N
Maximum Contact Pressure	117 MPa
Mean Contact Pressure	78 MPa
Maximum Lambda Ratio	0.05
Test Duration	2 hours
Sliding Distance	508 m
Reciprocating Frequency	5 Hz
Sliding Speed	0-0.11 ms^{-1}
Plate Surface Roughness (R_a)	0.5 µm
Pin surface roughness (R_a)	50 nm

To determine the response of the molybdenum additive structures to smooth surface contact, the TE77 plate surface roughness was reduced from 0.5 µm to 50 nm in 5.2.2. Tests were run under these smooth plate conditions at 25 N, which led to the same Hertzian contact pressures in Table 9 . Alteration of the surface roughness changed the maximum lambda ratio value of the tests. This change in surface ratio led to the contact conditions outlined in Table 10.

Table 10: TE77 additive performance characterisation 25 N smooth plate

Contact Parameter	Value
Contact Materials	AISI 52100 Bearing Steel
Pin Radius of Curvature	100 mm
Stroke Length	7 mm
Lubricant Bath Temperature	40°C
Load	100 N
Maximum Contact Pressure	117 MPa
Mean Contact Pressure	78 MPa
Maximum Lambda Ratio	0.51
Test Duration	2 hours
Sliding Distance	508 m
Reciprocating Frequency	5 Hz
Sliding Speed	0-0.11 ms^{-1}
Plate Surface Roughness (R_a)	50 nm
Pin surface roughness (R_a)	50 nm

In the investigation of lambda ratio for reciprocating contact in smooth plates, the load was increased in smooth plate conditions from 25 N to 300 N. This had the effect of altering the contact parameters in Table 11 to higher pressures and lower lambda ratio.

Table 11: TE77 additive performance characterisation 300 N smooth plate

Contact Parameter	Value
Contact Materials	AISI 52100 Bearing Steel
Pin Radius of Curvature	100 mm
Stroke Length	7 mm
Lubricant Bath Temperature	40°C
Load	100 N
Maximum Contact Pressure	268 MPa
Mean Contact Pressure	178 MPa
Maximum Lambda Ratio	0.04
Test Duration	2 hours
Sliding Distance	508 m
Reciprocating Frequency	5 Hz
Sliding Speed	0-0.11 ms^{-1}
Plate Surface Roughness (R_a)	50 nm
Pin surface roughness (R_a)	50 nm

4.3.2.2. Tribofilm formation for chemical analysis

In Chapter 6, tribofilms are created in reciprocating sliding contact for differing additive structures for chemical analysis. The conditions are outlined below in Table 12.

Table 12 Contact conditions for production of MoS_2 films for chemical analysis

Condition	Value
Load	100 N
Plate Surface Roughness (R_a)	40-60 nm
Frequency	5 Hz
Sliding speed	0-0.11 ms^{-1} (Reciprocating range) 0.07 ms^{-1} (mean)
Nominal contact pressure	343 MPa
Test Duration	2 hours
Lubricant Bath Temperature	100 °C
Pin radius of curvature	40 mm
Sliding Distance	504 m
Maximum Lambda Ratio	0.04

4.3.2.3. Molybdate ester Mo:S ratio testing

Tribotesting and friction performance characterisation of the binary molybdate ester + ZDDP and fully-formulated molybdate ester systems in Chapter 7 were carried out under the conditions outlines below in Table 13. The same conditions were utilised for investigation of the role of amine dispersants.

Table 13: Contact conditions for molybdate ester tribotesting

Condition	Value
Contact Materials	AISI 52100 Bearing Steel
Pin Radius of Curvature	40 mm
Stroke Length	7 mm
Lubricant Bath Temperature	100°C
Load	100 N
Maximum Contact Pressure	343 MPa
Mean Contact Pressure	228 MPa
Test Duration	2 hours
Sliding Distance	508 m
Reciprocating Frequency	5 Hz
Sliding Speed	0-0.11 ms^{-1}
Plate Surface Roughness (R_a)	50 nm and 500 nm
Pin surface roughness (R_a)	50 nm

4.3.2.4. Molybdate mechanism testing

In section 7.5.3 the TE77 is used to investigate the mechanistic steps in friction reduction for the molybdate ester under similar conditions to those outlined in Table 13. The only difference being a shorter test duration of 30 minutes, which corresponds to a test sliding distance of 127 m.

Table 14: Contact conditions for molybdate ester mechanism testing

Condition	Value
Contact Materials	AISI 52100 Bearing Steel
Pin Radius of Curvature	40 mm
Stroke Length	7 mm
Lubricant Bath Temperature	100 and 40°C
Load	100 N
Maximum Contact Pressure	343 MPa
Mean Contact Pressure	228 MPa
Test Duration	30 minutes
Sliding Distance	127 m
Reciprocating Frequency	5 Hz
Sliding Speed	0-0.11 ms^{-1}
Plate Surface Roughness (R_a)	50 nm
Pin surface roughness (R_a)	50 nm

Table 13: Contact conditions for molybdate ester tribotesting

4.4 High speed pin-on-disc tribometer

4.4.1 High speed pin-on-disc setup

For unidirectional tribometric testing, an in-house pin-on-disc tribometer was utilised. In this tribometer a disc rotates under a loaded stationary pin. The plate is held down by brackets so that it does not move, either due to the centrifugal force of the rotating stage or the friction of the pin. The pin is held in place by tension so that it does not roll, ensuring sliding contact. Both the pin and the plate are immersed in a temperature-controlled oil bath. The friction force of the rotating disc presses a steel bar against a load cell, which

measures the frictional force in real time. The measured force is then divided by the applied normal load to provide real-time friction coefficient data.

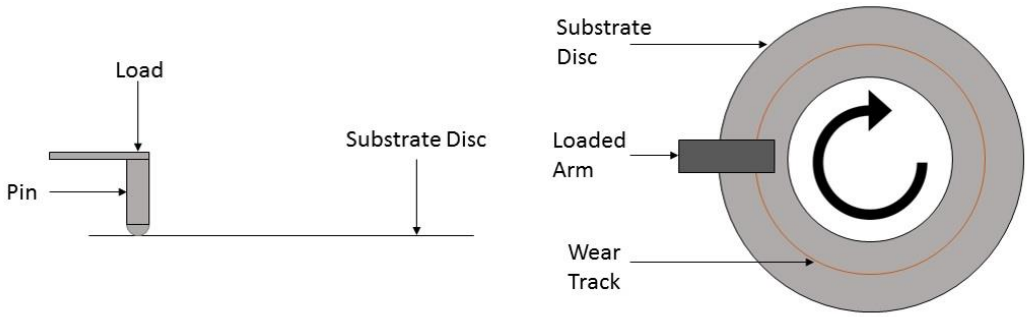


Figure 4.7 High speed pin-on-disc schematic

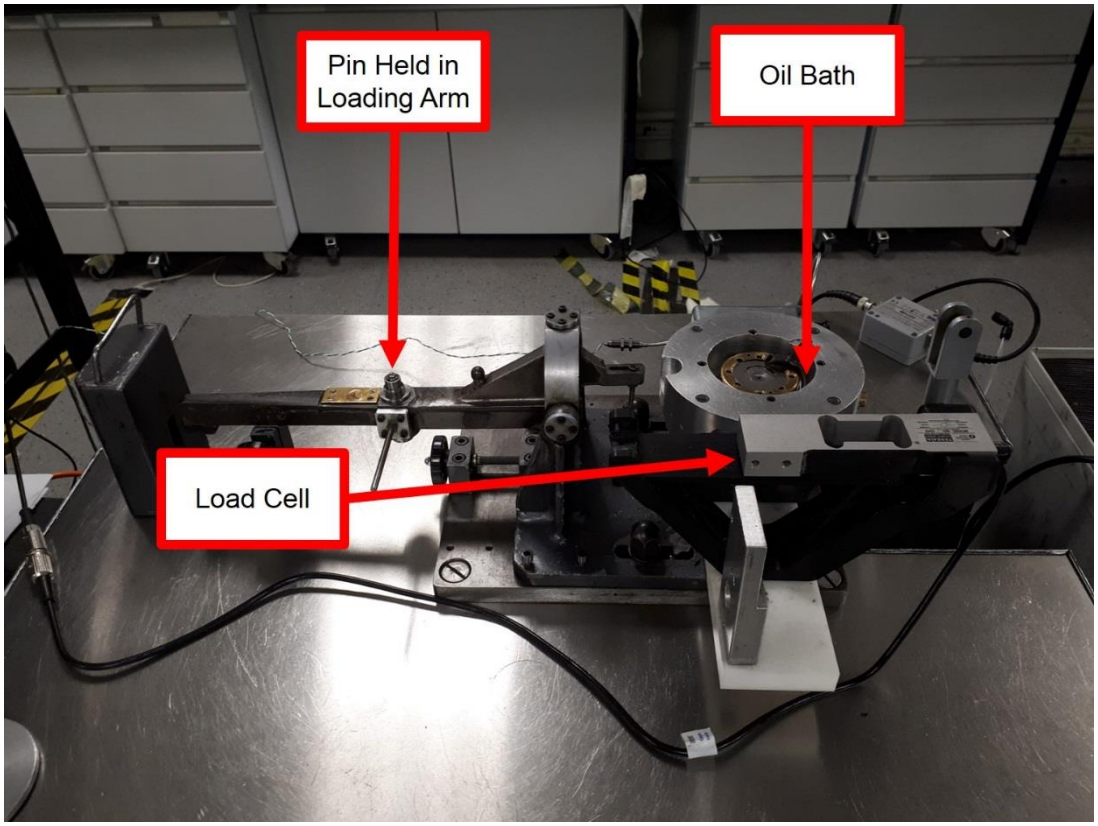


Figure 4.8 High speed pin-on-disc tribometer

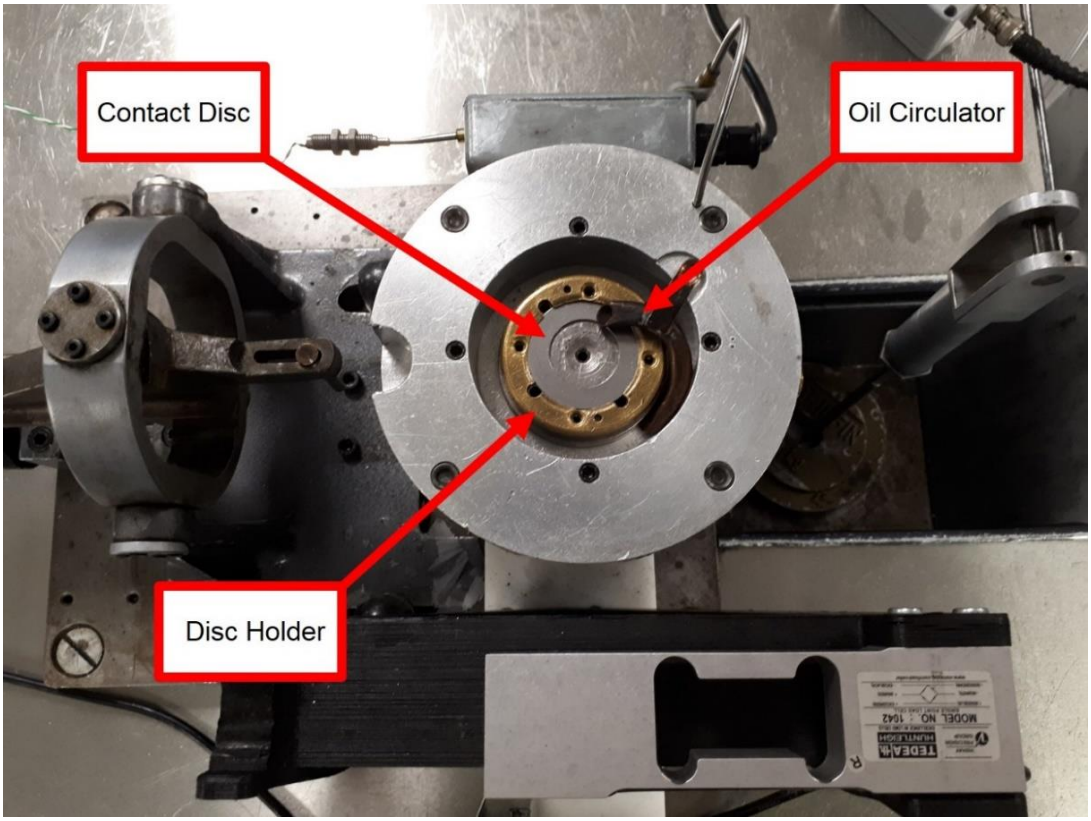


Figure 4.9 High speed pin-on-disc detailed disc view

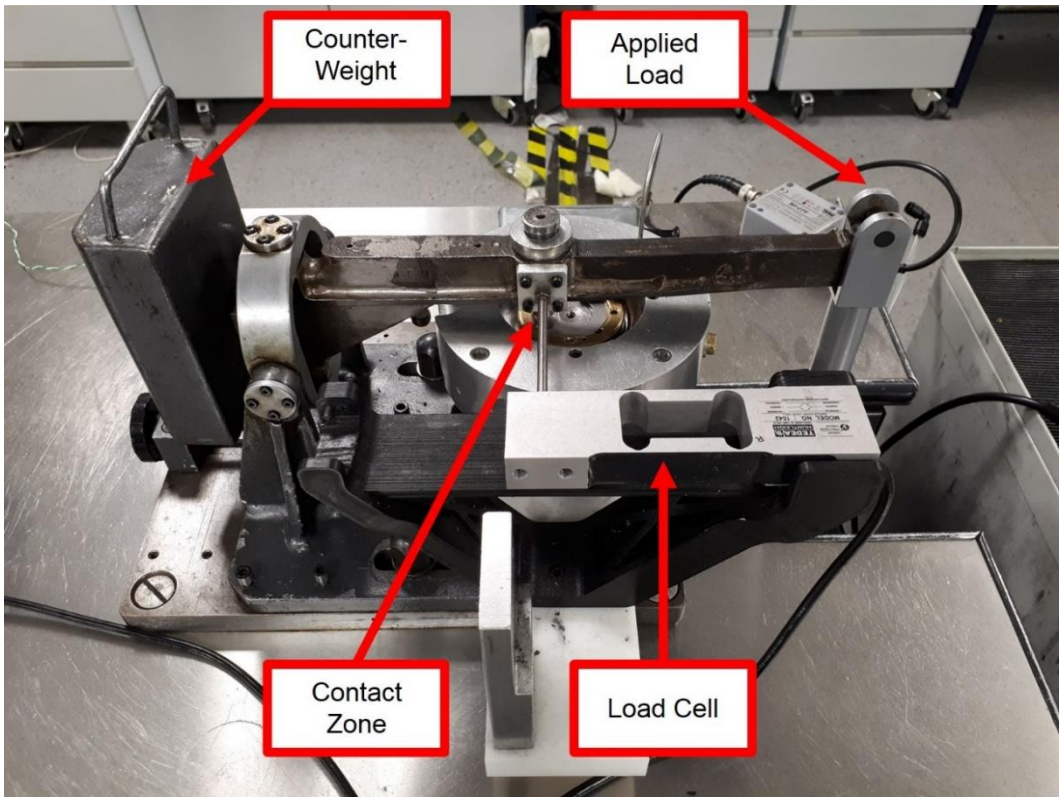


Figure 4.10 High speed pin-on-disc in usage configuration

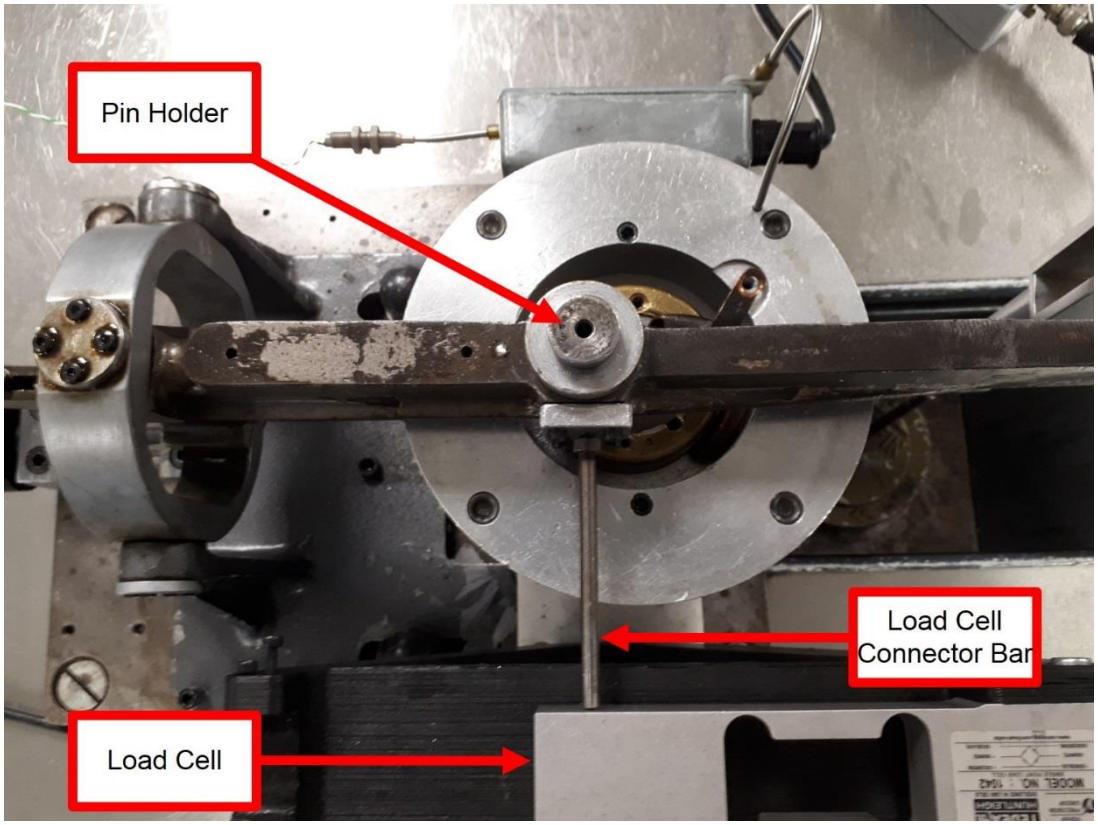


Figure 4.11 High speed pin-on-disc contact zone in usage configuration

4.4.2 High speed pin-on-disc tribotesting

Prior to tribotesting, the contacting surfaces, both pin and disc were ultrasonically cleaned in heptane for 10 minutes. The surfaces were then allowed to dry, contact side upwards for 5 minutes before being placed into the dry oil bath. The pin and disc were then fixed into position. The lubricant was then added to the oil bath and the oil bath was allowed to reach the desired temperature and left to equilibrate for 10 minutes.

Upon completion of the test, the pin was removed from the contact and the rotation of the disc was stopped. The oil bath was allowed to cool to room temperature. The contacting surfaces were then removed from the tribometer before being dried and then ultrasonically rinsed in heptane for 10 minutes. The samples were then allowed to air dry on a piece of blue roll for 5 minutes in order to remove residual heptane. The pin-on-disc samples were then wrapped in aluminium foil to prevent damage.

Tribological testing in the pin-on-disc tribometer was utilised to determine the friction response of the molybdenum additives at a range of temperatures, lambda ratio and sliding speeds. The range of conditions studied with this tribometer is outlined below:

Table 15: High speed pin-on-disc contact conditions

Contact Parameter	Value
Pin Radius of Curvature	3.25 mm
Load	6.5 N
Maximum Hertzian Contact Pressure	734 MPa
Mean Hertzian Contact Pressure	489 MPa
Sliding Speed	0.1649-1.649 ms^{-1}
Lubricant Temperature	40 -120 ˚C
Surface Roughness (R_a)	50-500 nm
Lambda Ratio	0.47-3.2
Contact Materials	AISI 52100 Steel

4.5 Viscosity determination

Viscosity of lubricants was determined with the use of a Malvern Kinexus Pro rotational rheometer. Viscosity profiles were taken at temperature intervals of 10°C between 25°C and 125°C at a shear rate of 1000 s^{-1}. For each viscosity point taken, the rheometer was allowed to reach the desired temperature and to thermally equilibrate with the lubricant for 5 minutes. Then the viscosity would be determined at a shear rate of 1000 s^{-1}.



Figure 4.12 Malvern rotational rheometer

4.6 Raman surface analysis

Raman spectroscopy was used for chemical identification and surface chemical characterisation of the MoS_2 in films formed from the various tribological tests. Raman is an effective technique for rapid chemical identification of crystalline species on a surface.

The instrument used for Raman spectroscopy was a Renishaw inVia Raman microscope with a 488 nm 16 mW laser.



Figure 4.13 Renishaw Raman Microscope

The spectrometer collects Raman scattered photons in a backscattering configuration. In the backscattering collection mode, the Raman scattered photons are collected at 180° reflection to the original laser beam. This allows for collection of Raman scattered light perpendicular to the sample surface [196]. The backscattering configuration of the Raman spectrometer is important as the E_{1g} MoS_2 vibration is nominally forbidden in this collection configuration. A simple outline of the optics of this configuration is presented in Figure 4.14.

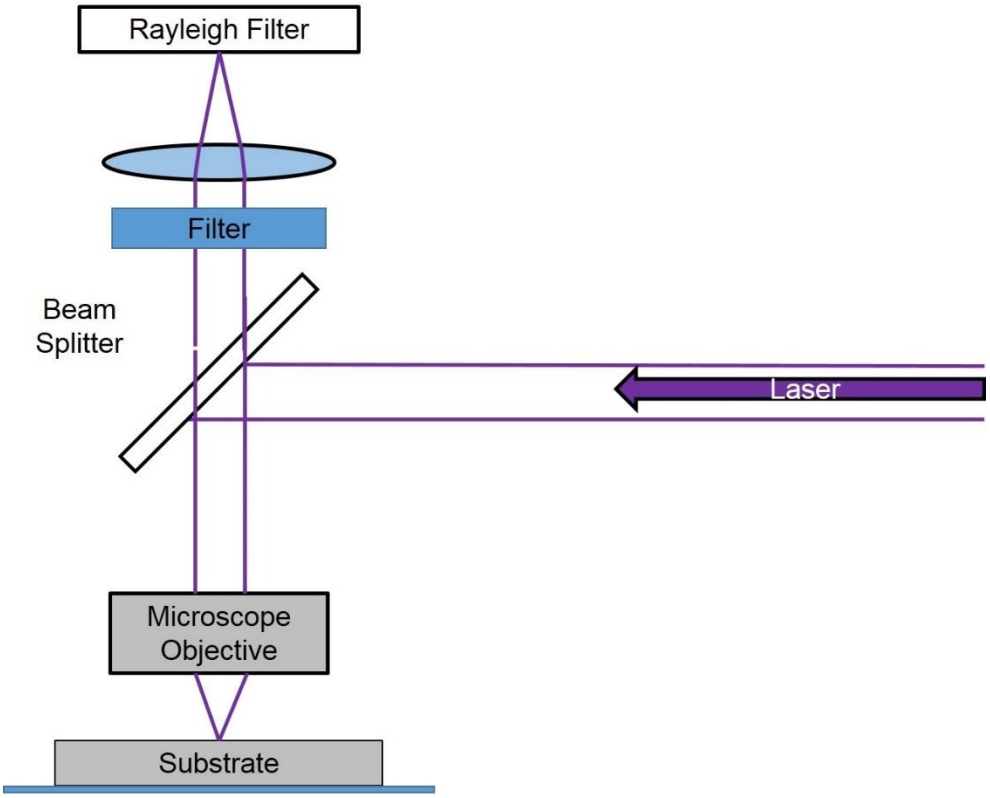


Figure 4.14 Raman backscattering optics configuration

Upon backscattering from the surface, holographic filters separate the scattered light from the light reflected from the laser surface. The light is then passed through a diffraction grating and Raleigh filtered before being focused onto a CCD camera.

It is well known that laser-induced heating of transition metal dichalcogenides can lead to oxidation. It has been found that this process can be prevented by limiting of the Raman laser power and exposure time [99]. In order to combat the effect of oxidation and ensure that any oxide species observed were not being formed by the laser, a standard set of conditions was used throughout the work. These spectral acquisition parameters were used unless otherwise stated:

Table 16: Standard Raman spectral acquisition parameters

Collection Parameter	Value
Accumulations	1
Laser Wavelength	488 nm
Laser Power	1.6 mW
Exposure Time	20 s

Samples which had been ultrasonically cleaned were analysed with the 20x and 50x objective microscope lenses. Two different types of analysis were performed on the contact surfaces studied.

1. Point analysis: A single spectrum is taken in a single spatial point of a sample.

2. Spot lattice mapping: A series of spectra are taken sequentially at different points in space. The Raman stage moves the sample by defined intervals during analysis. From this, a lattice of point spectra can be taken which allows for large areas of the wear scar to be analysed.

Point analysis was performed with the 50x objective lens. Raman mapping of the surfaces was performed using the 20x objective lens to limit focus loss upon changing analysis position. In the mapping spectra of MoS_2-containing samples, a minimum scattering threshold of 200 counts was employed. This minimum count threshold was used to prevent the random noise of the instrument from being interpreted as the presence of low levels of MoS_2. A representative TE77 plate wear scar showing a typical Raman mapping area in the central wear scar is shown in Figure 4.15.

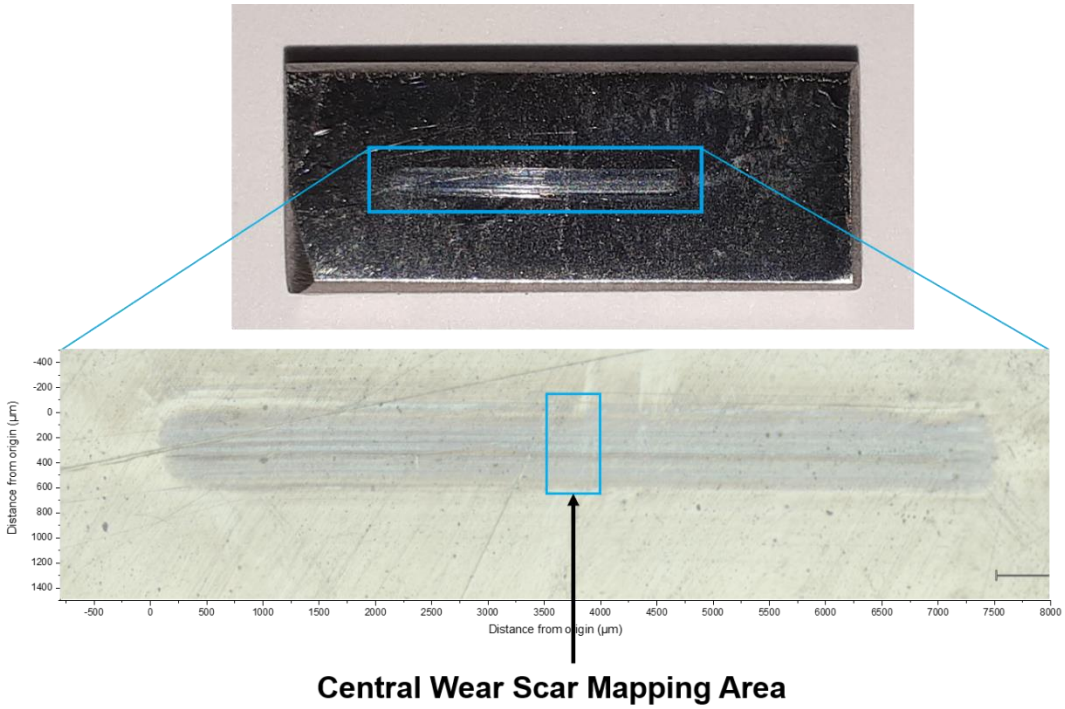


Figure 4.15 TE77 plate wear scar with highlighted Raman mapping area

4.7 X-Ray Photoelectron Spectroscopy (XPS)

X-Ray Photoelectron Spectroscopy provides information on the chemical composition of the surface of a solid sample. The technique functions by firing a beam of X-rays at constant energy onto a sample surface, this X-ray irradiation leads to release of electrons from core shells of surface atoms. The kinetic energy of the ejected electrons is dependent on the electron shell from which they originate, as such they can be used to determine the chemistry of the sample surface. Each element has multiple XPS peaks, for their s, p, d and f shells. In addition to elemental identification, the electron kinetic energy is also partially dependent on the chemical environment of atoms in the sample, so atoms bonded to highly electronegative atoms will have a greater binding energy and so will release electrons at a lower kinetic energy. In metallic systems this leads to lower oxidation states having lower binding energies, and therefore releasing higher kinetic energy electrons. Upon release of electrons from the surface, their kinetic energy is determined by passing through an analyser that discriminates electrons on their kinetic energy. The counts per second of electrons in the analyser is plotted against

the binding energy to produce an X-ray Photoelectron Spectrograph. Due to the small mean-free path of ejected photoelectrons in a solid, only those ejected from very near the surface (ca. 30 nm) are able to escape and enter the analyser. This means that only the topmost surface layers of a sample can be characterised by XPS.

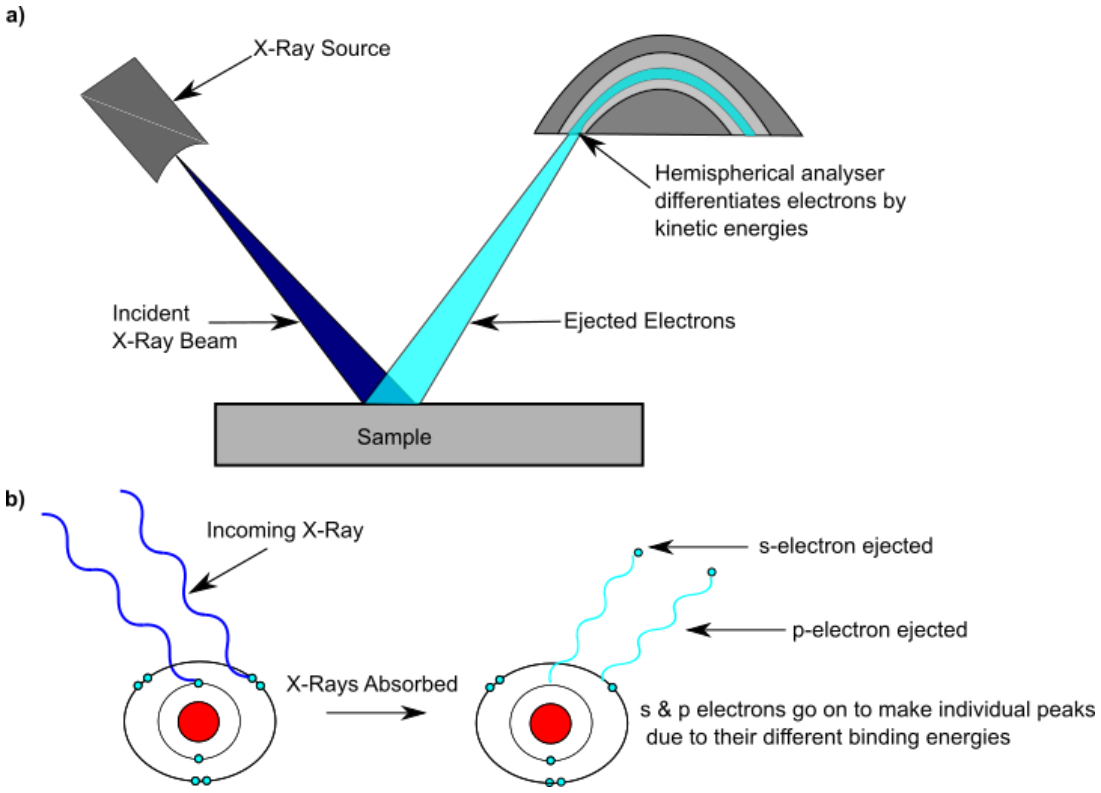


Figure 4.16 a) X-ray photoelectron spectrometer main component schematic. b) X-ray absorption leading to ejection of photoelectrons

X-Ray photoelectron spectroscopy was carried out upon TE77 sample plates that had been dried and ultrasonically rinsed in heptane remove any supernatant oil on the surface. Samples were studied by XPS to determine the chemical compositions on the tribofilms formed from the various molybdenum additives.

X-Ray photoelectron spectroscopy was performed using a UHV XPS module at the University of Leeds Versatile X-ray Source Facility (VXSF). Spectra were taken using a monochromatic Al Kα 1486.6 eV source.

The wear scars of TE77 plates were subjected to XPS in spot analysis mode. The spot size of the XPS instrument was a circle of 300 µm diameter. Survey spectra were taken at 50 eV pass energy and high-resolution spectra of specific elemental regions were taken at 30 eV pass energy. An electron gun was used to compensate for surface charging caused by the emission of surface electrons. Spectra were calibrated to the C1s peak at 285.0 eV to correct for any charging effects and fit using a Gaussian-Lorentzian peak model on a Shirley background in the CasaXPS peak-fitting software package. A Shirley background was chosen over a linear background in order to not omit the some of the peak areas in the spectra with a change in background signal intensity across the area of interest. A Tougaard background was also found not to be appropriate due to the number of expected peak overlaps in the Mo 3d and S 2p regions. A Shirley background was selected as it is sufficiently accurate to maintain appropriate peak areas, whilst not over-complicating the analysis procedure.

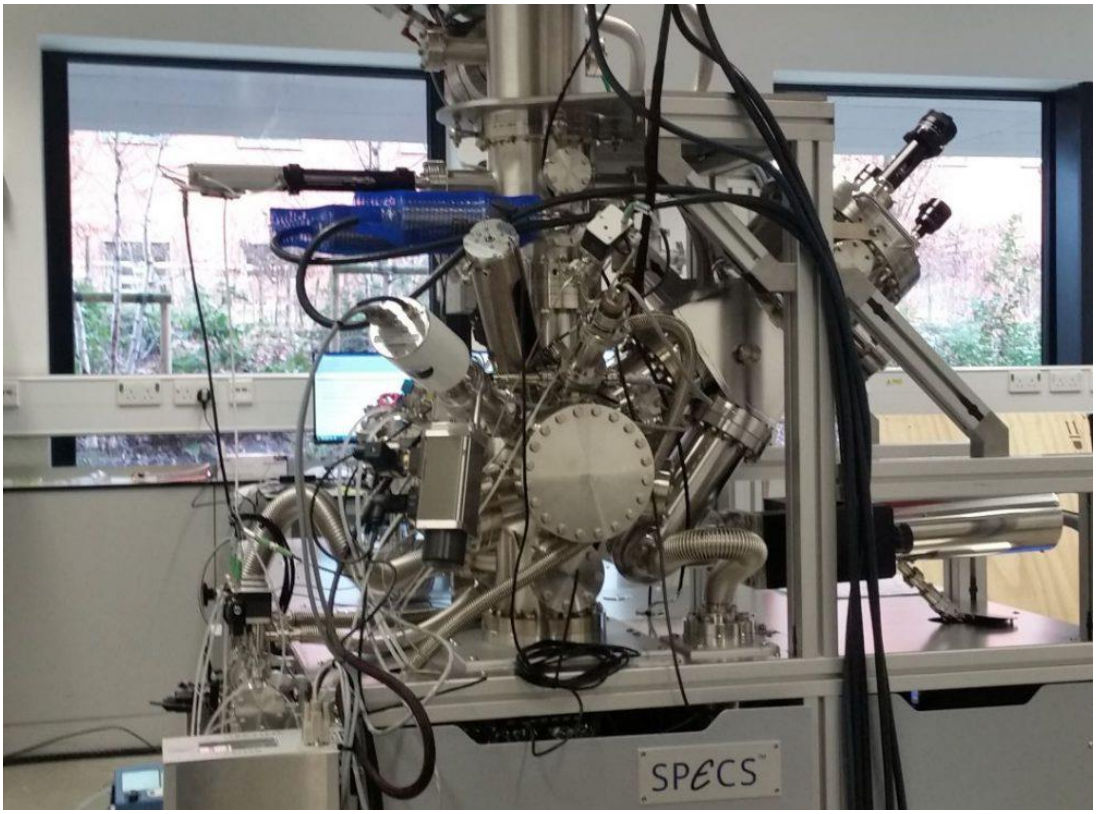


Figure 4.17 UHV XPS Spectrometer

4.8 Scanning electron microscopy (SEM-EDX)

Scanning electron microscopy in tandem with energy dispersive X-ray Spectroscopy is utilised to study surfaces at optical resolution greater than can be provided with light microscopy, and to identify the elements which compose the sample under study. In a SEM, a thermally produced electron beam is focused on a small spot, nanometres in size. This spot is then scanned over a sample to collect an image. The electron beam knocks out secondary electrons from the sample which are used to construct an image of the sample by collecting the secondary electrons in a detector. The number of secondary electrons detected for a given raster point determines the brightness of the image at that point.

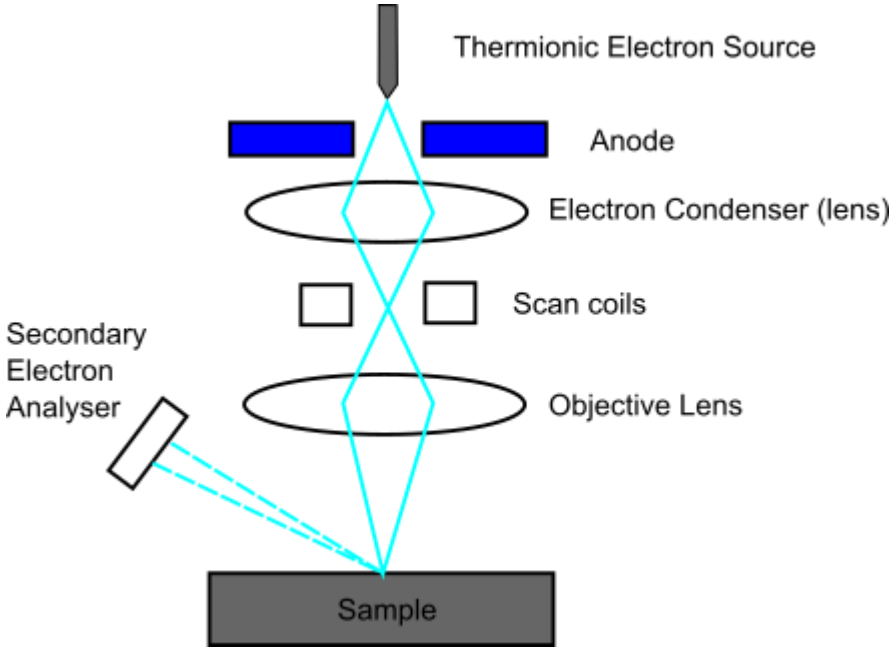


Figure 4.18 SEM Principle of operation

SEM-EDX was performed to optically and chemically characterise a molybdate precipitate using a Carl Zeiss EVO MA15 microscope with an acceleration voltage of 5 kV.

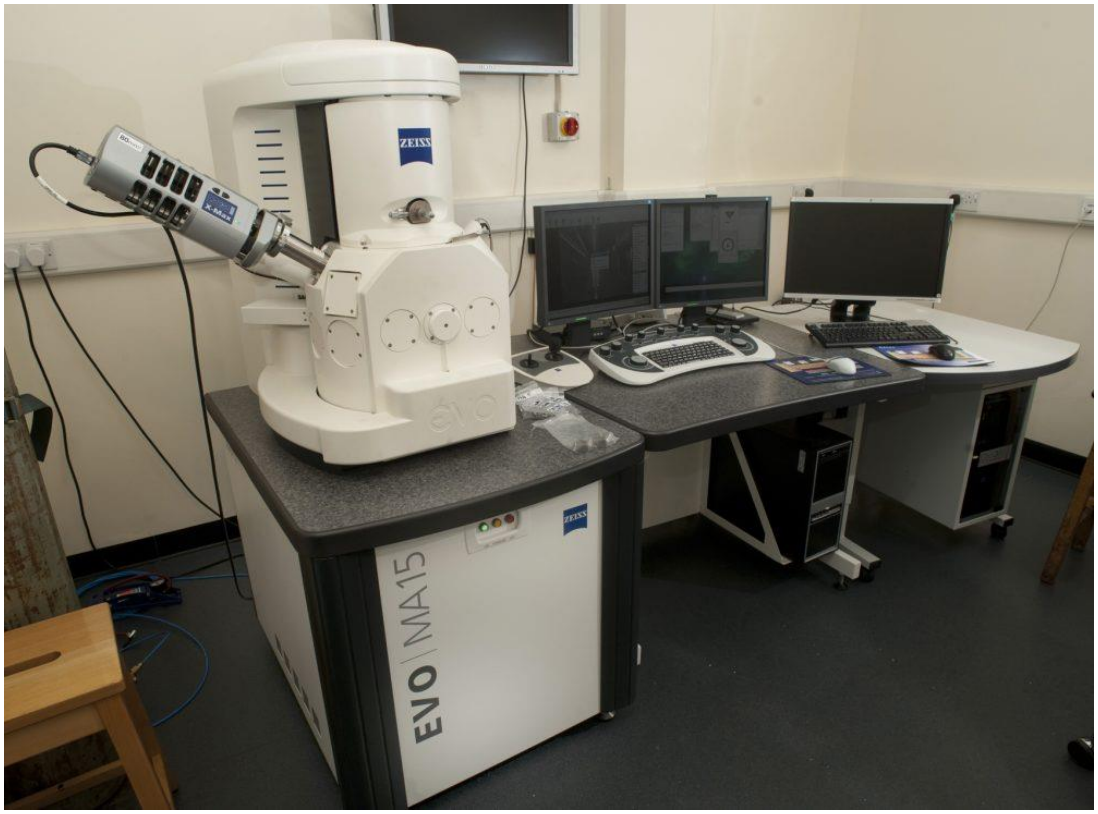


Figure 4.19 EVO MA15 scanning electron microscope

4.9 X-ray diffraction (XRD)

X-ray Diffraction (XRD) is used to determine the crystallinity and identity of crystalline materials. The technique works by measuring the diffraction of a beam of X-rays shone onto a crystal. The diffraction of X-rays detected depends upon the spacings in a material's crystal lattice structure. Common reflections observe Bragg's Law:

$$n\lambda = 2d \sin\theta$$

Equation 20 Bragg's Law

Where λ is the wavelength of the incoming X-ray beam, d is the spacing between diffracting planes of the crystal and θ is the angle of the incoming X-rays relative to the sample surface. By altering the incoming value of θ, the spacings in the crystal can be determined and used to identify the sample crystal group.

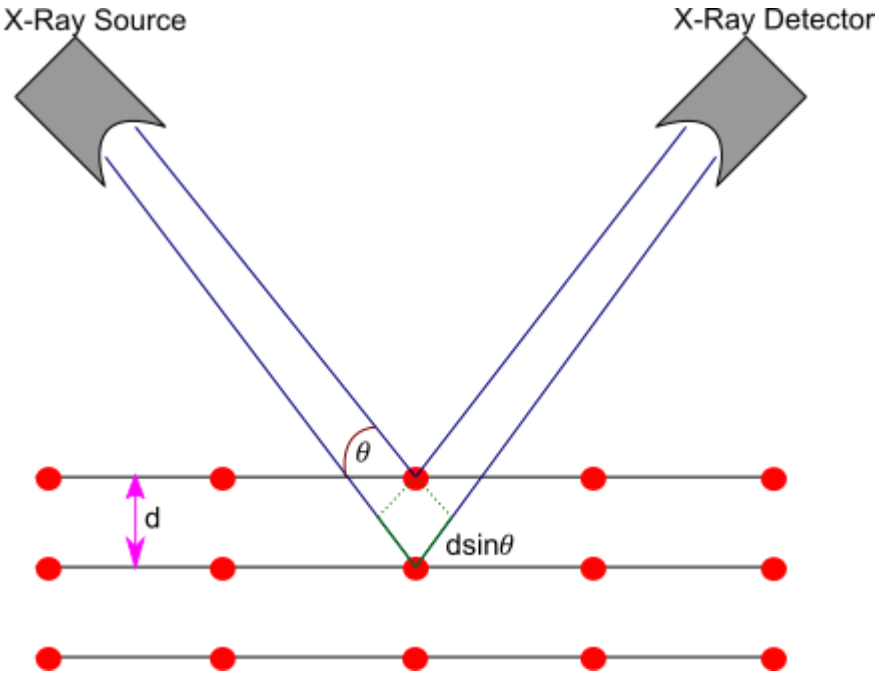


Figure 4.20 X-ray diffraction principle of operation

XRD was utilised to determine the crystallinity and chemical nature of a molybdate precipitate. X-ray diffraction was performed with a Bruker D8 powder diffractometer. Samples were prepared by drying in an oven overnight at 100 °C to drive off excess water of crystallisation. Then the samples were allowed to cool before transfer to the X-ray diffraction sample holder. The powder was compressed with a pestle and flattened with a glass slide to ensure a flat diffraction surface. X-ray scans were performed at 5° min^{-1} for 2θ values between 20 and 70°.



Figure 4.21 Bruker D8 X-ray diffractometer [197]

4.10 Transmission electron microscopy (TEM)

Cross sections of tribofilms were studied using Focussed ion beam transmission electron microscopy (FIB-TEM). Areas of highest MoS_2 Raman scattering intensity on the TE77 plate wear scars were chosen for FIB-TEM. Prior to FIB milling, the tribofilm surfaces were covered with a 100 nm thick platinum deposited film. This protective film prevents ion-induced crystallisation of the MoS_2 and ZDDP components of the tribofilms[198]. After

this, a 2 µm thick platinum layer was deposited on the surface to prevent damage to the cross section by the bombarding gallium ions.

Using a FEI Helios G4 CX FIB with gallium ion bombardment, tribofilm cross-sections of 5 µm width were cut. The Gallium ions bombarding the surface wear away at the substrate. By careful selection of impact angle and energy, sections can be cut from the surface and removed from it. The cut sections were then lifted out of the substrate surface and mounted on a TEM sample holder so that the FIB-section could be viewed as a function of tribofilm depth. The process of FIB milling and mounting is outlined in the figure below:

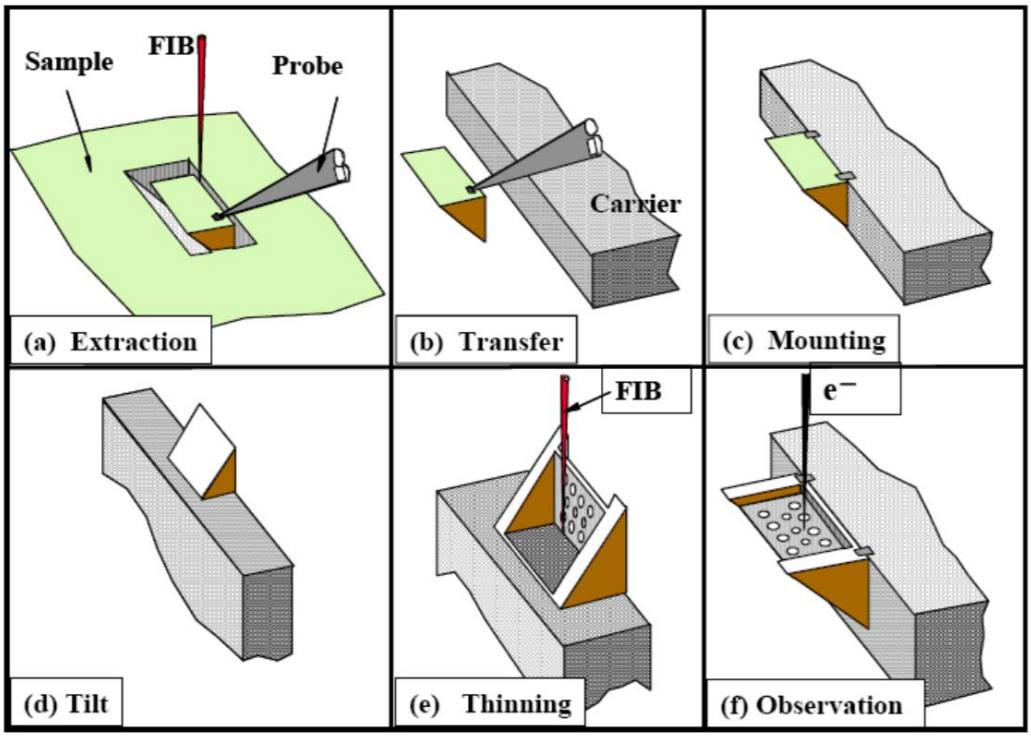


Figure 4.22 FIB milling method to prepare cross-sections of specific sites for TEM analysis[199]



Figure 4.23 FEI Helios G4 CX DualBeam FIB-SEM used to prepare tribofilm cross-sections

Transmission Electron Microscopy (TEM) was performed upon the FIB cross sections to view the tribofilms as a function of depth. The chemical composition of the film was studied with Energy-dispersive X-ray spectroscopy (EDX). A Thermofisher Titan Themis^3 was operated at 300 kV to acquire the TEM data. The bright field TEM images were collected on a Gatan OneView 16 Megapixel CMOS digital camera. The elemental maps were collected with a STEM probe current of 40 pA using Super-X EDX system with windowless 4-detector design and 0.7 srad solid angle.

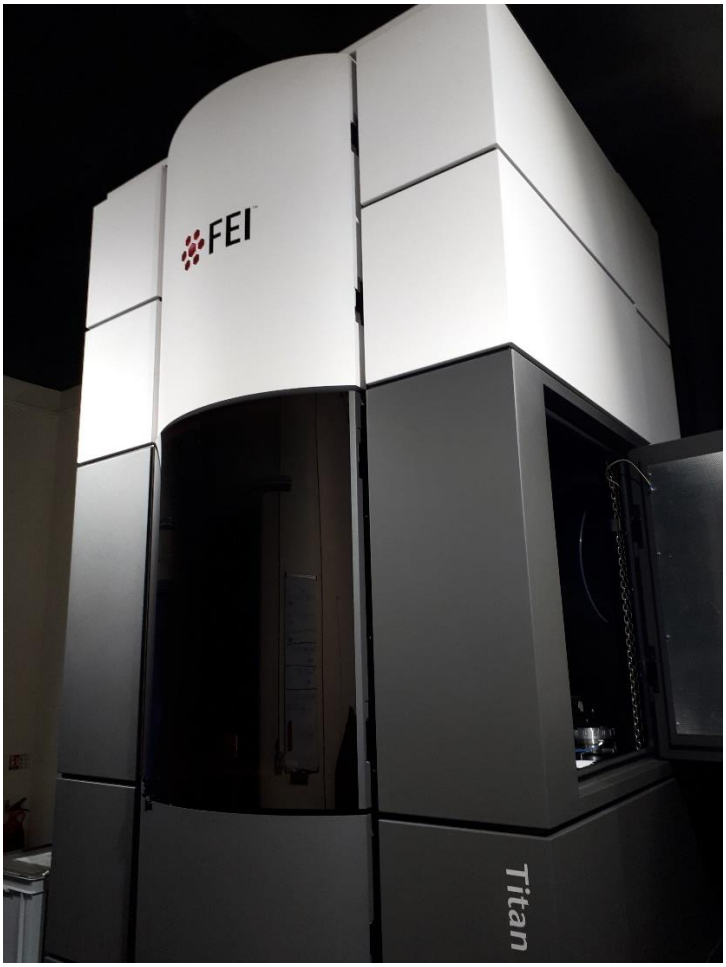


Figure 4.24 FEI Titan3 TEM used to analyse tribofilm cross-sections

4.11 Thermogravimetric analysis (TGA) of $(NH_4)_2MoS_4$

Thermogravimetric analysis was used to prepare a sample of amorphous MoS_3 while following the progress of the reaction through mass loss. This sample was prepared from the thermal decomposition of ammonium tetrathiomolybdate $(NH_4)_2MoS_4$.

Thermogravimetric analysis of ammonium tetrathiomolybdate $(NH_4)_2MoS_4$ was performed using a Shimadzu TGA50. Decomposition was performed under a nitrogen atmosphere from an initial temperature of 30°C at a temperature ramp rate of 10°Cmin^{-1}, followed by a 20 minute isotherm at 240 °C. After the heating cycle was completed, the sample was allowed to

cool to room temperature under a nitrogen atmosphere before being removed from the TGA.



Figure 4.25 Shimadzu TGA50 Thermogravimetric analyser[200]

4.12 Optical microscopy

Detailed images and preliminary wear analysis of the TE77 pins was performed using optical microscopy. In this study microscopy was performed using a Leica DM6000 optical microscope with 5x, 10x, and 20x magnification lenses. All samples were dried and ultrasonically rinsed in heptane for 10 minutes prior to viewing with optical microscopy. Wear scar diameters on the TE77 pins were determined through use of the Leica software distance-measuring tool under the 10x magnification lens.



Figure 4.26 Leica DM6000 optical microscope[201]

Chapter 5: Activation Of Molybdenum-Containing Additive Friction Reduction

5.1 Introduction

It is well established that friction reduction from molybdenum additives results from the formation of molybdenum disulfide. If new additives are to be developed, a better understanding of the relationship between chemical structure and the properties of the additives is required. In order to understand the friction-reducing ability of different additive structures, a systematic investigation of their responses to various contact conditions is required.

In this chapter, monoblend oils of five different molybdenum additives are subjected to a range of contact conditions in unidirectional and reciprocating sliding contact. The overall friction-reducing performance of the additives in contact is examined in terms of final friction coefficient and the severity of the contact conditions required to observe a reduction in friction, i.e. how difficult it is to “activate” friction reduction for each of the chemical structures. The friction responses of the oils are investigated as a function of a variety of contact parameters to produce trends wherein the friction responses of the additives can be predicted. The resulting tribofilms are then chemically characterised using Raman spectroscopy to confirm MoS_2 formation in relation to their friction performance.

5.2 Response of molybdenum additives to contact conditions

5.2.1 Effect of load

Each of the provided oils was first tested in the TE77 reciprocating pin-on-plate tribometer under a load of 100 N and 25 N, leading to maximum Hertzian contact pressures of 186 MPa and 117 MPa respectively. Pins with hemispherical heads of 100 mm radii of curvature were used. The low lubricant bath temperature of 40 °C was used to provide minimal thermal energy in the contact whilst maintaining a reliable constant temperature that would not be affected by fluctuations of temperature in the laboratory

environment. The low sliding speed range (0-0.11 ms^{-1}) provided only a small amount of bulk shear in the contact. Plates of R_a = 0.5 µm were used. The load was then reduced from the initial load of 100 N to 25 N to yield the following contact pressures and lambda ratio values:

Table 17: Contact conditions for changing load of TE77

Load	100 N	25 N
Maximum Lambda Ratio	0.04	0.05
Hertzian Contact area	0.320 mm^2	0.127 mm^2
Maximum contact pressure	178 MPa	117 MPa
Mean contact pressure	112 MPa	78 MPa

The complete contact conditions can be found in Table 8. The friction performance of the additives is characterised in terms of the induction period (the time between the start of the test and the beginning of a drop in friction coefficient), the final steady-state coefficient of the test and the time taken between the onset of friction reduction and the final friction coefficient. Figure 5.1 outlines the friction behaviour of each of the molybdenum additives studied. For each friction profile in this thesis a minimum of 4 repeats were performed, of which two representative friction traces are presented in each graph.

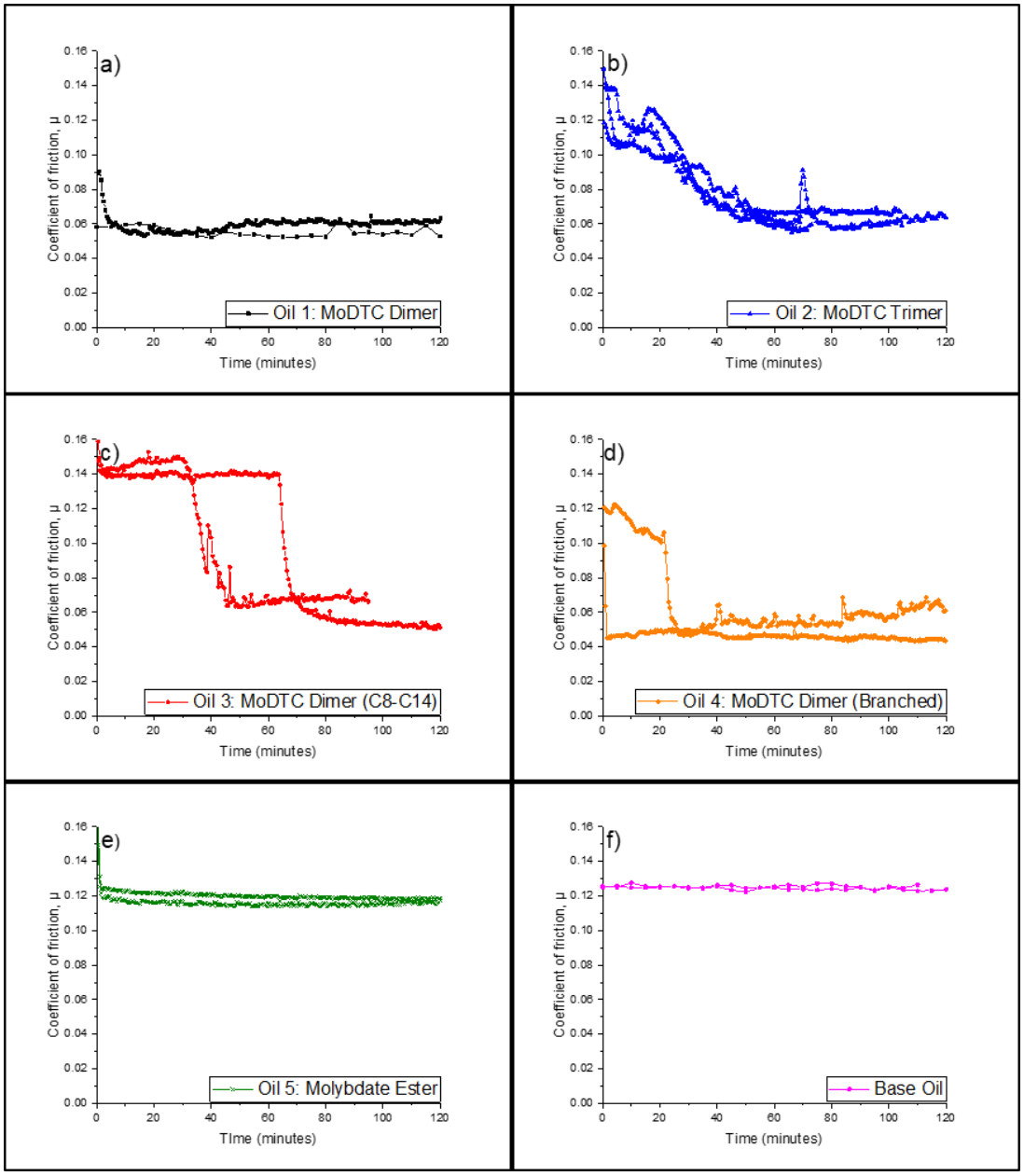


Figure 5.1 Individual friction profiles of molybdenum additives at 100 N

a) Oil 1: MoDTC Dimer, b) Oil 2: MoDTC Trimer, c) MoDTC Dimer (C8-C14), d) MoDTC Dimer (Branched), e) Oil 5: Molybdate Ester, f) Base Oil

Each of the sulfur-containing oils displayed a reduction in friction relative to base oil after an induction time of varying length. This friction behaviour is indicative of the formation of MoS_2 from all of these oils, despite their varying structures. Differences in the friction profiles of the additives are observed however, three of which are particularly distinct.

The MoDTC trimer shows an instant drop in friction as the dimeric structures do, but the reduction in friction occurs over a much longer timescale

than is observed for all of the dimeric species. In addition, this additive shows a slight increase in friction after its initial drop before friction then falls further.

The molybdate ester additive shows no friction reduction in its monoblend formulation relative to base oil, likely due to the lack of sulfur as no MoS_2 can be formed, but this is also indicative of a lack of formation of any lubricious oxides.

The C8-C14 dimer (Oil 3) displayed a friction profile like those of MoDTC dimers generally, with a high friction induction period followed by a rapid friction drop. However, the extent of the induction period was variable and much longer than was observed for the other additives.

The differences in friction performance between the sulfur-containing and sulfur-free systems can also be seen in the raw load cell data of the TE77 square waves. The amplitude of these square waves indicates the frictional force recorded by the load cell as the contact reciprocates. Their frequency depends on the contact reciprocating frequency. In systems where a friction reduction was observed, there is a smoothing of the central part of the square wave stroke that is not observed in the sulfur-free systems. This is indicative of a more consistent stroke in the systems where MoS_2 was formed, with less stick-slip behaviour than in the sulfur-free systems [202].

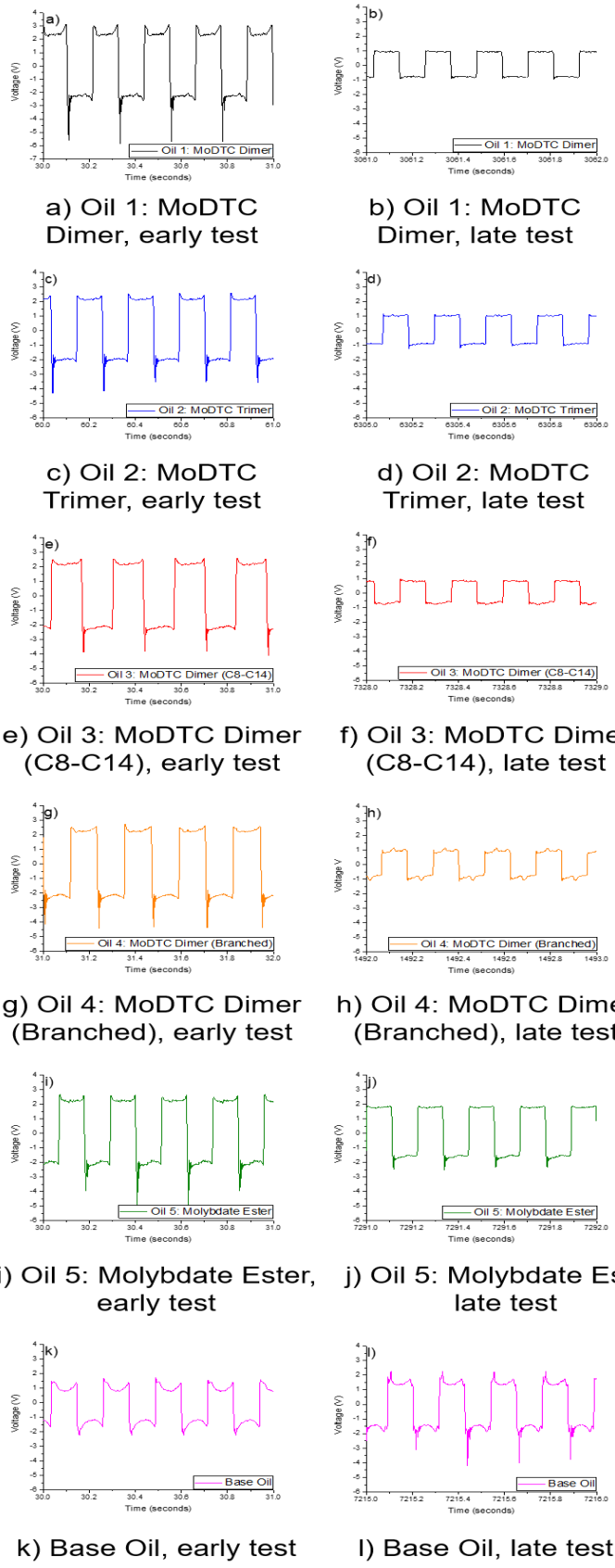


Figure 5.2 TE77 load cell waveforms in late and early stages of tribological testing for 100 N tests

Upon reduction of the applied load and associated contact pressure to 25 N conditions found in Table 9, the observed friction profiles remained similar to those found for the 100 N tests.

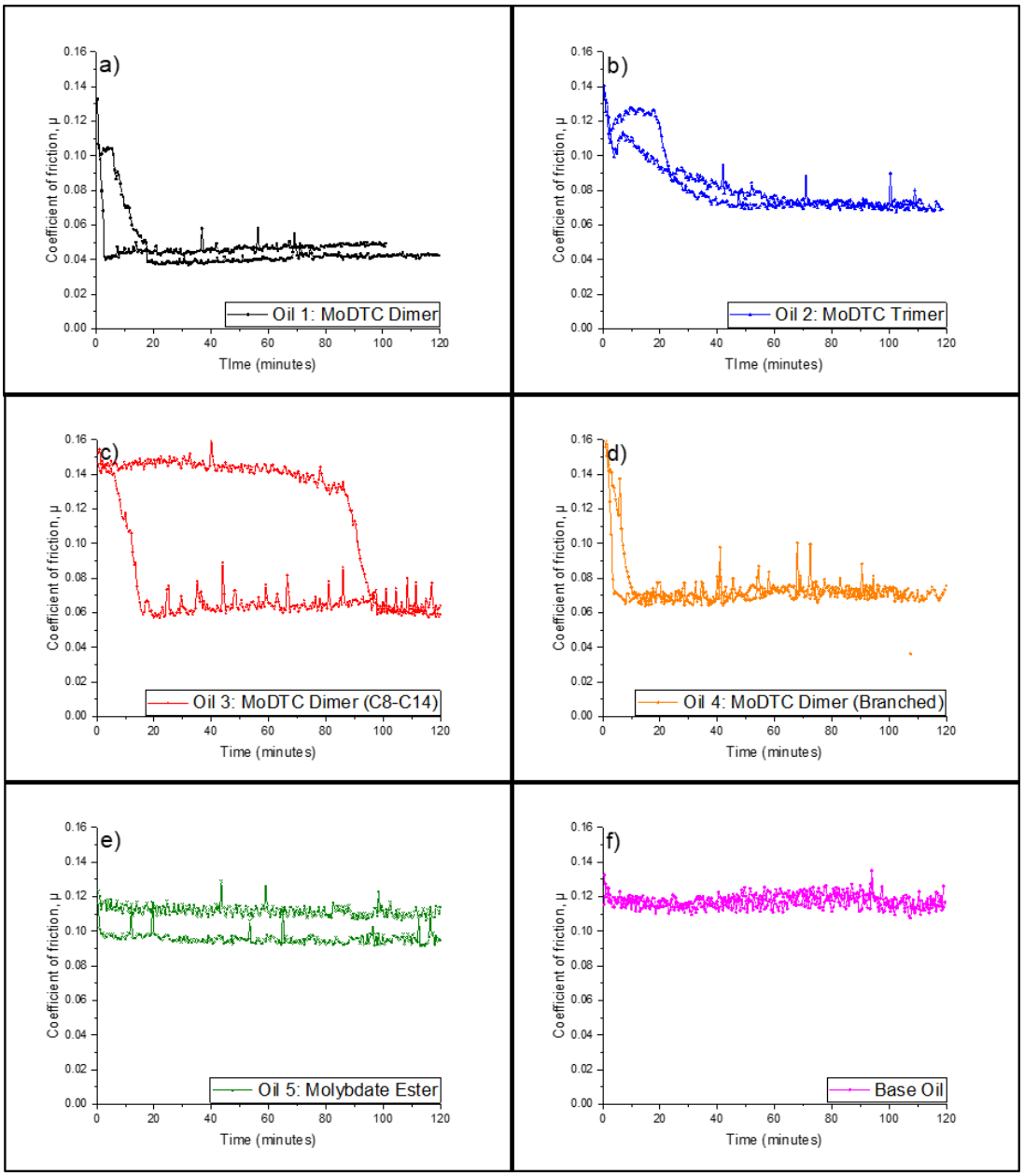


Figure 5.3 Individual friction profiles of molybdenum additives at 25 N

a) Oil 1: MoDTC Dimer, b) Oil 2: MoDTC Trimer, c) MoDTC Dimer (C8-C14), d) MoDTC Dimer (Branched), e) Oil 5: Molybdate Ester, f) Base Oil

Under 25 N load the friction profiles of the additives were much the same as at 100 N. Overall, the friction coefficient was slightly higher for all of the sulfur-containing additive systems than at 100 N. The Oil 1 MoDTC dimer displayed the lowest friction coefficient compared to the other additives. The other MoDTC dimeric structures held a higher final friction coefficient of μ = 0.07, compared to the lower value of the Oil 1 dimer at μ = 0.05.

No significant friction reduction was observed for the molybdate ester at either load value. The MoDTC trimer (Oil 2) displayed a longer friction drop than the dimeric species. The differences in induction period length for the Oil 3 MoDTC (C8-C14) dimer were greater than those observed at 100 N, which shows that the induction period length for this additive is very variable.

5.2.2 Effect of surface roughness

Each of the sulfur-containing additive systems effectively reduced friction at loads as low as 25 N. From this it was expected that decomposition of the additives to MoS_2 was occurring in all cases. The data also showed that the additive systems were capable of reducing friction at low loads and contact pressures. In order to find the point of mechanochemical activation, a further decrease in the severity of the contact conditions was required.

5.2.2.1. Reciprocating contact surface roughness

MoDTCs are known to display sub-optimal friction performance under smooth plate conditions[80,203]. This implies that surface roughness is an important contributing factor to the decomposition of MoDTCs. In order to investigate the effect of surface roughness on the friction performance of the additives, the TE77 plates were reduced in roughness from R_a = 0.5 µm to R_a = 50 nm. This led to an effective change in maximum lambda ratio from λ =0.04 to λ = 0.41. The tribological tests were then run on the additive systems using the same temperature and sliding speed conditions described previously, at a load of 25 N. The contact conditions are found in Table 10.

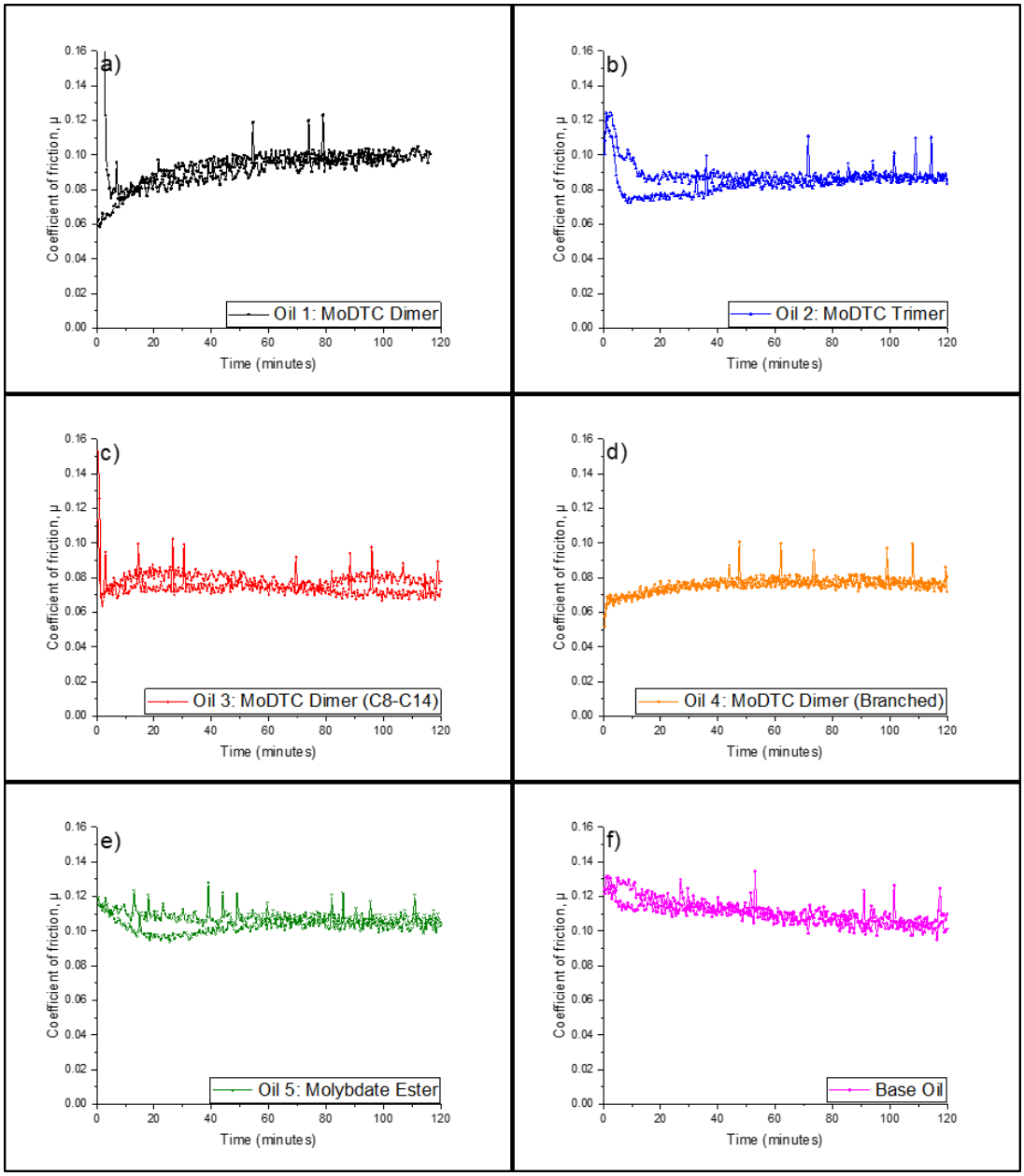


Figure 5.4 Individual smooth plate friction profiles of molybdenum additives at 25 N

a) Oil 1: MoDTC Dimer, b) Oil 2: MoDTC Trimer, c) MoDTC Dimer (C8-C14), d) MoDTC Dimer (Branched), e) Oil 5: Molybdate Ester, f) Base Oil

For the standard MoDTC dimer (Oil 1), under the higher lambda ratio contact there is a change in friction coefficient from the start of rubbing which settles in time to a steady state value of μ = 0.09. This value is lower than would be expected for steel-on-steel boundary contact but not typical of MoS_2 tribofilms which normally occupy the range μ = 0.04-0.06.

The MoDTC trimer's (Oil 2) friction performance was comparable to that of Oil 1. In these higher lambda ratio conditions, Oil 2 showed a more typical shape for a MoDTC friction profile than the unusual shape that was observed in the 500 nm roughness plate tests. The slight increase in friction was still observable after 10 minutes although was much less pronounced. A high friction induction period gave way to a rapid friction drop after 20 minutes. However, much like Oil 1, the steady state friction coefficient of $\mu = 0.08$ was not as low as would be expected from an MoS_2 tribofilm.

The C8-C14 dimer (Oil 3) displayed an almost instantaneous friction drop to the intermediate friction value of $\mu = 0.08$. Oils 3 and 4 displayed the lowest friction coefficients of all the additives under these higher lambda ratio conditions.

The sulfur-free additive (Oil 5) showed no friction reduction relative to the steady state base oil friction value of $\mu = 0.1$ under these contact conditions.

For all of the sulfur containing additives, the reduction in friction observed under the smooth plate conditions was less than that observed previously with the rougher plates. However, for the majority of systems, a reduction in friction relative to base oil was still observed.

To confirm that MoS_2 formation was still occurring in these smooth plate 25 N tests, Raman spectroscopy was performed on the TE77 plate wear scars. Representative spectra from the central wear scar for each additive are shown in Figure 5.5. MoS_2 scattering peaks at 380 cm^{-1} and 408 cm^{-1} were observed in the wear scars of all the sulfur-containing additives but were absent outside the wear scars and within the wear scars of the base oil and molybdate ester (Oil 5) plates.

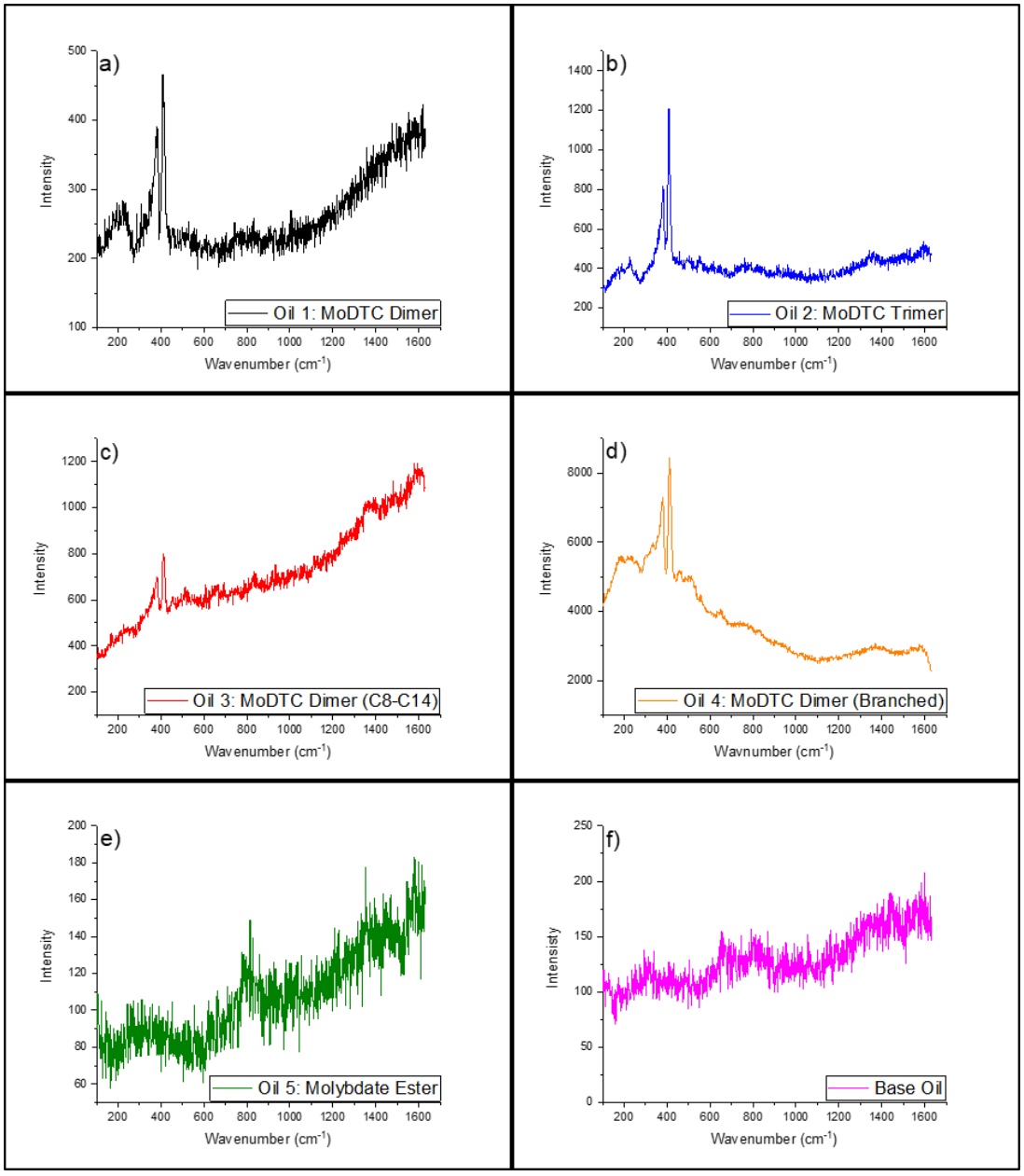


Figure 5.5 TE77 plate representative wear scar raman spectra

a) Oil 1: MoDTC Dimer, b) Oil 2: MoDTC Trimer, c) MoDTC Dimer (C8-C14), d) MoDTC Dimer (Branched), e) Oil 5: Molybdate Ester, f) Base Oil

In those spectra where MoS_2 was observed, the scattering peaks of this species dominated the spectra and no other species were observed. For the base oil and sulfur free molybdate ester, some peaks associated with haematite (Fe_2O_3) on the steel surface were observed at 820 cm^{-1}. No molybdates or oxides of molybdenum such as MoO_2 or MoO_3 were observed in any of the wear scars formed under these mild conditions.

In order to determine if the change in friction behaviour observed with smooth plates was due to the surface roughness or due to the change in lambda ratio between the roughened and smooth plates, the load was increased to 300 N. The result being that the lambda ratio with the smooth plates was lowered to the same value as had previously been tested for the rough plates. This allowed for lambda ratio to be altered whilst maintaining the same temperature and sliding speed conditions as all the other tests. The contact conditions are presented in Table 11. The change in load also led to changes in the Hertzian contact area and contact pressure as outlined in Table 18.

Table 18: Hertzian contact conditions for investigation of lambda ratio in reciprocating contact

Load	25 N (rough surfaces)	300 N (smooth surfaces)
Maximum Hertzian Contact Pressure (MPa)	117	268
Mean Hertzian Contact Pressure (MPa)	78	178
Hertzian contact area (mm^2)	0.127	0.666
Maximum Lambda Ratio	0.05	0.04

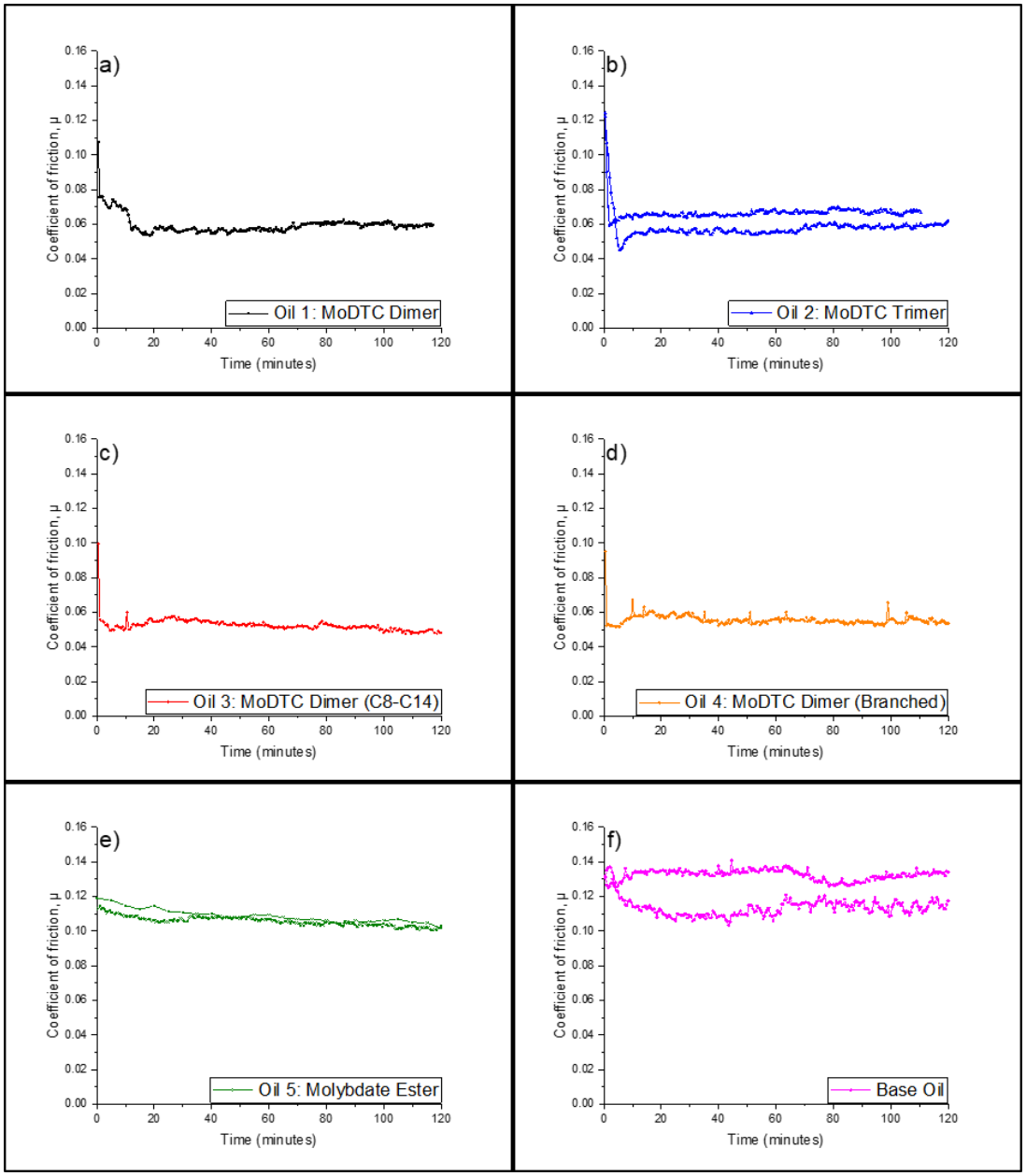


Figure 5.6 300N smooth plate individual friction profiles

a) Oil 1: MoDTC Dimer, b) Oil 2: MoDTC Trimer, c) MoDTC Dimer (C8-C14), d) MoDTC Dimer (Branched), e) Oil 5: Molybdate Ester, f) Base Oil

Under these highly-loaded conditions in Figure 5.6 the additives behaved in a similar manner to the rough plates. Each of the sulfur-containing additives showed a rapid friction drop upon the formation of molybdenum disulfide, after a brief induction period. Unlike in the rougher plate tests however, the (C8-C14) dimer (Oil 3 Figure 5.6c) had an induction period as short as the other sulfur-containing additives. The friction coefficient observed was $\mu \approx 0.06$ which is more typical of the rougher surface results rather than the

intermediate friction coefficient of μ = 0.08 observed with the smooth plates under low load.

The low lambda ratio tests which result either from high surface roughness, or from low surface roughness with high loads, both lead to clearly-activated friction responses from the additives. The smooth plate 25 N tests did not however. This suggests that either the lambda ratio, or the increased contact temperatures associated with low lambda ratios are the factors which affect whether a full drop in friction is observed from the additive systems. In reciprocating contact, such as the TE77 tests previously described, the lambda ratio is constantly changing with the sliding speed of the contact. This leads to the contact experiencing a range of lambda ratios through the cycle of a contact stroke. In order to investigate the effect of lambda ratio, and of contact temperature at constant lambda ratio, it is necessary to study a contact which can provide a fixed lambda ratio value throughout the duration of a test. This can be achieved using a unidirectional contact with a constant sliding speed, such as a High Speed Pin-on-Disc tribometer.

In reciprocating sliding conditions, the MoDTC dimeric structures maintained very similar friction profiles, with high friction induction periods followed by very rapid drops in friction. This is likely due to them having very similar chemistries, with identical molybdenum core structures, varying only in their alkyl chains. Therefore, in the case of each dimer, the friction-active chemical cores are identical. The MoDTC trimer (Oil 2) had a very different friction profile to the dimers, with a longer friction drop period and intermediate rise in friction mid-test. Unlike the dimer structures the MoDTC trimer has a fundamentally different molybdenum core structure, with bridging sulfido ligands and a Mo (IV) oxidation state. The differing core chemistry of these two additive systems suggests that if differences in performance are to be observed then it is likely to be most pronounced in these systems. In order to investigate these differences in greater details, the scope of additives was

reduced to investigation of the MoDTC dimer (Oil 1) and the MoDTC trimer (Oil 2).

5.2.2.2. Simulation of asperity contact pressures

The Hertzian contact analysis outlined in “2.7 Contact between surfaces” assumes that an applied load is distributed uniformly over the entire contact area. In truth, the true contact area over which the load is distributed is much smaller, with the load being held by the surface asperities. The height distribution of these asperities in the form of surface roughness will affect the expected contact area and, by extension, the pressures experienced by these asperity contacts.

To understand the effect of surface roughness on expected asperity contact pressures, the TE77 plate surfaces were modelled as self-affine fractal surfaces in contact with defined surface roughness. The computational model used was built upon a model developed by Ghanbarzadeh et al. [193] using surface digitisation employed by Tonder et al. [204]. The surface generation system can produce surfaces with desired surface roughnesses considered both vertically and laterally. The model can be used to determine contact pressures in either a perfectly elastic or in an elastic-plastic mode. The hardness of the material is used as an input to determine the expected plastic flow of material. This model of plastic flow is explained by Sahlin et al.[205].

Two plane surfaces of R_a = 50 nm and R_a = 500 nm, corresponding to the TE77 plate roughnesses were brought into contact with a third surface of R_a = 50 nm and 100 mm radius to simulate the TE77 pin. The simulation was carried out in an area of 100 µm x 100 µm with each node being 40 nm^2 in area. A pressure of 200 MPa was applied to the area, similar to the 100 N TE77 tests. This pressure also ensured that there would be significant surface contact, but that the load would still be supported by the asperities primarily, rather than increasing the contact area to an unrealistically high level.

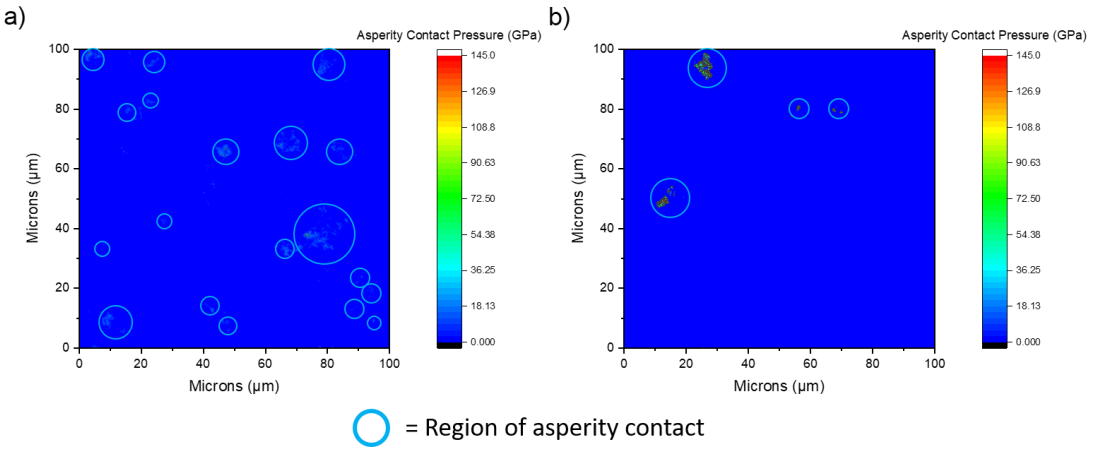


Figure 5.7 Elastic asperity pressure Distribution for a) 50 nm R_a and b) 500 nm R_a at 200 MPa

Regions of asperity contact are highlighted in blue circles for easier comparison of contact areas.

In the purely elastic analysis in Figure 5.7, it can be seen that there is a significant difference between the surfaces in both the expected asperity contact pressures, and the degree of surface coverage. In the 50 nm simulation, the load is supported over 3.9 % of the apparent contact area, whereas the 500 nm roughness simulation had a contact area of 0.5 % of the simulation area. This reduction in contact area with increased roughness led to an associated increase in mean asperity contact pressure from 5.0 GPa at 50 nm R_a to 39 GPa at 500 nm R_a.

A purely elastic analysis is expected to give an overestimate of the asperity contact pressure. Plastic deformation of asperities will increase the overall contact area and lead to a reduction in the asperity contact pressures. The simulations were run, taking account of the plastic deformation of asperities, and the pressure distribution maps are presented in Figure 5.8 (note the change in pressure scale from Figure 5.7).

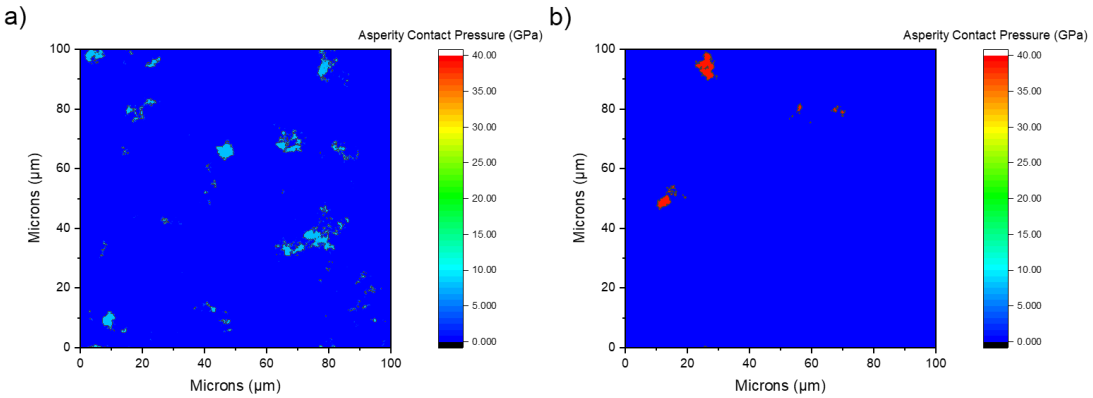


Figure 5.8 Elastic-plastic asperity pressure Distribution for a) 50 nm Ra and b) 500 nm Ra at 200 MPa

Note change in scale from Figure 5.7

When accounting for plastic deformation in Figure 5.8, the contact area of the smooth plate remains greater than the rough plate, as in the purely elastic simulation (4.4% and 0.5 % for the smooth and rough plates respectively). There was also little change in the average asperity contact pressures, 4.5 GPa for the smooth plate and 39 GPa for the rough plate.

The asperity contact pressures are compared in Figure 5.9. There is only a small difference in the mean asperity contact pressure between the plastic and elastic analysis, for a given surface roughness. This suggests that the contacts at these low pressures are primarily elastic in nature, consistent with the minimal wear observed for the plates in these systems. The major difference between the plastic and elastic analyses is found in the distribution of expected contact pressures for an asperity, in the form of the standard deviation of contact pressures. The plastic deformation criterion imposes a maximum contact pressure on an asperity and drastically reduces the expected variation in asperity contact pressures. This is especially true for the 500 nm R_a surface, which has a pressure standard deviation of 29 GPa in the elastic analysis but has a standard deviation on the order of individual Pascals in the plastic analysis.

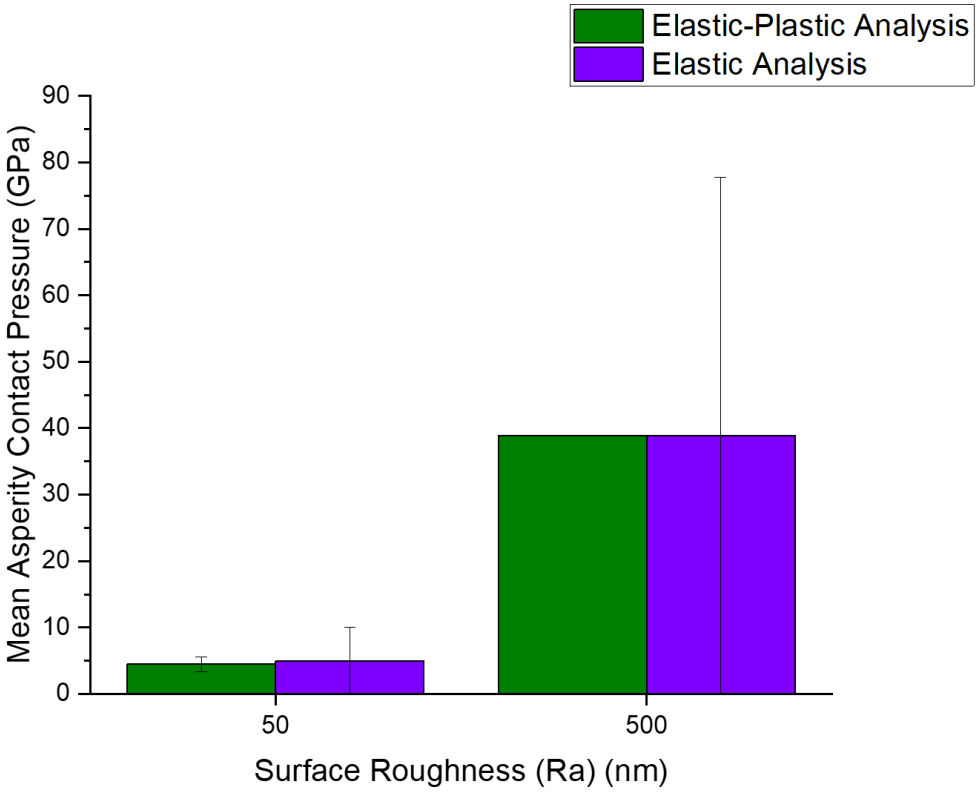


Figure 5.9 Comparison of asperity pressure distributions between elastic and plastic analysis

The simulation shows that despite nominally having the same applied Hertzian contact pressure, the surface roughness differences between TE77 plates are expected to lead to an almost order of magnitude difference in asperity contact pressures. These pressure differences are likely to manifest themselves as increase shear forces and flash temperatures which will contribute to the decomposition of molybdenum additives to form MoS_2, as seen in the experimental work in Section 5.2.2.1.

5.2.3 Effect of changing lambda ratio

In order to investigate the effect of changing lambda ratio upon the activation of the MoDTC additives, unidirectional tests were performed using a high speed pin-on-disc tribometer. The sliding speed was changed between 0.1649 ms^{-1} and 1.649 ms^{-1} (100 rpm and 800 rpm) whilst keeping all other contact conditions the same. Alteration of the sliding speed for a fixed test

duration will lead to different final sliding distance values between the tests. Overall sliding distance may be a factor in the length of the high-friction induction period of the dimeric additives as seen in Figure 5.1. The sliding speed results are for the Oil 1 MoDTC dimer are presented in Figure 5.10 and for the Oil 2 MoDTC trimer in Figure 5.11. This changing of conditions altered the lubricant film thickness and hence lambda ratio of the contact under study. A lubricant temperature of 40 °C was chosen to make the thermal energy of the tests comparable to that of the TE77 results. The contact pressure was 0.7 GPa with a load of 6.5 N. This lower load was chosen to find the limit of mechanochemical activation but the contact pressure was nominally higher due to the pin of the pin-on-disc tribometer having a smaller radius of curvature than the TE77 pins. The contact conditions are outlined in Table 15.

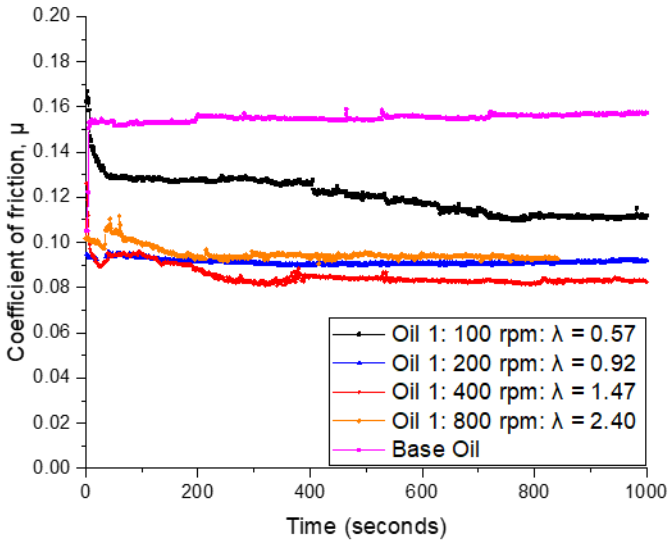


Figure 5.10 Friction response of MoDTC Dimer (Oil 1) with sliding speed and lambda ratio

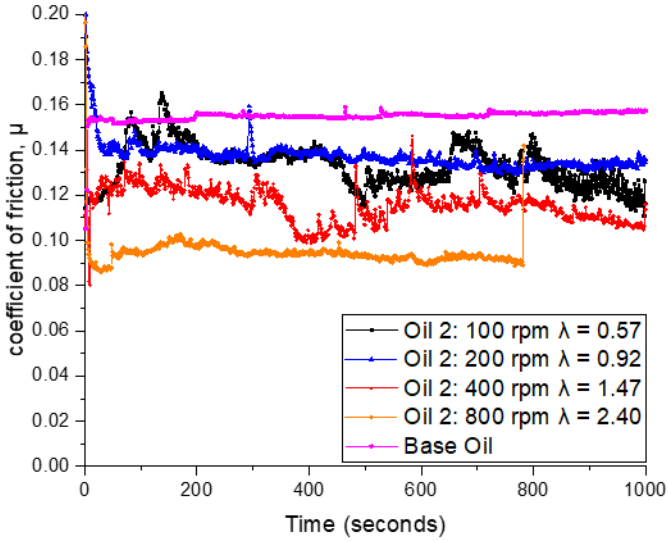


Figure 5.11 Friction response of MoDTC trimer (Oil 2) with sliding speed and lambda ratio

For both oil systems a slight reduction in friction occurred at all sliding speeds. For the MoDTC Dimer (Oil 1 Figure 5.10), there was a slight reduction in friction at λ = 0.57 and a greater reduction in friction for the higher sliding speeds to μ ≈ 0.10 which is still much higher than would be expected of a full MoS_2 tribofilm.

The MoDTC Trimer (Oil 2 Figure 5.11) displayed a similar pattern of friction reduction with lambda ratio to the MoDTC dimer. A small reduction in friction relative to base oil was observed at low sliding speeds, which became more pronounced at higher sliding speeds. At any given sliding speed, the friction coefficient of the MoDTC Trimer (Oil 2), was higher than that of the MoDTC Dimer (Oil 1). This suggests that less decomposition to MoS_2 is occurring for the Trimer than the dimer under these conditions.

Under these temperature conditions there was no MoS_2 formation observed on the discs at any sliding speed. The absence of MoS_2 was confirmed by Raman spectroscopic analysis of the disc wear scars for each sliding speed in Figure 5.12 and Figure 5.13.

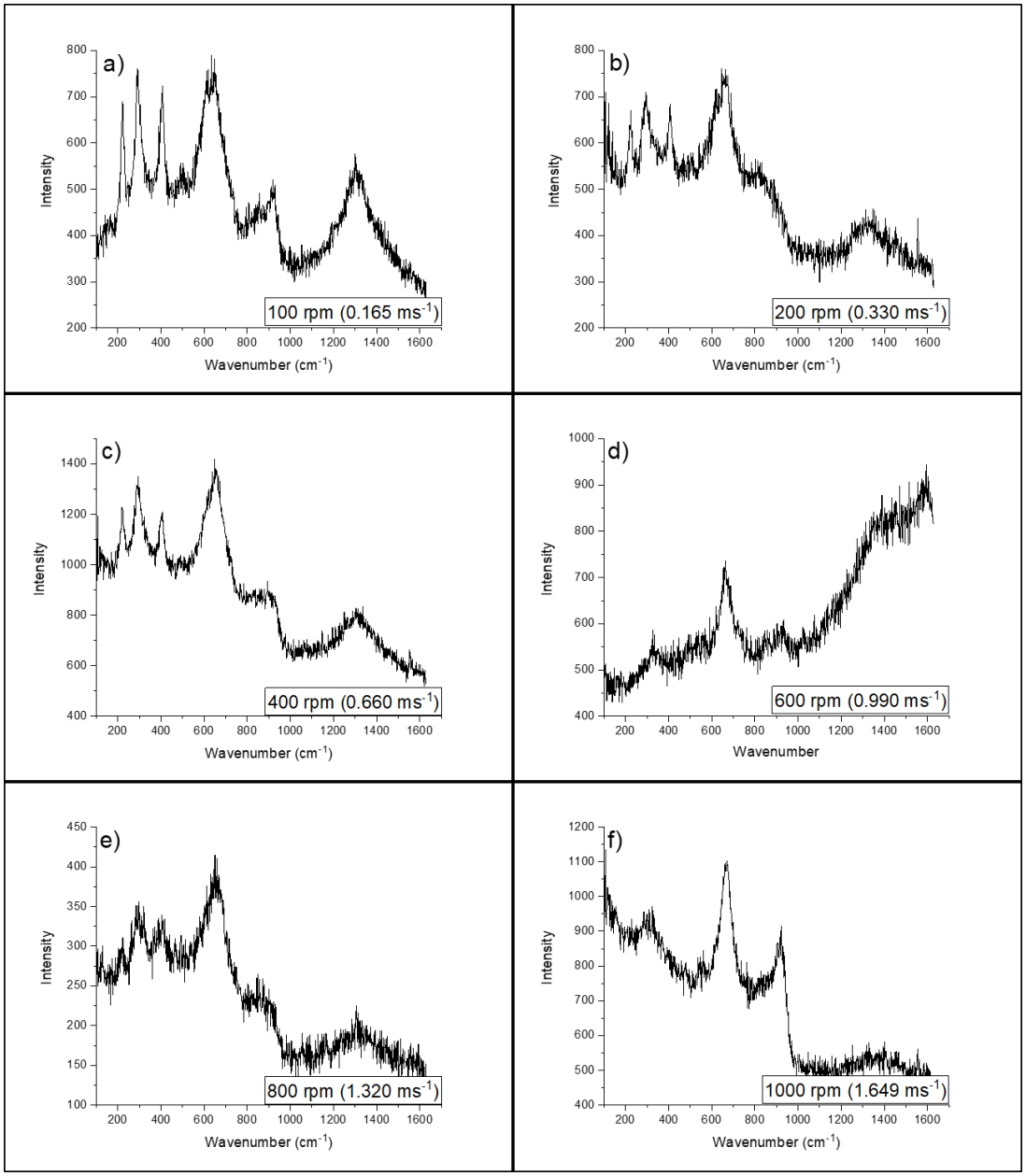


Figure 5.12 Oil 1 (MoDTC Dimer) wear scar Raman spectra for various sliding speeds

a) 100 rpm (0.165 ms^{-1}), b) 200 rpm (0.330 ms^{-1}), c) 400 rpm (0.660 ms^{-1}), d) 600 rpm (0.990 ms^{-1}), e) 800 rpm (1.320 ms^{-1}), f) 1000 rpm (1.649 ms^{-1})

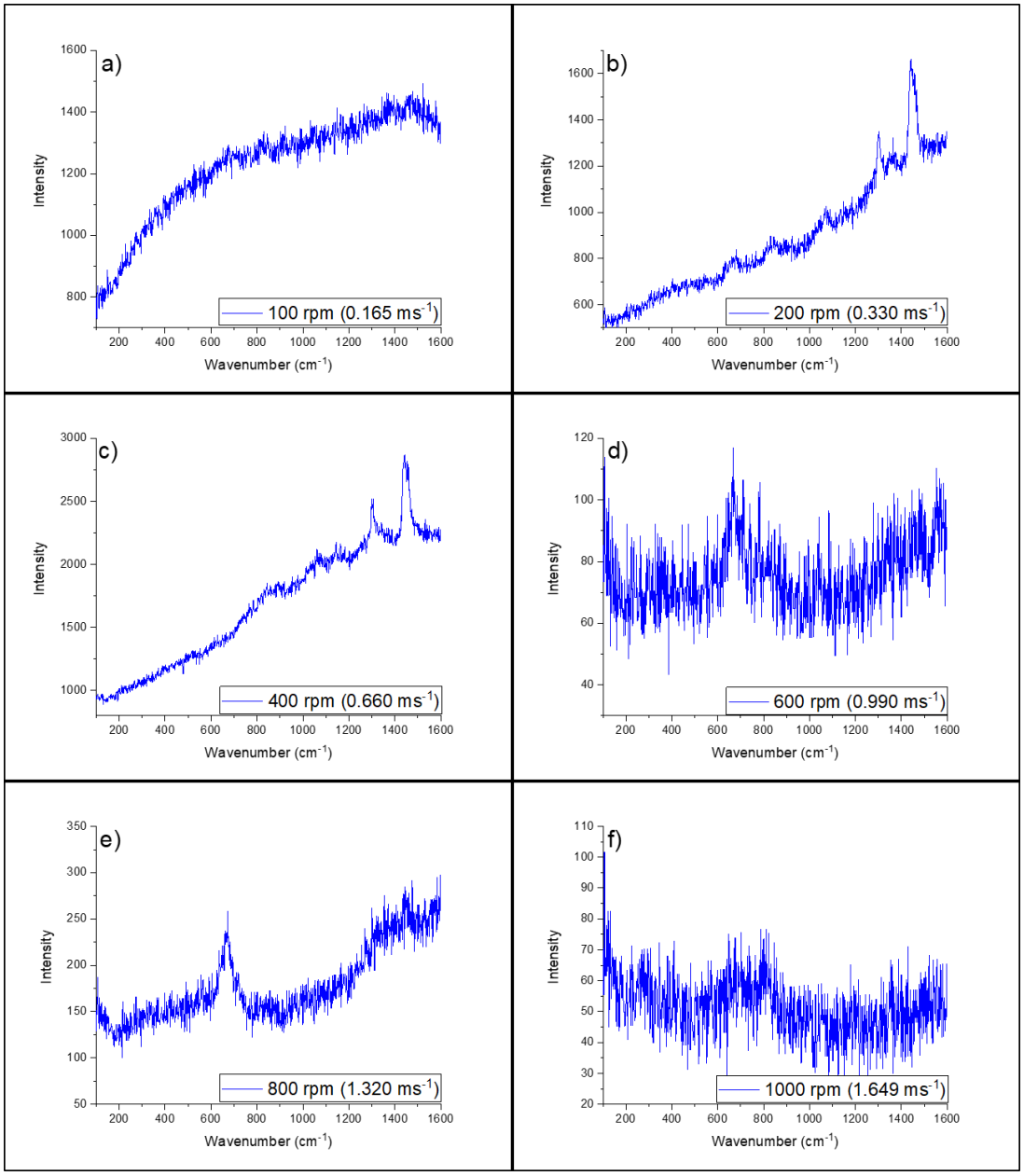


Figure 5.13 Oil 2 wear scar Raman spectra for various sliding speeds

a) 100 rpm (0.165 ms^{-1}), b) 200 rpm (0.330 ms^{-1}), c) 400 rpm (0.660 ms^{-1}), d) 600 rpm (0.990 ms^{-1}), e) 800 rpm (1.320 ms^{-1}), f) 1000 rpm (1.649 ms^{-1})

Through the alteration of the lubricant viscosity, a wider range of lambda ratios was investigated for the MoDTC dimer (Oil 1). In order to determine if there is an overall trend in friction performance as one moves from the deep boundary

regime towards the mixed regime. Across this wide range of contact conditions, no overall trend was observed; showing that the friction performance cannot be well defined by nominal lambda ratio.

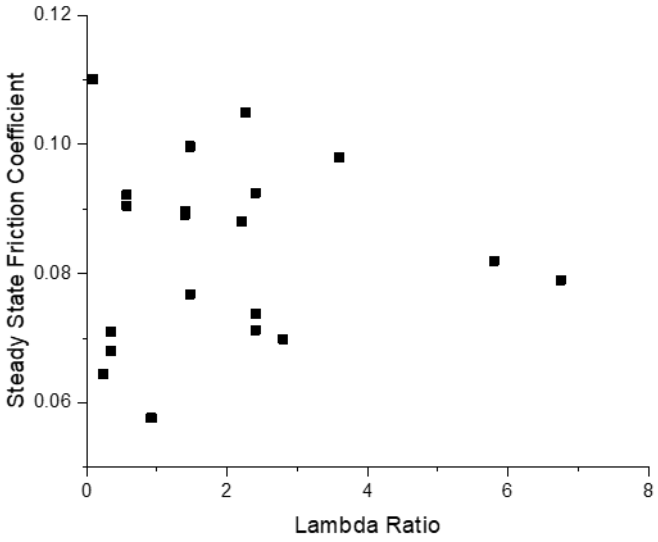


Figure 5.14: MoDTC dimer friction performance with changing lambda ratio in unidirectional sliding at 40°C

Although no simple relationship between lambda ratio and friction coefficient can be drawn for all possible conditions; from Figures 5.10 and 5.11, for a given set of boundary contact conditions the friction coefficient decreases with increasing lambda ratio. However, this trend runs contrary to what would be expected from lambda ratio alone, wherein lower lambda ratios would be considered harsher conditions where more additive decomposition would be expected. Instead, the decrease in friction coefficient with increasing sliding speed is suggestive of increased shear forces and contact temperatures being the driving forces for friction reduction. The friction reduction that is observed at higher lambda ratios may be due to a hydrodynamic component to the friction behaviour.

5.2.4 Effect of lubricant temperature

From the previous section, the key physical factors which determine friction reduction appear to be either the contact temperature (the combined effect of lubricant bath temperature and frictional flash temperature), or the shear forces in the contact.

The effect of temperature on the decomposition of the additive systems can be investigated independently of the shear forces and lambda ratio of a contact through the careful selection of lubricant base stock, whilst maintaining the same contact conditions. Three different lubricant base stocks were chosen for this study, labelled “Low”, “Medium” and “High” Viscosity. The tests previously performed all utilised the “Low” viscosity oil. The two extra oils of “Medium and “High” viscosity were supplied for the purpose of investigating the temperature dependence of friction reduction.

The temperature-viscosity behaviour of the oils was investigated using a rotational rheometer. Temperature sweeps of the oil systems were performed between 25°C and 125°C at 10°C intervals, at a shear rate of 1000 s^{-1}. The temperature was allowed to stabilise for 5 minutes prior to each point of viscosity determination. The temperature-viscosity sweeps for the oil systems are presented below in Figure 5.15.

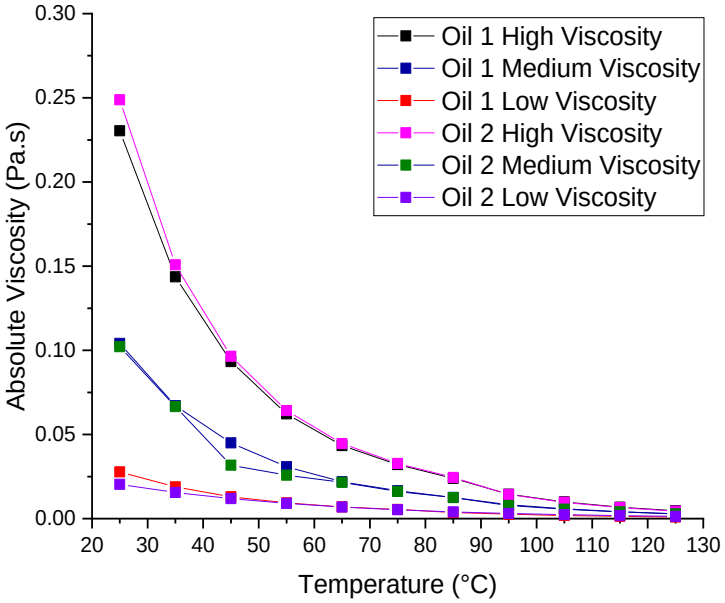


Figure 5.15 Temperature-viscosity profiles of base stocks

Exponential decay functions were fit to the viscosity profiles of the oils. From these, points of equivalent viscosity at different temperatures were determined for the three oil systems. It was found that the “Low” viscosity oil at 40°C, as previously tested, had an equivalent viscosity to the “Medium” oil at 80°C and the “High” oil at 120°C.

By fixing the viscosity whilst varying the temperature, the mechanical properties of the contact can remain constant in terms of contact and lubricant shear forces, whilst changing the thermal energy available to the additives. This method allows for determination of the effect of temperature as an independent variable. For each of these tests the sliding speed was fixed at 400 rpm (0.660 ms^{-1}) with a load of 6.5 N, providing a maximum Hertzian contact pressure of 0.77 GPa. The friction responses of the two additives as a function of temperature at fixed lambda ratio are presented in Figures 5.16 and 5.17.

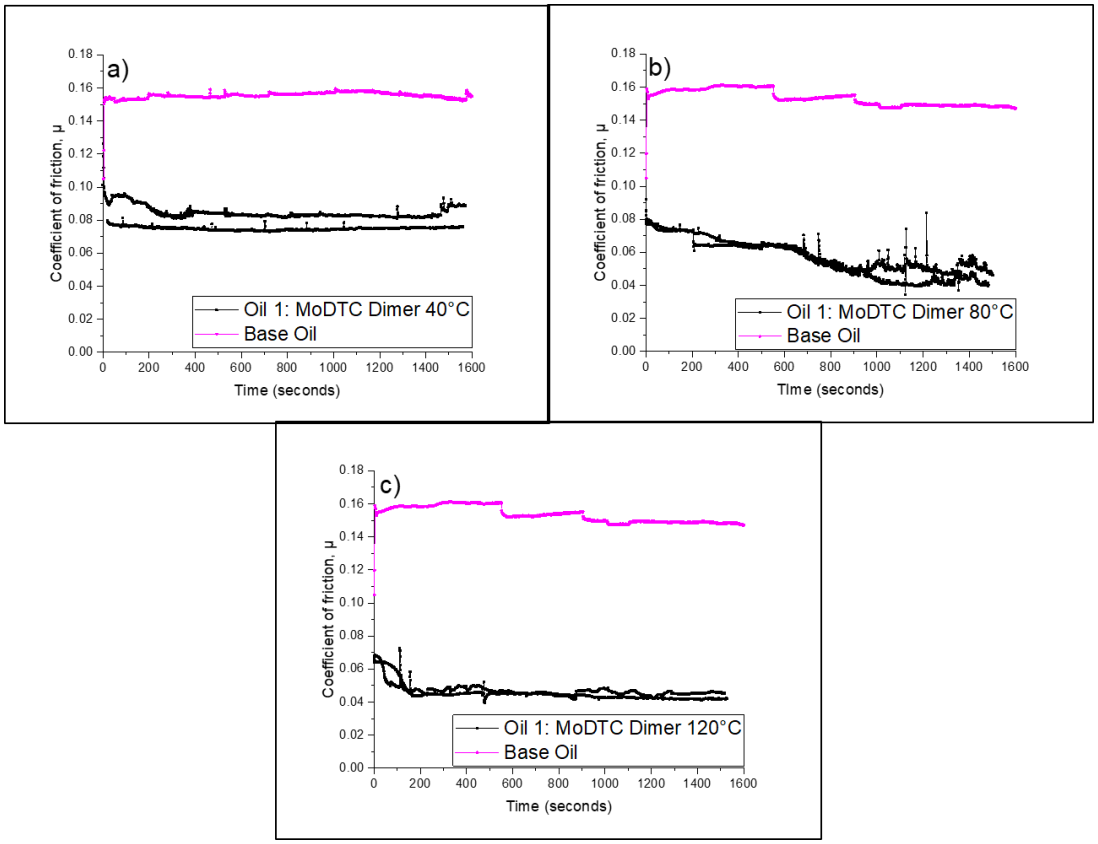


Figure 5.16 Friction response of MoDTC dimer (Oil 1) with temperature

a) 40°C low viscosity, b) 80°C medium viscosity, c) 120°C High Viscosity

In Figure 5.16, at 40°C, there is a reduction in friction for the MoDTC dimer (Oil 1) relative to base oil, as seen previously in Figure 5.10, but not to the low value typically associated with MoS_2 tribofilms. Upon increase in temperature to 80°C however, a further drop in friction occurs to $\mu = 0.05$, much more typical of MoS_2 films. At 80°C, the decay in friction coefficient occurred over the first 900 seconds before reaching the final value of $\mu = 0.05$. In contrast, the drop in friction coefficient was much more rapid for the test performed at 120°C. At this higher temperature, the friction dropped to $\mu = 0.05$ after a short induction period of 100 seconds.

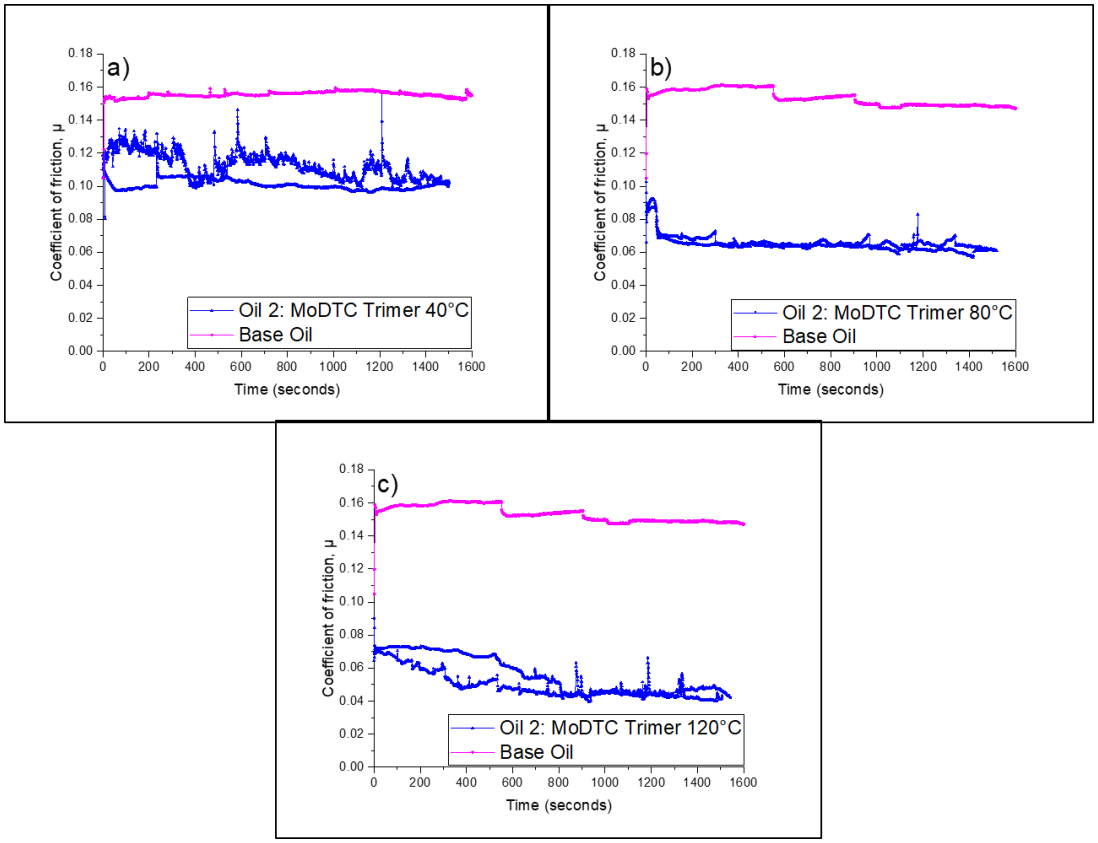


Figure 5.17 Friction response of MoDTC trimer (Oil 2) with temperature

a) 40°C low viscosity, b) 80°C medium viscosity, c) 120°C High Viscosity

Like the MoDTC Dimer (Oil 1), the MoDTC Trimer (Oil 2) in Figure 5.17 showed a decrease in friction relative to base oil at all temperatures and the degree of this friction reduction increased with increasing lubricant temperature. Unlike the MoDTC Dimer (Oil 1), the MoDTC Trimer (Oil 2) did not provide optimal friction reduction under 80°C conditions, instead displaying an intermediate friction coefficient of μ = 0.07. The lowest coefficient of friction of μ = 0.05 was only observed in the 120°C test for this additive, which was reached only towards the end of the test, via a 900 second friction decay period. Overlays of the friction profiles for the two additives at each temperature are provided in Figures 5.18, 5.19 and 5.20.

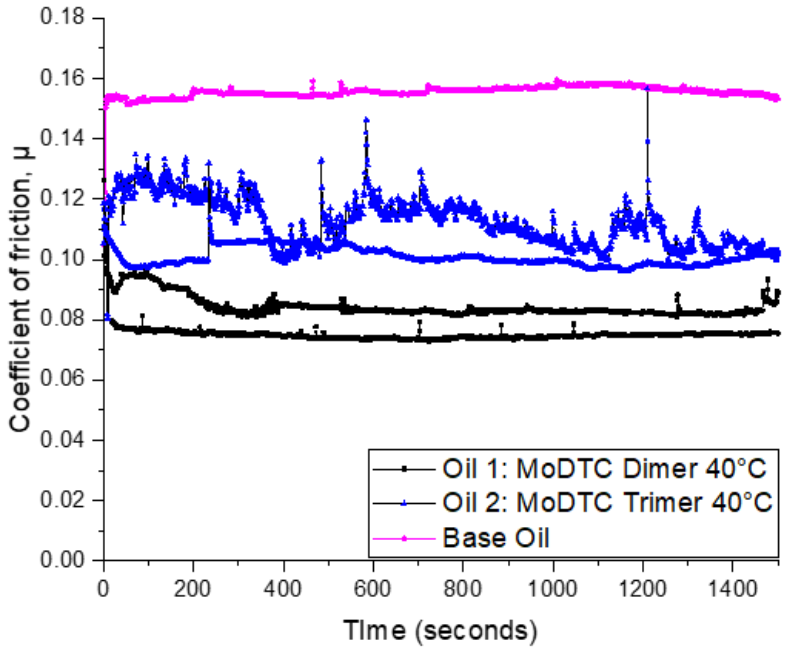


Figure 5.18 Additive friction response in low viscosity oil at 40°C

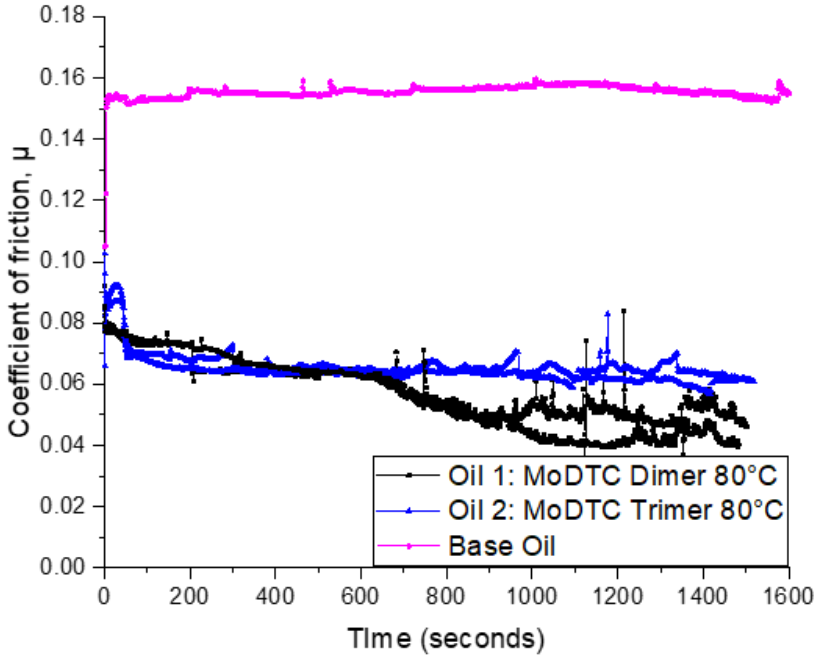


Figure 5.19 Additive friction response in medium viscosity oil at 80°C

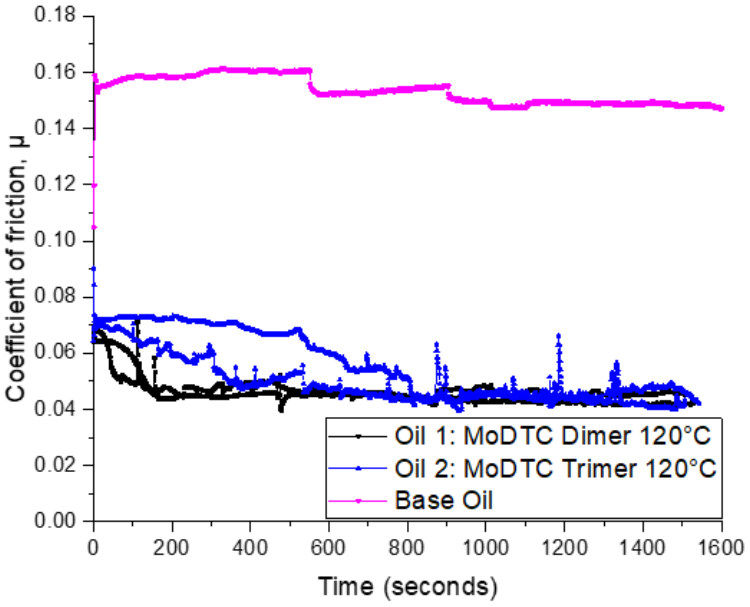


Figure 5.20 Additive friction response in high viscosity oil at 120°C

It can be seen from the above Figures that, like the sliding speed tests, the friction performance of the MoDTC dimer (Oil 1) is superior to that of the MoDTC Trimer (Oil 2). At 40°C and 80°C, the MoDTC dimer displays a lower coefficient of friction than the MoDTC Trimer. At 120°C the MoDTC dimer has a more rapid drop to low friction than the trimer, whilst maintaining a comparable final friction coefficient. The MoDTC dimer has lower friction at all temperatures. The lowest friction value of μ = 0.05 is reached first by the MoDTC dimer (Oil 1) at 80°C, whereas the MoDTC Trimer (Oil 2) does not reach this value until 120°C. Therefore, the MoDTC dimer is more sensitive to temperature than the MoDTC trimer and is more easily decomposed than the trimer. Overall, the friction drop for an MoDTC dimer is activated at milder conditions than for the MoDTC trimer. The contact parameter which affects this the most is the overall contact temperature, which is a product of the lubricant bath and the frictional flash temperature.

Raman analysis was performed on the disc wear scars to confirm the presence of MoS_2 in the low friction tests. In Figure 5.21, no MoS_2 was observed in the wear scars of either of the 40°C tests, with only hematite (Fe_2O_3) and magnetite (Fe_3O_4) peaks being observed at 220, 300, 410 and 1350 cm^{-1} for hematite and at 640 cm^{-1} for magnetite. In addition to the iron

oxide and molybdenum disulfide peaks, high wavenumber scattering was observed from small amounts of supernatant oil.

In Figure 5.21b, no MoS_2 is observed in the wear scar Raman spectrum, despite the MoDTC dimer displaying a lower friction coefficient than the MoDTC trimer under the 80°C conditions. This does not necessarily mean that there is no molybdenum disulfide in the wear scar at all but that there may be so little that it is below the detection threshold of the Raman spectrometer. In Figure 5.21e, only a very small amount of MoS_2 is observed for the trimer which is still dominated by iron oxide peaks. For the MoDTC dimer it may be that MoS_2 is being formed in the contact to reduce friction, but that this small amount is being removed from the contact area during sliding such that none remains for *post-mortem* surface analysis of the wear scar. The presence of MoS_2 in the 80°C wear scar of the MoDTC trimer suggests that the MoDTC trimer may create more Mo:S species on the surface, but that these may be inferior friction-reducing quality than those formed by the MoDTC dimer. In addition to the 80°C tests, a greater amount of MoS_2 is detected for the MoDTC trimer in the 120°C tests also (Figure 5.21c and f).

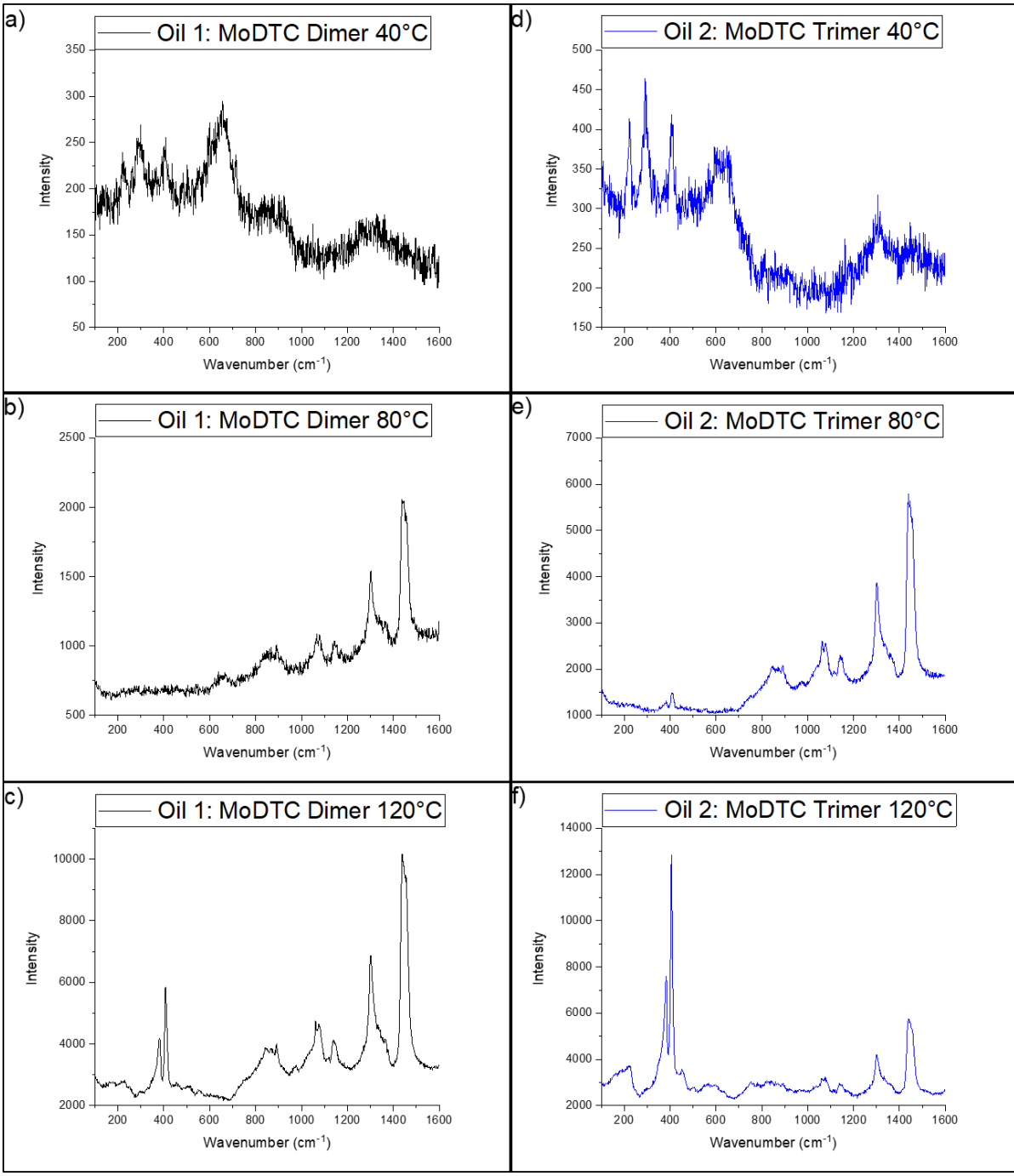
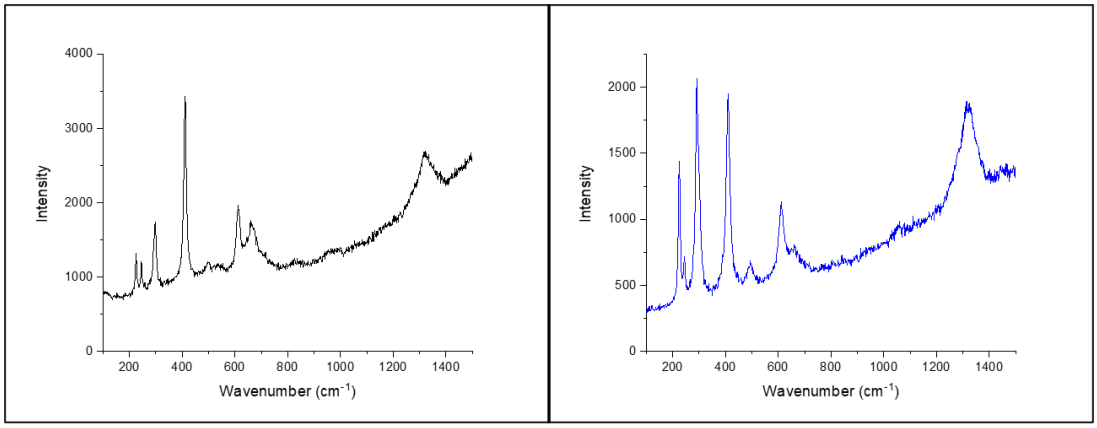


Figure 5.21 Representative wear scar Raman spectra for oils 1 and 2 with temperature

5.2.5 Thermal formation of MoS_2

In order to determine if the formation of iron oxides led to the catalytic formation of molybdenum disulfide, tests were run heating MoDTC dimer-

containing oil (Oil 1) outside of the contact. Firstly, tribological testing was performed with the 3.25 mm radius pins in the high-speed pin-on-disc tribometer in base oil under a load of 13 N to promote surface oxide formation. After 1 km sliding distance the disc was transferred to a heated bath of the MoDTC dimer-containing oil (Oil 1) held at 120 °C and allowed to stir for 1 hour. The same process was applied for MoDTC Trimer-containing oil (Oil 2) after the formation of surface oxides. Raman analysis of the resulting thermal films in Figure 5.22 did not display the presence of any molybdenum disulfide or iron molybdate on the surface, only magnetite scattering peaks with some scattering from supernatant oil. This result showed that some level of contact is needed and that an applied temperature in concert with the formation of surface oxides from wear is not sufficient to form MoS_2 on a surface.



a) Oil 1 MoDTC Dimer Thermal Film Raman Spectrum

b) Oil 2 MoDTC Trimer Thermal Film Raman Spectrum

Figure 5.22 Raman spectra of discs heated to 120°C in molybdenum additive-containing oil after tribological formation of surface iron oxides

5.2.6 Effect of Hertzian contact area in reciprocating contact

The formation of molybdenum disulfide was observed in reciprocating contact at much lower temperatures than was required to form it in the unidirectional contact, despite higher pressures and sliding speeds in the unidirectional tribometer. In the TE77 reciprocating contact, molybdenum disulfide was being formed easily at 40°C whereas in the unidirectional contact, temperatures of 80°C were required for any MoS_2 to be observed.

One major difference in the contact geometries between the TE77 reciprocating tests and the unidirectional tests is the radius of curvature of the pins. In the unidirectional tests, the pins have a radius of 3.25 mm, whereas the reciprocating tests had pins of 100 mm. This difference in contact radius is predicted to make significant changes in the Hertzian contact area, which in turn will affect the ability of the contact to remove heat from the contact in the form of frictional flash temperature. In order to test if this change in contact area had any effect on the performance of the additives through flash temperature, the TE77 tests were repeated under the conditions in Table 8 with lower radii of curvature of 10 mm and 40 mm. These changes in pin curvature lead to alterations in the Hertzian contact area outlined in Table 19.

Contact areas were calculated assuming a circular contact area of radius a as determined from Equation 12. Reduction of the pin radius from 100 mm to 10 mm raises the nominal contact pressure to levels comparable to that expected by the 3.25 mm radius pin used in the unidirectional pin-on-disc tests, but with a much larger nominal contact area.

Table 19: Hertzian contact areas with various pin radii

Pin radius (mm)	10	40	100	3.25 (PoD)
Maximum Hertzian contact pressure (MPa)	864	343	186	734
Mean Hertzian contact pressure (MPa)	575	228	124	489
Hertzian contact area (mm^2)	0.069	0.174	0.320	0.005

The effect of changing the pin radius, and by extension the Hertzian contact area for the oil systems can be seen for the Oil 1 MoDTC Dimer and Oil 2 MoDTC Trimer in Figure 5.23 and Figure 5.24 respectively. Comparative presentations of these data with both contact radius and additive nature can be found in Appendix B.

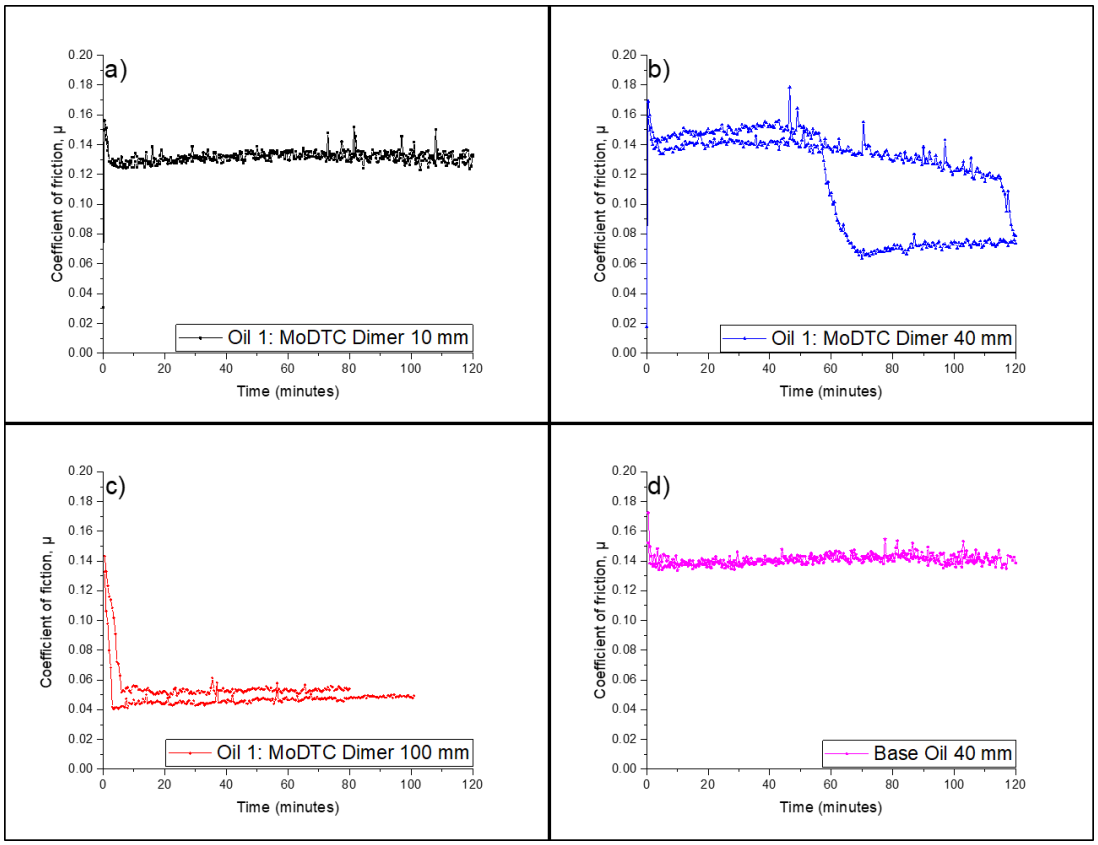


Figure 5.23 Effect of pin radius of curvature on Oil 1 (MoDTC Dimer)

a) 10 mm radius pin, b) 40 mm radius pin, c) 100 mm radius pin, d) Base oil 40 mm pin

For the MoDTC dimer, there is no significant reduction in friction relative to base oil using the 10 mm radius pin. This is despite having the same applied load and sliding speed as those tests in Figure 5.1 where a significant drop in friction was observed. In addition, the nominal contact pressures are expected to be greater for the 10 mm radius pin than in the previous tests with a 100 mm radius pin. Upon increase of the pin radius of curvature to 40 mm, a moderate reduction in friction is observed to μ = 0.08, but only after a significantly extended and variable induction period compared to previous tests. This behaviour is more like that of the Oil 3 MoDTC dimer (C8-C14). When a 100 mm radius pin was used, a rapid drop in friction with a short induction period was observed, similar to the behaviour of this additive in previous tests.

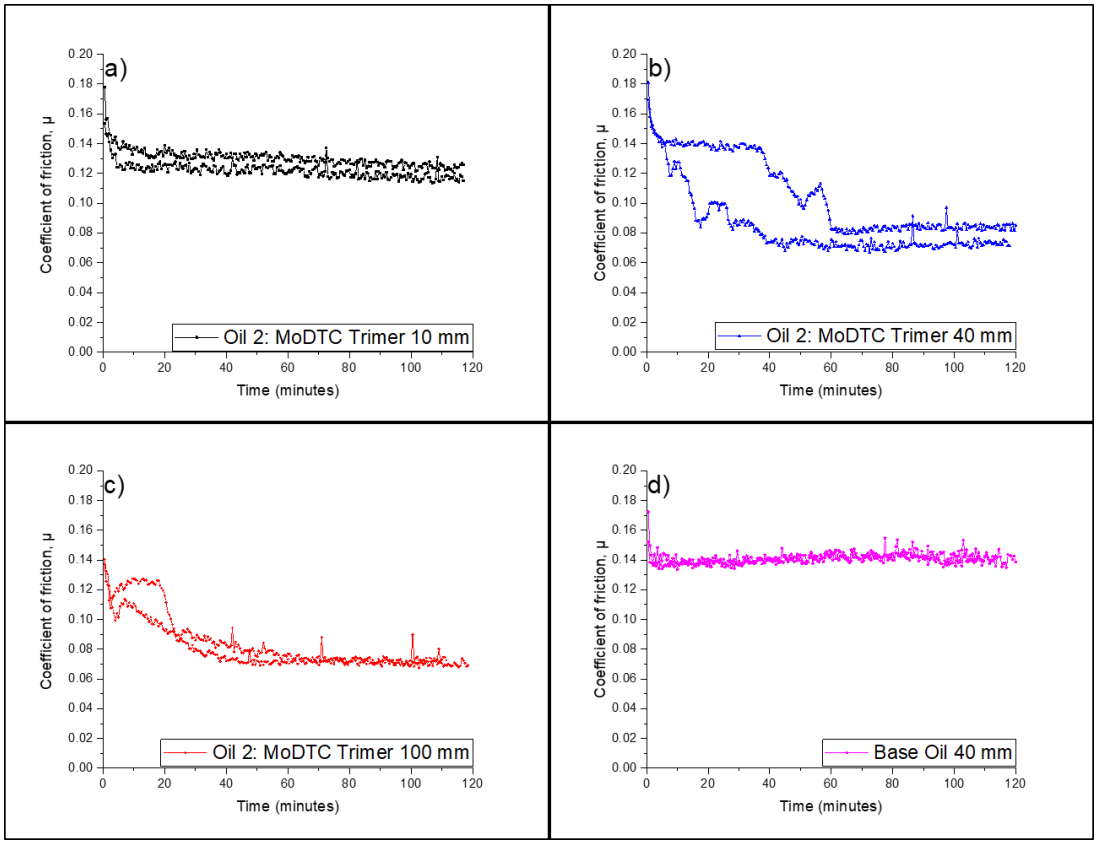


Figure 5.24 Effect of pin radius of curvature on Oil 2 (MoDTC Trimer)

b) 10 mm radius pin, b) 40 mm radius pin, c) 100 mm radius pin, d) Base oil 40 mm pin

For the MoDTC Trimer in Figure 5.24, a similar trend is observed to that of the MoDTC dimer. With a 10 mm radius pin, only a modest reduction in friction, relative to base oil is observed. Upon increase of radius of curvature to 40 mm, a greater reduction in friction is observed, but with a slightly extended induction period. For the 100 mm tests, the friction begins to drop at the beginning of the test and maintains the longer friction drop period that was observed in the previous tests.

The radius of curvature of the pins, and by extension the Hertzian contact area, have a profound effect on the friction profiles of the two additive systems at 40°C. This behaviour may be due to ability of the contact to dissipate thermal energy from the contact zone in small radius contacts, leading to lower frictional flash temperatures, which are unable to decompose the molybdenum additives to MoS_2. The expected thermal conditions of these contacts are investigated in the discussion.

5.3 Summary

In this chapter the friction-reducing performance of a variety of molybdenum additives was investigated under a range of contact conditions. The friction profiles and friction activation parameters were systematically studied. From the studies of the various additives, the following was observed:

- All of the molybdenum-sulfur containing additives were able to reduce friction relative to base oil under most conditions, even mild conditions with smooth surfaces, low loads low and sliding speeds.

- The sulfur-free molybdate ester is unable to reduce friction effectively under any conditions in its monoblend form, due to a lack of sulfur supply necessary for the formation of MoS_2.

- The MoDTC dimeric structures all had similar friction profiles, with high friction induction periods followed by very rapid drops in friction to MoS_2 values.

- The MoDTC dimer (C8-C14) had similar shaped friction profiles to the other dimeric structures. However, the induction period for this additive was highly variable, unlike the other dimeric additives.

- The MoDTC trimer additive has a distinct friction profile from the MoDTC dimers. The trimer has a much longer friction drop period which occurs over the course of minutes, rather than seconds.

- The friction performance of molybdenum-sulfur additives is activated more by surface roughness than by pressure, load or lambda ratio.

- Additive decomposition is driven primarily by the flash temperature, which is a complex product of the lubricant bath temperature and the severity of the asperity contacts.

- The friction performance of the additive systems is dependent on the radius of curvature of the pin in reciprocating contact, assuming all other contact conditions remain constant.

- The MoDTC Dimer additive requires less mechanochemical activation energy in order provide optimum friction performance than does the MoDTC Trimer. Therefore, molybdenum additives are not necessarily interchangeable as they show different degrees of friction reduction depending on the contact conditions.

The work of this chapter has shown that the chemistry of the molybdenum additives in a formulation affects that formulation's ability to reduce friction. In the next chapter, the tribofilms derived from the various additives will be studied in order to determine if changes in additive structures alter the nature of the MoS_2 films formed from those additives.

Chapter 6: Differences In Tribofilm Structures Derived From Varying Molybdenum-Sulfur Chemistries

6.1 Introduction

The friction experiments in the previous chapter have shown that the performance of additives is not only dependent upon the contact conditions employed, but also on the chemistry of the additives themselves. It is not the case that all molybdenum-sulfur additives decompose in the same way, or that they can be treated interchangeably in formulation.

In the friction tests previously described, it has been shown that the MoDTC Trimer has a higher coefficient of friction than the MoDTC dimer, up to a point where both additives decompose completely to MoS_2 at higher temperatures. In these tests MoS_2 was observed on the surfaces by Raman, even when the two additives displayed different final friction coefficients. It is of interest to determine then what is different about the MoS_2 films derived from these additives which causes them to have differing degrees of friction performance. Work has previously been performed relating the surface coverage of MoS_2 in a system to its friction performance [126,136,147]. In general, MoS_2 films derived from different additives have been believed to be equivalent, but it is of interest to lubricant formulators to determine if the additive chemistry has any effect on the chemical and physical properties of the MoS_2 tribofilms formed from different structures. This can help to characterise what properties of MoS_2 films are most desirable in order to maximise these properties from future additive chemistries.

In this chapter, the tribofilms derived from three different additive systems (MoDTC Dimer, MoDTC Trimer and Molybdate Ester) are characterised with Raman spectroscopy, X-Ray Photoelectron Spectroscopy, and Transmission Electron Microscopy. The additive structures are shown in Figure 6.1. From the chemical analysis, the differences in structure and performance of the MoS_2 tribofilms are related to the chemical structures of the additives and their ability to form decomposition intermediates.

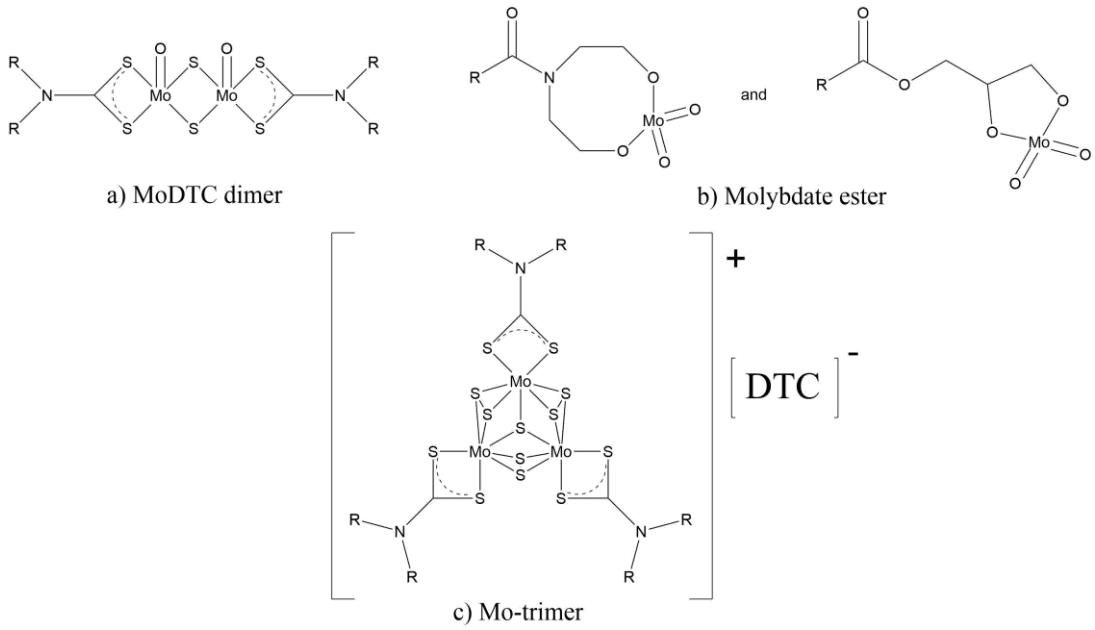


Figure 6.1 Molybdenum additives subjected to tribofilm characterisation

a) MoDTC dimer, b) Molybdate ester, c) Mo-trimer also known as MoDTC trimer

6.2 Tribofilm formation

Tribofilms were prepared for chemical characterization using a TE77 reciprocating pin-on-plate tribometer, under the conditions in Table 12.

Both monoblend and fully formulated oils of each additive system were subjected to friction testing in order to produce films for chemical analysis. Base Oil and a Molybdenum-free fully formulated oil were used as controls for the monoblends and fully formulated systems respectively.

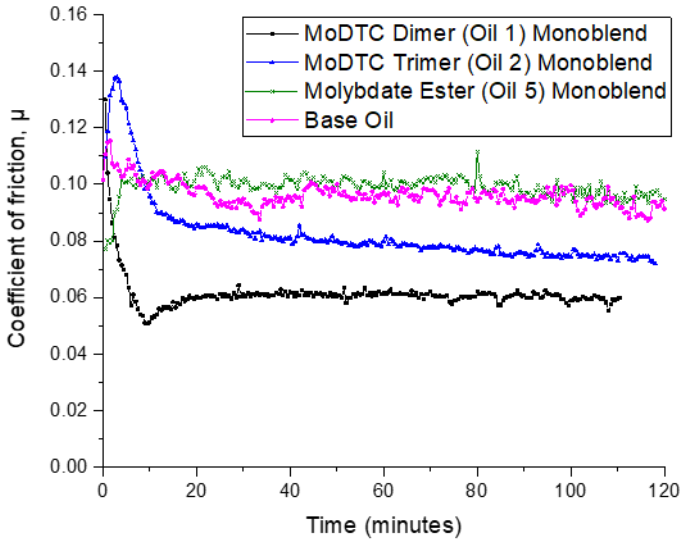


Figure 6.2 Friction profiles of molybdenum additive tribofilms

In the monoblend oil systems the sulfur-containing additives displayed a friction drop relative to base oil. As outlined in the previous chapter, the magnitude of this friction drop was greater for the MoDTC dimer (Oil 1) than for the MoDTC Trimer (Oil 2). In addition, the friction drop period for MoDTC dimer (Oil 1) was shorter than the more prolonged friction drop of MoDTC Dimer (Oil 2). The MoDTC Dimer reached its steady state friction coefficient after 20 minutes, whereas the MODTC trimer did not reach its final friction value until after 60 minutes.

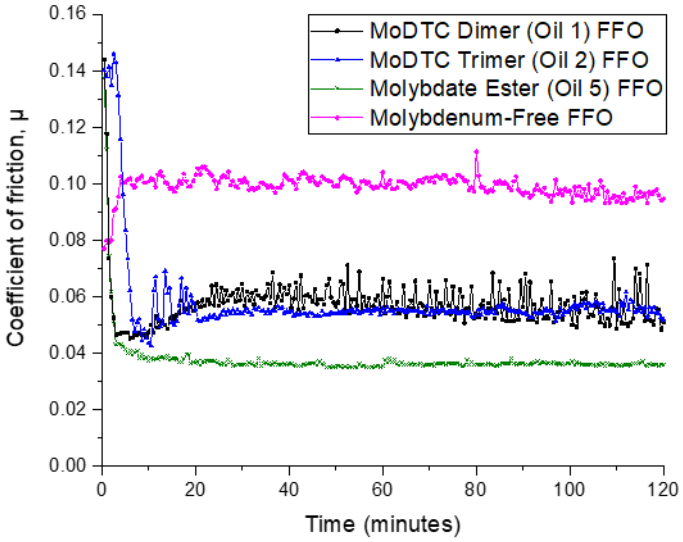


Figure 6.3 Friction profiles for molybdenum additive fully-formulated systems

In the fully-formulated tests, the friction performances of the MoDTC Dimer (Oil 1) and the MoDTC Trimer (Oil 2) were comparable, with each settling to a final friction coefficient of μ = 0.55 after a period of 20 minutes. Like the monoblends, the MoDTC trimer (Oil 2) did show a slightly longer induction period than the dimer, but the difference was not as pronounced as in the monoblends.

The overall friction performance of the oil systems is summarised in Figure 6.4. The final friction coefficient was determined by taking the mean friction coefficient from all the data points in the last ten minutes of the test.

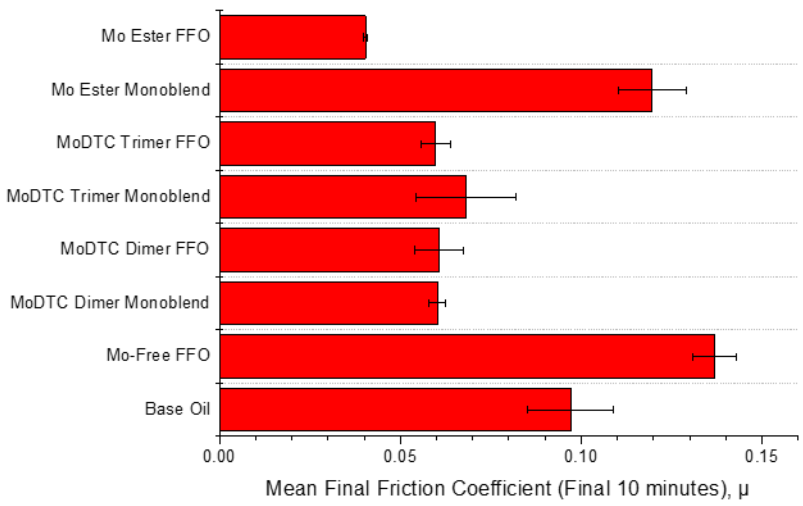


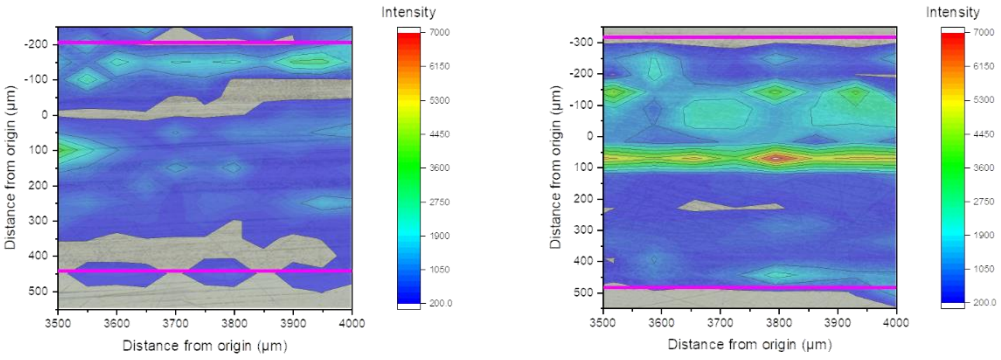
Figure 6.4 Final friction performance of molybdenum oil systems

The friction performance of the MoDTC Dimer (Oil 1) and MoDTC Trimer (Oil 2) was comparable in the fully-formulated systems, with the MoDTC trimer displaying slightly higher friction than the dimer in the monoblends. The molybdate ester (Oil 5) consistently displayed a lower final friction coefficient than the MoDTC Dimer (Oil 1), or Trimer (Oil 2) in the fully-formulated systems. This is somewhat surprising as this additive must undergo some sulfur-exchange reaction in order to form MoS_2, unlike the MoDTC Dimer (Oil 1) and Trimer (Oil 2), which are able to form MoS_2 from unimolecular decomposition.

6.3 Raman analysis of tribofilm wear scars

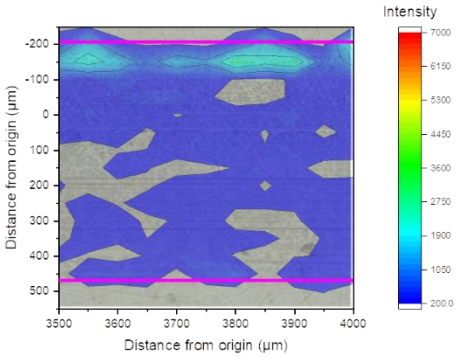
In previous work, it has been suggested that the key determinant in the friction performance of a MoS_2 tribofilm is the coverage of MoS_2 which is placed down on the contacting surfaces [126,136,147]. In order to determine if the differences in friction performance between the additive systems were due to the level of MoS_2 surface coverage, the wear scars were subjected to Raman spectroscopic mapping. By applying a lattice of point Raman spectra in a spatial distribution, the surface coverage of MoS_2 scattering peaks is determined across the wear scar. These are presented in Figure 6.5 and

Figure 6.6 for the fully-formulated systems and monoblends respectively. The maps display the intensity of the 410 cm^{-1} A_{1g} vibration, superimposed on the wear scar, with a minimum intensity threshold of 200 counts. The minimum intensity threshold was set so that random noise did not show up in the map spectrum.



a) MoDTC Dimer (Oil 1) FFO

b) MoDTC Trimer (Oil 2) FFO



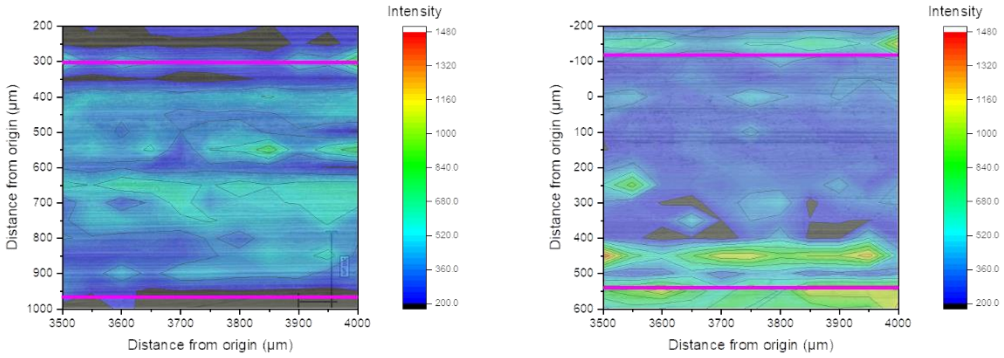
c) Molybdate Ester (Oil 5) FFO

Figure 6.5 MoS_2 410 cm^{-1} surface distribution in fully-formulated oil systems. Pink lines show the outer bounds of the wear scar area.

For all of the fully-formulated systems, the distribution of MoS_2 was patchy, with pockets of higher intensity scattering interspersed in an incomplete film of low intensity spectra. In these fully-formulated systems the areas of highest intensity were found outside the wear scar where MoS_2 is likely to be pushed as wear debris, and in the centre of the stroke where tribological conditions are likely to be their most harsh. The scattering intensity was greater for the MoDTC trimer than for the MoDTC dimer. The MoDTC

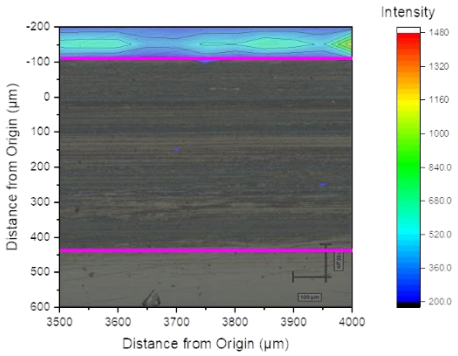
trimer also appeared to display a more consistent film than either the MoDTC dimer or the molybdate ester.

The molybdate ester, despite having the lowest friction coefficient, displayed the lowest scattering intensity and surface coverage of all of the oil systems. The small patches of higher intensity scattering observed for this system actually occur as wear debris outside of the wear scar.



a) MoDTC Dimer (Oil 1) Monoblend

b) MoDTC Trimer (Oil 2) Monoblend



c) Molybdate Ester (Oil 5) Monoblend

Figure 6.6 MoS_2 410 cm^{-1} surface distribution in monoblend systems. Pink lines show the outer bounds of the wear scar area.

Like the fully-formulated systems, the monoblend systems displayed a patchy distribution of MoS_2 scattering intensity within the wear scar. In contrast to the fully formulated systems however, the scattering within the wear scar of the MoDTC dimer was greater than that of the trimer.

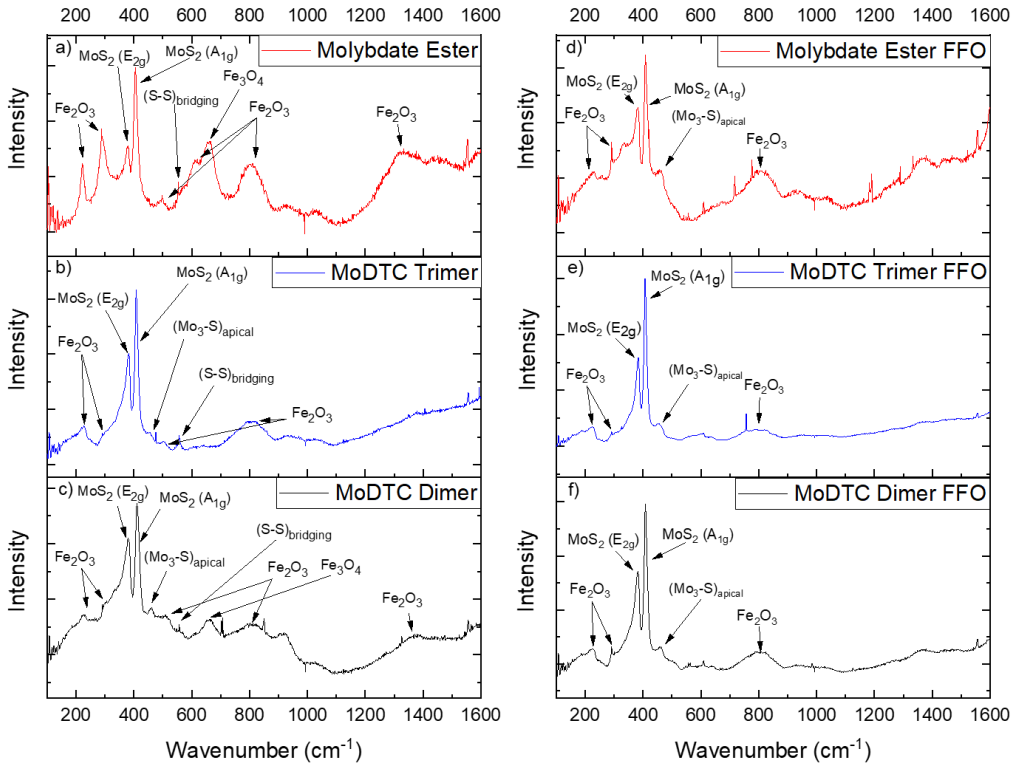
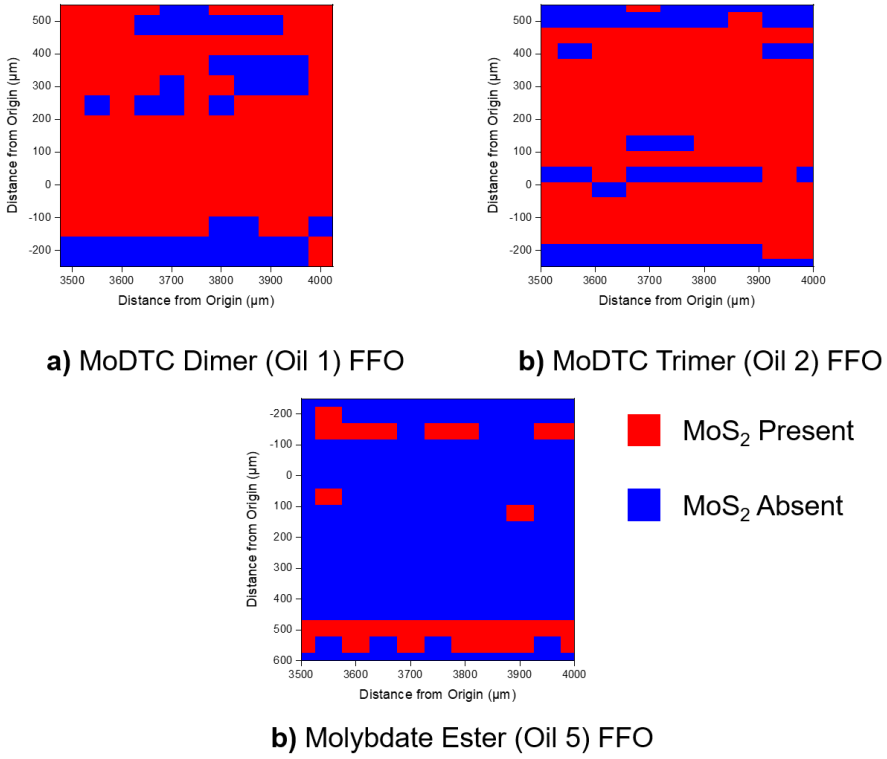


Figure 6.7 Mean Raman spectra derived from Raman mapping data of fully-formulated and monoblend additive tribofilms

a) Molybdate ester monoblend, b) MoDTC trimer monoblend, c) MoDTC dimer monoblend, d) Molybdate ester fully-formulated oil, e) MoDTC trimer fully-formulated oil, f) MoDTC dimer fully-formulated oil

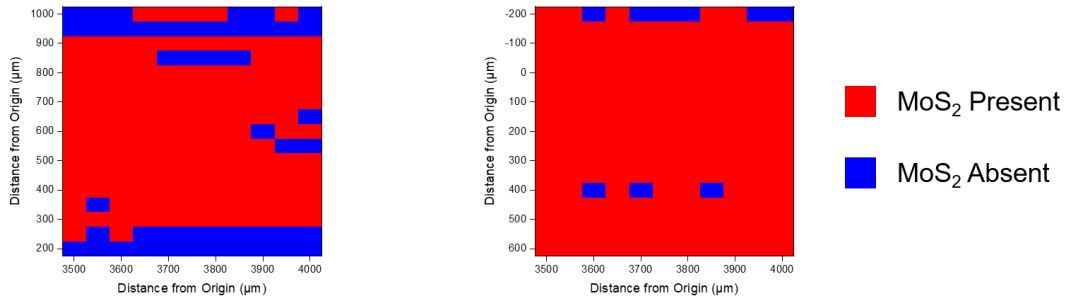
In Figure 6.5 and Figure 6.6, the minimum scattering intensity was 200 counts. This value can be exceeded by noise in some spectra, especially those with high scattering peaks from iron oxides. However, to raise the threshold further would lead to some MoS_2 scattering peaks to be missed out on the coverage maps. These higher noise value spectra can skew the perceived level of surface coverage from the Raman maps, and make it appear that MoS_2 surface coverage is actually greater than it is. In order to provide a more accurate picture of the MoS_2 surface coverage, individual spectra which compose the Raman maps were inspected and the presence or absence of MoS_2 A_{1g} and E^1_{2g} peaks noted. Binary maps showing the presence or absence of MoS_2 are presented in Figure 6.8 and Figure 6.9.



a) MoDTC Dimer (Oil 1) FFO **b)** MoDTC Trimer (Oil 2) FFO

b) Molybdate Ester (Oil 5) FFO

Figure 6.8 Binary MoS_2 distribution in fully-formulated oils



a) MoDTC Dimer (Oil 1) Monoblend **a)** MoDTC Trimer (Oil 2) Monoblend

Figure 6.9 Binary MoS_2 distribution in monoblend oils

It can be seen from the MoS_2 distribution maps in Figure 6.88 that there is less area coverage of MoS_2 in the wear scar of the molybdate ester system than the dimer and trimer systems. The MoDTC dimer and MoDTC trimer showed an even surface coverage across the wear scar. In contrast, the molybdate ester had only a very patchy distribution in the wear scar, with MoS_2 wear debris found outside of the wear scar. This result contrasts with the results of Oumahi et al. [102] who found that surface coverage of MoS_2 derived

from the molybdate ester of greater than 60 % were required to achieve a friction coefficient value of μ = 0.04.

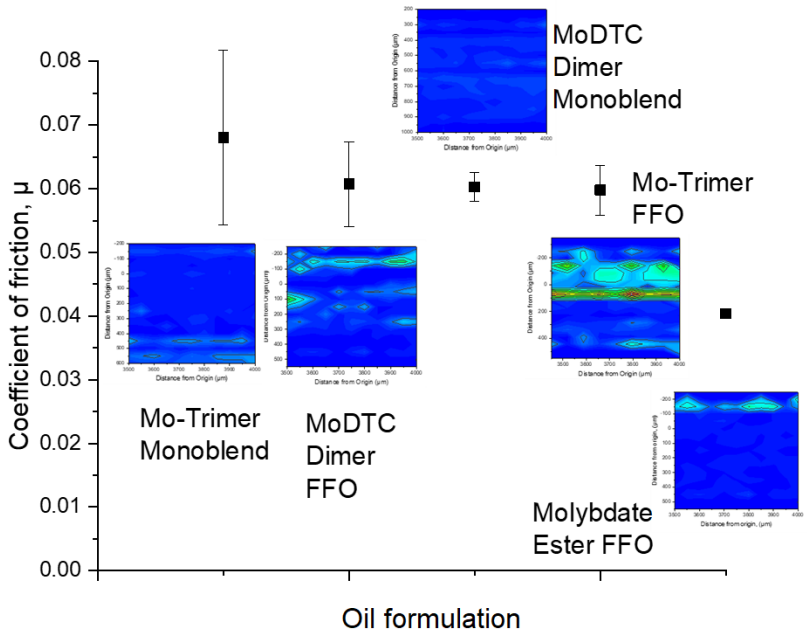


Figure 6.10 Raman surface coverage maps superimposed upon friction performance

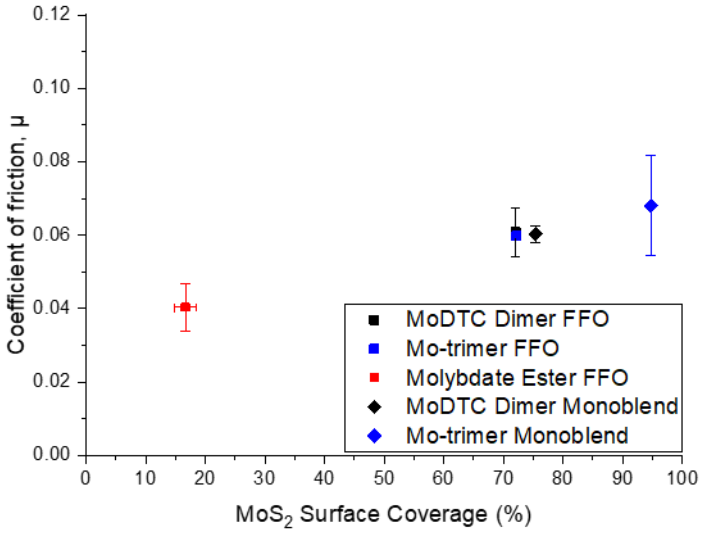


Figure 6.11 Friction performance of additive systems with MoS_2 Raman surface coverage

In addition to the A_{1g} and E^1_{2g} peaks of MoS_2 studied, the tribofilms all displayed an additional peaks at 456, 518 and 555 cm^{-1} that can be identified as the vibration of molybdenum with the apical sulfur in Mo_3S_{13} core units, S-S terminal and S-S bridging vibrations such as those found in the structure of the MoDTC trimer [206]. This spectral feature was found for all of the additive films to some degree but was more prevalent for the trimer (Figure 6.12). This suggests this feature is a common part of the decomposition products of all of the additives.

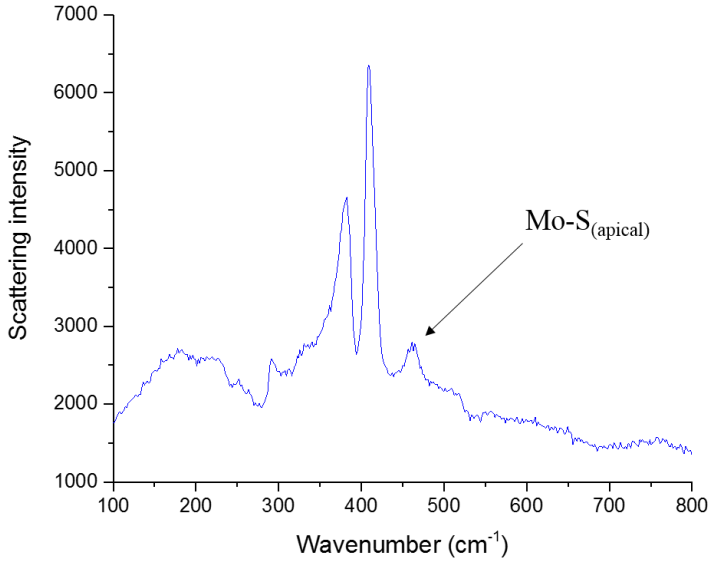


Figure 6.12 Representative MoDTC trimer Raman spectrum

To determine if any of the oil systems showed had a greater contribution from amorphous MoS_3 peaks than the others, the peak ratios between the Fe_2O_3 291 cm^{-1} vibrational mode and the three identifiable MoS_3 peaks at 456 cm^{-1} (Mo_3-S_{apical}), 518 cm^{-1} (S-$S_{terminal}$) and 555 cm^{-1} (S-S)$_{bridging}$ were calculated for the mapping spectra which contained an MoS_2 A_{1g} scattering intensity of 200 counts or greater, as in Figure 6.5 and Figure 6.6. This 291 cm^{-1} Fe_2O_3 peak was chosen as it is common in the mapping spectra, has a sharply defined maximum unlike the 220 cm^{-1} and 808 cm^{-1} peaks and like the MoS_3 peak region, is affected by the MoS_2 fluorescence signal more closely than the other iron oxide peaks. The peak intensity ratios are presented in Figure 6.13. In both the monoblends and the fully-formulated systems a slight

increase in the relative MoS_3 peak intensity was observed for the MoDTC trimer compared to the other two additives.

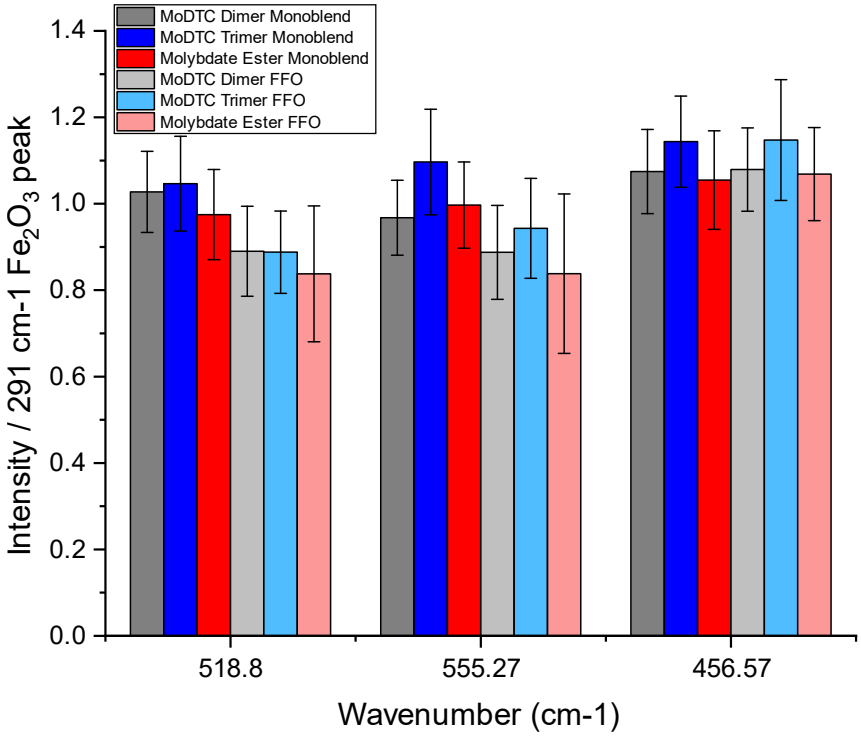


Figure 6.13 Relative peak intensity of MoS_3 scattering peaks to the 291 cm^{-1} Fe_2O_3 peak

6.4 XPS characterisation of tribofilms

The molybdenum centres in the three additive structures are present in differing oxidation states in their molecular forms. The MoDTC dimer has a Mo (V) centre, whereas the molybdenum centres of the MoDTC trimer and the molybdate ester are in Mo (IV) and Mo (VI) oxidation states respectively. To determine if the additive oxidation state had any effect upon the distribution and abundances of oxidation states present on the surface, XPS was performed on the plate wear scars. The Mo 3d region can be used to easily distinguish between Mo oxidation states. The sulfur S 2p region is also an effective indicator of the presence and chemical state of surface sulfur. XPS was performed on both the fully formulated systems (Figure 6.14) and the

monoblend systems (Figure 6.15). Peaks were fit with a Gaussian-Lorentzian peak model on a Shirley background, the reasoning for which is outlined on page 106. Peak widths and intensity ratios were determined by comparison to molybdenum and sulfur standards presented in the XPS Handbook [207], using a fitting strategy outlined by Sherwood [208]. Peak positions were determined by comparison with selected references of molybdenum and sulfur compound standards, along with previous literature of electrochemically-deposited and tribologically-derived MoS_3 and MoS_2 films [96,97,208–213].

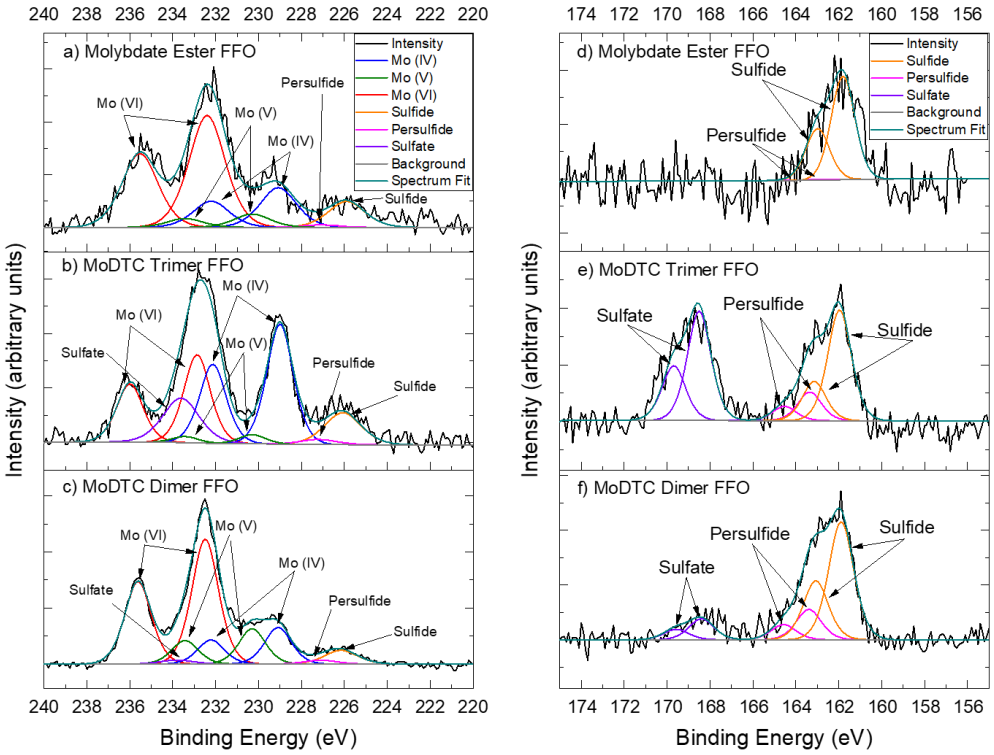


Figure 6.14 Wear scar XPS of fully-formulated Mo 3d and S 2p environments

a) Molybdate ester fully-formulated oil Mo 3d region, b) MoDTC trimer fully-formulated oil Mo 3d region, c) MoDTC dimer fully-formulated oil Mo 3d region, d) Molybdate ester fully-formulated oil S 2p region, e) MoDTC trimer fully-formulated oil S 2p region, f) MoDTC dimer fully-formulated oil S 2p region

Table 20: XPS peak information for the fully-formulated oil tribofilms

	MoDTC Dimer FFO			MoDTC Trimer FFO			Molybdate Ester FFO		
Peak	Position (eV)	FWHM	% At conc	Position (eV)	FWHM	% At conc	Position (eV)	FWHM	% At conc
Mo (VI) 5/2	232.49	1.46	22.86	232.87	1.45	7.20	232.40	1.98	21.05
Mo (VI) 3/2	235.62	1.46	13.15	236.00	1.45	4.14	235.53	1.98	12.10
Mo (V) 5/2	230.30	1.46	7.11	230.30	1.45	0.84	230.30	1.98	2.58
Mo (V) 3/2	233.43	1.46	4.13	233.43	1.45	0.49	233.43	1.98	1.50
Mo (IV) 5/2	229.09	1.46	7.78	229.00	1.45	11.60	229.11	1.98	8.89
Mo (IV) 3/2	232.22	1.46	4.48	232.13	1.45	6.68	232.24	1.98	5.12
S2s Sulfide	226.16	1.81	27.30	226.07	2.00	32.10	225.90	2.00	44.55
S2s Persulfide	227.10	1.81	7.47	227.20	2.00	4.89	227.10	2.00	4.23
S2s Sulfate	233.80	1.81	5.72	233.62	2.00	32.07	N/A		
S2p Sulfide (3/2)	161.89	1.37	43.96	161.96	1.29	25.67	161.80	1.21	60.61
S2p Sulfide (1/2)	163.07	1.37	21.98	163.14	1.29	9.11	162.98	1.21	30.30
S2p Persulfide (3/2)	163.40	1.37	11.33	163.35	1.29	6.64	163.22	1.21	6.06
S2p Persulfide (1/2)	164.58	1.37	5.67	164.53	1.29	3.32	164.40	1.21	3.03
S2p Sulfate (3/2)	168.40	1.37	13.14	168.51	1.29	42.57	N/A		
S2p Sulfate (1/2)	169.58	1.37	3.92	169.69	1.29	12.79	N/A		

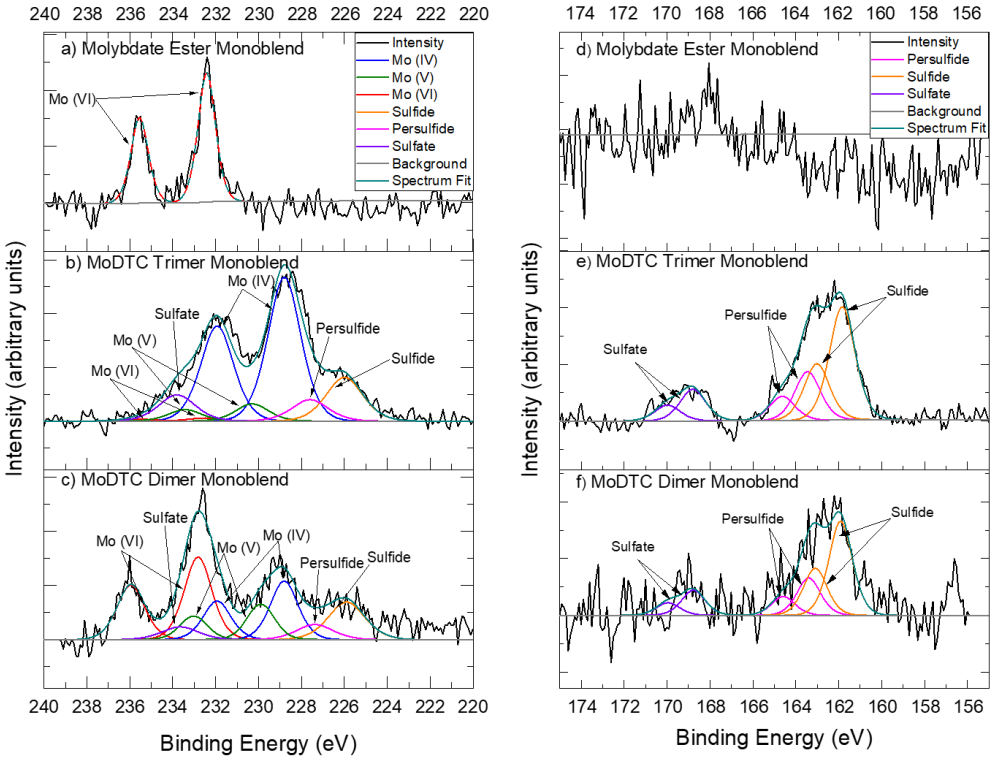


Figure 6.15 wear scar XPS of monoblend Mo 3d and S 2p environments

a) Molybdate ester monoblend oil Mo 3d region, b) MoDTC trimer monoblend oil Mo 3d region, c) MoDTC dimer monoblend oil Mo 3d region, d) Molybdate ester monoblend oil S 2p region, e) MoDTC trimer monoblend oil S 2p region, f) MoDTC dimer monoblend oil S 2p region

Table 21: XPS peak information for the monoblend oil tribofilms

	MoDTC Dimer Monoblend			MoDTC Trimer Monoblend			Molybdate Ester Monoblend		
Peak	Position (eV)	FWHM	% At conc	Position (eV)	FWHM	% At conc	Position (eV)	FWHM	% At conc
Mo (VI) 5/2	232.81	1.53	8.19	232.5	1.80	0.32	232.41	0.96	63.48
Mo (VI) 3/2	235.94	1.53	4.71	235.63	1.80	0.19	235.55	0.96	36.52
Mo (V) 5/2	229.90	1.53	3.65	230.30	1.80	1.53	N/A		
Mo (V) 3/2	233.03	1.53	2.12	233.43	1.80	0.89	N/A		
Mo (IV) 5/2	228.83	1.53	4.71	228.80	1.80	15.16	N/A		
Mo (IV) 3/2	231.96	1.53	3.86	231.93	1.80	8.72	N/A		
S2s Sulfide	225.90	2.00	43.63	226.01	2.00	38.87	N/A		
S2s Persulfide	227.34	2.00	16.56	227.6	2.00	17.76	N/A		
S2s Sulfate	233.64	2.00	10.57	233.8	2.00	16.56	N/A		
S2p Sulfide (3/2)	161.91	1.29	37.30	161.84	1.40	35.07	N/A		
S2p Sulfide (1/2)	163.09	1.29	18.65	163.02	1.40	35.07	N/A		
S2p Persulfide (3/2)	163.40	1.29	14.86	163.40	1.40	15.12	N/A		
S2p Persulfide (1/2)	164.58	1.29	7.43	164.63	1.40	7.56	N/A		
S2p Sulfate (3/2)	168.78	1.29	16.76	168.80	1.40	16.48	N/A		
S2p Sulfate (1/2)	169.96	1.29	5.00	169.98	1.40	8.24	N/A		

Each of the three molybdenum additive systems, MoDTC dimer, MoDTC trimer and molybdate ester, displayed both Mo (IV) and Mo (VI) oxidation state environments for the fully-formulated oil systems (Figure 6.14) in the Mo 3d binding energy region. This assignment of oxidation states agrees with those determined by previous XPS studies [85,96,143,213,214]. The presence of Mo (IV) is due to the presence of MoS_2 and amorphous Mo:S species. The molybdate ester monoblend (Figure 6.15 **f)**) showed no Mo (IV) state corresponding to MoS_2, and no surface sulfur in the S 2p region, confirming the lack of MoS_2 formation in this system inferred from friction results. However, molybdenum was still found on the steel surface for this system in a Mo (VI) oxidation state, at a binding energy of 232.5 eV typically associated with molybdenum trioxide (MoO_3). No MoO_3 was observed in the Raman spectra of any of the additive systems studied. The MoDTC dimer and the MoDTC trimer showed both Mo (IV) and (VI) environments in the monoblends (Figure 6.15) but did so with different relative ratios of oxidation states.

The MoDTC trimer XPS spectra found a greater proportion of the Mo (IV) state on the surface relative to the MoDTC dimer and the molybdate ester. This suggests a greater relative abundance of Mo (IV) species on the surface, due either to a greater proportion of MoS_2 and Mo:S amorphous Mo (IV) species in the film, or a resistance of the formed film to oxidation.

6.5 Nanoscale tribofilms

To determine if the MoDTC trimer's increased relative abundance of the Mo (IV) oxidation state was the result of a greater proportion of Mo:S species on the surface, FIB-TEM sections were cut to determine the film thicknesses and distributions of the films on the nanoscale. Areas of highest scattering within the monoblend wear scars were selected for FIB sectioning. The elemental distributions within the tribofilms were studied with EDX.

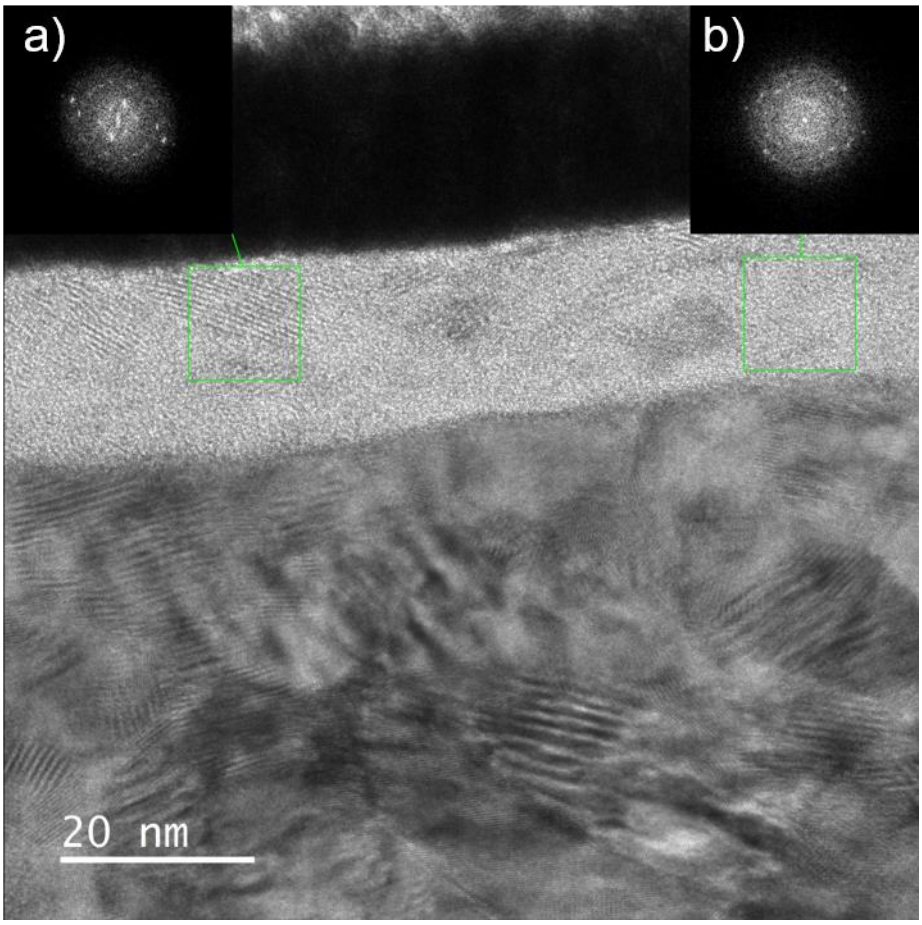


Figure 6.16 MoDTC trimer tribofilm crystallinity

(inset) a) FFT of crystalline region, b) FFT of amorphous region

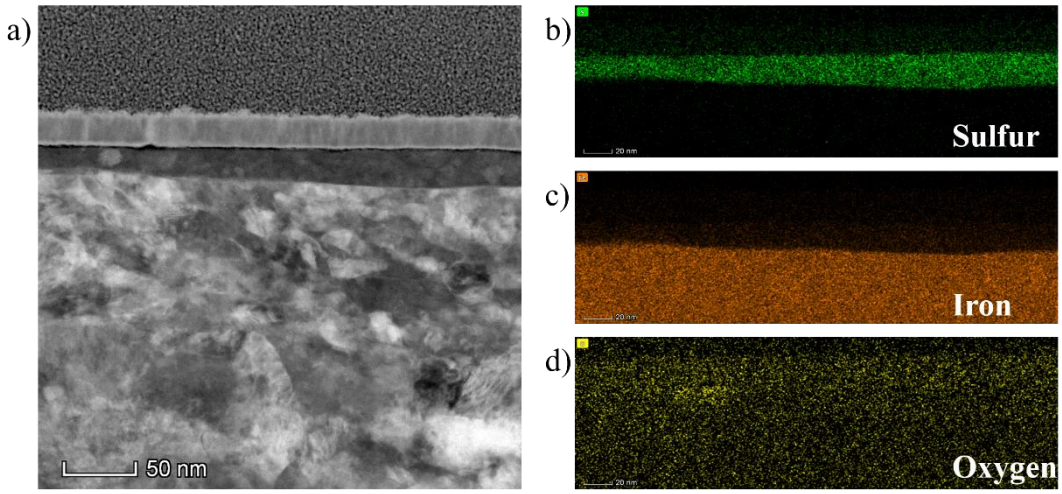


Figure 6.17 FIB-TEM cross-section of MoDTC trimer tribofilm

a) High Resolution image of MoDTC Trimer tribofilm b) Sulfur EDX of zoomed out tribofilm, c) Iron EDX of tribofilm, d) Oxygen EDX of tribofilm

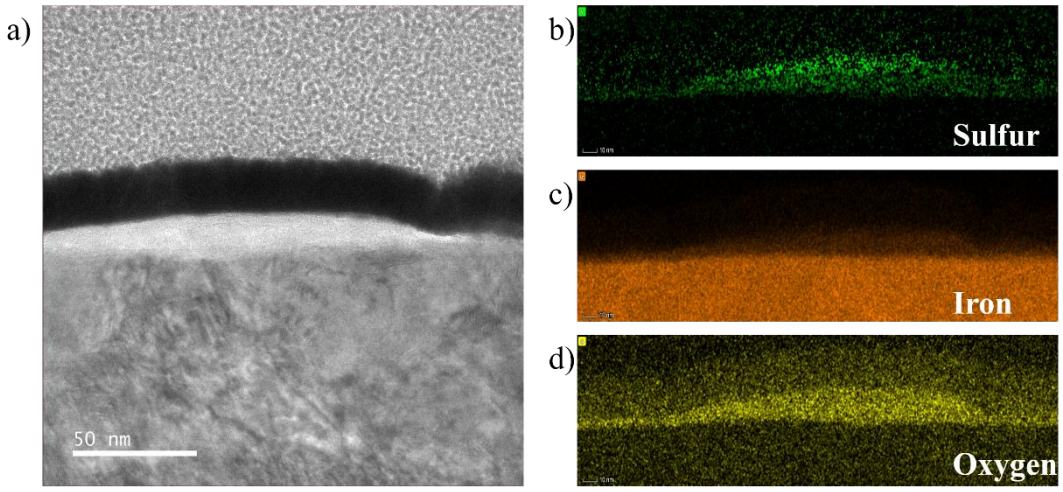


Figure 6.18 FIB-TEM cross-section of MoDTC dimer tribofilm

a) High resolution image of MoDTC dimer tribofilm b) Sulfur EDX of tribofilm c) Iron EDX of tribofilm, d) Oxygen EDX of tribofilm

The MoDTC trimer monoblend (Figure 6.17) tribofilm shows a consistent layer across FIB section of Mo:S species (as shown by EDX). The film is composed of a mixture of amorphous and crystalline domains highlighted in Figure 6.16. Amorphous regions of Mo:S have been proposed as intermediates in MoS_2 formation by Khaemba and Oumahi and can be seen in the tribofilms of Rai et al. [134,145,147]. The MoS_2 crystalline domains are oriented in the sliding direction at the very surface but the subsurface crystalline regions have random orientations. The film had a consistent distribution of iron particles within it (Figure 6.17c). In contrast to the structure of the MoDTC trimer film, the MoDTC dimer tribofilm did not show a consistent layer of Mo:S species across the FIB section and these elements were only found in increased concentration in small patches atop iron oxide asperities. This can be seen in the sulfur EDX image (Figure 6.17b) of the dimer, there is a localised increase in sulfur concentration at the top of the iron oxide particle surface.

6.6 Tribofilm durability

The TEM cross sections of the MoDTC dimer and MoDTC trimer monoblends show that the film derived from the MoDTC dimer monoblend is much thinner than that formed from the MoDTC trimer, which displays a consistent 20 nm thick layer across the entire steel surface.

In order to determine if this increase in amount of Mo:S species observed in the MoDTC trimer TEM resulted in a more durable tribofilm, a durability test similar to that conducted by Morina and Neville was performed [74]. A tribofilm was created for the MoDTC dimer and MoDTC trimer monoblends under the conditions listed in Table 12 and after thirty minutes the additive-containing oil was removed, the oil bath cleaned with heptane and then filled with base oil. The components were removed and ultrasonically rinsed in heptane for 10 minutes to ensure no residual additive-containing oil was present before being replaced in the tribometer. Similar tests were performed for the fully-formulated systems except in these tests the replacement oil inserted after 30 minutes was a Mo-free fully-formulated oil, rather than base oil.

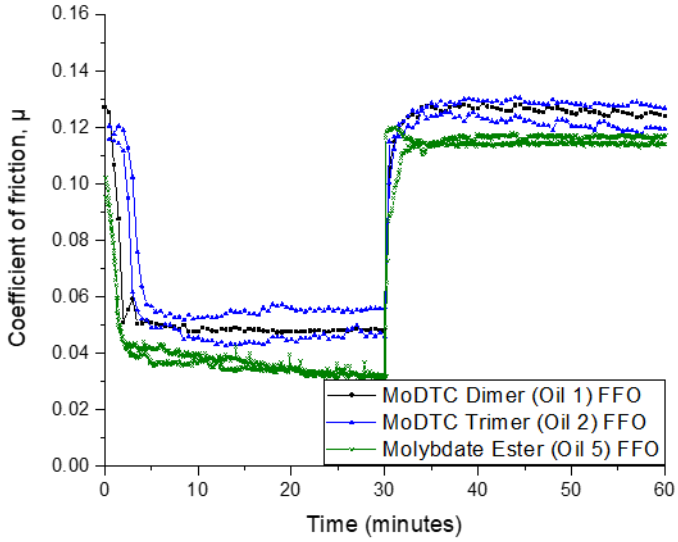


Figure 6.19 Fully-formulated tribofilm durability test friction profile

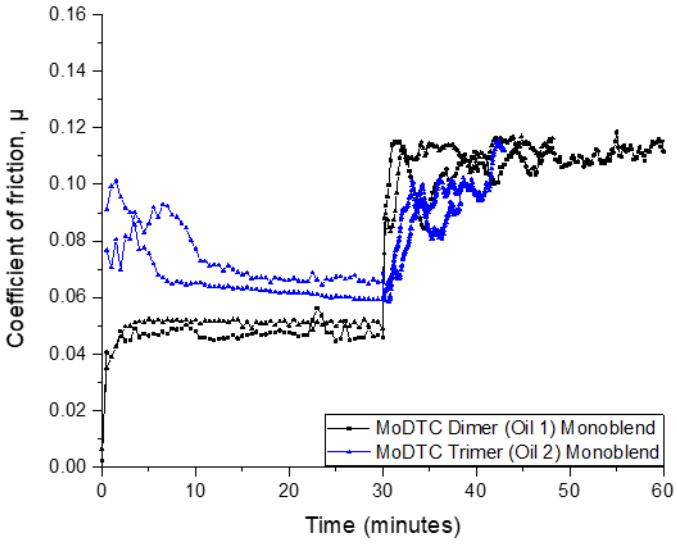


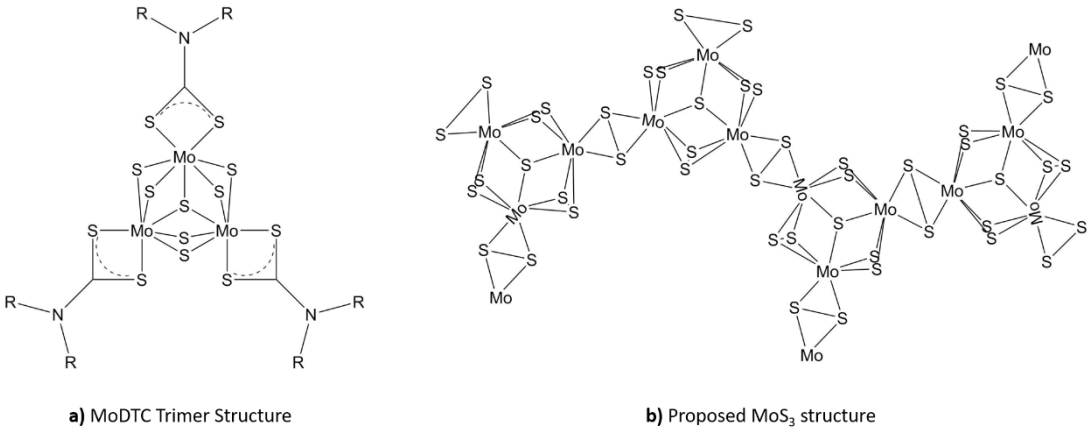
Figure 6.20 Monoblend tribofilm durability test friction profile

Figure 6.20 shows that the MoDTC trimer took slightly longer to reach base oil friction levels again upon oil replacement by base oil than did the MoDTC dimer, but both additives had effectively returned to base oil friction coefficients after ten minutes. This suggests additives which deposit more Mo:S species on the surface may create more durable tribofilms. In the fully-formulated systems (Figure 6.19) there was no difference in rate of friction rise between the additives, unlike the monoblends. This suggests that the MoS_2 sheets in the fully-formulated systems sit upon the top of a ZDDP layer in a much thinner configuration than those bound to the iron surface in the monoblends.

6.7 Amorphous molybdenum sulfides as a decomposition intermediate

The MoDTC trimer TEM displayed a sulfur-rich tribofilm with amorphous and crystalline domains. As the structure of the MoDTC trimer has excess sulfur, with a Mo_3S_{13} core (Figure 6.21) it is perhaps not surprising that such a sulfur-rich film is formed upon decomposition. A series of mixed stoichiometry amorphous molybdenum sulfides are known of the form MoS_x. These species have been found to be effective catalysts for hydrogen

evolution and have been proposed as decomposition intermediates in the formation of MoS_2 from both the MoDTC dimer and molybdate ester [98,102,215]. One of the better known of these species is molybdenum trisulfide (MoS_3), which shares a proposed structural form with the core of the MoDTC trimer. MoS_3 is proposed to exist as chains of triangular Mo_3S_{13} units joined by bridging disulfide ligands [216,217].



a) MoDTC Trimer Structure

b) Proposed MoS_3 structure

Figure 6.21 Structure of MoDTC trimer and MoS_3

In order to determine if the amorphous species observed in the TEM images was likely to be MoS_3, a sample was created thermally by the thermal decomposition of ammonium tetrathiomolybdate under a nitrogen atmosphere.

Ammonium tetrathiomolybdate thermally decomposes in two stages. The first at 180 °C with the release of ammonia and hydrogen disulfide to form MoS_3 and a second stage at 350 °C to form MoS_2 (Equation 21) [103,104,140]. Each step of this reaction is accompanied by a change in mass, so the progress of the reaction can be determined by following the mass loss of the reactants. To create the MoS_3 sample in this study, a sample of ammonium tetrathiomolybdate was heated under nitrogen from room temperature to 240°C and held at this isotherm for 20 minutes. This was performed in a thermogravimetric analyser to ensure that the reaction stopped after the production of MoS_3 and no MoS_2 was formed. The thermogravimetric profile of the decomposition is presented in Figure 6.22. Figure 6.21 shows the first reaction step corresponding to the formation of the MoS_3 decomposition

intermediate. XPS analysis of the Mo 3d and S 2p regions was performed on the resulting black solid (Figure 6.23 and Figure 6.24).

$$(NH_4)_2MoS_4 \xrightarrow{180°C} MoS_3 + 2NH_3 + H_2S \xrightarrow{350°C} MoS_2 + S$$

Equation 21 Thermal decomposition of ammonium tetrathiomolybdate $(NH_4)_2MoS_4$

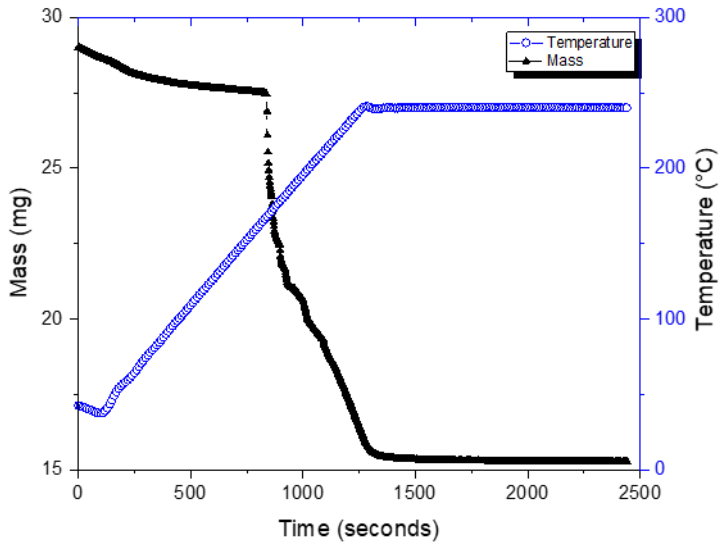


Figure 6.22 Thermogravimetric profile of MoS_3 preparation from ammonium tetrathiomolybdate

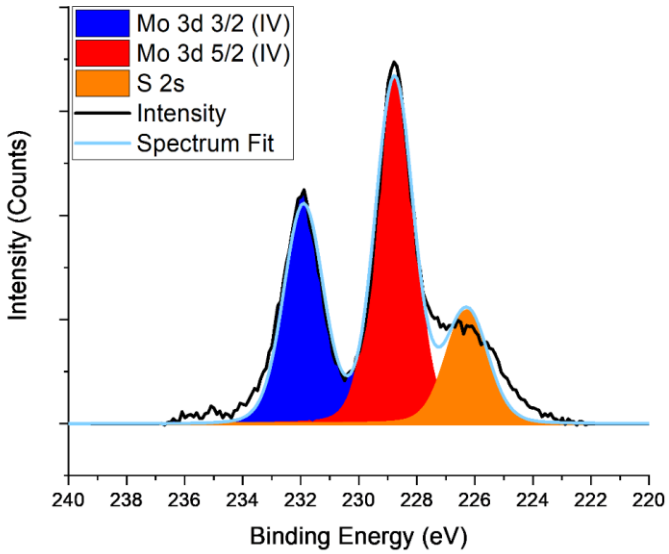


Figure 6.23 XPS spectrum of MoS_3 sample Mo 3d region

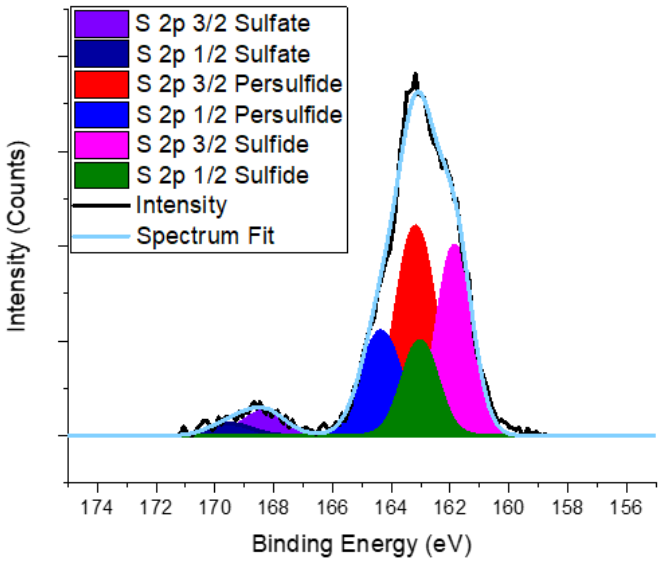


Figure 6.24 XPS spectrum of MoS_3 sample Mo S 2p region

In Figure 6.23 and Figure 6.24, the MoS_3 standard displayed only a Mo (IV) oxidation state and a mixture of sulfide and persulfide environments in the S 2p region. A small amount of sulfate-type S environment was observed at 174 eV due to surface oxidation. The XPS assignments of the S 2p environment agree well with those of films of deposited Mo_3S_{13} clusters found

in the literature [218,219]. The spectrum of the Mo 3d environment suggests that MoS_3 is a candidate for the increased amount of Mo (IV) amorphous species displayed by the MoDTC trimer in XPS. MoS_3 is one of a series of amorphous molybdenum sulfides which can have a Mo (IV) oxidation state [106,220,221]. Therefore, it cannot be conclusively stated that MoS_3 specifically is present on the surface, but it can be confidently asserted that amorphous molybdenum sulfides of MoS_3-type are formed.

To confirm that the thermal decomposition product was MoS_3, and had not gone on to form crystalline MoS_2, Raman spectroscopy was performed under the conditions described in Table 16, except in this instance, 20 accumulations were performed to improve the signal-to-noise ratio, as amorphous MoS_3 is a poor Raman scattering species. The results are presented in Figure 6.25**.** If crystalline MoS_2 were present in the sample, the scattering peaks of MoS_2 would drown out any of the MoS_3 peaks. There is a peak observed in the 380 cm^{-1}, but no corresponding peaks around 410 cm^{-1} which sits in the valley of the MoS_3 spectrum. From this, it is concluded that there is no significant amount of crystalline MoS_2 in the thermally prepared MoS_3 sample.

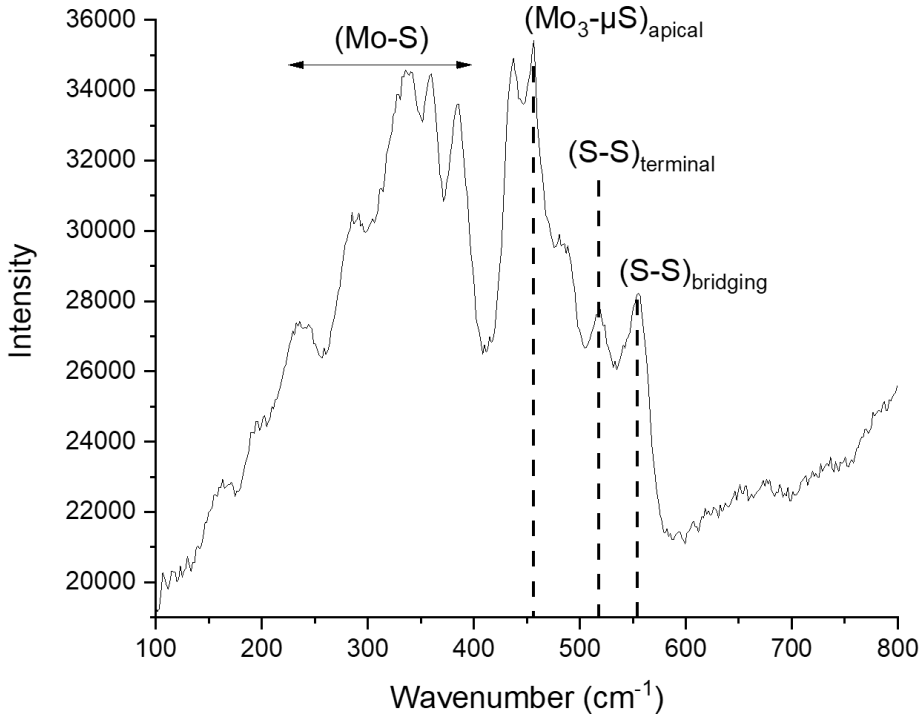


Figure 6.25 Raman spectrum of MoS_3 sample

6.8 Summary

In this Chapter the nature of tribofilms derived from differing molybdenum additive chemistries were studied. The films were characterised in terms of their friction coefficients, surface distribution, chemical composition, nanoscale structure and mechanical durability. The following behaviour was observed for the range of additives studied:

- Each of the additives studied had comparable friction performance typical of MoS_2-based tribofilms. The formation of MoS_2 was confirmed with Raman spectroscopy in all cases except the molybdate ester monoblend which was unable to form a MoS_2 film.

- The tribofilms formed from all of the additives were chemically very similar, displaying a mixture of Mo (IV) MoS_2 and Mo (VI) species in similar proportions. The MoDTC trimer displayed a slight preference for the Mo (IV) oxidation state than the MoDTC dimer and the molybdate ester. This is due to the formation of the MoS_3 decomposition intermediate that is common to all of the additives, as found in the Raman and XPS spectra of all the additive tribofilms.

- Under identical tribological conditions, the MoDTC trimer monoblend produces a consistent Mo:S layer across the surface whilst the MoDTC dimer monoblend produced a much thinner film that appeared patchy and was only formed on iron oxide asperities. The MoDTC trimer produced a thicker Mo:S film because of its structural similarity to the amorphous MoS_3 decomposition intermediate.

- The thicker film formed from the MoDTC trimer monoblend led to a modest improvement in the durability of this additive relative to that of the MoDTC dimer.

- It is clear from the analysis of the films that despite there being little chemical difference observable by Raman and XPS between the films formed from the additives, there are notable physical differences in film thickness, oxidation state distribution and surface coverage. The design of the molecular additives and their interactions with other additives in the formulation do have an effect on the physical characteristics of the MoS_2 films formed.

Chapter 7: The Behaviour Of Sulfur-Starved Molybdate Ester Formulations

7.1 Introduction

In order to reduce the environmental impact of lubricant formulations, it is necessary to develop low-sulfur alternatives to current formulations. This will require the development of sulfur-free additives such as molybdate esters, which are oxymolybdate structures with amide or glycerol monooleate organic groups (Figure 7.1).

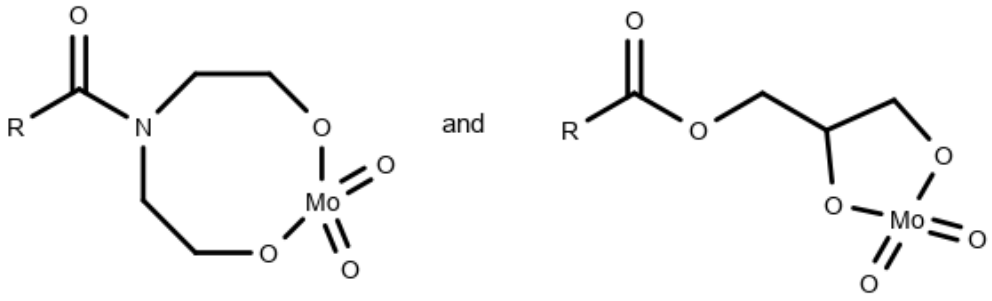


Figure 7.1 Molybdate ester structure mixture

In addition, this goal will require the reduction of sulfur content from other sulfur additives such as ZDDP. The molybdate ester is reliant on a sulfur-transfer reaction with sulfur-containing systems like ZDDP in order to form MoS_2, according to the proposed mechanism in Figure 7.2. In sulfur-rich formulations, with ZDDP concentrations of 400 ppm or greater, the molybdate ester can provide comparable friction performance to MoDTCs [137,222–224]. Some work has briefly investigated the effect of molybdate ester and ZDDP concentration on friction in a four-ball tribometer [137]. However, no systematic study of the sulfur-dependence of molybdate ester has been determined in order to find a limiting value of sulfur concentration below which the friction performance of molybdate ester is adversely affected.

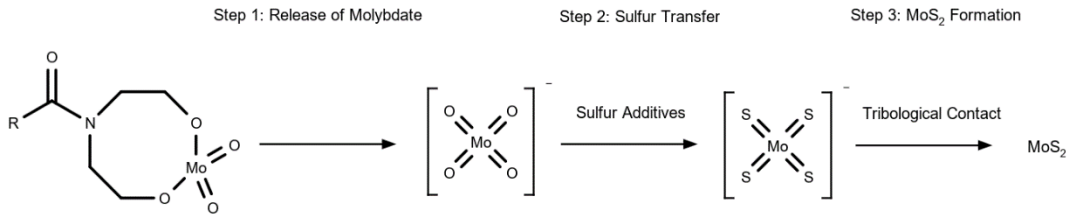


Figure 7.2 Proposed molybdate ester MoS_2 formation mechanism

The molybdate ester's friction performance has also been shown to be improved by the addition of fatty amines to the formulation [143,149]. It has been proposed that this effect is due to amine stabilisation of the molybdate ion intermediate [143].

In this chapter, the sulfur-dependence of the molybdate ester is studied in both binary systems containing just molybdate ester and ZDDP, and in fully-formulated systems. The mechanical activation parameters for friction reduction in the two oil systems are investigated. The role of additive interactions in the form of amine dispersants are studied in terms of tribofilm development and friction performance. Finally, the mechanism of MoS_2 formation from the molybdate ester is investigated to propose a rate-determining step for friction reduction.

7.2 Friction performance of molybdate ester systems

In order to investigate the sulfur-dependence of molybdate ester friction performance, a range of molybdate ester oil systems with varying degrees of sulfur starvation were studied. The oil systems all contained molybdate ester at a concentration of 400 ppm by [Mo]. Sulfur starvation levels were determined through oil systems with varying Mo:S ratio, where the sulfur concentration was varied by control of the ZDDP concentration in the oil. A Mo:S ratio of 1:2 represents a typical sulfur loading in a commercial oil.

Molybdate ester fully-formulated oil systems were subjected to tribological testing under the conditions outlined in Table 13 with smooth TE77 plates of R_a = 50 nm, at a load of 100 N and a lubricant bath temperature of 100°C. An oil containing only ZDDP, with no molybdate ester was used as a control.

7.2.1 Fully-formulated systems

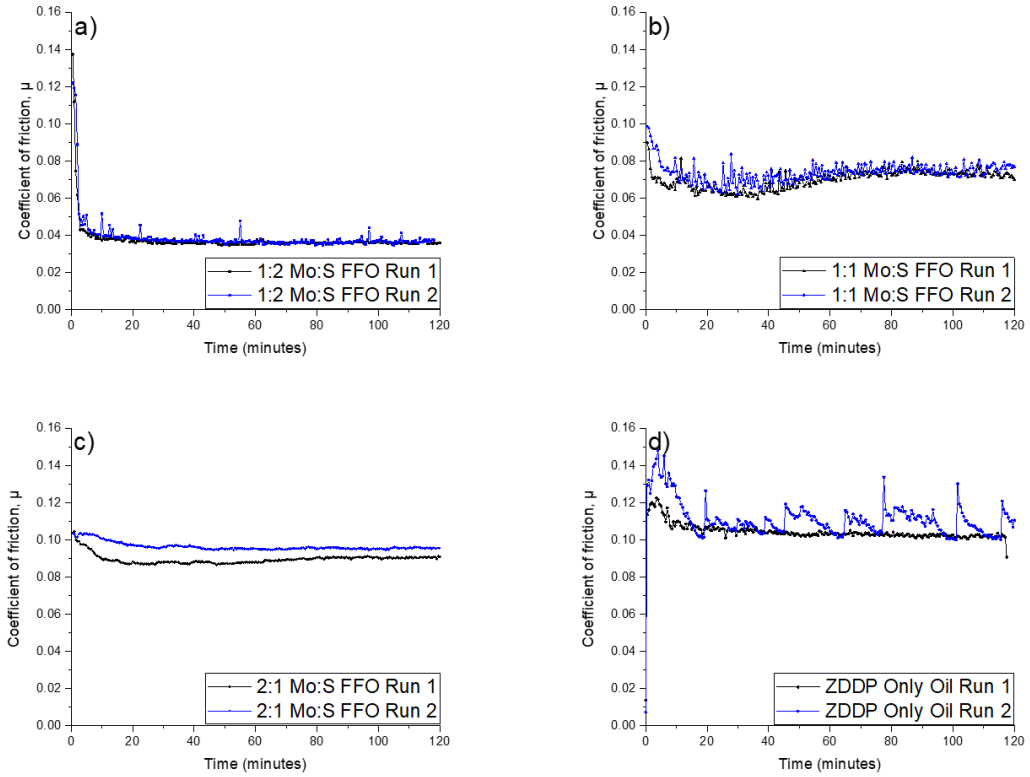


Figure 7.3 Individual friction profiles of molybdate ester FFO Mo:S ratio oils under smooth plate conditions

a) 1:2 Mo:S FFO, b) 1:1 Mo:S FFO, c) 1:1 Mo:S FFO, d) ZDDP-only control oil

In the fully-formulated systems, friction reduction was observed for all the systems relative to the ZDDP-only oil. Optimal friction performance was observed only for the 1:2 Mo:S ratio oil, where a final friction coefficient of μ = 0.04 was observed in all tests. Any reduction in the sulfur content of the oils was matched by an increase in the friction coefficient. The 1:1 and 2:1 Mo:S ratio had final friction coefficients of μ = 0.08 and 0.10 respectively. The 2:1 Mo:S ratio oil displayed only a modest improvement in friction compared to the ZDDP control.

In order to understand the relative amount of MoS_2 on the surfaces for the oil systems, Raman maps of the 410 cm^{-1} A_{1g} vibration were constructed

to analyse the surface coverage and relative intensities of MoS_2 scattering in each system.

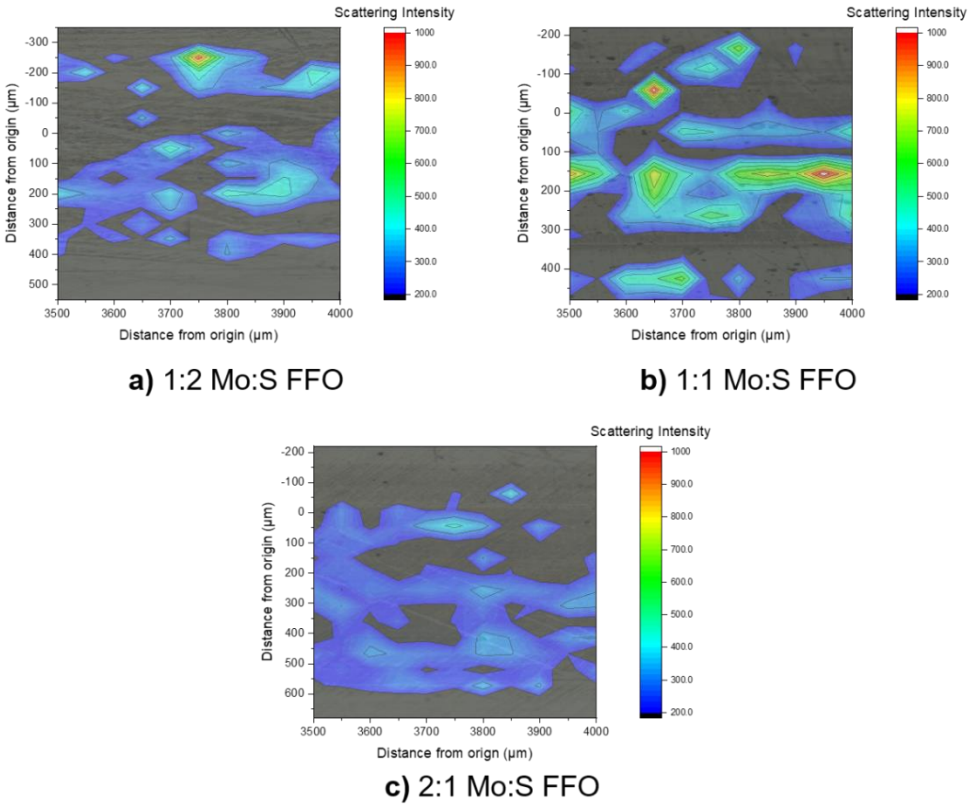


Figure 7.4 Raman surface coverage maps of 410 cm^{-1} A_{1g} vibration for Mo:S ratio FFO oils

The greatest scattering intensity was observed for the 1:1 Mo:S oil and it appears that the greatest coverage was for this oil also. However, a lot of the scattering intensity observed for the higher Mo:S ratio oils was due to the presence of iron oxides. Figure 7.7 shows the actual MoS_2 surface coverage for the Raman maps. The surface coverage decreases with increasing Mo:S ratio. As observed in the previous chapter, the surface coverage of the molybdate ester fully-formulated systems, even the low friction 1:2 ratio oil, was much lower than that observed from the sulfur-containing molybdenum additives.

7.2.2 Binary systems

7.2.2.1. Binary systems – smooth surfaces

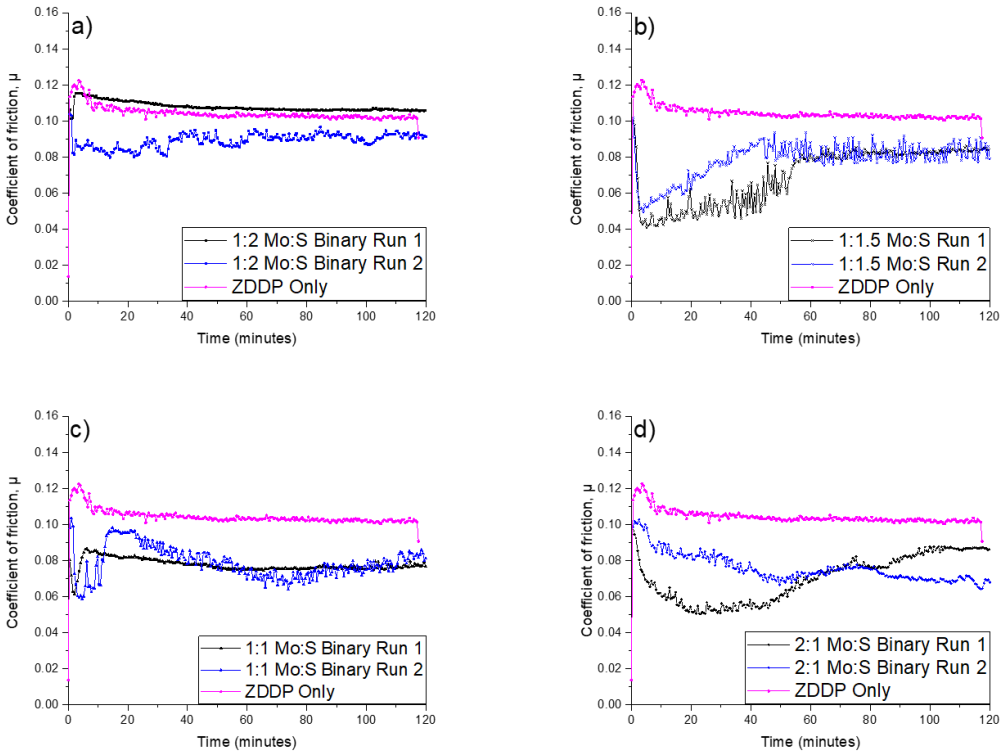


Figure 7.5 Individual profiles of molybdate ester binary Mo:S ratio oils under smooth plate conditions

a) 1:2 Mo:S binary oil, b) 1:1.5 Mo:S binary oil, c) 1:1 Mo:S binary oil, d) 2:1 Mo:S binary oil

Figure 7.5 shows the friction performance of the binary molybdate ester + ZDDP oil systems under the same conditions as the fully-formulated systems described previously. The friction performance of the binary systems was inferior to that of the fully-formulated systems, for all Mo:S ratio values except the 2:1 ratio oil.

In addition, the binary systems displayed a distinct friction profile. The friction coefficient would initially drop for a period, followed by a rise in friction towards the end of the test where the oils would tend to a friction coefficient of $\mu \approx 0.08$.

Unlike the fully-formulated oils, no clear trend in final friction coefficient was observed with Mo:S ratio. From these data it is clear that the overall friction response of the binary molybdate ester systems has not been

“activated” to provide the friction performance commonly associated with MoS_2 tribofilms.

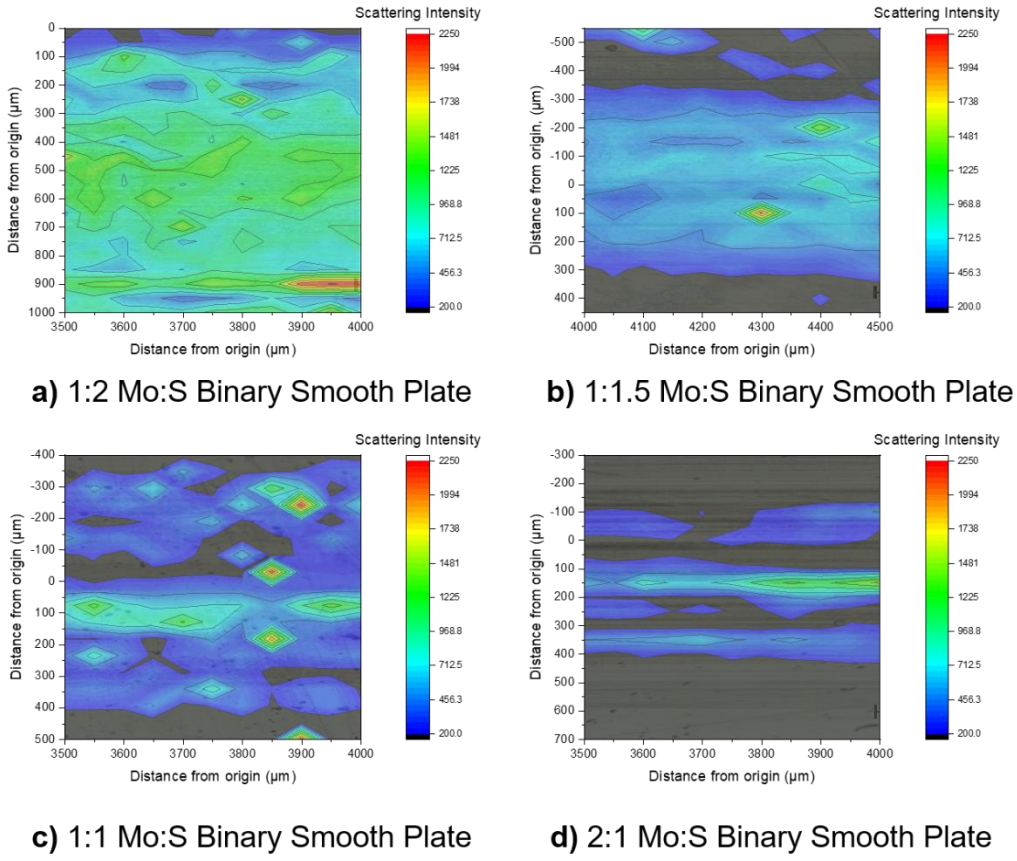


Figure 7.6 Raman surface coverage maps of 410 cm^{-1} A_{1g} vibration for Mo:S ratio binary oils in smooth plate conditions

Figure 7.6 shows the 410 cm^{-1} Raman intensity maps of the central wear scar for the binary oils. In the binary systems a distinct trend is observed of decreasing scattering intensity with increasing Mo:S ratio. However, this trend does not correlate with the actual MoS_2 surface coverage as determined from manual inspection of the spectra. Figure 7.7 shows the MoS_2 surface coverage determined from manual inspection of the mapping spectra for the presence of MoS_2.

The surface coverages of the binary systems were greater than those observed for the fully-formulated systems, but all of the molybdate ester systems had lower MoS_2 surface coverage than the MoDTC system studied in Figure 6.11.

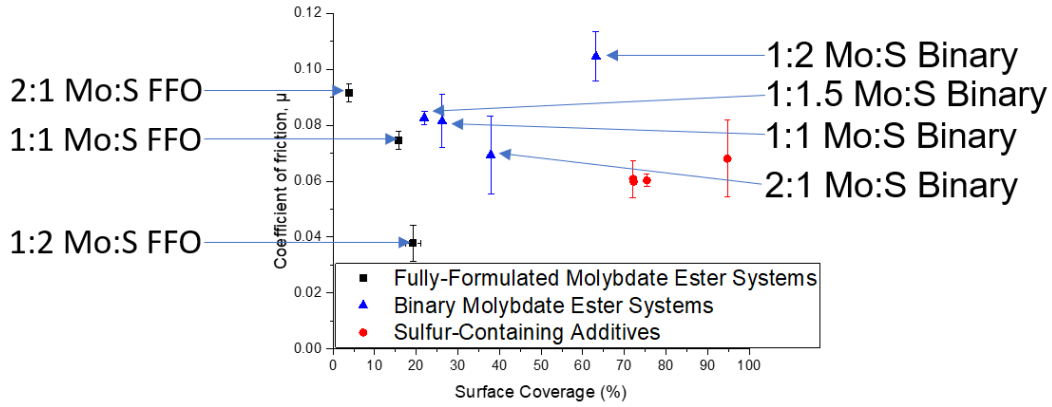


Figure 7.7 Raman surface coverage of binary and FFO Mo:S ratio oil systems with friction

7.2.2.2. Binary systems – rough plates

In the previous tests, no optimal reduction in friction was observed for the binary systems. In the literature it has been shown that binary mixtures of molybdate ester and ZDDP can provide friction coefficients of μ = 0.04 or less under conditions harsher than those studied above [143,222]. In order to understand the dependence of these binary mixtures upon sulfur ratio when their friction response had been activated, tests were run with rougher plate surfaces of R_a = 0.5 μm, maintaining all other contact conditions the same as previously. As a control to make sure the FFO friction behaviour was the same as in smooth plate conditions, the FFO tests were repeated with R_a = 0.5 μm plates.

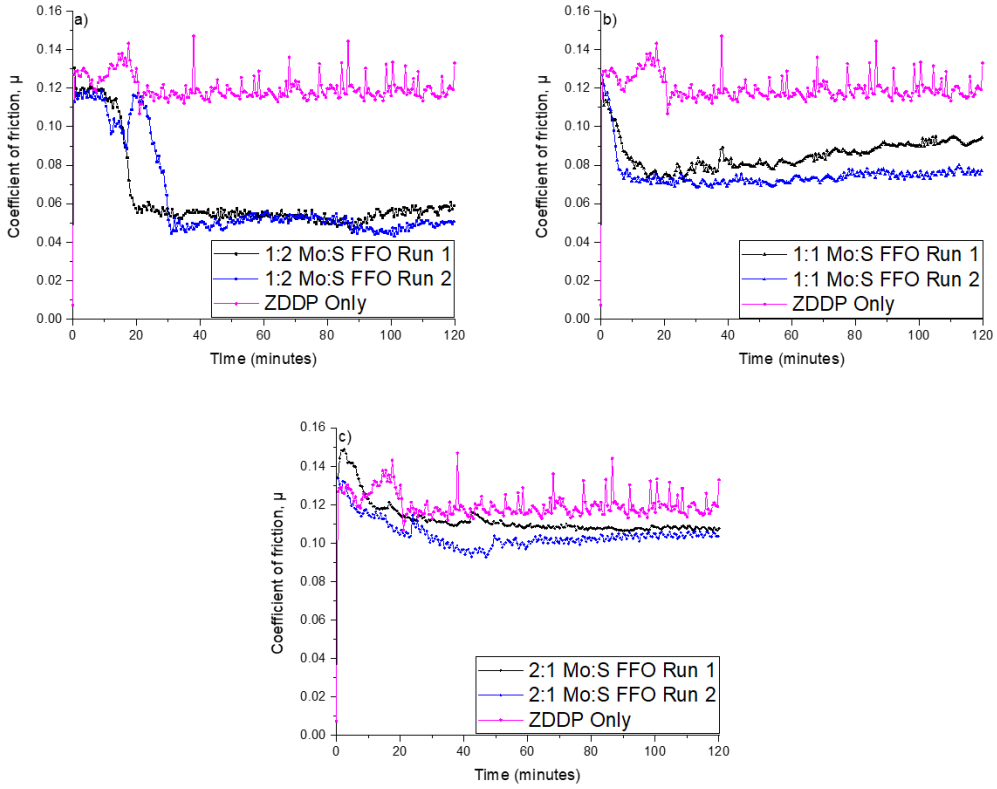


Figure 7.8 Fully-formulated Mo:S ratio oils with rough plates

With rough plates, the friction behaviour of the fully-formulated systems was similar to the FFO smooth plate conditions. A clear trend is observed with increasing friction coefficient as the sulfur supply in the formulation is reduced.

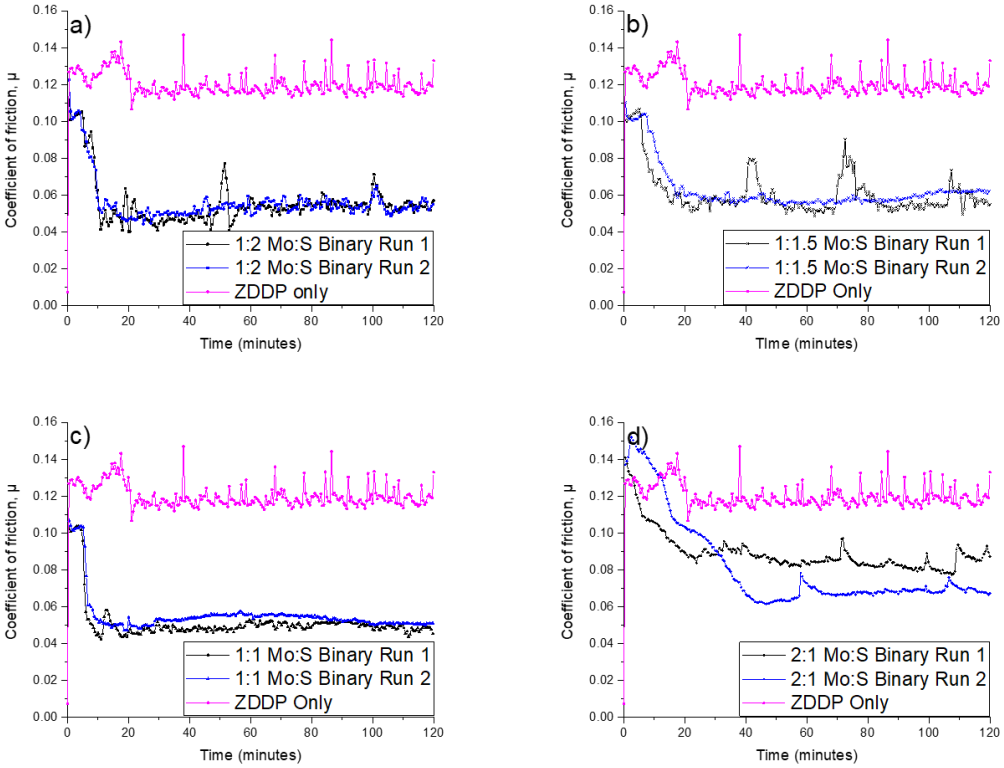


Figure 7.9 Individual profiles of binary molybdate ester Mo:S ratio oils under rough plate conditions

a) 1:2 Mo:S binary oil, b) 1:1.5 Mo:S binary oil, c) 1:1 Mo:S binary oil, d) 2:1 Mo:S binary oil

Under these harsher conditions shown in Figure 7.9, the binary mixtures all displayed a consistent reduction in friction after an initial induction period. Unlike the fully-formulated systems, no distinct trend was observed between friction coefficient and Mo:S ratio, with the majority of the systems showing comparable friction performance. The exception to this rule was the 2:1 oil, which produced higher final friction coefficients than the other systems.

The Raman intensity maps for these tests are presented in Figure 7.10, in these tests MoS_2 was found at much higher scattering intensities than in the fully-formulated or binary smooth surfaces tests in clear lines along the centre and the edges of the wear scar.

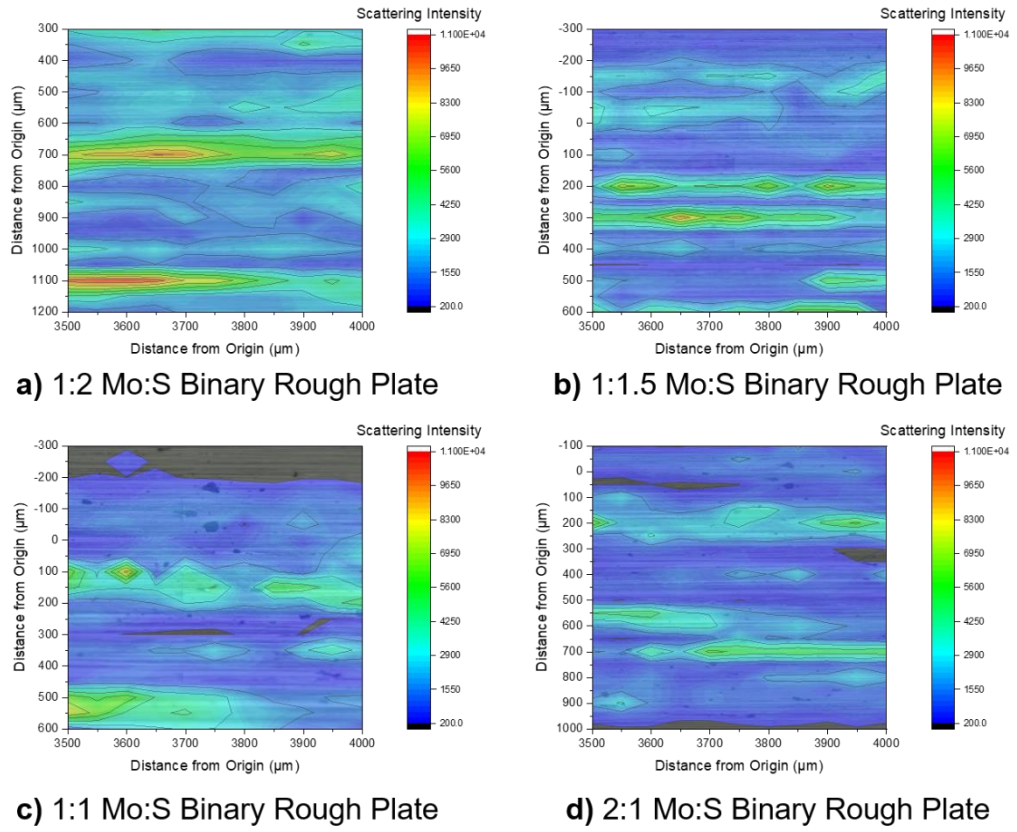


Figure 7.10 Raman surface coverage maps of 410 cm^{-1} A_{1g} vibration for Mo:S ratio binary oils in rough plate conditions

The overall summary of the friction performance of the oil systems studied under these standard conditions is summarised in Figure 7.11. For the 2:1 Mo:S ratio systems, the friction coefficient was comparable in all cases. This is indicative of insufficient formation of sufficient good-quality MoS_2 to provide low friction and provides an absolute limit to minimum relative sulfur content required to observe friction reduction of molybdate ester relative to ZDDP.

The binary systems in smooth plates testing displayed a wide variance in friction coefficient that was broadly independent of Mo:S ratio. This is indicative of insufficient activation of the chemistry required to induce and effective and steady friction response.

Both the fully-formulated oils under smooth conditions and the binary oils under rough plate conditions showed consistent friction responses for a given Mo:S ratio. This can be seen from the small variance in the friction results from these systems. The fully-formulated systems are more sensitive

to changing Mo:S ratio than the binary systems, although it is not clear if this is a product of the contact conditions. The difference in sensitivity to Mo:S ratio could be due to increased formation of MoS_2 induced by greater frictional flash temperatures in the rough plate conditions.

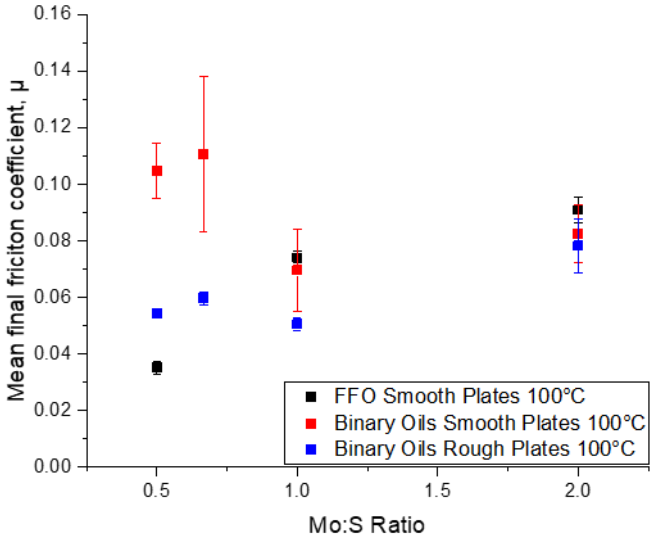


Figure 7.11 Friction performance of binary and FFO oils as a function of Mo:S ratio

7.2.3 Temperature dependence of molybdate ester systems

To investigate the role of temperature, and by extension frictional flash temperature, the friction responses of the fully-formulated and binary systems were studied under the contact conditions described previously. The lubricant bath temperature was reduced to 40°C. Figure 7.12 shows that the lower Mo:S ratio fully-formulated oils both display a significant increase in friction upon reduction of the lubricant bath temperature. The same trend was also observed in Figure 7.13 for the binary oils in rough plate friction conditions.

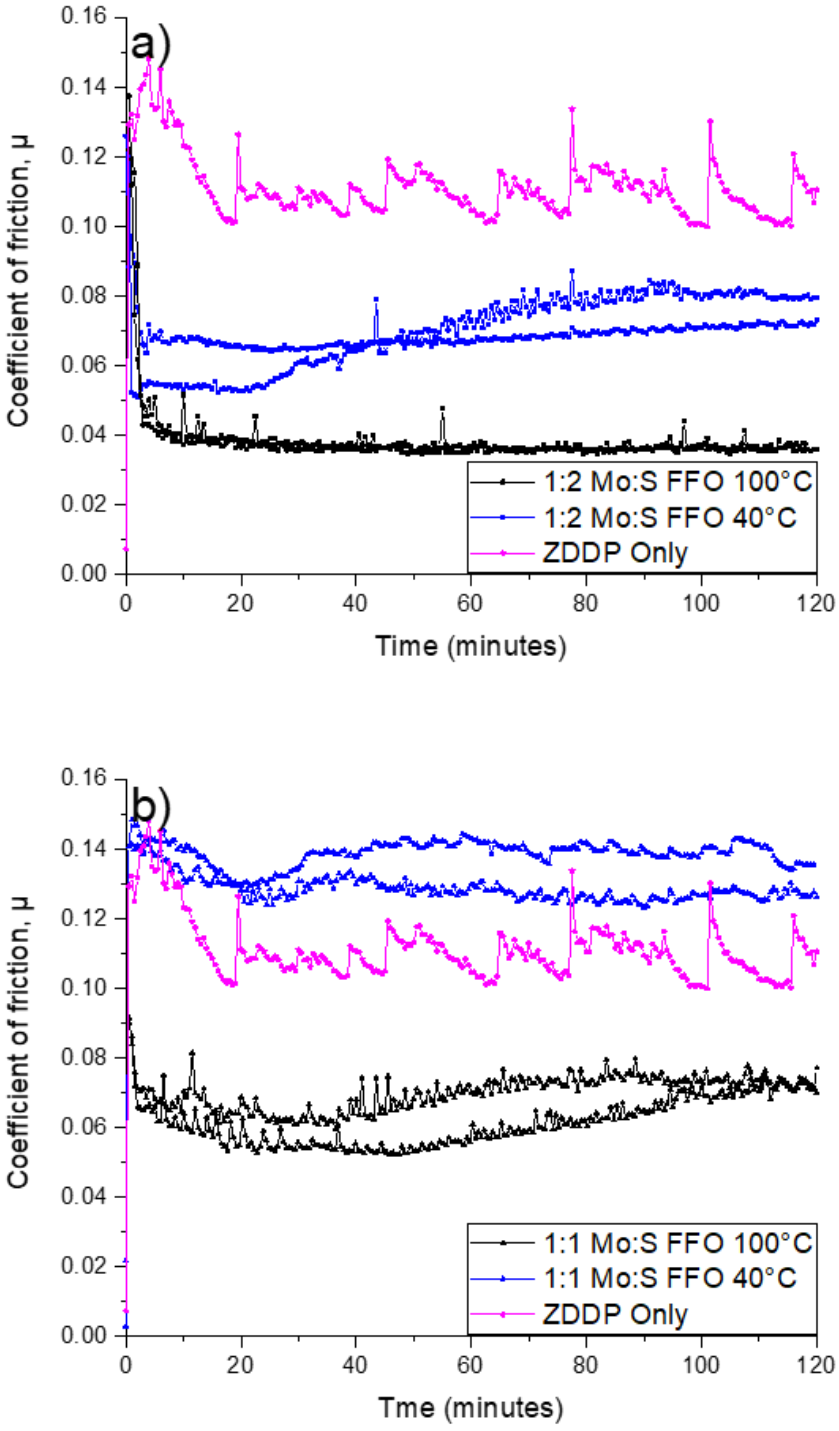


Figure 7.12 Friction performance of Mo:S ratio FFOs with lubricant bath temperature

a) 1:2 Mo:S Fully-Formulated Oil, b) 1:1 Mo:S Fully-Formulated Oil

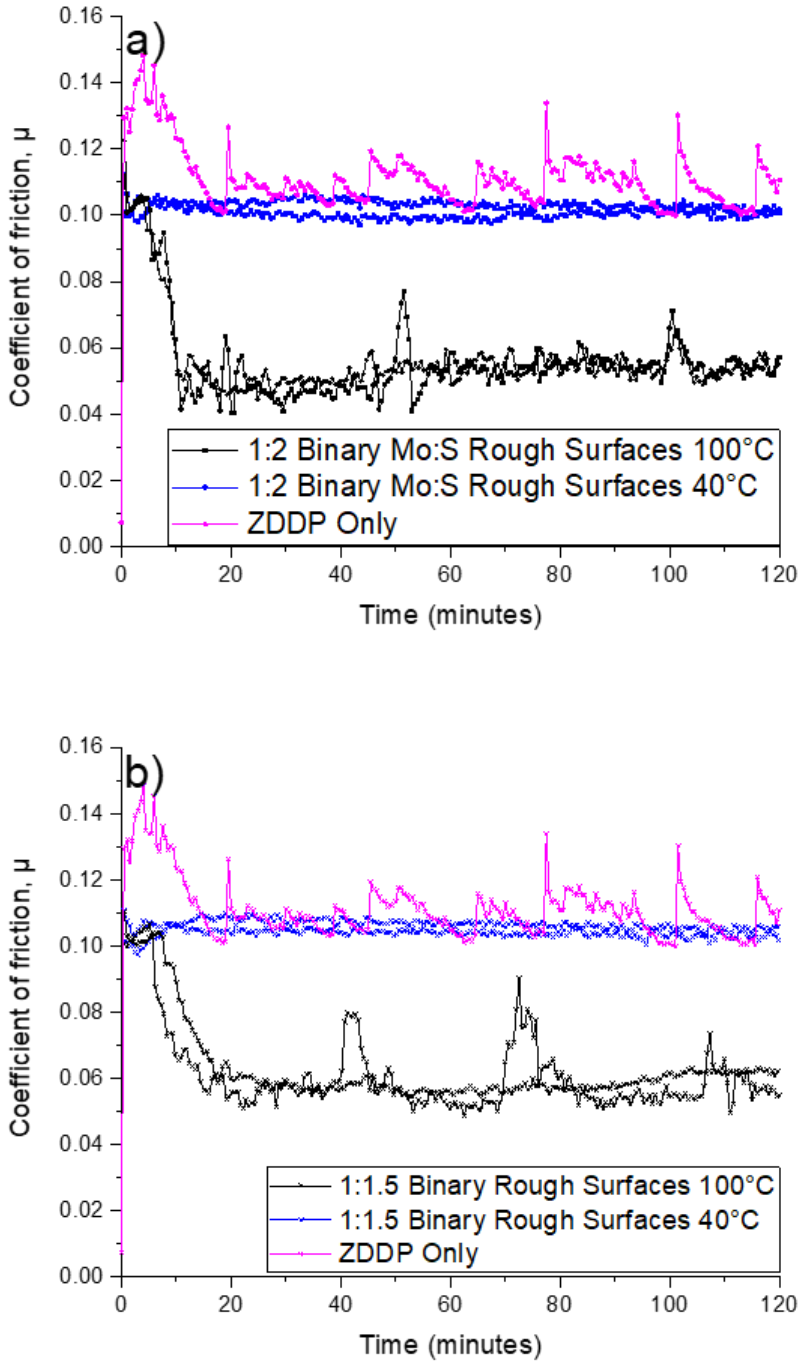


Figure 7.13 Friction performance of Mo:S ratio binary oils with lubricant bath temperature

a) 1:2 Mo:S Binary Oil, b) 1:1.5 Mo:S Binary Oil

From these results, it is clear that the contact temperature plays a significant role in the performance of molybdate ester systems. The friction performance of these oils is much more sensitive to temperature than the

sulfur-containing molybdenum additives studied in Chapter 5. The MoDTC Dimer and MoDTC Trimer systems both showed a significant drop in friction at 40°C in Figure 5.1 which were not observed for the molybdate ester systems. Therefore, some part of the molybdate ester MoS_2-formation mechanism is not occurring effectively under lower temperatures.

7.3 Fatty amine booster effect

In addition to the contact dependence of molybdate ester systems, molybdate esters are known to show improved friction performance relative to binary systems in the presence of amine dispersants [143]. Therefore, it is believed that there is an interaction between the molybdate ester and the dispersant additives. De Barros Bouchet et al. [143] proposed that the amine dispersants stabilise the formation of the molybdate ion intermediate outlined in Figure 7.2.

The amine used in these studies is a long-chain fatty amine, developed by AkzoNobel, named “Triameen” [143,149]. By addition of 500 ppm Triameen to a binary molybdate ester/ZDDP mixture, De Barros Bouchet et al.[143] observed a reduction in final friction coefficient from μ = 0.04 to μ = 0.02.

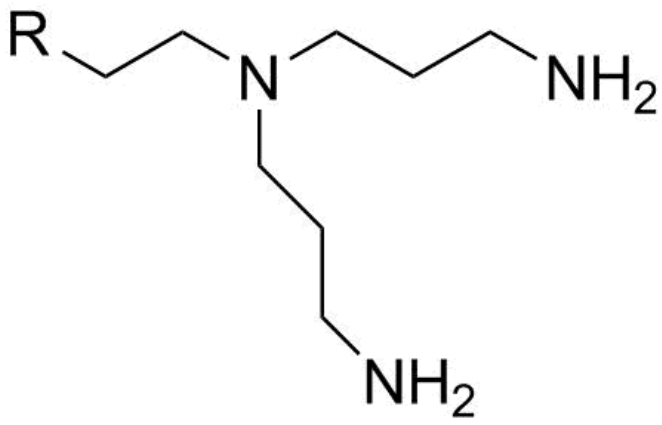


Figure 7.14 Structure of Triameen “fatty amine”

The additive interactions between amines and the molybdate ester systems seem to facilitate the development of low friction, but it is not clear whether this merely reduces the friction of pre-formed MoS_2 films, or if the

dispersants can facilitate a friction drop where none was observed before. Similar dispersants are found in the fully-formulated systems which have been studied. The additive interactions between dispersants and the oil systems may help to explain the overall superior friction performance of the fully-formulated systems over the binary systems, despite both being able to create MoS_2 under the contact conditions presented previously.

1 wt. % of Triameen was blended into the 1:2 Mo:S binary molybdate ester/ZDDP oil at 60°C for four hours before being allowed to cool and settle. This ternary oil mixture was then subjected to tribotesting with smooth surfaces under the conditions previously described (Table 13) at a lubricant bath temperature of 100°C, the friction results are presented in Figure 7.15.

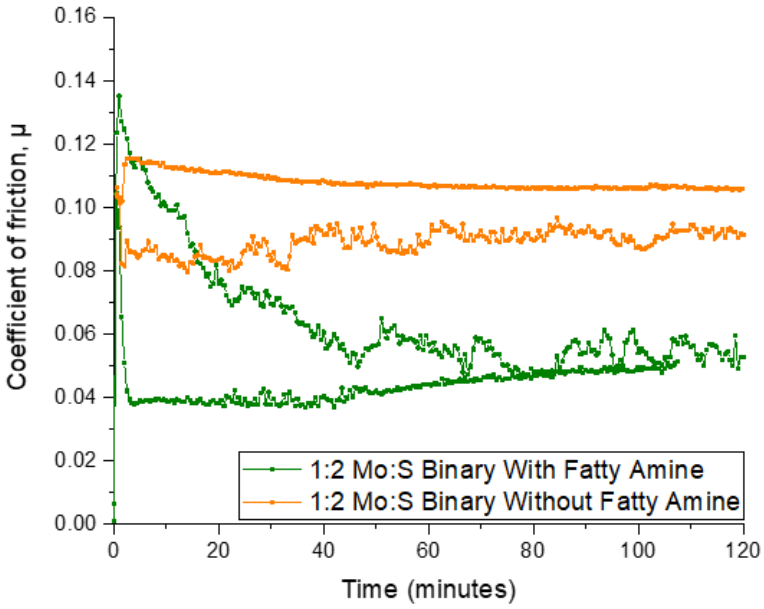


Figure 7.15 Response of 1:2 Mo:S ternary Oil with fatty amine dispersant

Upon addition of Triameen to create a 1:2 Mo:S ternary oil system, a reduction in friction to a final friction coefficient of $\mu = 0.05$ was observed. This is lower than had been observed for any of the binary systems in Figure 7.5. It appears from the behaviour of the ternary mixture that the additive interactions of the amine dispersants can not only improve the friction performance of a fully-formed MoS_2 film, but can initiate a friction drop under milder conditions than would be expected from a binary mixture alone.

In addition, it is interesting to note that the friction profile of the ternary amine oils was also distinct from those of the binary oils. In the binary oil systems, a general trend of low-friction, followed by a rise in friction up to μ = 0.08 had been observed, whereas the ternary oils showed a friction profile more typical of an MoDTC, with an induction period, followed by a friction drop which was maintained. This behaviour is explored in more depth in the next section.

The Triameen, being a long-chain amine, shares a structure which may act as an organic friction modifier [225,226]. In order to confirm that the friction behaviour observed in Figure 7.15 was not merely a synergy between MoS_2 and OFM friction reduction, a model oil of 1 wt.% Triameen in ZDDP-only oil was blended and tested in Figure 7.16. No significant friction reduction was observed in the amine oil relative to the ZDDP-only oil. Therefore, the data suggests that the friction reducing effect of amine/molybdate ester blends is indeed a result of additive interactions, rather than any friction-reducing behaviour from the amine acting as an organic friction modifier.

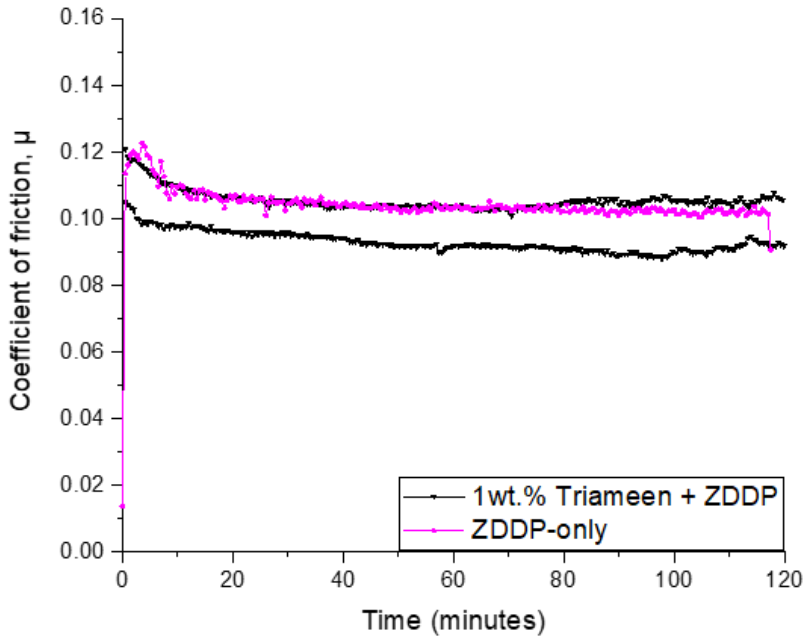
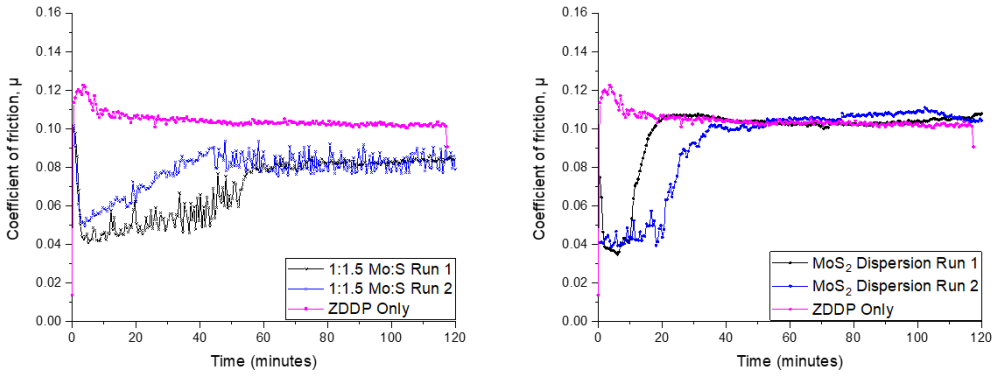


Figure 7.16 Friction response of Triameen blended in ZDDP-only oil

7.4 Role of friction-reducing precipitate in molybdate ester binary mixture friction performance

7.4.1 Role of precipitate in friction

In the binary oil, smooth plate friction profiles outlined in Figure 7.5, the majority of the friction profiles show a drop in friction, followed by a rise later on in the tests where the friction coefficient stabilises. This behaviour is unlike the fully-formulated systems where the friction coefficient stabilises rapidly. The friction profiles of the binary systems show some similarity with those of a dispersion of solid MoS_2 in oil, where friction drops while MoS_2 is present in the contact, rising as the supply of MoS_2 in the contact slowly depletes [227]. MoS_2 dispersion-lubricated contacts become starved of MoS_2 due to insufficient mixing of the oil by the contact leading to inadequate entrainment of the MoS_2 solid into the contact. To compare, a solid dispersion of 1wt. % of MoS_2 in ZDDP-only oil was prepared and tribotested under the same conditions as the binary mixtures, the results of which are presented alongside the binary mixture friction profile in Figure 7.17.



a) 1:1.5 Mo:S Binary Mixture **b)** MoS_2 Dispersed in ZDDP Oil

Figure 7.17 Comparision of binary mixture and MoS_2 dispersed in oil

The friction profile of solid MoS_2 displays a low friction coefficient of μ = 0.04 while MoS_2 is being effectively entrained into the contact, which then increases towards the ZDDP-only oil values as the supply of MoS_2 in the contact runs out.

In a similar fashion to solid MoS_2, the binary oil friction profile contains a similar down and up profile. However, unlike a solid MoS_2 dispersion, there was always an even mixing and entrainment of the precipitate into the contact. Prior to each of the tests outlined in Figure 7.5 the binary oils had been shaken vigorously to effectively mix the oil. To determine if there was a solid in the oil similar to MoS_2 which was determining the friction performance in the early stages of the test, a sample of the oil was taken and allowed to settle for two weeks. After a two-week period, a precipitate was observed at the bottom of the sample vial (Figure 7.18). The settled oil was then tested without the precipitate was then subjected to friction testing, which is compared to the well-mixed oil in Figure 7.19. From the friction data, it is clear that in the absence of this solid precipitate, no friction reduction takes place and that the precipitate dominates the friction behaviour of the binary systems.

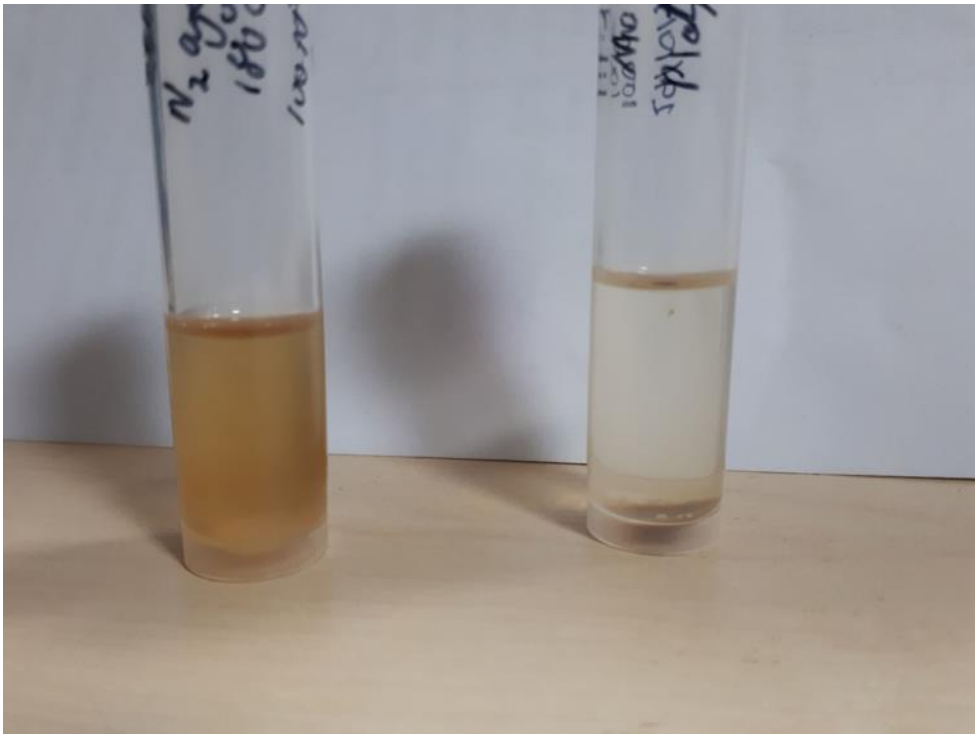


Figure 7.18 Precipitate settling in oil

Left) binary mixture oil Right) Binary mixture oil after being allowed to settle for two weeks

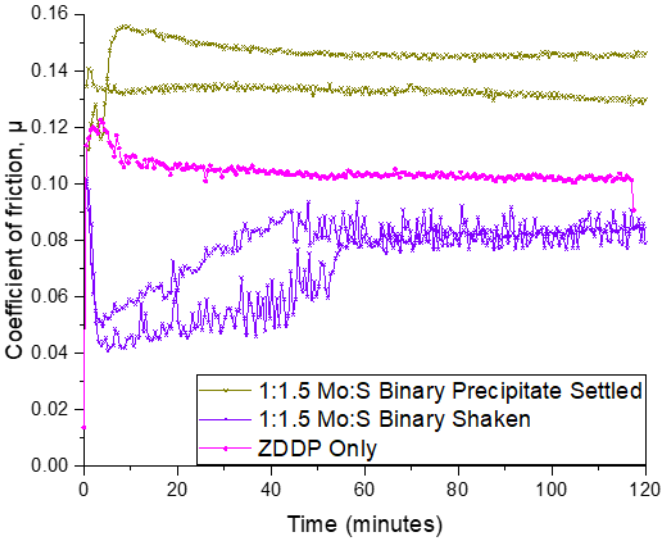


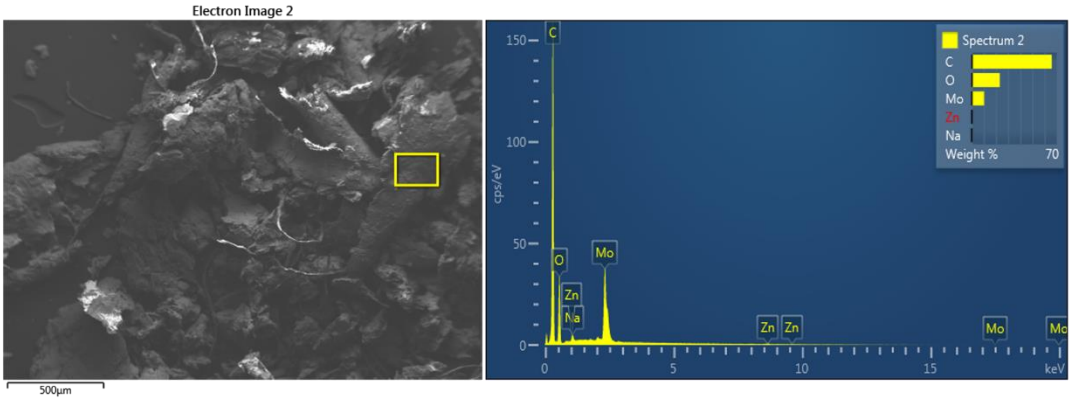
Figure 7.19 Friction response of binary mixture with and without precipitate

7.4.2 Chemical identification of friction-reducing precipitate

The precipitate in the binary mixtures is responsible for friction reduction in these systems, in order to study the precipitate, it was filtered out from the settled oil, dried and then washed with heptane 3 times. Chemical characterisation of the precipitate was performed by SEM-EDX, Raman spectroscopy and X-ray diffraction.

7.4.2.1. SEM-EDX characterisation

SEM-EDX characterisation of the precipitate showed that the microstructure of the precipitate was a flaky, soft solid composed primarily of Mo, O, and C with small traces of zinc (Figure 7.20). As molybdenum and sulfur have overlapping EDX peaks, it is uncertain if the precipitate is sulfur-containing. In order to better understand the chemistry of the precipitate and distinguish between whether bonding is primarily between molybdenum and either oxygen or sulfur, Raman spectroscopy was performed.



a) Precipitate SEM Image

b) Precipitate EDX Spectrum Of Highlighted Area

Figure 7.20 SEM characterisation of friction-reducing precipitate

7.4.2.2. Raman characterisation

Raman spectra of the dried precipitate are presented in Figure 7.21. Spectral acquisition parameters are the same as those outlined in Table 16 except the laser power and number of accumulations were varied as shown in Figure 7.21. At 10% laser power, the spectrum from the precipitate was quite indistinct, even after 50 accumulations. This is suggestive of a significant amount of carbon in the precipitate structure. Some peaks were observed however at 199, 222, 348, 486, 725, 817 and 960 cm^{-1}. Upon increase of the laser power to 100% (16 mW), laser-induced oxidation of the precipitate occurred, and the peak structure closely matched that of molybdenum dioxide (MoO_2). A spectrum of a reference sample of MoO_2 is presented in Figure 7.21 for comparison.

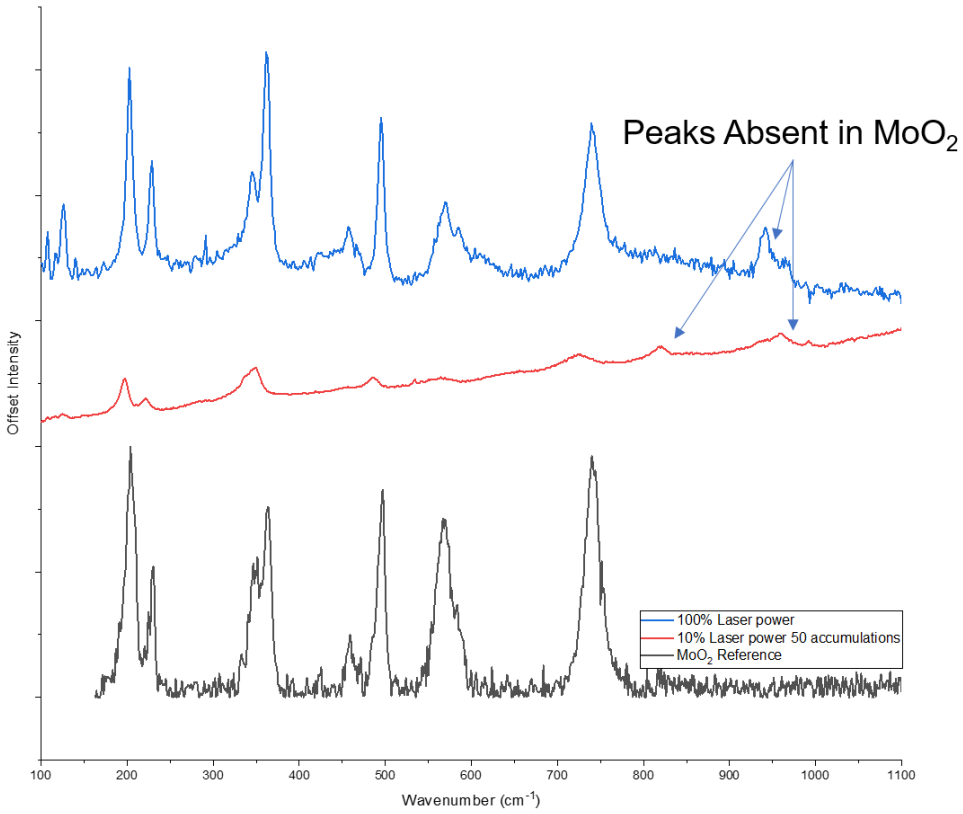


Figure 7.21 Raman characterisation of precipitate under higher laser powers

The precipitate did display some peaks not associated with MoO_2 under both 10% and 100% laser power at 817 and 957 cm^{-1}. To determine if these are also oxidation-induced peaks, the laser power was reduced to 1% for 50 accumulations. The resulting spectrum is presented in Figure 7.22. The peaks around 820 cm^{-1} and 950 cm^{-1} remain but the oxidation peaks of MoO_2 are absent. The peaks at 820 cm^{-1} and 950 cm^{-1} are associated with M=O double bond stretching modes in molybdate crystals [228,229]. Such stretches would be expected in the molybdate molecular structure which features two such M=O double bonds.

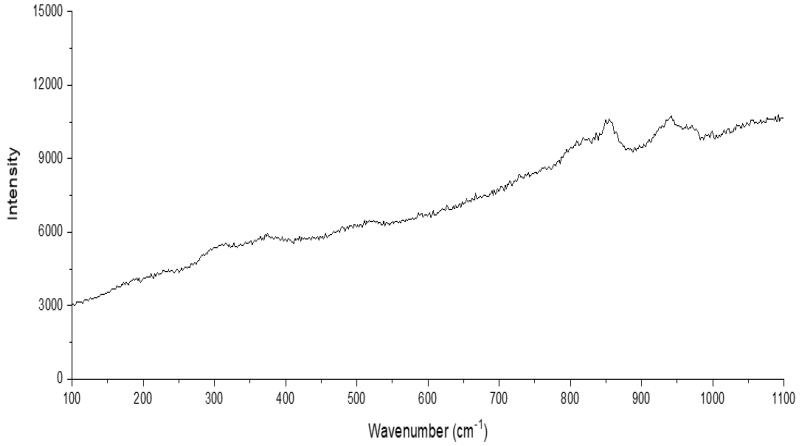


Figure 7.22 Low laser power Raman spectrum of precipitate

7.4.2.3. X-Ray diffraction

In order to confirm the crystalline or amorphous nature of the precipitate, and whether crystalline MoO_2 is part of the precipitate's structure, XRD was performed. The diffractogram of the precipitate is presented in Figure 7.23. Even at slow scanning rates of 5°min^{-1}, no crystal reflection peaks were observed, this suggests that the precipitate is ultimately amorphous in nature.

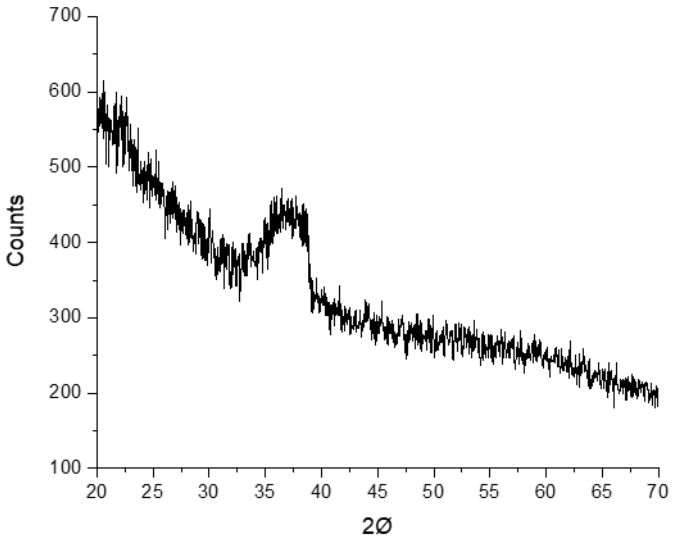


Figure 7.23 X-Ray diffractogram of friction reducing precipitate

From the results of the elemental analysis by SEM-EDX and chemical analysis from XRD and Raman spectroscopy, it can be stated that the precipitate is primarily composed of amorphous oxymolybdate species with a significant amount of carbon. From this, it seems reasonable to conclude that the precipitate is merely the molybdate ester additive itself falling out of solution, rather than an insoluble product resulting from an interaction with ZDDP.

7.5 Effect of a ZDDP film and additive interactions on the friction performance of molybdate ester formulations

From the previous section describing the friction performance of the molybdate ester, some factors which affect the performance have become clear. Dispersants in a fully-formulated oil or a ternary mixture with ZDDP, molybdate ester and Triameen aid in the development of low friction, and that increasingly harsh contact conditions induced by increase surface roughness improve friction performance.

Optical microscopy of the TE77 pin wear scars derived from each of the testing conditions show a distinct trend. That those oil systems which display the development of a macroscopic ZDDP film have high final friction coefficients, whereas those tests with friction coefficients of $\mu = 0.05$ or 0.04 do not.

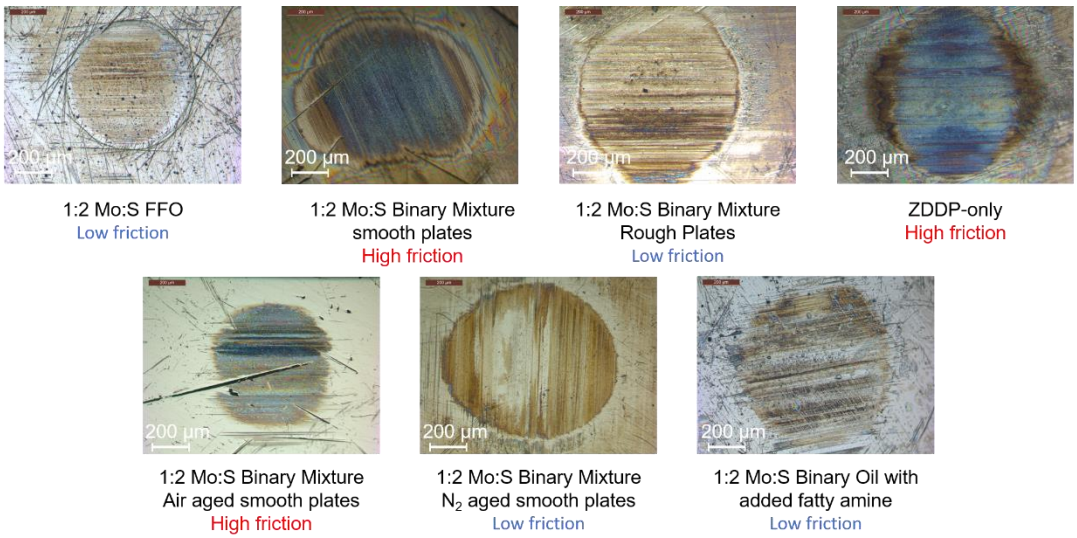


Figure 7.24 Optical microscope images of 1:2 Mo:S TE77 pin wear scars derived from a range of conditions

In the case of rougher surfaces, it is likely the case that the rough surfaces prohibit the formation of such a bulk film, which maintains the high frictional flash temperatures required to lower friction for this additive. In the case of fully-formulated oils and ternary oils with Triameen, the behaviour may be due to two possible reasons.

1. The basic nature of amines, leading to the release of free thiophosphorylate which aid in the sulfur-transfer reaction and subsequent formation of MoS_2.

2. ZDDP-dispersant antagonisms which reduce the ZDDP film thickness and prevent any reduction in flash temperatures caused by the smooth ZDDP film.

7.5.1 Basic nature of amines

Amines, by virtue of the lone pair on the nitrogen atom, are able to act as bases. Upon their interaction with ZDDP to form basic ZDDP, there is release of thiophosphorylate ions, which may act as a sulfur source that can undergo sulfur-exchange with the molybdate ester [159]. The reaction for the formation of basic ZDDP from amines is presented in Figure 7.25 below.

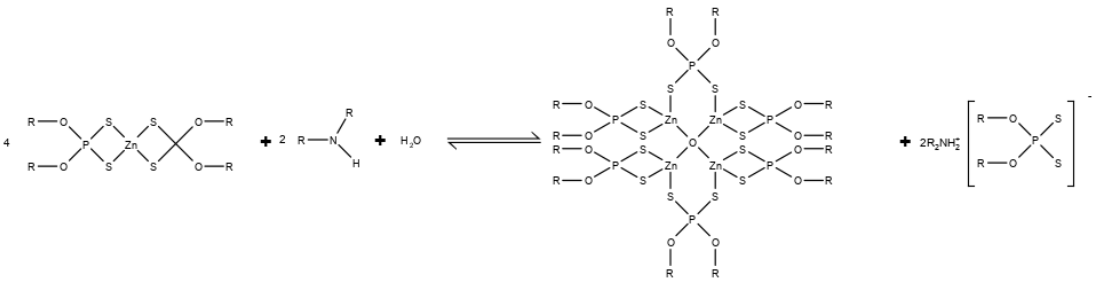
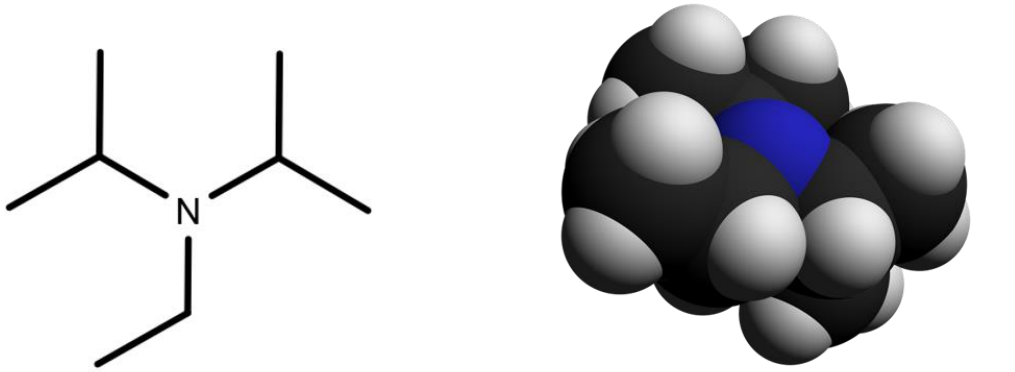


Figure 7.25 Formation of basic ZDDP through action of amines

In addition to their basic nature, amines can act as ligands and as nucleophiles. In order to isolate the basic effect of amines to test as the cause of a friction drop, careful choice of chemistry is required. Diisopropyl ethylamine (DIPEA) is a sterically-hindered amine, wherein the nitrogen centre is sterically hindered by the surrounding alkyl groups. The result of this hindrance is that the nitrogen centre is unable to act as an effective ligand or nucleophile, but still being able to act as a base by being able to bind protons. The structure of DIPEA and the sterically-hindered nature of its nitrogen centre are highlighted in Figure 7.26.



a) DIPEA Structure **b)** Space-filling DIPEA Structure

Figure 7.26 Structure of diisopropylethylamine (DIPEA)

The space-filled structure in b) highlights the steric hinderance of the nitrogen centre. DIPEA is unable to bind electrophiles larger than a proton

1 wt. % DIPEA was blended into the 1:2 binary mixture oil and subjected to tribotesting under the smooth plate conditions described previously (Table 13), at a lubricant bath temperature of 100°C. The friction profile of the oil with added DIPEA was much the same as the binary oil alone, with a slight drop in friction towards the start of the test which increased after a period. This was unlike the response observed with Triameen in Figure 7.15 where a sustained drop in friction was observed upon addition of the binary mixture. These results suggest that it is not the basic nature of the amines which leads to the "fatty amine booster effect".

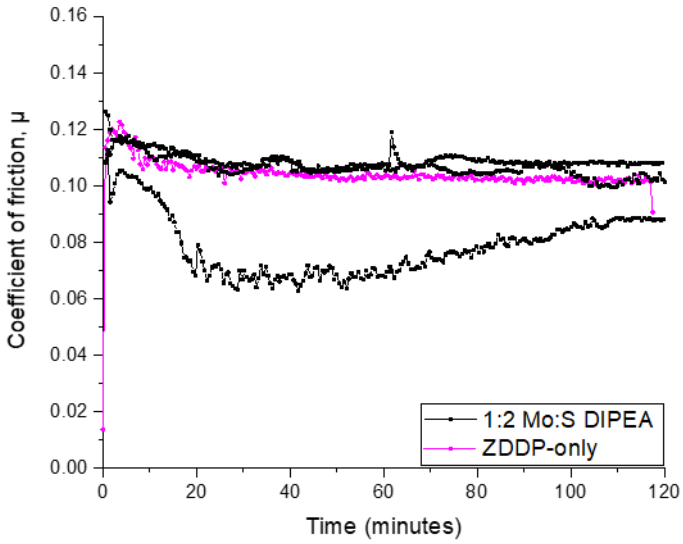


Figure 7.27 Friction profile of binary mixture with DIPEA

This leaves the antagonistic interactions between the amine dispersants and ZDDP films as a possible source for the amine booster effect. It is well known that amine dispersants reduce the thickness of ZDDP tribofilms, and at high concentrations can completely eliminate tribofilm formation [180,181]. It may be that the elimination of the formation of glassy ZDDP tribofilm increases flash temperatures to a point where effective friction reduction can occur from the binary mixtures under mild conditions. This would mean that the "down and up" friction profiles of binary systems result from initial low friction where ferrous surface contact occurs which is then inhibited by an interposing glassy ZDDP film which reduces contact pressures to a point

where the molybdate ester is unable to form sufficient MoS_2 to effectively, leading to increased friction.

7.5.2 Oil ageing and removal of ZDDP thermally

If the absence of a thick ZDDP film is important for steady-state low friction coefficients, then any removal of a ZDDP film which maintains the supply of sulfur to the molybdate ester should result in a sustained drop in friction. The effective power of ZDDP to form a film can be removed without addition of other additives, through thermal ageing of the oil.

The 1:2 Mo:S binary oil was heated under a nitrogen atmosphere for 4 hours at 220°C. ZDDP is known to thermally decompose at 120°C, with rapid thermal decomposition occurring above 170°C [159,230,231]. Upon reaching 200°C, the oil rapidly changed colour to a deep orange as free sulfur was released upon ZDDP decomposition. This effect is observed in Figure 7.28.



Figure 7.28 Ageing of binary oil

(Left) fresh binary mixture of molybdate ester/ZDDP, (Right) Nitrogen aged binary mixture

The aged oil was then subjected to tribotesting under the smooth plate conditions described in Table 13 at a lubricant bath temperature of 100°C. The results are presented in Figure 7.29.

Like the fatty amine tests, and rough surface tests, the friction profile of the nitrogen aged oil in Figure 7.29 was more similar to that which would be expected of a molybdenum additive. There was a high friction induction period, followed by a sustained drop in friction to μ = 0.06. Optical inspection of the TE77 pin wear scar in Figure 7.30 showed no formation of a bulk ZDDP tribofilm. The small black film observed across the centre of the wear scar is magnetite (Fe_3O_4).

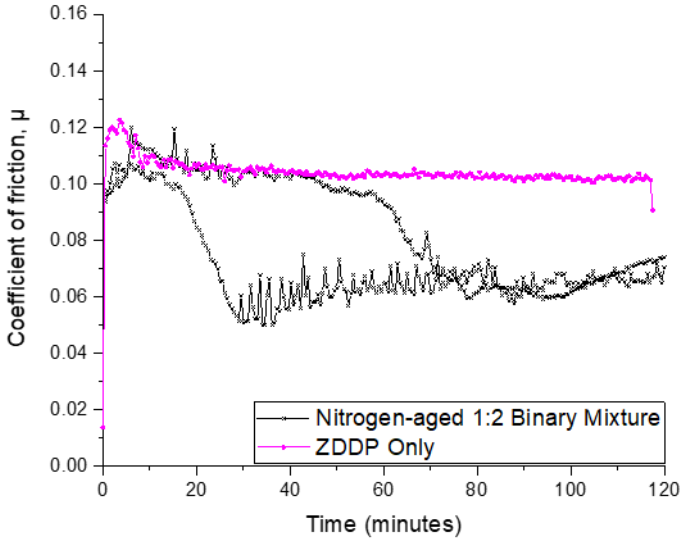


Figure 7.29 Friction profile of nitrogen aged binary oil

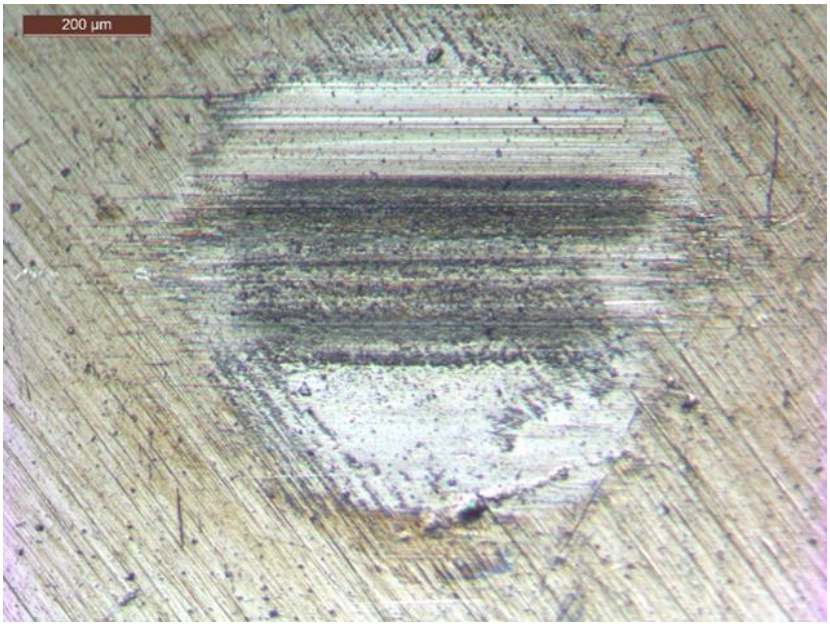


Figure 7.30 TE77 pin wear scar of nitrogen aged binary oil

These results show that the formation of a bulk ZDDP film is detrimental to the friction performance of the binary molybdate ester formulations. The prevention of the formation of a thick ZDDP film, either through contact conditions, additive interactions or thermal decomposition of ZDDP, allow for the maintenance of high enough contact temperatures for the effective formation of MoS_2 from molybdate ester oils.

7.5.3 Investigation of molybdate ester mechanism

The proposed mechanism for how the molybdate ester reduces friction is outlined in Figure 7.2. The mechanism if divided into three distinct steps:

1. The release of free molybdate from the additive structure.

2. The transfer of sulfur from other additives to convert the molybdate into a thiomolybdate.

3. The decomposition of the tetrathiomolybdate to MoS_2.

In order for effective friction reduction to occur from the molybdate ester, all the steps in the process must occur, so that enough MoS_2 of sufficient quality is created to reduce friction. In the sulfur-starved fully-formulated tests, the second sulfur-transfer step is not occurring at a sufficient rate to produce enough thiomolybdate. So, in these cases, the second step is the rate-determining step.

In the binary oil smooth plate tests in Figure 7.5 sub-optimal friction performance is observed for all of the Mo:S ratios investigated. For these tests it is not as simple to determine what the rate-determining step is.

7.5.3.1. Friction testing

In order to determine the limiting chemical step in friction reduction, a series of tribological tests were performed with intermediate compounds along the mechanistic pathway. Intermediate compounds were blended into ZDDP-containing oil at 1 wt% concentration and subjected to friction testing under the conditions described in Table 14. As the intermediate compounds were quite polar, they were only sparingly soluble in the oil. The intermediate compounds used to analyse the molybdate ester mechanism were:

1. The precipitate was used as a model for the molybdate ester additive for Step 1 (The release of free molybdate from the additive structure) as the precipitate appears to be the molybdate ester additive, unchanged by any bulk oil chemistry.

2. Ammonium molybdate $(NH_4)_2MoO_4$ was used to model the free molybdate ion in the sulfur transfer process in Step 2.

3. Ammonium tetrathiomolybdate was used to model the thiomolybdate ion in the final MoS_2 formation process in Step 3.

The friction results from the molybdate ester mechanism testing are presented at 100°C for the molybdate precipitate and ammonium molybdate in Figure 7.31. No tests were performed for ammonium tetrathiomolybdate at this temperature due to safety concerns regarding the potential release of H_2S

gas. Each of the intermediate compounds was also blended into a low-sulfur PAO base oil as a control.

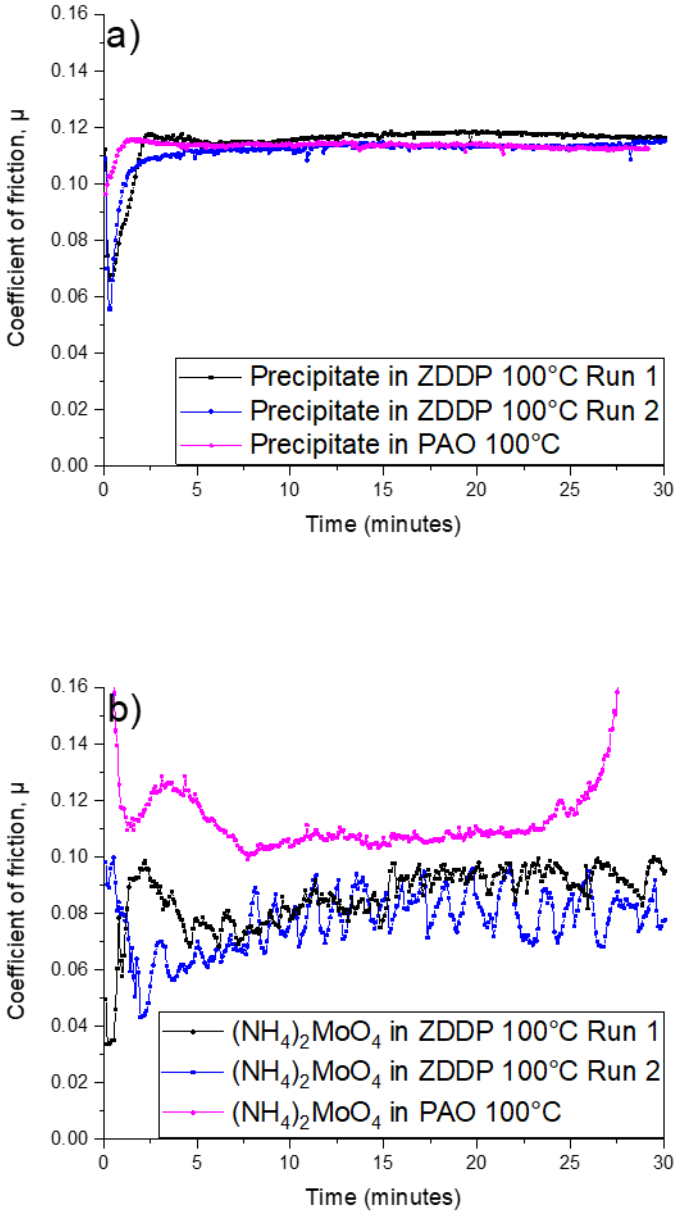


Figure 7.31 Molybdate mechanism testing friction profiles 100°C

a) Molybdate precipitate 100°C, b) Ammonium molybdate 100°C

In Figure 7.31, at 100°C a slight friction reduction was observed from the molybdate precipitate in ZDDP-only oil. After 3 minutes, this friction reduction was effectively lost as the friction climbed to the same value as the PAO control. The ammonium molybdate showed a significant drop in friction, with both of the tests reaching the friction coefficient low associated with MoS_2

tribofilms of μ = 0.04 - 0.05. After this, the friction coefficient rose slowly as the poorly soluble ammonium molybdate was pushed out of the contact. However, it appears that when plentiful ammonium molybdate is available in the contact, the performance is superior to the equivalent amount of molybdate ester precipitate.

Tests were performed again at 40°C and presented in Figure 7.32. This lower temperature was chosen both to safely include the ammonium tetrathiomolybdate in the study, and to increase the lubricant viscosity in order to reduce the effect of losing the active compounds from the contact zone.

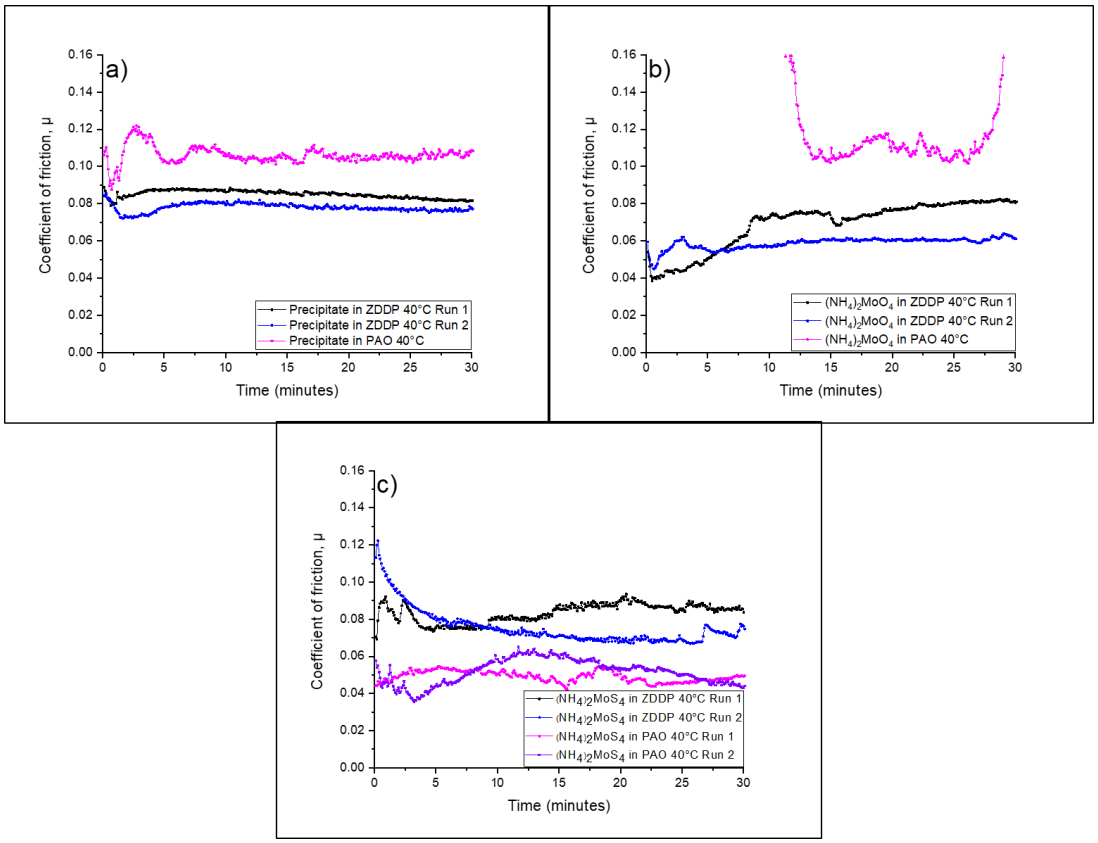


Figure 7.32 Molybdate mechanism testing friction profiles 40°C

a) Molybdate precipitate 40°C, b) Ammonium molybdate 40°C, c) Ammonium tetrathiomolybdate 40°C

At 40°C, there some, but very little friction reduction by the molybdate precipitate. The ammonium molybdate and the thiomolybdate both displayed significant and sustained drops in friction down to typical MoS_2 friction values. From these results, it appears that the rate limiting step to friction reduction in

sulfur-rich systems is the release of free molybdate from the molybdate ester additive.

7.5.3.2. Raman analysis

To confirm that the friction reduction observed for the molybdate and tetrathiomolybdate were due to MoS_2 formation, rather than any lubricious oxide species, Raman analysis was performed on the TE77 plate wear scars.

The results for the 100°C mechanism tests are presented in Figure 7.33. For the ammonium molybdate a significant amount of MoS_2 was observed in the spectrum in the ZDDP oil in which friction reduction was observed. MoS_2 was also observed in the ZDDP testing of the molybdate ester precipitate, but the intensity of MoS_2 scattering was very small compared to the spectral background. In the PAO tests, MoS_2 was observed for the sulfur-containing tetrathiomolybdate, but not for the oxymolybdate or precipitate tests, which showed only iron oxides and MoO_2 respectively.

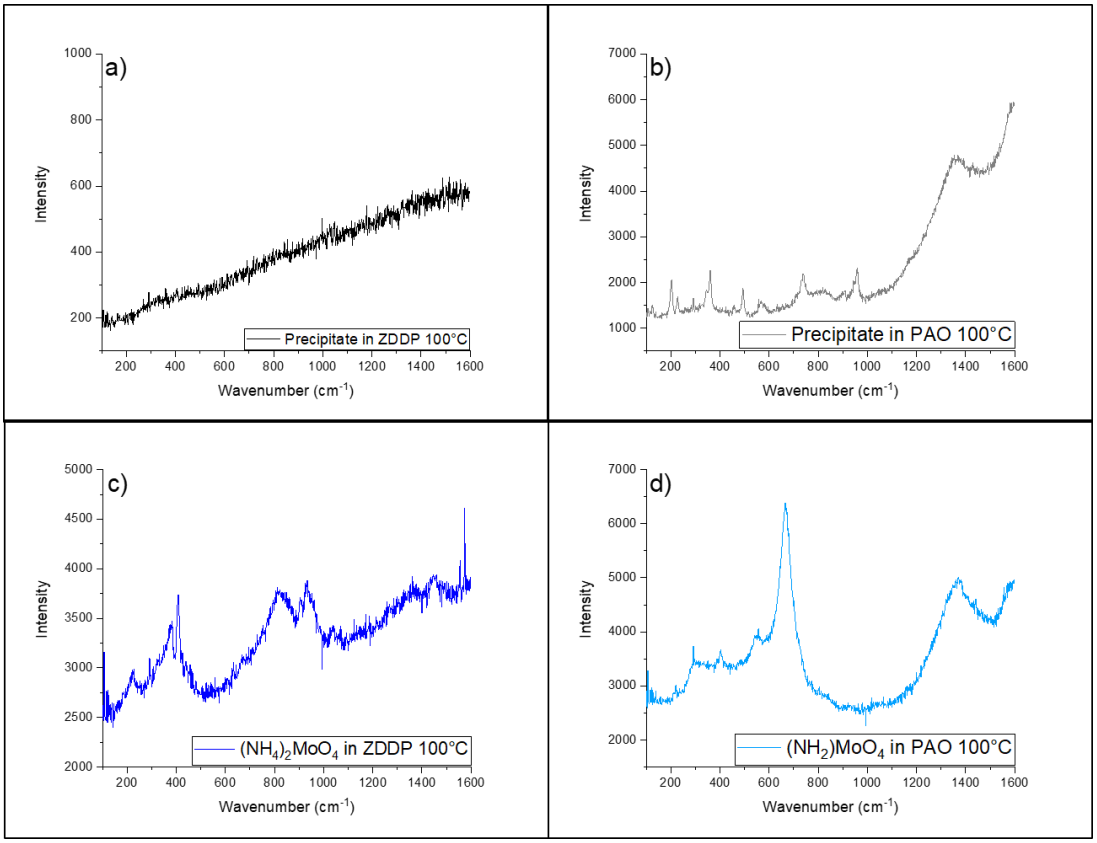


Figure 7.33 Raman spectra of molybdate mechanism testing wear scars for 100°C tests

a) Molybdate precipitate in ZDDP-containing oil, b) Molybdate precipitate in PAO base oil, c) Ammonium molybdate in ZDDP-containing oil, d) Ammonium molybdate in PAO base oil

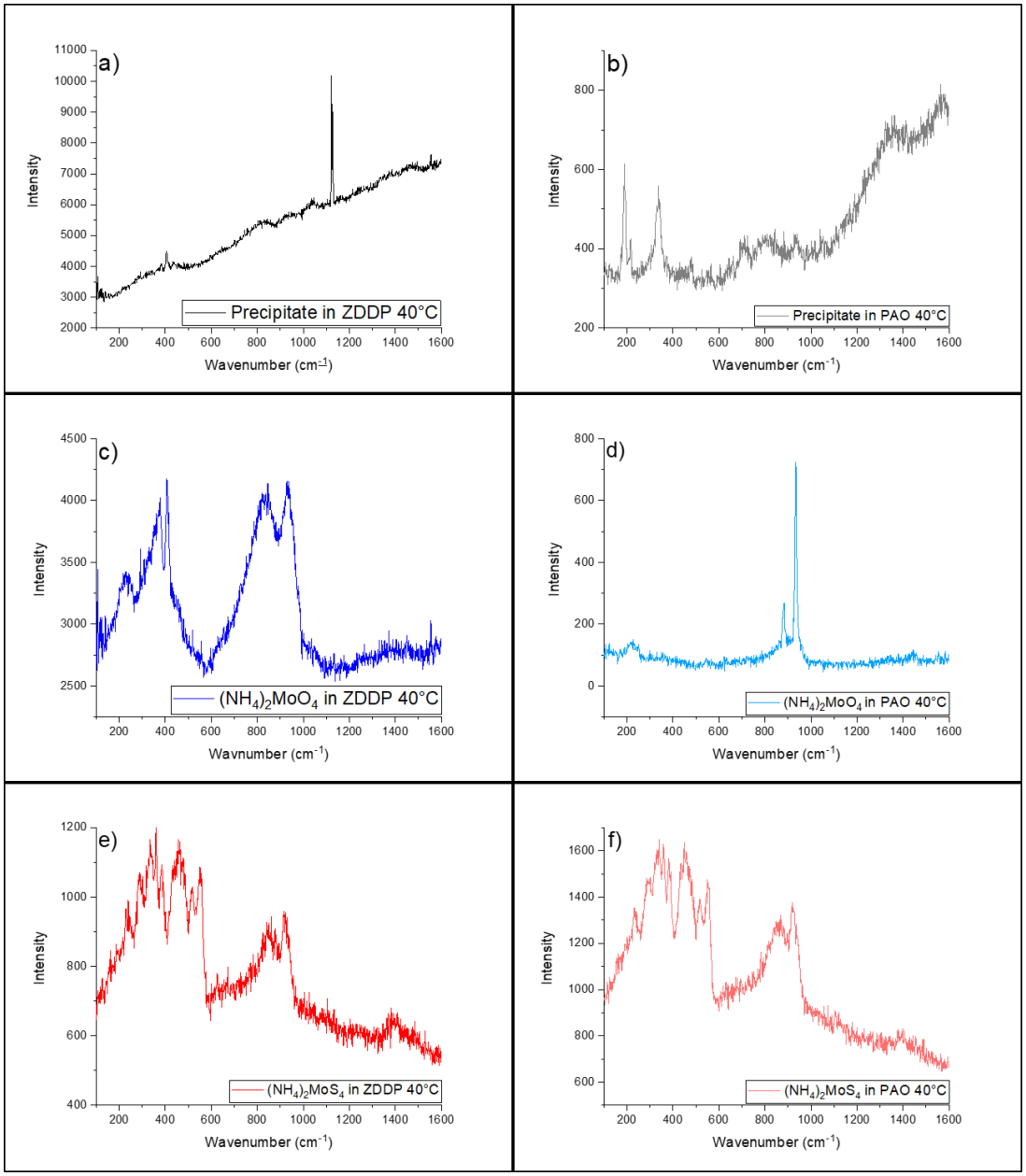


Figure 7.34 Raman spectra of ammonium tetrathiomolybdate wear scar after rubbing at 40°C in PAO base oil

a) Molybdate precipitate in ZDDP-containing oil, b) Molybdate precipitate in PAO base oil, c) Ammonium molybdate in ZDDP-containing oil, d) Ammonium molybdate in PAO base oil e) Ammonium tetrathiomolybdate in ZDDP-containing oil, f) Ammonium tetrathiomolybdate in PAO base oil

7.6 Summary

In this chapter, the sulfur and formulation dependence of the sulfur-free molybdate ester friction modifier was studied. The friction performance of the fully-formulated molybdate ester systems and binary molybdate ester + ZDDP systems were characterised under a range of contact conditions. Then the role of amines in the “fatty amine booster effect” was investigated as an activation parameter and the role of amines was investigated in terms of ZDDP film formation antagonisms. The overall friction performance of all the systems was examined in terms of the formation of bulk ZDDP films, followed by a mechanistic investigation of the kinetics of the molybdate ester MoS_2-formation mechanism. From this work, the following was observed:

- In fully-formulated systems, the friction performance of the molybdate ester was highly dependent on Mo:S ratio, with optimal friction performance only observed for a 1:2 Mo:S ratio with sulfur-loading comparable to a commercial oil.

- Binary oils systems were unable to reduce friction effectively under smooth plate conditions, but were able to with rough surfaces, as seen previously in the literature. In rough surface conditions, the binary oils were less dependent on Mo:S ratio than the fully-formulated oils were with smooth surfaces.

- The friction performance of fully-formulated and binary oils is highly temperature dependent.

- Binary systems can produce effective friction reduction on smooth surfaces in the presence of a fatty amine dispersant. This shows that the fatty amine booster effect not only improves the friction performance of fully-formed MoS_2 films but can also activate effective friction reduction.

- The fatty amine booster effect increases the effectiveness of molybdate ester friction response by inhibiting the formation of

bulk ZDDP films and keeping contact conditions harsh enough to sufficient MoS_2 formation to keep friction low.

- In sulfur-rich systems where a full ZDDP film inhibits the formation of MoS_2 from the molybdate ester, the rate limiting step in MoS_2 formation is likely to be the breaking of the organic molybdate bonds to release free molybdate. In sulfur-poor systems, the rate-determining step in providing low friction performance is likely to be the exchange of sulfur with free molybdate to form thiomolybdates.

- In general, harsher contact conditions, and in particular higher temperatures needed for the molybdate ester to act as a friction modifier comparable to the MoDTC dimer or MoDTC trimer additives.

Chapter 8: Discussion

8.1 Introduction

Results from the tribological testing of all of the additive systems in Chapter 5 show that friction performance is strongly affected by both the contact conditions employed and the additive chemistry in the lubricant formulation. It has also been shown that some contact conditions make a greater contribution to the effective action of molybdenum-based friction modifiers than others.

Chemical analysis of the tribofilms in Chapter 6 has shown that the additive chemistry employed leads to notable differences in the natures of the tribofilms formed from those additives. These differences manifest themselves in terms of surface coverage, film thickness and the distributions of chemistries forming the films. The tribochemistry of the additives is key to understanding the tribological performance of oils in boundary lubrication.

In the case of the molybdate ester in Chapter 7, the additive effectiveness has been shown to depend upon the formulation of the lubricant system and the interactions with other additives.

From the collective results presented earlier, it is clear that molybdenum additives are far from interchangeable and their chemistry has a distinct effect on their behaviour and the tribofilms they form. In this chapter, the results outlined in the previous chapters are interpreted and discussed. The discussion is split into the following themes:

- The relative importance of tribological contact parameters to the decomposition of molybdenum additives.
- The role of MoS_3 as a decomposition intermediate and how additive structure may affect its formation.
- The properties of molybdenum-derived tribofilms which affect friction performance and durability.

- The formulation dependence of molybdate ester/ZDDP oils.

8.2 The relative importance of contact parameters to the decomposition of molybdenum additives

In Chapter 5, the friction responses of a variety of molybdenum-based friction modifier additives were investigated under a range of contact conditions. One of the aims of this chapter was to identify the most important contact parameters for the effective reduction of friction by these additives. Mild contact conditions were chosen in order to create a mixture of conditions wherein the friction response of the molybdenum additives would be activated in some tests but not others.

In both reciprocating and unidirectional sliding contact, the friction responses of the additives were found to not be greatly affected by the applied load (Figure 5.1 & Figure 5.3) and Hertzian contact pressure. The Hertzian contact pressures of the unidirectional tests (Figure 5.10 & Figure 5.11) were often much higher than those expected of the reciprocating sliding tests, yet it was observed that friction reduction occurred in the nominally lower pressures of the reciprocating sliding contacts and not in those of the higher pressure pin-on-disc tests. In addition, in Figure 5.23 & Figure 5.24 when TE77 pins of smaller radius were used, which would be expected to raise the Hertzian contact pressures outlined in Table 19, the rise in contact pressure actually led to a higher coefficient of friction being observed.

Similar to the Hertzian contact pressure, the sliding speed and lambda ratio were observed to only make minor differences to whether friction reduction was observed or not (Figure 5.10 & Figure 5.11) . By far the most notable differences in performance were the changes in lubricant bath temperature at constant λ (Figure 5.16 & Figure 5.17), and the roughness of the contacting surfaces (Figure 5.3 & Figure 5.4). Both of these factors are likely to affect the temperature in the contact, by changing the bulk and contact flash temperatures respectively. Increased overall contact temperature will facilitate the decomposition of molybdenum additives to MoS_2.

8.2.1 Flash temperatures

To understand the expected contact temperatures from the conditions studied, the flash temperatures of the tribometer systems were calculated using a Blok and a Peclet treatment of the contact conditions. The maximum predicted contact temperature rise above ambient in Blok theory is given by Equation 22 [91,94,232].

$$T_{max} = 1.1\left(\frac{P_{max}\mu U}{(C_p \kappa \rho)^{\frac{1}{2}}}\right)\left(\frac{a}{U}\right)^{\frac{1}{2}}$$

Equation 22 Blok frictional flash temperature rise

Where P_{max} is the maximum Hertzian contact pressure, μ is the friction coefficient, U is the sliding speed, C_p is the specific heat capacity of the contacting materials, κ is the thermal conductivity of the plate, ρ is the material density and a is the width of the contact area.

The Peclet temperature rise is given by:

$$T_{max} = \frac{2}{\sqrt{\pi}}\left(\frac{\mu P_{max} U a}{\kappa}\right) P_e^{\frac{-1}{2}}$$

Equation 23 Peclet frictional flash temperature rise [233]

Where a is the contact area radius and P_e is the Peclet number of the contacting pin.

The predicted flash temperatures for the contact conditions in Chapter 5 are presented in Table 22 below.

Table 22: Hertzian contact pressures and predicted flash temperatures for tribological tests with 100 mm radius TE77 pins outlined in chapter 5 at 40°C

	25 N TE77	100 N TE77	300 N TE77	6.5 N Pin-on-disc
Max Hertzian Contact Pressure (MPa)	117	186	268	735
Mean Hertzian Contact Pressure (MPa)	78	124	179	489
Hertzian Contact Area (mm^2)	0.127	0.320	0.666	0.005
Maximum Predicted Blok flash temperature (°C)	8	16	27	27 (at 0.165 ms^{-1}) 86 (at 1.649 ms^{-1})
Maximum Predicted Peclet Flash Temperature (°C)	8	16	28	28 (at 0.165 ms^{-1}) 88 (at 1.649 ms^{-1})
Mean Final Friction Coefficient (Oil 1 MoDTC Dimer), μ	0.05	0.05	0.06	0.10

Molybdenum additives thermally decompose to form MoS_2 only at temperatures above 300°C [64,66,234,235]. The expected contact temperatures of the conditions studied here are insufficient to thermally decompose molybdenum additives, even at lubricant bath temperatures of 120°C. One major disadvantage of the Hertzian contact treatment is that it does not account for the surface roughness which was an important factor for molybdenum additives to provide a friction drop.

8.2.2 Role of surface roughness

In the simulation work found in 5.2.2.2, it was observed that the Hertzian contact pressure is a poor indicator of the actual pressures found on the contacting asperities (Figure 5.7 & Figure 5.8). If instead of the Hertzian contact pressure the mean asperity contact pressure is used at a reduced contact area, the predicted flash temperatures increase. Using the percentage surface contact as a contact area and the plastic average asperity pressure derived from the contact model, the predicted flash temperatures were recalculated and presented below in Table 23.

Table 23: Effect of asperity contact pressures and surface roughness on predicted flash temperatures at constant Hertzian pressure of 200 MPa

Surface Roughness, R_a, (nm)	50 nm	500 nm
Percentage of contact are compared to Hertzian analysis, (%)	4.4	0.5
Mean Plastic Asperity Contact Pressure (GPa)	5.0	39
Maximum Predicted Blok flash temperature (°C)	173	872
Maximum Predicted Peclet Flash Temperature (°C)	177	894

Consideration of the localised contact temperatures at asperity junctions provides a stark contrast in predicted flash temperatures between the smooth and rough plate systems. The investigation of surface roughness in Chapter 5 took place at a lubricant bath temperature of 40°C (Figure 5.3 & Figure 5.4). When the flash temperature is accounted for with the smooth 50 nm surface, an overall contact temperature of 217°C would be expected, below the 300°C needed for appreciable formation of MoS_2. The formation of MoS_2 was still observed in Figure 5.5 by Raman spectroscopy for the 25 N smooth plate tests however, but only in limited amounts, insufficient to provide optimal friction performance. This result is consistent with a previous investigation of MoDTC performance on smooth surfaces undertaken by Khaemba et al. [80], wherein small amounts of MoS_2 formation was observed even in high friction conditions.

Some MoS_2 formation is likely to occur even in these low-load, smooth plate conditions for two reasons: Firstly, the asperity contact pressure defined by the model is an average, around which there will be some asperity contacts of higher pressure than the mean used in the model. Secondly, the simulation model defining the asperity contact pressures does not account for tractive contributions to the asperity pressures, only the normal component. In a sliding contact the asperities will be subject to both normal and tractive

pressures which will lead to an underprediction of the asperity contact pressures and flash temperatures from the numerical model.

For the 500 nm roughness plates, the same Hertzian contact pressure provides much more thermal energy for MoS_2 formation, with a predicted flash temperature rise of > 800°C. The thermal energy provided leads to more MoS_2 being formed and a reduction in friction coefficient, relative to 50 nm roughness plates at equivalent load.

The role of asperity contact pressure provides an explanation for why the surface roughness has a particularly notable effect on the activation of molybdenum additives. A Hertzian analysis is a poor indicator of the likely local conditions experienced by additive molecules in a contact, which act not upon the macroscopic contact conditions, but only on their sub-asperity-scale localised environment.

8.2.3 Contact pin radius of curvature

The activation of molybdenum additives was found to be dependent on the radius of curvature of the contacting pin in Figure 5.23 & Figure 5.24. In tests with a 10 mm radius pin, neither the MoDTC dimer nor the MoDTC trimer reduced friction effectively. When the pin radius was increased to 40 mm, friction reduction did occur, but with a long induction period. Upon increase of the pin radius of curvature to 100 mm, friction reduction occurred rapidly and consistently.

This is perhaps surprising, as the reduction in radius of curvature leads to an increase in the overall pressure within the contact which would facilitate additive decomposition. The same power input from the contact conditions is also held in a smaller contact area, which might be expected to increase the thermal energy per unit area of the contact. This behaviour is reflected in the expected Hertzian flash temperatures calculated from these conditions in Table 24.

Table 24: Hertzian contact areas and predicted flash temperatures for tribological tests with 100 N load TE77 tests outlined in chapter 5 at 40°C

Pin radius of curvature (mm)	10 TE77	40 TE77	100 TE77	3.25 Pin-on-disc
Max Hertzian Contact Pressure (MPa)	864	343	186	735
Mean Hertzian Contact Pressure (MPa)	575	228	124	489
Hertzian Contact Area (mm^2)	0.069	0.174	0.320	0.005
Maximum Predicted Blok flash temperature (°C)	49	25	16	27 (at 0.165 ms^{-1}) 86 (at 1.649 ms^{-1})
Maximum Predicted Peclet Flash Temperature (°C)	51	25	16	28 (at 0.165 ms^{-1}) 88 (at 1.649 ms^{-1})
Mean Final Friction Coefficient (Oil 1 MoDTC Dimer), μ	0.13	0.08	0.06	0.10

Using the Blok (Equation 22) and Peclet (Equation 23) expressions for the Hertzian flash temperature, it would be expected that the flash temperatures would decrease with increasing Hertzian contact area. This is because the expected drop in the P_{max} term is greater than the increase in the a and r terms. However, the analysis of the asperity contact pressures and contact areas from modelling have shown that the Hertzian contact analysis is a poor indication of the actual asperity-scale contact conditions experienced by the MoDTC additives (Table 23). The P_{max} and subsequent flash temperatures experienced by the asperities is primarily dependent on the surface roughness. When the applied pressure is changed for a fixed surface roughness, the asperity pressure does not change very much beyond the elastic limit, but instead the load is more evenly spread by increased plastic deformation and subsequent increase in the real contact area. As the contact area increases towards the expected Hertzian value, the flash temperatures at the asperities decrease [94,236]. The response of the computational model to various applied pressures is presented below in Figure 8.1.

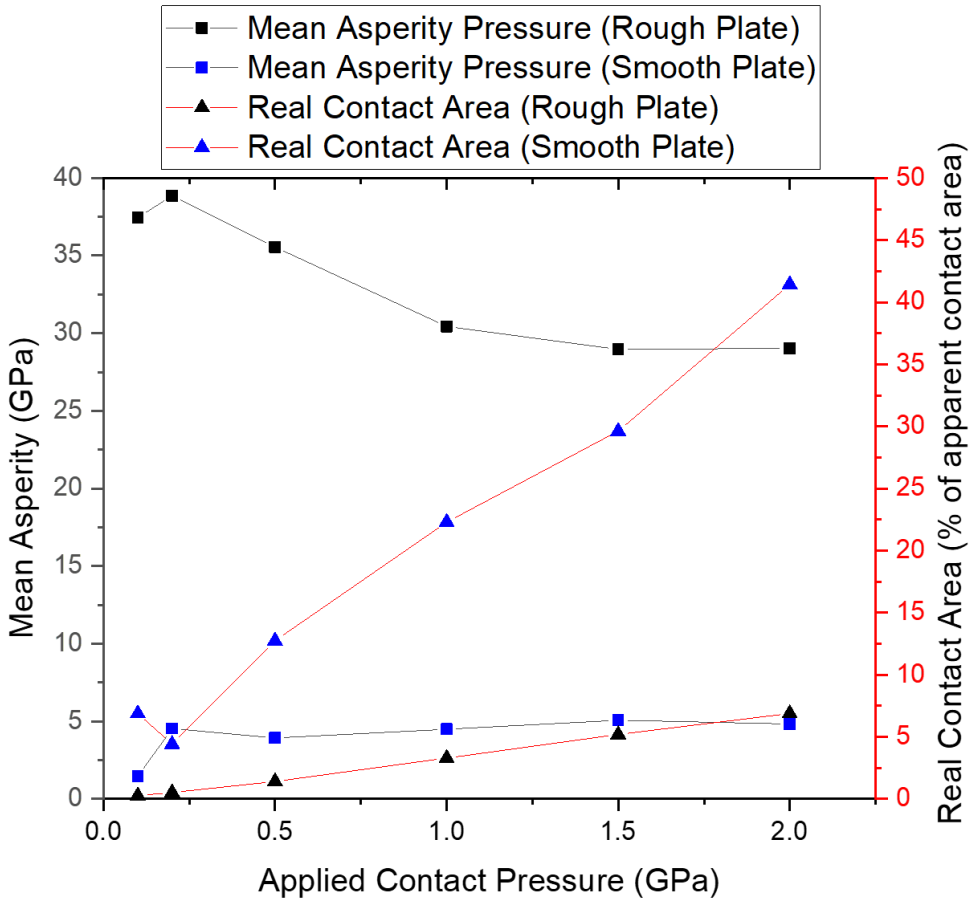


Figure 8.1 Computational model response to increasing applied Hertzian contact pressure

The overall increase in the contact area associated with increased pin radius increases the likelihood of MoDTC decomposition through flash temperature in two ways: First, a wider contact area increases the length of time that a given region of the plate is in contact with the pin [237,238]. This extends the length of time over which frictional heating takes place for any given contact area. Secondly, it takes some time for the overall contact temperature to build up in the contact. The ability of the contact to dissipate the build-up of contact temperature is lessened when the contact zone is larger. This is particularly the case for the pin surface, which is in constant contact with a continuous supply of frictional heat energy [239,240]. A larger contact leads to a greater steady-state frictional temperature. This build-up of temperature may explain the observed behaviour of the MoDTC dimer with the 40 mm radius pin in Figure 5.23 and for the Oil 3 MoDTC dimer in Figure

5.1. The 10 mm pin conditions are insufficiently harsh to reduce friction, but the 40 mm conditions show a reduction in friction but only after a very extended high-friction induction period. This may be due to the build-up of temperature in the contact which exceeds the value needed for appreciable MoS_2 formation, but only after an extended time in contact. Another possibility however may be that MoS_2 friction reduction is a balance between MoS_2 formation and wear processes and MoS_2 is only able to reduce friction after the running-in wear period is completed, this may also act to explain the apparent variability of these induction periods as wear processes show great variability in the time they take to occur.

8.2.4 Temperature of the bulk lubricant & Triboactivation

Increasing the bulk temperature of the lubricant led to reduction in friction for both the MoDTC dimer and the MoDTC trimer. At lubricant bath temperatures of 40°C friction reduction was more modest than at temperatures in excess of 100°C. Increased bulk lubricant temperature facilitates MoS_2 formation in two ways, both chemically and tribologically. The reaction rate for the formation of MoS_2 is composed of two components, a thermal chemical one and a tribological one.

Chemically, the thermal formation rate constant of MoS_2 can be described by an Arrhenius-type behaviour:

$$k_{thermal} = A_0 e^{\frac{-E_a}{\boldsymbol{RT}}}$$

Equation 24 Thermal rate constant Arrhenius behaviour

Where $k_{thermal}$ is the thermal component of the reaction rate constant, A_0 is the pre-exponential factor, E_a is the activation energy of the MoDTC decomposition reaction, $\boldsymbol{R}$ is the ideal gas constant and T the reaction temperature. As the lubricant bath temperature increases, the level of extra thermal energy needed to overcome the reaction activation energy is reduced, increasing the overall reaction rate.

8.2.4.1. Mechanical component of tribochemical reaction rate

In addition to this chemical reaction rate it has been proposed that the fluid stress in the contact has an effect on the reaction rate behaviour to provide a mechanical component to the reaction rate. It has often been noted that reactions in tribological contact can occur at much lower temperatures than would be expected thermally [241]. In order to explain this a theoretical framework has been developed in which the mechanical stresses in a contact effectively reduce the required activation energy of additive decomposition, relative to the thermal reaction alone [191–194,242,243]. This understanding of tribological reaction rate increase builds upon the work of Bell who observed increased reaction rates in cells subjected to shear forces [244]. The effect of the applied mechanical bond stretching is to reduce the effective activation energy, relative to the thermal reaction.

$$k_{tribo} = k_{thermal} e^{\left(\frac{\sigma \Delta V^{\ddagger}}{k_b T}\right)}$$

Equation 25 Tribological-thermal rate relationship [191,245]

Where σ is the shear stress applied to the MoDTC molecule $\Delta V^{\ddagger}$ is the molecule's activation volume. The activation volume of the molecule is the product of the area of the molecule over which the applied shear stress can act A_r and the change in bond length required to break the chemical bond of interest $\Delta x^{\ddagger}$. The reduction of the lubricant viscosity with increasing temperature will increase the reaction rate by increasing the magnitude of the shear forces to which the MoDTC molecules are exposed.

The MoDTC dimer and MoDTC trimer additive studied in this work will have differing tribological contributions to their tribochemical decomposition rate. As the two structures vary in size, they will each present different areas, A_r , and hence activation volumes to the shear forces acting upon them in the contact.

X-ray crystallographic and chemical modelling studies have been undertaken to accurately determine the dimensions of the MoDTC dimer and

MoDTC trimer molecules [246,247]. The MoDTC dimer, with ethyl R-groups, has unit cell dimensions smaller than those of the MoDTC trimer with the same alkyl chains. As such, on average, the MoDTC dimer will present a smaller area over which shear forces can act than the MoDTC trimer. The unit cell sizes of the MoDTC dimer and MoDTC trimer structures (with ethyl R groups) are presented in Table 25.

Table 25: Unit cell sizes of MoDTC Dimer and MoDTC Trimer (R = ethyl)

Unit cell dimension (Å)	MoDTC Dimer	MoDTC Trimer
a	33.961	24.782
b	6.9879	17.849
c	18.086	16.429
Volume ($Å^3$)	4127.9	7267.1

In one dimension, the unit cell structure of the MoDTC dimer is much smaller than the MoDTC trimer, because the MoDTC dimer is an almost planar molecule. However, in solution the molecules will tumble around in all orientations, so it makes more sense to consider the average area presented to the contact, which is 1.76 times greater for the MoDTC trimer. If all other factors are assumed to be equal, the change in activation volume from the MoDTC dimer to the MoDTC trimer would lead to a 2.13 factor increase in k_{tribo} from mechanochemical considerations alone. This increase to the tribological reaction rate doesn't translate into improved friction performance for the MoDTC dimer however. This is because the chemistry of the two additives is not the same and has a greater effect on the friction behaviour of the additives than the mechanical component of the decomposition reaction. For both molecules, the loss of the dithiocarbamate ligands is expected to be the most energetically favourable from computational studies in the gas phase [248]. This study supports the Grossiord proposition for the MoDTC decomposition mechanism [85]. If this computational view of decomposition is correct, it will have consequences for the resulting steric and kinetic behaviour of the additives.

The MoDTC dimer molecule is almost planar and can lie on the contacting surfaces more effectively for decomposition than the MoDTC trimer. In addition to the steric effect of increased likelihood of binding the MoDTC dimer to the surface, this also allows for greater shear stress to act along the line of the chemical bonds than in the trimer. Shear stress can then act in-line with the Mo-S bonds of adsorbed MoDTC dimer in a way that is impossible for the unadsorbed MoDTC trimer due to steric hinderance of its alkyl groups in all three dimensions. In order to effectively bind to the surface, the MoDTC trimer would need to dissociate one of its dithiocarbamate ligands, whereas the planar MoDTC dimer molecule can interact with the iron surface prior to any ligand loss [249].

8.2.4.2. The role of thermal energy in the tribochemical reaction rate

The importance of the thermal component of the reaction rate increase can be seen from Figure 5.16 and Figure 5.17 where the viscosity of the lubricant was kept constant in order to reduce the contribution of the tribological rate increase component. At low temperature, some friction reduction was observed relative to base oil despite little MoS_2 being observed by Raman, but when the temperature was increased the friction coefficient was reduced with increased MoS_2 production. The shear stress was increased independent of the thermal component in the sliding speed tests in Figure 5.10 & Figure 5.11. The shear stress in the form of sliding speed was found to have a minor impact on the ability to reduce friction, but not as great an effect as altering the bulk lubricant temperature (Figure 5.16 & Figure 5.17).

From these observations it appears that the thermal contribution to the tribochemical reaction rate is greater than the tribological contribution in the types of bench tribological tests typically studied by lubricant formulators. The tribological component of the model is more useful for smaller-scale AFM studies on individual molecules rather than macroscale testing on tribometers as the σ and $\Delta V^{\ddagger}$ terms are highly dependent on the localised asperity entrainment environments and molecular orientation respectively. Therefore, the reaction rate will be affected more strongly in some parts of the contact

over others. This may explain why MoS_2 is sometimes observed in contacts without any drop in friction occurring as some localised environments are tribologically capable of MoS_2 formation, but not enough is formed to affect the overall friction behaviour. The tribochemical reaction rate depends also upon the energy potentials of given bonds, making comparisons between different additives difficult [191].

8.2.5 Interactions between the additive and surface chemistry

In addition to the tribological and thermal contributions to the reaction rate, there is of course a role to be played by the chemistry of the additives and the surfaces of the tribological contact. The molecular shape, orientation, bond dissociation energies and surface affinities will all play a role in the likelihood of additive decomposition. Just as important as the chemistry of the additives is the nature of the additive interactions with the tribosurface, both chemically by adsorption and physically through sterics.

The lack of steric hinderance experienced by the MoDTC dimer is proposed to facilitate the decomposition of this additive to MoS_2 by allowing it to access the catalytic effect of an iron surface. Khaemba observed thermal formation of MoS_2 in the presence of iron that was absent from heating the lubricant alone [99]. Molecular modelling studies by Peeters et al. [248,249] have shown that the initial steps of MoDTC decomposition are more energetically favourable in the presence of an iron surface than in the gas phase. The orientation of MoDTC dimer adsorption may also assist in the formation of basally-oriented MoS_2 sheets that are critical for effective friction performance [250,251].

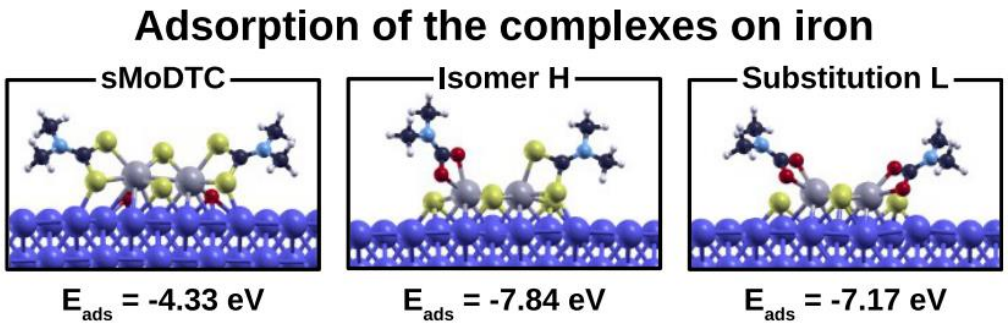


Figure 8.2 Adsorption behaviour of MoDTCs on an iron surface [249]

This energetically more favourable decomposition in the presence of iron may explain previous experimental work that has shown a lack of MoS_2 formation from MoS_2 in non-ferrous contacts. In DLC-DLC contacts or ceramic-DLC contacts, the level of MoS_2 production is less than when one of the counterfaces is ferrous [252–254]. As DLCs and ceramic materials can have greater hardness and elastic modulus than steels, it seems likely that this is a chemical effect rather than a lack of harsh contact conditions which cause the limited MoS_2 production. In this work, all friction testing has been performed in steel-steel contacts, so any catalytic effect of iron has always been present in friction tests.

Steric hinderance of the MoDTC trimer to the iron surface prevents the molybdenum core from benefitting from iron's catalytic effect unless the MoDTC trimer has lost a dithiocarbamate ligand prior to adsorption. The lack of orientation of this species on the surface may offer some explanation of the more amorphous nature of the MoDTC trimer film observed in Figure 6.17 as the molybdenum sulfides formed from this additive do not benefit from basal orientation as the MoDTC dimer sulfides do.

The computational studies by Peeters et al. [248,249] also suggest that the presence of oxygen in the additive structure can improve the adsorption of the additive on iron, facilitating the molecular orientation required for MoS_2 formation. The lack of oxygen in the sulfur-rich MoDTC trimer may encourage the formation of amorphous molybdenum sulfides, whereas the oxygenated MoDTC dimer and molybdate ester are more likely to bind favourably to the iron surface in order to decompose into well-oriented, crystalline MoS_2 sheets.

8.3 MoS_3 as a decomposition intermediate

Tribological testing with the MoDTC dimer, MoDTC trimer and molybdate ester in Chapter 6 under identical tribological conditions developed tribofilms which had different properties. These differences manifested themselves in terms of friction coefficient, MoS_2 surface coverage, tribofilm thickness and the distribution of oxidation states in the tribofilms.

Despite differences in additive structure, the formulations lead to similar surface chemistry. All of the fully-formulated oil systems led to the formation of MoS_2 as observed by Raman and XPS. In fully formulated oil systems, the tribofilms all had similar XPS spectra in the Mo 3d region also, showing a range of Mo (IV) and Mo (VI) oxidation states (Figure 6.14 and Figure 6.15), despite the additives all beginning their decomposition from different oxidation states.

The chemically similar natures of the films suggest that the additives form a common decomposition intermediate on the contact surface. It has been proposed that MoS_2 can be formed on the surface from amorphous MoS_3 [102,143]. An amorphous molybdenum-sulfur tribofilm can be seen in the TEM cross-section of the MoDTC trimer monoblend (Figure 6.17). MoS_3 is also a potential intermediate candidate for the additive decomposition intermediate as it is known to thermally decompose itself to form MoS_2 [140]. MoS_3 is composed of (S^{2-}) and (S_2^{2-}) ligands bonded to Mo (IV) centres and has the same Mo 3d binding energy as MoS_2 [107,150,151]. The proposed structure of MoS_3 is a coordination polymer of trimeric molybdenum-sulfur units in a Mo (IV) or (V) oxidation state presented below in Figure 8.3.

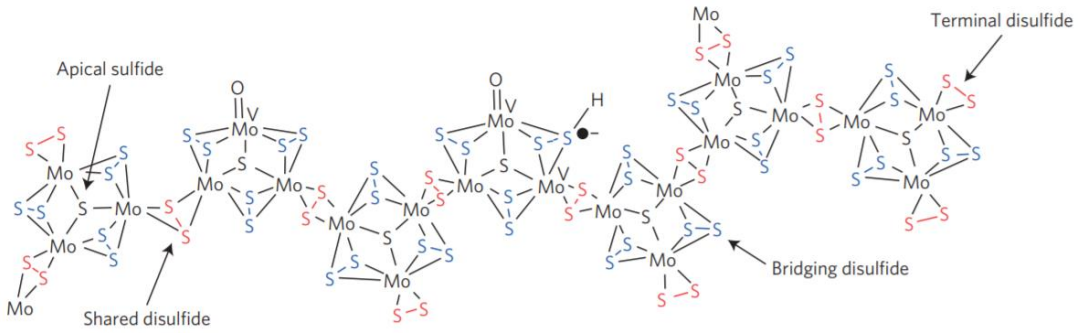


Figure 8.3 Structure of MoS_3 [216]

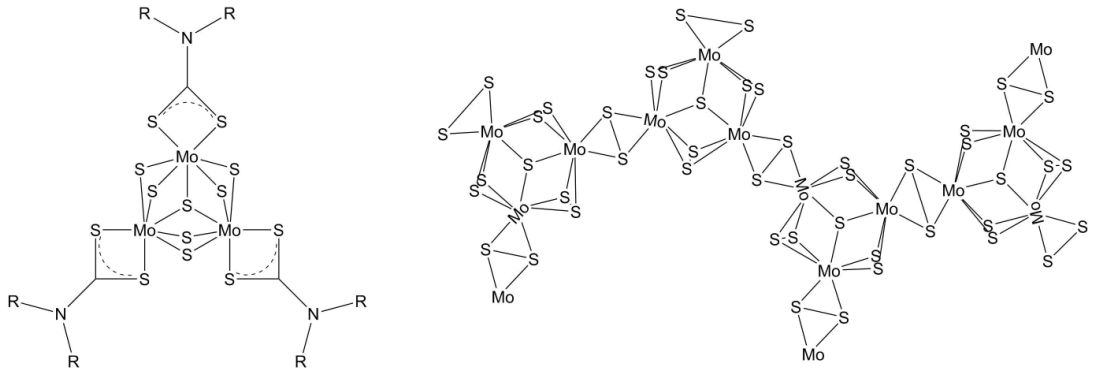
All of the additive tribofilms displayed the Raman vibration associated with apical sulfur at 460 cm^{-1} found in the Raman spectra of MoS_3 extended structures of Mo_3S_{13} unit polymers (Figure 6.7). This vibration is also observed in the Raman spectrum of thermally prepared MoS_3 (Figure 6.25). The increased amount of amorphous molybdenum sulfides displayed by the MoDTC trimer in its FIB-TEM cross-section (Figure 6.17) and increased proportion of Mo(IV) in its XPS spectra (Figure 6.14 & Figure 6.15) may be due to an increased ability of MoDTC trimer to form MoS_3 relative to the other additives. The trimer produced a thicker, more consistent film of amorphous sulfides than the MoDTC dimer or the molybdate ester and this is reflected in both TEM and the levels of "MoS_2" surface coverage (Figure 6.11).

The friction performance of the MoDTC trimer under mild conditions was also consistent with the formation of a full film of MoS_3. MoS_3 has been prepared as a solid lubricant which provides a small degree of friction reduction relative to base oil, but is not as effective as MoS_2. Liu et al. [255] prepared an MoS_3 powder lubricant which reduced friction in sliding contact with an intermediate friction coefficient between that of unlubricated contact and an MoS_2 solid lubricant. In harsher conditions MoS_3 nanoparticles have been shown to form MoS_2 and reduce friction further in the wear scar [256]. In the mild contact conditions outlined in Figure 6.2 and Figure 5.3 an intermediate friction coefficient was observed of $\mu = 0.08$. This behaviour was only observed for the monoblend trimer system. In the fully-formulated systems in Figure 6.3 the MoDTC trimer friction performance was similar to that of the dimer. This is due to a preference for the formation of MoS_2 rather

than MoS_3 in fully-formulated systems. This is discussed further in Section 8.4.

8.3.1 MoDTC trimer's increased ability to form MoS_3

It is possible that the formation of MoS_3 from MoDTC trimer is more energetically favourable than from the other additives. Upon loss of a dithiocarbamate ligand, bridging sulfurs are exposed which can polymerise into the MoS_3 structure. A greater degree of structural rearrangement, and a change in oxidation state is required for the MoDTC dimer and molybdate ester, whereas the molecular MoDTC trimer structure is already in the Mo (IV) state.



a) MoDTC Trimer Structure **b)** Proposed MoS_3 structure

Figure 8.4 Structural relation between MoDTC trimer and MoS_3

Another potential reason for increased MoS_3 deposition from the MoDTC trimer is an increased tribochemical decomposition rate from the increase in the molecular area between the dimeric MoDTC and the MoDTC trimer. This would lead to an increase in the effective $\Delta V^{\ddagger}$ and subsequent increase in the expected k_{tribo}.

8.3.2 MoS_3 vs MoS_2 formation

The differences in performance between the MoDTC trimer and the other additives manifested themselves primarily under mild contact conditions. Under harsh tribological conditions the friction performance of the molybdenum additive systems was very comparable with a coefficient of

friction of μ = 0.05-0.06. Examples of such conditions are the 100 N rough surface tests in Figure 5.1, the 300 N smooth plate tests in Figure 5.6 and the high temperature unidirectional tests in Figure 5.20. Under these harsh conditions the coefficient of friction dropped relative to the highly amorphous MoDTC trimer tribofilm which was observed by TEM (friction profile in Figure 6.2). This drop in friction suggests an increase in crystallinity of the film and the formation of more MoS_2. As the MoS_2 which reduces friction is formed under harsher conditions than those which form the amorphous sulfides it is likely that all the MoDTC trimer films pass through this intermediate prior to formation of MoS_2, with the activation energy to form MoS_2 being greater than that to form MoS_3.

8.4 Idealised properties of molybdenum sulfide tribofilms

The three additives which formed part of the more detailed study in Chapter 6 (MoDTC dimer, MoDTC trimer and molybdate ester) displayed both physical differences in their tribofilm properties and variations in friction performance between the additive structures. The varying natures of the films formed from the additives can offer some insight into what aspects of a lubricant-derived tribofilm are desirable for given properties. Information about the properties of an “ideal” film can be used to inform the chemical properties of future additive development.

8.4.1 Friction performance

The fully-formulated oils of the MoDTC dimer and MoDTC trimer showed comparable friction performance under the conditions studied. The fully-formulated molybdate ester oil however showed a consistently lower friction coefficient than either the MoDTC dimer or MoDTC trimer. This has previously been observed in the literature and is proposed to be due to the action of amine dispersants in fully-formulated oils [143].

In the monoblend systems there was variation in the final friction performance of all three additives. The friction coefficient of the MoDTC dimer was lower than that of the MoDTC trimer. The molybdate ester was unable to

reduce friction in the monoblend due to lack of sulfur in the formulation. The relative friction performance of the systems can be found in Figure 6.4.

8.4.1.1. MoS_2 surface coverage

One common factor which is utilised in the assessment of molybdenum additives is their ability to create as much MoS_2 surface coverage on the tribofilm surface as possible. The level of MoS_2 surface coverage is often related to the overall friction performance of the additive [75,102,203]. It is often assumed that a greater degree of MoS_2 surface coverage will lead to a lower friction coefficient. This was not found to be the case with the additive systems studied in this work, indeed the opposite trend to this could be said to be true (Figure 6.5).

The greatest MoS_2 surface coverage, as determined through Raman spectroscopy, belonged to the MoDTC trimer monoblend, which also showed the highest friction coefficient (Figure 6.11). The lowest MoS_2 surface coverage was found for the molybdate ester fully-formulated system which had the lowest final friction coefficient also (Figure 6.8). Indeed, despite having a higher friction coefficient, the MoDTC trimer showed a greater level of MoS_2 scattering intensity both in terms of surface coverage and absolute scattering intensity than the MoDTC dimer and molybdate ester (Figure 6.5 and Figure 6.6).

8.4.1.1.1. Film crystallinity

One possible explanation for this behaviour may be that friction reduction is not due to the bulk deposition of molybdenum-sulfur species. Rather, the quality of the molybdenum disulfide must be sufficient to reduce friction effectively. In order to effectively reduce friction, the MoS_2 formed from lubricant additives must be crystalline and basally-oriented with respect to the sliding surfaces. Amorphous sulfides have been observed in the literature by TEM during the induction period of MoDTC additives in high friction conditions [84]. In the TEM samples of the trimer tribofilm taken in this work, crystalline MoS_2 domains were observed embedded in a matrix of amorphous sulfides,

with only some of the surface layers oriented in the sliding direction (Figure 6.17).

In addition to the amorphous sulfides observed by TEM, the presence of MoS_2 was observed in higher friction conditions in the pin-on-disc tests during the investigation of the role of lubricant temperature (Figure 5.21). This is consistent with work by Khaemba and Oumahi who noted MoS_2 formation by Raman during sub-optimal friction performance [80,102].

These observations suggest that additives are able to make large quantities of amorphous and poorly-crystalline MoS_2 without providing optimal friction performance, as observed in the tests with the MoDTC trimer. In order to be effective, the MoS_2 deposited on the surface must be deposited at the interface, not buried in a film, it must be basally-oriented in the sliding direction and must be sufficiently crystalline for sliding between MoS_2 layers to occur. The MoS_2 crystal chain length has been proposed as a determining factor in the improvement in performance of molybdate esters in the presence of amines [70,143].

From the observed behaviour of the additives it seems likely that the molybdate ester fully-formulated oil is the most effective friction modifier under the TE77 testing conditions because it is able to form highly-crystalline sheets of MoS_2. Whereas the MoDTC trimer, although it deposits a large quantity of molybdenum-sulfur species, these are amorphous and unable to act as friction modifiers. The low Raman surface coverage observed for the molybdate ester is not an issue because MoS_2 is formed in areas of surface contact, which are known to be only a small proportion of the apparent contact area.

8.4.1.1.2. Raman MoS_2 surface coverage as an analysis technique

The comparison of the levels of MoS_2 surface coverage determined by Raman with the friction coefficient has shown that MoS_2 surface coverage is a poor indicator of predicted tribofilm performance. The ability of an additive to reduce friction is primarily determined by its chemistry, therefore comparisons of MoS_2 surface coverage determined by Raman is a poor indicator of expected friction performance when comparing different additives. When comparing conditions with the same additive however, the correlation

between surface coverage and friction seems valid, as evidenced by the drop in surface coverage with increasing friction coefficient for the molybdate ester systems with changing ZDDP concentration in Figure 7.7. A model exploring this behaviour for the MoDTC dimer was created by Xu et al [86].

8.4.2 Tribofilm durability

In the durability tests of the tribofilms derived from the three main additive structures, the friction durability of the MoDTC trimer monoblend film was greater than the any of the other monoblend or fully-formulated systems for the other additives (Figure 6.20). Indeed, the MoDTC trimer monoblend film was the only one which did not show an almost instantaneous reversion to base oil friction coefficients upon removal of the molybdenum supply from the contact. This durability performance is likely a product of the unique nature of the MoDTC trimer monoblend tribofilm.

8.4.2.1. Monoblend tribofilms

Unlike the MoDTC dimer, the MoDTC trimer monoblend tribofilm produces a thick 30 nm thick layer of molybdenum-sulfur species (Figure 6.17). The MoDTC dimer monoblend tribofilm consisted of only a few layers of MoS_2 (Figure 6.18). When the MoS_2 tribofilm is rubbed in base oil, the MoS_2 is expected to be removed through wear. The MoS_2 tribofilm is sacrificial and therefore is lost from the surface with rubbing [257]. As the durability tests were performed under the same conditions for the MoDTC dimer and trimer monoblend oils, it stands to reason that the overall MoS_2 film removal rate would be equivalent across the whole wear scar area for both systems. The thinner MoS_2 film derived from the MoDTC dimer will be depleted more quickly than the thicker MoDTC trimer film and the friction-reducing effect of MoS_2 will be removed from the contact more quickly. This is consistent with the more rapid rise in friction observed in the MoDTC dimer durability tests (Figure 6.20).

In addition to the increased friction durability provided by the film thickness, another potential contributing factor to the friction durability of the MoDTC trimer tribofilm is the possibility of further MoS_2 formation. It is possible

that the MoDTC trimer film is able to continue making some MoS_2 in contact from the amorphous sulfides which form part of the film. As the severity of the contact conditions do not change upon changing the oil to base oil, the conditions remain the same as those which were able to form an MoS_2 tribofilm in the presence of molybdenum additives. Therefore, the conditions remain sufficiently harsh to form MoS_2 when the oil is switched for base oil, there simply is a lack of molybdenum supply. Therefore, there is likely to be some conversion of the amorphous molybdenum sulfides in the MoDTC trimer monoblend tribofilm into crystalline MoS_2 as the tribofilm is worn away and new layer of molybdenum sulfides is exposed. The conversion of amorphous molybdenum sulfides to MoS_2 has been shown to occur in solid coatings [255,256]. This further formation of MoS_2 is likely to contribute to the maintenance of lower friction than if the MoS_2 were removed instantly.

8.4.2.2. Fully-formulated tribofilms

The fully-formulated oil tribofilms all showed a near instantaneous rise in friction upon replacement of the molybdenum additive-containing oil with a molybdenum-free fully-formulated oil (Figure 6.19). This is consistent with previous studies on friction durability of the MoDTC dimer performed by Morina [74]. Unlike the monoblends, this behaviour was observed for all three additives, including the MoDTC trimer. This implies that the previous behaviour for the MoDTC trimer monoblend regarding film thickness and formation of amorphous sulfides may not apply in a fully-formulated system.

In fully-formulated oil systems containing ZDDP, the tribofilm thickness is determined primarily by the ZDDP phosphate glass film. The MoS_2 which forms in the contact can be either embedded in this film during the film growth process or it can sit atop the ZDDP film. It is the MoS_2 film which sits atop the ZDDP phosphate glass which determines the ultimate frictional characteristics of the film, as this is the junction point between the sliding surfaces. FIB-TEM samples of MoDTC trimer films formed with ZDDP show only a very thin surface MoS_2 film of ca. 3-5 nm thickness, similar to the MoDTC dimer [89]. ZDDP films are known to be more durable than MoS_2 films, showing little

reduction in thickness in durability tests [163]. Ueda tested the durability of tribofilms derived from various ZDDPs and noted no reduction in film thickness even after an hour of rubbing in PAO [166]. The maintenance of the durable ZDDP film thickness is likely to prevent any embedded molybdenum sulfides from reaching the surface and reducing friction, as such the friction coefficient rises rapidly upon removal of the molybdenum-containing oil. Therefore, in fully-formulated systems, the overall tribofilm durability behaviour is dominated by ZDDP, which produces a thick phosphate glass upon which only a limited amount of MoS_2 can form, and whose durability also prevents residual Molybdenum species buried in the tribofilm from acting upon the friction behaviour of the film.

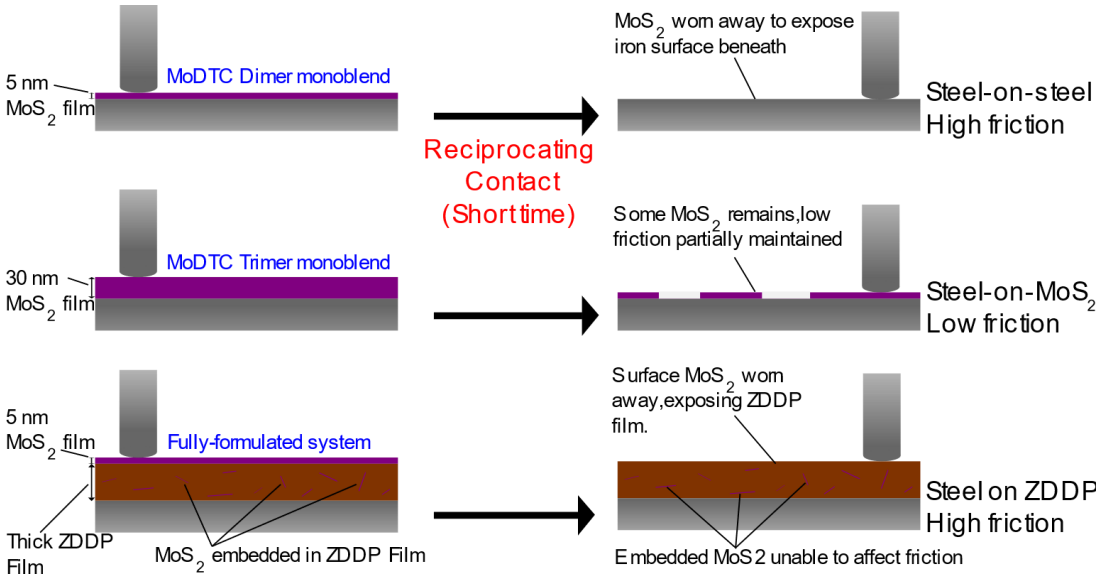


Figure 8.5 Effect of tribofilm nature on the durability of friction performance

8.4.2.3. An ideal MoS_2 film

From the behaviour of the additives and the nature of their tribofilms, some basic properties of tribofilm behaviour can be laid out:

1. The friction performance is not primarily determined by the surface coverage of MoS_2 by the additive, but the nature of MoS_2 is more important.

2. Amorphous molybdenum sulfides do not reduce friction as effectively as crystalline MoS_2.

3. The durability of friction reduction is controlled by the MoS_2 film thickness.

4. Amorphous sulfides can still reduce friction relative to base oil, either by conversion to crystalline MoS_2 through sliding, or by their own action.

Therefore, an idealised film that can be formed from molybdenum additives would be one which produces highly crystalline MoS_2 in the first instance, rather than amorphous sulfides. For the maintenance of friction reduction where the oil supply is not constant the film formed should be as thick as possible. Whilst beneficial from a durability perspective, it is not necessary to fully cover the surface in MoS_2 in order to provide optimal friction performance.

8.5 The formulation dependence of molybdate ester additive systems

In Chapter 7 the formulation dependence of the molybdate ester systems was investigated. The friction performance of the molybdate ester oil systems was found to be dependent on the supply of sulfur to the additive in the form of ZDDP. The friction behaviour of the molybdate ester was also found to be affected by the addition of an oil-soluble amine dispersant.

8.5.1 Dependence on sulfur supply in fully-formulated conditions

In section 7.2.1 the friction performance of fully-formulated molybdate ester systems was investigated as a function of the Mo:S ratio in the oil. The Mo:S ratio was altered by keeping a constant concentration of Mo of 400 ppm and changing the ZDDP loading in the formulation from that typical of a fully-formulated oil of 400 ppm downwards. The fully-formulated tests are the most interesting for discussion around the performance and chemistry of molybdate

ester tribofilms with changing sulfur supply, as these tests do not suffer from the interfering effects of bulk ZDDP films and solubility issues observed for the smooth plate binary mixture tests in 7.2.2. Upon altering the Mo:S ratio from 1:2 to 2:1 the coefficient of friction rose from μ = 0.04 to μ = 0.09.

The decomposition reaction of the molybdate ester is proposed to function through the exchange of sulfur with ZDDP, followed by the decomposition a sulfur-molybdate species to MoS_2. Alteration of the Mo:S ratio is likely to affect the kinetics of this reaction.

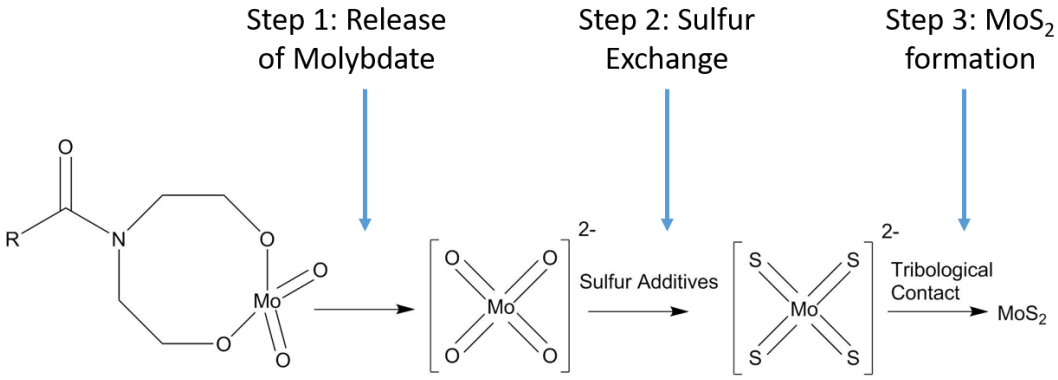


Figure 8.6 Molybdate ester sulfur transfer mechanism

As the Mo:S ratio was increased a decrease in the MoS_2 surface coverage was observed (Figure 7.7). This implies that this sulfur transfer reaction was occurring at a reduced rate. It is not clear whether full sulfurization of the molybdate intermediate is necessary for MoS_2 formation or whether mixed oxythiomolybdates can decompose to form an oxygen-rich MoO_xS_{2-x} oxysulfide analogue of MoS_2. MoS_2 has been shown to form thermally from the mixed oxythiomolybdate Cs_2MoOS_3 when heated in air [258]. Oxygen-rich MoS_2 of the form MoO_xS_{2-x} would have inferior sliding properties as oxygen incorporation disrupts the lattice layer structuring so critical for the effective friction performance of MoS_2 [259,260]. In either case, the total amount and coverage of good-quality MoS_2 is reduced as sulfur becomes less available for the molybdate. This reduction in MoS_2 formation leads to impaired friction performance in sulfur-starved formulations.

In the binary molybdate ester/ZDDP formulations, the same dependence on Mo:S ratio is observed in Figure 7.9, but a consistent friction response was

only observed for these systems at elevated temperatures and with roughened plates. This was not the case for the sulfur-containing additive systems studied in Chapter 5 and suggests that it may require harsher conditions to elicit a friction response form the molybdate ester than sulfur-containing additives.

8.5.2 The relative difficulty in activation of molybdate ester friction response

The sulfur-containing additive systems outlined in Chapter 5 were capable of reducing friction to μ ≈ 0.05 both with smooth plates and at a lubricant bath temperature of 40°C. In contrast, the molybdate ester FFO systems only showed optimal friction reduction at a temperature of 100°C. Reduction of the lubricant bath temperature to 40°C led to an increase in the friction coefficient for these conditions as outlined in Figure 7.12. This was also the case for the binary systems, except in these examples, long-term friction reduction was only possible in rough plate conditions.

It may be initially considered that the molybdate is harder to activate to form MoS_2 because it must undergo a two-step reaction with ZDDP to form MoS_2, whereas the sulfur-containing additives can simply decompose to this product. However, the molybdate mechanism testing in 7.5.3 showed that the rate-determining step of friction reduction was release of free molybdate from the additive structure. Once a free molybdate was available to the formulation, friction reduction was easily achieved, even at a lubricant bath temperature of 40°C. The sulfidation of the molybdate can occur at ambient temperature [141,145]. Therefore, it is likely that the removal of organic groups from the molybdate ester structure is the single step inhibiting bulk MoS_2 formation in these systems. An increased degree of input energy required to decompose the molybdate additives is consistent with the low surface coverage observed for these systems by Raman spectroscopy (Figure 7.4). Previous thermogravimetric analysis of the molybdate ester structure has shown that it decomposes with one mass-loss step at 295°C, comparable to MoDTCs [222].

In the molybdate ester friction tests, optimal friction reduction only occurred in systems where a thick ZDDP film was not formed (Figure 7.24). In the case of binary systems, friction initially dropped, but then climbed as a ZDDP anti-wear film was formed (Figure 7.5). The formation of a ZDDP film inhibits the formation of MoS_2 from the molybdate ester by reducing the severity of the contact conditions to the point that molybdate ester decomposition can no longer occur. In the initial stages of contact, the contact properties are steel-on-steel, which has an elastic modulus of 220 GPa [170,261]. Upon formation of the ZDDP film, the surface mechanical properties are controlled then by the properties of the ZDDP tribofilms on the pin and plate surfaces. ZDDP tribofilms have temperature-dependent mechanical properties wherein the elastic modulus decreases with increasing lubricant temperature [261]. At the temperatures studied in this work, the elastic modulus of a ZDDP tribofilm is around 100 GPa, significantly lower than steel surfaces. This will lead to a greater degree of energy dissipation as energy is lost to plastic deformation of the ZDDP tribofilm and subsequently lower contact temperatures. In addition to the action of ZDDP as an anti-wear additive, the formation of a ZDDP tribofilm reduces the severity of the contact conditions to a point that the molybdate ester is unable to effectively reduce friction. Furthermore, the formation of a ZDDP film on both contacting surfaces removes the possibility of molybdenum additives binding directly to the steel surface, which has been shown to facilitate the formation of MoS_2 films through favourable scission of bonds [249]. The absence of a free ferrous surface in the contact zone (as it becomes a ZDDP surface) further increases the difficulty of forming MoS_2 in the contact.

The molybdate ester can be made to reduce friction in ZDDP-containing formulations by increasing the severity of the contact conditions, such as by increasing the surface roughness of the contacting plates. This alteration affords an increase in the tribochemical activation energy sufficient to reliably reduce friction even in binary formulations (Figure 7.9). In previous works surrounding the action of the molybdate ester, the contacts have been studied at high pressures and surface roughnesses to elicit a strong friction response [137,222]. Friction reduction can also be achieved by preventing the formation

of a bulk ZDDP film through thermal decomposition of the additive. In section 7.5.2, ZDDP was thermally decomposed under nitrogen so that it was unable to form a thick tribofilm, whilst maintaining the sulfur supply in the oil. Friction testing of this aged oil in Figure 7.29 showed a consistent reduction in friction, unlike the binary system from which the oil was derived. The TE77 pin for these test also did not display a thick ZDDP film in Figure 7.30 and Figure 7.24, consistent with maintaining steel-on-steel contact, providing sufficiently harsh conditions for the molybdate ester to form MoS_2 and reduce friction.

8.5.3 The effect of amines/dispersants on the activity of molybdate ester formulations

In addition to increasing the severity of contact conditions and inhibiting formation of a bulk ZDDP film by increasing the contact surface roughness, ZDDP bulk film formation can be inhibited chemically. The addition of a fatty amine to the binary Mo:S oil formulations led to a consistent drop in friction absent in the binary formulations themselves (Figure 7.15). This improvement in molybdate ester friction performance by addition of an amine has been termed the “fatty amine booster effect”. It has been proposed by De Barros Bouchet et al. [143] that this effect is caused by stabilisation of a free molybdate intermediate to form an ammonium salt. Fatty amines have also been shown to slightly improve the friction coefficient behaviour of MoDTC systems that contain ZDDP [149].

Lundgren et al. have proposed that the fatty amine is able to improve the friction performance of MoDTCs by acting in tandem with this additive as an organic friction modifier [149]. However, this does not appear to be the case in this work, as the fatty amine does not reduce friction relative to a ZDDP control oil under the conditions studied (Figure 7.16). This disparity is likely due to the conditions studied. OFM systems display better friction characteristics when there is some degree of rolling contact, such as the MTM tests which are often used to characterise these species. In purely sliding contacts such as the TE77 and high-frequency reciprocating rigs (HFRRs),

friction coefficients are dominated by extreme pressure additives such as molybdenum additives and ZDDP [262].

The low-friction tests involving the addition of fatty amine to the binary formulations do not display the formation of a thick ZDDP film on the contacting pins (Figure 7.24). This is also consistent with the behaviour of the fully-formulated oil systems, which contain dispersants of various kinds. It has previously been observed that succinimide dispersants can effectively reduce the development of a ZDDP film, and at higher concentrations completely prevent their formation [180,263]. As both the fully-formulated tests with dispersant and the fatty amine friction tests reduce friction effectively at the cost of forming a bulk ZDDP film, it appears likely that the fatty amine is acting in the same form as a dispersant in this case. By inhibiting the development of a bulk ZDDP tribofilm, the amine-containing system maintains the harsher conditions of steel-on-steel contacts necessary for molybdate ester friction reduction. Also, the lack of ZDDP film coverage maintains the presence of a free ferrous surface to facilitate additive decomposition and MoS_2 formation.

There may be some contribution to the fatty amine booster-effect from stabilisation of a molybdate or thiomolybdate intermediate. As amines are basic, they stabilise the simple molybdate and thiomolybdate anions proposed in the decomposition mechanism [141,145]. Under more acidic conditions these species construct larger molybdate structures such as heptamolydate [264]. If this effect does also occur in oil formulations, it does not seem to contribute as much as ZDDP-dispersant antagonisms. The tests in Figure 7.27 using DIPEA as an added amine showed no better friction reduction then the binary systems alone. DIPEA’s steric hindrance allows it to make a basic environment without being able to interact with the surface as strongly as the primary fatty amine. Therefore, if the basicity of dispersant amines does stabilise the molybdate intermediates as proposed by De Barros Bouchet et al. [143] then this effect is not as significant as the surface effects of dispersant-ZDDP interactions.

Chapter 9: Conclusions & Future Work

9.1 Conclusions

9.1.1 Contact conditions for activation of Molybdenum additive friction responses

- Whether a friction response is observed from a molybdenum additive depends upon the severity of the contact conditions and the additive's chemistry, as does the degree of friction reduction from that additive.

- In sliding contacts (both reciprocating and unidirectional), molybdenum additive friction responses are most strongly initiated by increasing the surface roughness of the contacting surfaces and the temperature of the lubricant bath. The increase in surface roughness provides an increase in local asperity contact pressures and flash temperatures. Increases in lubricant bath temperature provide increased shear stresses and more thermal energy to overcome the tribochemical reaction barrier to additive decomposition.

- Increases in the Hertzian contact area initiated by changes in pin radius of curvature increase the likelihood of an MoS_2 friction response for a given set of conditions and reduce the length of the MoDTC high-friction induction period.

9.1.2 Molybdenum additive structure-activity relationships

- Under the reciprocating studied the different additive structures displayed alternate friction profiles. These manifested themselves primarily in the behaviour of the high-friction induction period. The trimeric structure showed an extended, slow decay type of induction period. The MoDTC dimer (C8-C14) shared a similar profile to the standard MoDTC dimer, but with a very variable length of induction period, dependent on the severity of the contact conditions.

9.1.3 MoS_2 tribofilm properties

- The friction coefficient of a molybdenum additive system is not primarily determined by the level of Mo:S species surface coverage as has previously been proposed, at least not on the macroscale. Despite consistently showing the lowest MoS_2 surface coverage by Raman, the molybdate ester had the lowest friction coefficient under the conditions studied.

- The greater bulk deposition and film thickness of Mo:S species observed for the MoDTC trimer monoblend afforded this system a greater degree of friction-reducing durability than the MoDTC dimer system which deposited a thinner film on the surface. Therefore, the Mo:S film thickness likely determines friction durability of a tribofilm.

- The MoDTC trimer produced a more amorphous tribofilm structure with a preference for Mo (IV) and MoS_3 scattering peaks than the other additive systems. This amorphous tribofilm observed by TEM for the MoDTC trimer monoblend had a higher friction coefficient than the other monoblend systems. The amorphous nature of the film prevents MoS_2 layers from sliding over one another. Therefore, the crystallinity of an MoS_2 tribofilm is likely an important determining factor in its friction performance, with more crystalline films providing lower friction coefficients.

- The increased deposition of amorphous species by the MoDTC trimer suggests a preferential formation of amorphous MoS_3 from this additive as it shares structural features with the MoS_3 coordination polymer.

9.1.4 Molybdate Ester behaviour

- The friction behaviour of molybdate esters is dependent on the Mo:S ratio of the oil formulation and the contact conditions. In mild conditions, reductions in the concentration of sulfur increase the observed friction coefficient in tribological testing. Under harsh conditions the friction performance is less sensitive to Mo:S ratio, but still dependent upon it.

- Molybdate ester friction performance is more temperature sensitive than MoDTC dimer and MoDTC trimer systems. Higher lubricant temperatures are needed for optimal friction performance in the TE77 reciprocating contact conditions studied in this work.

- Molybdate ester friction performance is inhibited by the formation of a bulk ZDDP phosphate film on the surface. In binary systems, friction begins low but increases as a thick phosphate film develops and reduces the severity of the contact conditions.

- The development of a thick phosphate film to maintain optimal friction performance can be achieved in three ways:

    1. By increasing the severity of the contact conditions to prevent a large-scale phosphate film forming.

    2. By thermally decomposing ZDDP so that it is unable to form a film on the surface, whilst still maintaining the sulfur supply of the formulation.

    3. Inhibition of the ZDDP film-forming ability through the addition of amine dispersants which reduce the development of a thick ZDDP phosphate film.

- The “fatty amine booster effect” allows molybdate esters to reduce friction in ZDDP-containing systems better than the binary systems

alone. The notable effect of amines on the formation of a ZDDP film and subsequent decrease in friction suggests that this is a ZDDP-centred effect rather than a molybdate-centred effect as previously thought.

9.2 Future Work

9.2.1 The kinetic behaviour of the MoDTC dimer induction period

Under mild tribological conditions, some MoDTC dimeric structures, such as the C8-C14 dimer in Figure 5.1 and the standard MoDTC dimer in Figure 5.23, displayed an extended high friction induction period. This extended induction period behaviour appears to occur when the conditions are not sufficiently harsh to effectively reduce friction. However, at the very start of the test, before the surfaces conform through running-in wear, the conditions for MoS_2 formation should be harshest and most favourable. It would be interesting to note the behaviour of the surface in a time-resolved manner throughout this induction period to understand the nature of the tribofilm and the surface chemistry before and after a friction drop. Some work has been performed in this area by Rai et al. [87] who took time-resolved Raman and TEM slices before and after an induction period. In this work, the authors used a standard MoDTC dimer formulation and the induction period was short and predictable (ca. 5 minutes). It would be of interest to determine if the results of this work (that amorphous Mo:S was on the surface in the induction period and crystalline MoS_2 is observed after it) can be extended to determine if this is the case for systems with variable induction periods seen in this study.

Improved temporal resolution of TEM slices during the friction drop period will allow determination of if improved crystallisation of the deposited Mo:S film is the trigger for a reduction in friction. If FIB-TEM cross sections can be found at intervals during the friction drop period, the percentage area coverage of crystalline vs amorphous species in the FIB section can be analysed as a measure of degree of crystallinity. This work may be able to answer if the crystallinity of a film is indeed the driving factor for low friction, as opposed to the current thinking of MoS_2 volume deposition.

9.2.2 Quantitative XPS for determination of Mo/S ratio in MoS_x species

Amorphous molybdenum sulfides such as those seen in this study have a greater Mo/S ratio in their structure than crystalline MoS_2. Sulfides of the form MoS_x (where $x > 2$) can be seen as intermediates towards the formation of crystalline MoS_2. By comparison of the Mo/S ratio in tribofilm samples prepared by thermal decomposition by XPS, a calibration curve of Mo/S ratio for tribofilms can be created. Upon studying a tribofilm, the quantitative Mo/S ratio determined through XPS peak areas can be used as a more non-destructive indication of the level of crystallinity in the tribofilm for monoblend species. This quantitative understanding of Mo/S ratios in films would prevent the need for FIB-TEM slices to be taken of tribofilms in order to understand crystallisation which destroys the sample for further analysis during the FIB coating process.

9.2.3 Harsh conditions and the role of iron molybdates

In this work, no iron molybdates were noted on the surface by Raman spectroscopy. In other works, such as those by Khaemba [98] and Okubo [265], iron molybdates were observed on the surface but these tribological tests were performed under much higher contact pressures and sliding conditions. This suggests that under harsh enough conditions, the MoDTC molybdate structures can interact with iron, but that the formation of this species is not necessary for MoS_2 formation or optimal friction performance. Tribological tests under harsh conditions should be attempted to determine if there is a tribochemical activation point for the formation of iron molybdates on the iron surface. In addition, tribological tests to form iron molybdates should be run with the molybdate ester monoblends as well as MoDTC to determine if the formation of these species is a mechanistic step unique to MoDTC dimer or if any oxygenated molybdenum species is capable of interacting with a ferrous surface this way. It is notable in this work that iron molybdates were not even seen in the molybdate mechanism testing Raman

spectra where ammonium orthomolybdate $(NH_4)_2MoO_4$ was used as a model compound (Figure 7.34).

9.2.4 Molybdates with non-film-forming sulfur sources

In this work, the molybdate ester reduced friction only in ZDDP-containing systems. The addition of ZDDP to formulations makes it more challenging to understand the fundamental chemical behaviour of the molybdate ester as the interfering effect of ZDDP film formation masks the MoS_2 film behaviour of the molybdate ester.

In order to better study MoS_2 films derived from molybdate esters, alternate oil-soluble sulfur sources should be investigated that do not form their own tribofilms. This will ensure that model molybdate ester formulations only form MoS_2 films such that the tribofilms of this additive can be compared with MoDTC monoblends more effectively. Oil-soluble thiols (mercaptans) and organic disulfide species would be appropriate candidates for potential sulfur candidates that do not form an interfering inorganic tribofilm.

Allowing the formation of a purely Mo:S tribofilm will allow comparisons of MoS_2 film thickness and crystallinity for a molybdate ester “monoblend” in a similar manner to the MoDTC dimer and MoDTC trimer comparisons outlined in Chapter 6. Only in the absence of a ZDDP film can the ultimate behaviour and chemistry of molybdate esters be fully confirmed.

9.2.5 Tungstates as DLC-friendly molybdate analogues

One issue in oil formulations regarding the use of molybdenum additives is their antagonistic interactions with friction-reducing diamond-like carbon (DLC) surfaces. The use of common MoS_2-forming additives leads to an acceleration of DLC coating wear [266,267]. This issue means that there is a need for molybdenum-free, oil-soluble friction modifier that can reduce friction without unduly damaging DLC-coated surfaces. Tungsten is frequently used in DLC as a performance-improving dopant [268–270].

Tungsten shares a lot of similar chemistry with molybdenum and tungsten disulfide WS_2 has been shown to act as an effective friction modifier for PVD coatings and nanoparticle formulations [271,272]. Organic tungstates of similar form to the molybdate ester can be formulated as oil-soluble lubricant additives for similar tribological characterisation as has been performed for the molybdenum compounds in this study. The sulfur-dependence of these additives and their film formation properties in relation to ZDDP should be determined in order to characterise their suitability as friction modifiers. If successful, these additives may offer lubricant formulations opportunities for DLC-coated contacts.

9.2.6 Quantitative nanoscale dispersant antagonisms

The ZDDP film-reducing effect of fully-formulated oil dispersant and fatty amine behaviour warrants further investigation. In the tests in this work a 1 wt% addition of fatty amine was made to binary mixtures to investigate the effect. In order to quantify this behaviour, a range of different formulations should be created with varying loading of fatty amine and the ZDDP films should be grown *in-situ*.

This experiment can be achieved through the use of an atomic force microscope (AFM). ZDDP films can be made through rubbing of an AFM tip in oil on a steel surface. The thickness of a ZDDP film can then be measured by the change in the topography of the surface. By monitoring the ZDDP film growth as a function of time for various loading of fatty amine in the oil formulation, the inhibiting effect of a fatty amine on ZDDP film growth can be quantified by determination of the percentage film thickness at a given time relative to an amine-free system.

One issue with this experiment is that it would only allow a small thickness of film to be studied in the AFM. For a reduction in precision, a more representative macroscale experiment would involve monitoring the ZDDP film thickness with a Spacer Layer Imaging (SLIM) device attached to a tribometer. Similar work has been performed by Spikes et al. [161,262]. This device tracks the film thickness of ZDDP tribofilms in sliding-rolling contact. Utilising the macroscale test will allow for the degree of surface coverage by

the ZDDP film to be determined as well as the film thickness as a function of fatty amine/dispersant doping.

List of References

[1] Holmberg K, Andersson P, Erdemir A. Global energy consumption due to friction in passenger cars. Tribol Int 2012;47:221–34. https://doi.org/10.1016/j.triboint.2011.11.022.

[2] Spikes H. Friction Modifier Additives. Tribol Lett 2015;60:1–26. https://doi.org/10.1007/s11249-015-0589-z.

[3] Ratoi M, Niste VB, Alghawel H, Suen YF, Nelson K. The impact of organic friction modifiers on engine oil tribofilms. RSC Adv 2014;4:4278–85. https://doi.org/10.1039/c3ra46403b.

[4] Ratoi M, Niste VB, Alghawel H, Suen YF, Nelson K. The impact of organic friction modifiers on engine oil tribofilms. RSC Adv 2014;4:4278–85. https://doi.org/10.1039/C3RA46403B.

[5] Davidson JE, Hinchley SL, Harris SG, Parkin A, Parsons S, Tasker PA. Molecular dynamics simulations to aid the rational design of organic friction modifiers. J Mol Graph Model 2006;25:495–506. https://doi.org/10.1016/j.jmgm.2006.03.006.

[6] Ratoi M, Anghel V, Bovington C, Spikes HA. Mechanisms of oiliness additives. Tribol Int 2000;33:241–7. https://doi.org/10.1016/S0301-679X(00)00037-2.

[7] Anghel V, Bovington C, Spikes HA. Thick Boundary Film Formation by Friction Modifier Additives. Lubr Sci 1999;11:313–35.

[8] Ratoia M, Bovington C, Spikes H. In situ study of metal oleate friction modifier additives. Tribol Lett 2003;14:33–40. https://doi.org/10.1023/A:1021714231949.

[9] Tang Z, Li S. A review of recent developments of friction modifiers for liquid lubricants (2007-present). Curr Opin Solid State Mater Sci 2014;18:119–39. https://doi.org/10.1016/j.cossms.2014.02.002.

[10] Choo JH, Forrest AK, Spikes HA. Influence of organic friction modifier on liquid slip: A new mechanism of organic friction modifier action. Tribol Lett 2007;27:239–44. https://doi.org/10.1007/s11249-007-9231-z.

[11] Koshy CP, Rajendrakumar PK, Thottackkad MV. Evaluation of the tribological and thermo-physical properties of coconut oil added with MoS2 nanoparticles at elevated temperatures. Wear 2015;330–331:288–308. https://doi.org/10.1016/j.wear.2014.12.044.

[12] Verma A, Jiang W, Abu Safe HH, Brown WD, Malshe AP. Tribological behavior of deagglomerated active inorganic nanoparticles for advanced lubrication. Tribol Trans 2008;51:673–8. https://doi.org/10.1080/10402000801947691.

[13] Spreadborough J, Bollmann W. © 1960 Nature Publishing Group. Nature 1960;186:29–31. https://doi.org/10.1038/186029a0.

[14] Torregrosa AJ, Broatch A, García A, Mónico LF. Sensitivity of combustion noise and NOx and soot emissions to pilot injection in PCCI Diesel engines. Appl Energy 2013;104:149–57. https://doi.org/10.1016/j.apenergy.2012.11.040.

[15] Castoldi L, Matarrese R, Lietti L, Forzatti P. Simultaneous removal of NOx and soot on Pt-Ba/Al 2O3 NSR catalysts. Appl Catal B Environ 2006;64:25–34. https://doi.org/10.1016/j.apcatb.2005.10.015.

[16] Farrauto RJ, Heck RM. Catalytic converters: State of the art and perspectives. Catal Today 1999;51:351–60. https://doi.org/10.1016/S0920-5861(99)00024-3.

[17] Kaleli H. Engine emissions and poisoning effect of synthetic oil's additives on catalytic converter using an engine dynamometer. Ind Lubr Tribol 2003;55:162–77. https://doi.org/10.1108/00368790310480353.

[18] Dowson D. History of Tribology. 2nd ed. London: Professional Engineering Publishing; 1997.

[19] Jost P. Lubrication (Tribology) A report on the present position and industry's needs. London: 1966.

[20] Williams J. Engineering Tribology. 1st ed. Cambridge University Press; 2005.

[21] Straffelini G. A simplified approach to the adhesive theory of friction. Wear 2001;249:78–84. https://doi.org/10.1016/s0043-1648(01)00524-5.

[22] Halling J. A retired lecturer's presentation of the theory of friction first presented by Bowden and Tabor. Tribol Int 1995;28:29–32. https://doi.org/10.1016/0301-679X(95)99490-C.

[23] Hamrock BJ, Dowson D. Isothermal Elastohydrodynamic Lubrication of Point Contacts: Part I—Theoretical Formulation. J Lubr Technol 1977:223–8. https://doi.org/10.1115/1.3453074.

[24] Hamrock BJ, Dowson D. Isothermal Elastohydrodynamic Lubrication of Point Contacts: Part II—Ellipticity Parameter Results. J Lubr Technol 1976:375–81. https://doi.org/10.1115/1.3452861.

[25] Hamrock BJ, Dowson D. Isothermal Elastohydrodynamic Lubrication of Point Contacts: Part III - Fully-flooded Results. J Lubr Technol 1977:264–75.

[26] Hamrock BJ, Dowson D. Isothermal Elastohydrodynamic Lubrication of Point Contacts: Part IV- Starvation Results. J Lubr Technol 1977:15–23. https://doi.org/10.1115/1.3453074.

[27] Serest EA, Akbarzadeh S. Mixed-elastohydrodynamic analysis of helical gears using load-sharing concept. Proc Inst Mech Eng Part J J Eng Tribol 2014;228:320–31.

[28] Wilson JA, Yoffe AD. The transition metal dichalcogenides discussion and interpretation of the observed

optical, electrical and structural properties. Adv Phys 1969;18:193–335. https://doi.org/10.1080/00018736900101307.

[29] Schmidt K H, Muller A. Schwingungspektren von Ubergangsmetall-Chalkogenverbindungen. Coord Chem Rev 1974;14:115–79.

[30] Wu Z, Wang D, Sun A. Surfactant-assisted preparation of hexagonal molybdenum disul fi de nanoparticles. Mater Lett 2009;63:2591–3. https://doi.org/10.1016/j.matlet.2009.07.050.

[31] Zhao ZY, Liu QL. Study of the layer-dependent properties of MoS2 nanosheets with different crystal structures by DFT calculations. Catal Sci Technol 2018;8:1867–79. https://doi.org/10.1039/c7cy02252b.

[32] Pardee RP. The effect of humidity on low-load frictional properties of a bonded solid film lubricant. ASLE Trans 1972;15:130–42. https://doi.org/10.1080/05698197208981409.

[33] Khare HS, Burris DL. The effects of environmental water and oxygen on the temperature-dependent friction of sputtered molybdenum disulfide. Tribol Lett 2013;52:485–93. https://doi.org/10.1007/s11249-013-0233-8.

[34] Serpini E, Rota A, Ballestrazzi A, Marchetto D, Gualtieri E, Valeri S. The role of humidity and oxygen on MoS2 thin films deposited by RF PVD magnetron sputtering. Surf Coatings Technol 2017;319:345–52. https://doi.org/10.1016/j.surfcoat.2017.04.006.

[35] Zhao X, Perry SS. The role of water in modifying friction within MoS2 sliding interfaces. ACS Appl Mater Interfaces 2010;2:1444–8. https://doi.org/10.1021/am100090t.

[36] Lince JR, Frantz PP. Anisotropic oxidation of MoS2 crystallites studied by angle-resolved X-ray photoelectron spectroscopy. Tribol Lett 2001;9:211–8. https://doi.org/10.1023/A:1018869107511.

[37] Levita G, Restuccia P, Righi MC. Graphene and MoS2 interacting with water: A comparison by ab initio calculations. Carbon N Y 2016;107:878–84. https://doi.org/10.1016/j.carbon.2016.06.072.

[38] Levita G, Righi MC. Effects of Water Intercalation and Tribochemistry on MoS_2 Lubricity: An Ab Initio Molecular Dynamics Investigation. ChemPhysChem 2017:1475–80. https://doi.org/10.1002/cphc.201601143.

[39] Donnet C, Martin JM, Le Mogne T, Belin M. The origin of super-low friction coefficient of MoS2 coatings in various environments. Tribol Ser 1994;27:277–84. https://doi.org/10.1016/S0167-8922(08)70317-1.

[40] Radisavljevic B, Radenovic A, Brivio J, Giacometti V, Kis A. Single-layer MoS2 transistors. Nat Nanotechnol 2011;6:147–50. https://doi.org/10.1038/nnano.2010.279.

[41] Frey GL, Tenne R, Matthews MJ, Dresselhaus MS, Dresselhaus G. Raman and resonance Raman investigation of MoS2 nanoparticles. Phys Rev B - Condens Matter Mater Phys 1999;60:2883–92. https://doi.org/10.1103/PhysRevB.60.2883.

[42] Jiménez Sandoval S, Yang D, Frindt RF, Irwin JC. Raman study and lattice dynamics of single molecular layers of MoS2. Phys Rev B 1991;44:3955–62. https://doi.org/10.1103/PhysRevB.44.3955.

[43] Ribeiro-Soares J, Almeida RM, Barros EB, Araujo PT, Dresselhaus MS, Cançado LG, et al. Group theory analysis of phonons in two-dimensional transition metal dichalcogenides. Phys Rev B - Condens Matter Mater Phys 2014;90:1–32. https://doi.org/10.1103/PhysRevB.90.115438.

[44] Pimenta MA, Corro E Del, Carvalho BR, Fantini C, Malard LM. Comparative study of raman spectroscopy in graphene and MoS2-type transition metal dichalcogenides. Acc Chem Res 2015;48:41–7. https://doi.org/10.1021/ar500280m.

[45] Cai Y, Lan J, Zhang G, Zhang YW. Lattice vibrational modes and phonon thermal conductivity of monolayer MoS 2. Phys Rev B - Condens Matter Mater Phys 2014;89:1–8. https://doi.org/10.1103/PhysRevB.89.035438.

[46] Ye M, Winslow D, Zhang D, Pandey R, Yap YK. Recent advancement on the optical properties of two-dimensional molybdenum disulfide (MoS2) thin films. Photonics 2015;2:288–307. https://doi.org/10.3390/photonics2010288.

[47] Chen JM, Wang CS. Second order Raman spectrum of MoS2. Solid State Commun 1974;14:857–60. https://doi.org/10.1016/0038-1098(74)90150-1.

[48] Verble JL, Wietling TJ, Reed PR. Rigid-layer lattice vibrations and van der waals bonding in hexagonal MoS2. Solid State Commun 1972;11:941–4. https://doi.org/10.1016/0038-1098(72)90294-3.

[49] Wieting TJ, Verble JL. Infrared and Raman studies of long-wavelength optical phonons in hexagonal MoS2. Phys Rev B 1971;3:4286–92. https://doi.org/10.1103/PhysRevB.3.4286.

[50] Gołasa K, Grzeszczyk M, Bozek R, Leszczyński P, Wysmołek A, Potemski M, et al. Resonant Raman scattering in MoS2- From bulk to monolayer. Solid State Commun 2014;197:53–6. https://doi.org/10.1016/j.ssc.2014.08.009.

[51] Viršek M, Jesih A, Milošević I, Damnjanović M, Remškar M. Raman scattering of the MoS2 and WS2 single nanotubes. Surf Sci 2007;601:2868–72. https://doi.org/10.1016/j.susc.2006.12.050.

[52] Wang Y, Cong C, Qiu C, Yu T. Raman spectroscopy study of lattice vibration and crystallographic orientation of monolayer mos2 under uniaxial strain. Small 2013;9:2857–61. https://doi.org/10.1002/smll.201202876.

[53] Li H, Zhang Q, Yap CCR, Tay BK, Edwin THT, Olivier A, et al. From bulk to monolayer MoS 2: Evolution

of Raman scattering. Adv Funct Mater 2012;22:1385–90. https://doi.org/10.1002/adfm.201102111.

[54] Mrstik BJ, Kaplan R, Reinecke TL, Van Hove M, Tong SY. Surface-structure determination of the layered compounds MoS2 and NbSe2 by low-energy electron diffraction. Phys Rev B 1977;15:897–900. https://doi.org/10.1038/2071238d0.

[55] Chakraborty B, Matte HSSR, Sood AK, Rao CNR. Layer-dependent resonant Raman scattering of a few layer MoS2. J Raman Spectrosc 2013;44:92–6. https://doi.org/10.1002/jrs.4147.

[56] Anees P, Valsakumar MC, Panigrahi BK. Anharmonicity of optic modes in monolayer MoS2. Appl Phys Lett 2016;108. https://doi.org/10.1063/1.4943546.

[57] Livneh T, Sterer E. Resonant Raman scattering at exciton states tuned by pressure and temperature in 2H -MoS2. Phys Rev B - Condens Matter Mater Phys 2010;81:1–9. https://doi.org/10.1103/PhysRevB.81.195209.

[58] Bagnall AG, Liang WY, Marseglia EA, Welber B. Raman studies of MoS2 at high pressure. Phys B+C 1980;99:343–6. https://doi.org/10.1016/0378-4363(80)90257-0.

[59] Sugai S, Ueda T. High-pressure Raman spectroscopy in the layered materials 2H-MoS2, 2H-MoSe2, and 2H-MoTe2. Phys Rev B 1982;26:6554–8. https://doi.org/10.1103/PhysRevB.26.6554.

[60] Nayak AP, Pandey T, Voiry D, Liu J, Moran ST, Sharma A, et al. Pressure-dependent optical and vibrational properties of monolayer molybdenum disulfide. Nano Lett 2015;15:346–53. https://doi.org/10.1021/nl5036397.

[61] Blanco É, Afanasiev P, Berhault G, Uzio D, Loridant S. Resonance Raman spectroscopy as a probe of the crystallite size of MoS2 nanoparticles. Comptes Rendus Chim 2016;19:1310–4. https://doi.org/10.1016/j.crci.2015.08.014.

[62] Hulanicki A. Complexation reactions of dithiocarbamates. Talanta 1974;14:979–1004.

[63] Gleu K, Schwab R. Disubstituierte Dithiocarbamate („Carbate") als Fällungsreagenzien für Metalle. Angew Chemie 1950;62:320–4. https://doi.org/10.1002/ange.19500621307.

[64] Sakurai T, Okabe H, Isoyama H. The Synthesis of Di-m-thio-dithio-bis (dialkyldithiocarbamates) Dimolybdenum (V) and Their Effects on Boundary Lubrication. Bull Japan Pet Inst 1971;13:243–9.

[65] Lozano R, Moragues A, Roman J. Thermal studies on molybdenum(IV) dialkyl dithiocarbamate adducts with pyridine. Thermochim Acta 1986;108:1–7. https://doi.org/10.1016/0040-6031(86)85072-9.

[66] Lozano R, Román J, Avilés JC, Moragues A, Jerez A, Ramos E. Thermal decomposition of molybdenum(IV) dialkyldithiocarbamates: application of a new method to kinetic studies. Transit Met Chem 1987;12:289–91. https://doi.org/10.1007/BF01024014.

[67] Sharma AK. Thermal behaviour of metal-dithiocarbamates. Thermochim Acta 1986;104:339–72. https://doi.org/10.1016/0040-6031(86)85208-X.

[68] Udupa MR, Nagaraja KS. Mass spectral and thermogravimetric studies of molybdenum dithiocarbamates. Thermochem Acta 1982;56:241–5.

[69] Martin JM, Le Mogne T, Bilas P, Vacher B, Yamada Y. Effect of oxidative degradation on mechanisms of friction reduction by MoDTC. Tribol Ser 2002;40:207–13.

[70] De Feo M, Minfray C, De Barros Bouchet MI, Thiebaut B, Le Mogne T, Vacher B, et al. Ageing impact on tribological properties of MoDTC-containing base oil. Tribol Int 2015;92:126–35. https://doi.org/10.1016/j.triboint.2015.04.014.

[71] De Feo M, Minfray C, De Barros Bouchet MI, Thiebaut B, Martin JM. MoDTC friction modifier additive degradation: Correlation between tribological performance and chemical changes. RSC Adv 2015;5:93786–96. https://doi.org/10.1039/C5RA15250J.

[72] Ponjavic A, Lemaigre T, Southby M, Spikes HA. Influence of NOxand Air on the Ageing Behaviour of MoDTC. Tribol Lett 2017;65:1–7. https://doi.org/10.1007/s11249-017-0836-6.

[73] Morina A, Neville A. Tribofilms: aspects of formation, stability and removal. J Phys D Appl Phys 2007;40:5476–87. https://doi.org/10.1088/0022-3727/40/18/S08.

[74] Morina A, Neville A. Understanding the composition and low friction tribofilm formation/removal in boundary lubrication. Tribol Int 2007;40:1696–704. https://doi.org/10.1016/j.triboint.2007.02.001.

[75] Graham J, Spikes H, Jensen R. The friction reducing properties of molybdenum dialkyldithiocarbamate additives: part ii - durability of friction reducing capability. Tribol Trans 2001;44:637–47. https://doi.org/10.1080/10402000108982505.

[76] Miklozic KT, Graham J, Spikes H. Chemical and physical analysis of reaction films formed by molybdenum dialkyl-dithiocarbamate friction modifier additive using Raman and atomic force microscopy. Tribol Lett 2001;11:71–81. https://doi.org/10.1023/A:1016655316322.

[77] Yamamoto Y, Gondo S. Friction and wear characteristics of Molybdenum Dithiocarbamate and Molybdenum Dithiophosphate. Tribol Trans 1989;32:251–7. https://doi.org/10.1080/10402008908981886.

[78] Graham J, Spikes H, Korcek S. The friction reducing properties of molybdenum dialkyldithiocarbamate additives: part i — factors influencing friction reduction. Tribol Trans 2001;44:626–36. https://doi.org/10.1080/10402000108982504.

[79] Khaemba DN, Neville A, Morina A. New insights on the decomposition mechanism of Molybdenum DialkyldiThioCarbamate (MoDTC): A Raman spectroscopic study. RSC Adv 2016;6:38637–46. https://doi.org/10.1039/c6ra00652c.

[80] Khaemba DN, Jarnias F, Thiebaut B, Neville A, Morina A. The role of surface roughness and slide-roll ratio on the decomposition of MoDTC in tribological contacts. J Phys D Appl Phys 2017;50:085302. https://doi.org/10.1088/1361-6463/aa5905.

[81] Wu H, Li X, He X, Lu J, Wang L, Zhou B, et al. An investigation on the lubrication mechanism of MoS2nanoparticles in unidirectional and reciprocating sliding point contact: The flow pattern effect around contact area. Tribol Int 2018;122:38–45. https://doi.org/10.1016/j.triboint.2018.02.013.

[82] Wu H, Qin L, Zeng Q, Dong G. Understanding the Physical Adsorption Action Mechanism of MoS2Nanoparticles in Boundary Lubrication with Different Polyisobutyleneamine Succinimide (PIBS) Concentrations. Tribol Lett 2015;60:1–12. https://doi.org/10.1007/s11249-015-0604-4.

[83] Graham J, Spikes H, Jensen R. The Friction Reducing Properties of Molybdenum Dialkyldithiocarbamate Additives: Part I - Factors Influencing Friction Reduction. Tribol Trans 2001;44:626–36. https://doi.org/10.1080/10402000108982505.

[84] Rai Y, Neville A, Morina A. Transient processes of MoS2 tribofilm formation under boundary lubrication. Lubr Sci 2016;28:449–71. https://doi.org/10.1002/ls.

[85] Grossiord C, Varlot K, Martin J, Mogne T Le, Esnouf C. MoS2 single sheet lubrication by molybdenum. Tribol Int 1998;31:737–43.

[86] Xu D, Wang C, Espejo C, Wang J, Neville A, Morina A. Understanding the Friction Reduction Mechanism Based on Molybdenum Disulfide Tribofilm Formation and Removal. Langmuir 2018;34:13523–33. https://doi.org/10.1021/acs.langmuir.8b02329.

[87] Rai Y, Neville A, Morina A. Transient processes of MoS2 tribofilm formation under boundqary lubrication. Lubr Sci 2016;28:449–71. https://doi.org/10.1002/ls.

[88] Komaba M, Kondo S, Suzuki A, Kurihara K, Mori S. The effect of temperature on lubrication property with MoDTC-containning lubricant —temperature dependence of friction coefficient and tribofilm structure—. Tribol Online 2018;13:275–81. https://doi.org/10.2474/trol.13.275.

[89] Gorbatchev O, De Barros Bouchet MI, Martin JM, Léonard D, Le-Mogne T, Iovine R, et al. Friction reduction efficiency of organic Mo-containing FM additives associated to ZDDP for steel and carbon-based contacts. Tribol Int 2016;99:278–88. https://doi.org/10.1016/j.triboint.2016.03.035.

[90] De Barros Bouchet MI, Martin JM, Le Mogne T, Bilas P, Vacher B, Yamada Y. Mechanisms of MoS2 formation by MoDTC in presence of ZnDTP: effect of oxidative degradation. Wear 2005;258:1643–50. https://doi.org/10.1016/j.wear.2004.11.019.

[91] Blok H. The flash temperature concept. Wear 1963;6:483–94. https://doi.org/10.1016/0043-1648(63)90283-7.

[92] Archard JF. The temperature of rubbing surfaces. Wear 1959;2:438–55. https://doi.org/10.1016/0043-1648(59)90159-0.

[93] Francis H a. Interfacial Temperature Distribution Within a Sliding Hertzian Contact. A S L E Trans 1971;14:41–54. https://doi.org/10.1080/05698197108983226.

[94] Kalin M. Influence of flash temperatures on the tribological behaviour in low-speed sliding: A review. Mater Sci Eng A 2004;374:390–7. https://doi.org/10.1016/j.msea.2004.03.031.

[95] Grossiord C, Varlot K, Martin JM, Le Mogne T, Esnouf C, Inoue K. MoS2 single sheet lubrication by molybdenum dithiocarbamate. Tribol Int 1998;31:737–43. https://doi.org/10.1016/S0301-679X(98)00094-2.

[96] Spevack PA, McIntyre NS. A Raman and XPS investigation of supported molybdenum oxide thin films. 2. Reactions with hydrogen sulfide. J Phys Chem 1993;97:11031–6. https://doi.org/10.1021/j100144a021.

[97] Lichtman D, Craig JH, Sailer V, Drinkwine M. AES and XPS spectra of sulfur in sulfur compounds. Appl Surf Sci 1981;7:325–31. https://doi.org/10.1016/0378-5963(81)90080-5.

[98] Khaemba DN, Neville A, Morina A. New insights on the decomposition mechanism of Molybdenum DialkyldiThioCarbamate (MoDTC): a Raman spectroscopic study. RSC Adv 2016;6:38637–46. https://doi.org/10.1039/C6RA00652C.

[99] Khaemba DN, Neville A, Morina A. A methodology for Raman characterisation of MoDTC tribofilms and its application in investigating the influence of surface chemistry on friction performance of MoDTC lubricants. Tribol Lett 2015;59:1–17. https://doi.org/10.1007/s11249-015-0566-6.

[100] Rai Y. In-situ Interface Chemical Characterisation of a Boundary Lubricated Contact 2015:184–5.

[101] Braithwaite ER, Haber J. Molybdenum: An Outline of its Chemistry and Uses. 1st ed. Elsevier; 1994.

[102] Oumahi C, De Barros-Bouchet MI, Le Mogne T, Charrin C, Loridant S, Geantet C, et al. MoS2formation induced by amorphous MoS3species under lubricated friction. RSC Adv 2018;8:25867–72. https://doi.org/10.1039/c8ra03317j.

[103] Poisot M, Bensch W, Fuentes S, Alonso G. Decomposition of tetra-alkylammonium thiomolybdates characterised by thermoanalysis and mass spectrometry. Thermochim Acta 2006;444:35–45.

https://doi.org/10.1016/j.tca.2006.02.025.

[104] Walton RI, Dent AJ, Hibble SJ. In Situ Investigation of the Thermal Decomposition of Ammonium Tetrathiomolybdate Using Combined Time-Resolved X-ray Absorption Spectroscopy and X-ray Diffraction. Chem Mater 1998;10:3737–45. https://doi.org/10.1021/cm980716h.

[105] O NHMS, O NHMS, Hibble SJ, Feaviour MR. An in situ structural study of the thermal decomposition reactions of 2001;2:2607–14. https://doi.org/10.1039/b103129p.

[106] Benck JD, Chen Z, Kuritzky LY, Forman AJ, Jaramillo TF. Amorphous Molybdenum Sul fi de Catalysts for Electrochemical Hydrogen Production: Insights into the Origin of their Catalytic Activity 2012:2–9. https://doi.org/10.1021/cs300451q.

[107] Cao P, Peng J, Liu S, Cui Y, Hu Y, Chen B, et al. Tuning the Composition and Structure of Amorphous Molybdenum Sulfide / Carbon Black Nanocomposites by Radiation Technique for Highly Efficient Hydrogen Evolution. Sci Rep 2017:1–11. https://doi.org/10.1038/s41598-017-16015-y.

[108] Escalera-López D, Niu Y, Park SJ, Isaacs M, Wilson K, Palmer RE, et al. Hydrogen evolution enhancement of ultra-low loading, size-selected molybdenum sulfide nanoclusters by sulfur enrichment. Appl Catal B Environ 2018;235:84–91. https://doi.org/10.1016/j.apcatb.2018.04.068.

[109] Zhang Z, Yamaguchi ES, Kasrai M, Bancroft GM. Tribofilms generated from ZDDP and DDP on steel surfaces: Part 1, growth, wear and morphology. Tribol Lett 2005;19:211–20. https://doi.org/10.1007/s11249-005-6148-2.

[110] Haque T, Morina A, Neville A, Kapadia R, Arrowsmith S. Effect of oil additives on the durability of hydrogenated DLC coating under boundary lubrication conditions. Wear 2009;266:147–57. https://doi.org/10.1016/j.wear.2008.06.011.

[111] Haque T, Morina A, Neville A. Influence of friction modifier and antiwear additives on the tribological performance of a non-hydrogenated DLC coating. Surf Coatings Technol 2010;204:4001–11. https://doi.org/10.1016/j.surfcoat.2010.05.017.

[112] Okubo H, Sasaki S. In situ Raman observation of structural transformation of diamond-like carbon films lubricated with MoDTC solution: Mechanism of wear acceleration of DLC films lubricated with MoDTC solution. Tribol Int 2017;113:399–410. https://doi.org/10.1016/j.triboint.2016.10.009.

[113] Okubo H, Yonehara M, Sasaki S. In Situ Raman Observations of the Formation of MoDTC-Derived Tribofilms at Steel/Steel Contact Under Boundary Lubrication. Tribol Trans 2018;61:1040–7. https://doi.org/10.1080/10402004.2018.1462421.

[114] Kosarieh S, Morina A, Lainé E, Flemming J, Neville A. The effect of MoDTC-type friction modifier on the wear performance of a hydrogenated DLC coating. Wear 2013;302:890–8. https://doi.org/10.1016/j.wear.2012.12.052.

[115] Kosarieh S, Morina A, Flemming J, Lainé E, Neville A. Wear Mechanisms of Hydrogenated DLC in Oils Containing MoDTC. Tribol Lett 2016;64. https://doi.org/10.1007/s11249-016-0737-0.

[116] Teo BK, Antonio MR, Averill BA. Molybdenum K-Edge Extended X-ray Absorption Fine Structure (EXAFS) Studies of Synthetic Mo-Fe-S Clusters Containing the MoS4 Unit: Development of a Fine Adjustment Technique Based on Models. J Am Chem Soc 1983;105:3751–62. https://doi.org/10.1021/ja00350a001.

[117] Zhou HC, Su W, Achim C, Rao PV, Holm RH. High-nuclearity sulfide-rich molybdenum-iron-sulfur clusters: Reevaluation and extension. Inorg Chem 2002;41:3191–201. https://doi.org/10.1021/ic0201250.

[118] Braithwaite ER, Cheetham AK, Chippindale AM, Dilworth JR, Garner CD, Green MLH, et al. Molybdenum Sulphur Chemistry. In: Braithwaite ER, Haber J, editors. Molybdenum An Outl. its Chem. Uses. 1st ed., Amsterdam: Elsevier B.V.; 1994, p. 185–250.

[119] Arai K, Yamada M, Asano S, Yoshizawa S, Ohira H, Hoshino K, et al. Lubricant technology to enhance the durability of low friction performance of gasoline engine oils. SAE Tech Pap 1995;104:1964–72. https://doi.org/10.4271/952533.

[120] Stiefel EI, McConnachie JM, Leta DP. United States Patent. 5,888,945, 1999.

[121] Hartley RJ, Waddoups M, Bell IAW, Bidwell ThR, Farnsworth GR, Miyoshi T. United States Patent. 6,300,291 B1, 2001.

[122] Waddoups M, Hartley RJ, Miyoshi T. United States Patent. 6,074,993, 2000.

[123] De Barros Bouchet MI, Martin JM, Oumahi C, Gorbatchev O, Afanasiev P, Geantet C, et al. Booster effect of fatty amine on friction reduction performance of Mo-based additives. Tribol Int 2018;119:600–7. https://doi.org/10.1016/j.triboint.2017.11.039.

[124] Haque T, Morina A, Neville A, Kapadia R, Arrowsmith S. Non-ferrous coating/lubricant interactions in tribological contacts: Assessment of tribofilms. Tribol Int 2007;40:1603–12. https://doi.org/10.1016/j.triboint.2007.01.023.

[125] Haque T, Morina A, Neville A. Influence of friction modifier and antiwear additives on the tribological performance of a non-hydrogenated DLC coating. Surf Coatings Technol 2010;204:4001–11. https://doi.org/10.1016/j.surfcoat.2010.05.017.

[126] Francis JN. United States Patent. 4,990,271, 1991.

[127] Abraham WD, Manka JS, Roby SH, Supp JA. United States Patent. 5,712,230, 1998.

[128] Tang Z, Li S. A review of recent developments of friction modifiers for liquid lubricants (2007-present). Curr Opin Solid State Mater Sci 2014;18:119–39. https://doi.org/10.1016/j.cossms.2014.02.002.

[129] Sutton M, Kocsis JA, Nakagawa I. Improved friction modifiers to aid in future fuel economy targets. SAE Tech Pap 2007;116:1035–9. https://doi.org/10.4271/2007-01-4134.

[130] Li J, Xu X, Wang Y, Ren T. Tribological studies on a novel borate ester containing benzothiazol-2-yl and disulfide groups as multifunctional additive. Tribol Int 2010;43:1048–53. https://doi.org/10.1016/j.triboint.2009.12.030.

[131] Wang Y, Li J, Ren T. Tribological study of a novel borate ester containing dialkylthiophosphate group as multifunctional additive. Ind Lubr Tribol 2009;61:33–9. https://doi.org/10.1108/00368790910929511.

[132] Coupland K, Smith CR. United States Patent, 1979. https://doi.org/10.1016/0375-6505(85)90011-2.

[133] Rowan, Eugene V, Karol, Thomas J, Farmer, Homer H. United States Patent : 4,889,647. 4,889,647, 1985.

[134] Price JA, Neblett RF. United States Patent No:3,285,942. 3,285,942, 1966. https://doi.org/10.1111/j.1559-3584.1927.tb04229.x.

[135] Karol TJ. United States patent No: 5,137,647, 1992. https://doi.org/10.1016/0375-6505(85)90011-2.

[136] Yan L, Yue W, Wang C, Wei D, Xu B. Comparing tribological behaviors of sulfur- and phosphorus-free organomolybdenum additive with ZDDP and MoDTC. Tribol Int 2012;53:150–8. https://doi.org/10.1016/j.triboint.2012.04.002.

[137] Hu JQ, Wei XY, Dai GL, Fei YW, Xie F, Zong ZM. Tribological behaviors and mechanism of sulfur- and phosphorus-free organic molybdate ester with zinc dialkyldithiophosphate. Tribol Int 2008;41:549–55. https://doi.org/10.1016/j.triboint.2007.11.020.

[138] Chinas-Castillo F, Lara-Romero J, Alonso-Núñez G, Barceinas-Sánchez JDO, Jiménez-Sandoval S. Friction reduction by water-soluble ammonium thiometallates. Tribol Lett 2007;26:137–44. https://doi.org/10.1007/s11249-006-9179-4.

[139] Chiñas-Castillo F, Lara-Romero J, Alonso-Núñez G, Barceinas-Sánchez JDDO, Jiménez-Sandoval S. MoS 2 films formed by in-contact decomposition of water-soluble tetraalkylammonium thiomolybdates. Tribol Lett 2008;29:155–61. https://doi.org/10.1007/s11249-007-9292-z.

[140] Brito JL, Ilija M, Hernández P. Thermal and reductive decomposition of ammonium thiomolybdates. Thermochim Acta 1995;256:325–38.

[141] Laurie SH. Thiomolybdates — Simple but Very Versatile Reagents. Eur J Inorg Chem 2000:2443–50.

[142] Srinivasan BR. Does an all-sulphur analogue of heptamolybdate exist ? J Chem Sci 2004;116:251–9.

[143] De Barros Bouchet MI, Martin JM, Oumahi C, Gorbatchev O, Afanasiev P, Geantet C, et al. Booster effect of fatty amine on friction reduction performance of Mo-based additives. Tribol Int 2018;119:600–7. https://doi.org/10.1016/j.triboint.2017.11.039.

[144] Vorlicek TP, Chappaz A, Groskreutz LM, Young N, Lyons TW. A new analytical approach to determining Mo and Re speciation in sulfidic waters. Chem Geol 2015;403:52–7. https://doi.org/10.1016/j.chemgeo.2015.03.003.

[145] Erickson BE, Helz GR. Molybdenum(VI) speciation in sulfidic waters: Geochim Cosmochim Acta 2000;64:1149–58. https://doi.org/10.1016/s0016-7037(99)00423-8.

[146] Wu H, Wang YG, Ren TH. The tribological properties and action mechanism of non-active organic molybdate ester and its combination with ZDDP. Tribol Int 2012;49:90–5. https://doi.org/10.1016/j.triboint.2012.01.004.

[147] Oumahi C, De Barros-Bouchet MI, Le Mogne T, Charrin C, Loridant S, Geantet C, et al. MoS2 formation induced by amorphous MoS3 species under lubricated friction. RSC Adv 2018;8:25867–72. https://doi.org/10.1039/c8ra03317j.

[148] Miklozic KT, Forbus TR, Spikes HA. Performance of friction modifiers on zddp-generated surfaces. Tribol Trans 2007;50:328–35. https://doi.org/10.1080/10402000701413505.

[149] Lundgren SM, Eriksson K, Rossenaar B. Boosting the Friction Performance of Amine Friction Modifiers with MoDTC. SAE Int J Fuels Lubr 2015;8:27–30. https://doi.org/10.4271/2015-01-0684.

[150] Weber T, Muijsers JC, Niemantsverdriet JW. Structure of amorphous MoS3. J Phys Chem 1995;99:9194–200. https://doi.org/10.1021/j100022a037.

[151] Hibble SJ, Wood GB. Modeling the Structure of Amorphous MoS3: A Neutron Diffraction and Reverse Monte Carlo Study. J Am Chem Soc 2004;126:959–65. https://doi.org/10.1021/ja037666o.

[152] Tran PD, Tran T V., Orio M, Torelli S, Truong QD, Nayuki K, et al. Coordination polymer structure and revisited hydrogen evolution catalytic mechanism for amorphous molybdenum sulfide. Nat Mater 2016;15:640–6. https://doi.org/10.1038/nmat4588.

[153] Lee CH, Lee S, Lee YK, Jung YC, Ko Y Il, Lee DC, et al. Understanding the origin of formation and active sites for thiomolybdate [Mo3S13]2- Clusters as hydrogen evolution catalyst through the selective control of sulfur atoms. ACS Catal 2018;8:5221–7. https://doi.org/10.1021/acscatal.8b01034.

[154] Fu W, Yang S, Yang H, Guo B, Huang Z. 2D amorphous MoS3 nanosheets with porous network

structures for scavenging toxic metal ions from synthetic acid mine drainage. J Mater Chem A 2019;7:18799–806. https://doi.org/10.1039/c9ta05861c.

[155] Freuler HC. United States Patent. 2364284, 1944.

[156] Frueler HC. United States Patent. 2364283, 1941. https://doi.org/10.1145/178951.178972.

[157] Cook EW, Thomas JWD. United States Patent. 2344392, 1941.

[158] Asseff PA. United States Patent. 2261047, 1941. https://doi.org/10.1145/178951.178972.

[159] Spikes H. The history and mechanisms of ZDDP. Tribol Lett 2004;17:469–89. https://doi.org/10.1023/B:TRIL.0000044495.26882.b5.

[160] Topolovec-Miklozic K, Forbus TR, Spikes HA. Film thickness and roughness of ZDDP antiwear films. Tribol Lett 2007;26:161–71. https://doi.org/10.1007/s11249-006-9189-2.

[161] Zhang J, Spikes H. On the Mechanism of ZDDP Antiwear Film Formation. Tribol Lett 2016;63:1–15. https://doi.org/10.1007/s11249-016-0706-7.

[162] Johnson D, Hils J. Phosphate Esters, Thiophosphate Esters and Metal Thiophosphates as Lubricant Additives. Lubricants 2013;1:132–48. https://doi.org/10.3390/lubricants1040132.

[163] Suominen Fuller ML, Rodriguez Fernandez L, Massoumi GR, Lennar WN, Kasrai M, Bancroft GM. The use of x-ray absorption spectroscopy for monitoring the thickness of antiwear films from ZDDP. Tribol Lett 2000;8:187–92. https://doi.org/10.1023/A:1019195404055.

[164] Yin Z, Kasrai M, Fuller M, Bancroft GM, Fyfe K, Tan KH. Application of soft X-ray absorption spectroscopy in chemical characterization of antiwear films generated by ZDDP Part I: The effects of physical parameters. Wear 1997;202:172–91. https://doi.org/10.1016/S0043-1648(96)07272-9.

[165] Parsaeian P, Van Eijk MCP, Nedelcu I, Neville A, Morina A. Study of the interfacial mechanism of ZDDP tribofilm in humid environment and its effect on tribochemical wear; Part I: Experimental. Tribol Int 2017;107:135–43. https://doi.org/10.1016/j.triboint.2016.11.012.

[166] Ueda M, Kadiric A, Spikes H. On the Crystallinity and Durability of ZDDP Tribofilm. Tribol Lett 2019;67:1–13. https://doi.org/10.1007/s11249-019-1236-x.

[167] Gauvin M, Minfray C, Belin M, Aquilanti G, Martin JM, Dassenoy F. Pressure-induced amorphization of zinc orthophosphate-Insight in the zinc coordination by XAS. Tribol Int 2013;67:222–8. https://doi.org/10.1016/j.triboint.2013.07.011.

[168] Martin JM, Onodera T, Minfray C, Dassenoy F, Miyamoto A. The origin of anti-wear chemistry of ZDDP. Faraday Discuss 2012;156:311–23. https://doi.org/10.1039/c2fd00126h.

[169] Onodera T, Morita Y, Suzuki A, Sahnoun R, Koyama M, Tsuboi H, et al. A theoretical investigation on the abrasive wear prevention mechanism of ZDDP and ZP tribofilms. Appl Surf Sci 2008;254:7976–9. https://doi.org/10.1016/j.apsusc.2008.04.057.

[170] Aktary M, McDermott MT, McAlpine GA. Morphology and nanomechanical properties of ZDDP antiwear films as a function of tribological contact time. Tribol Lett 2002;12:155–62. https://doi.org/10.1023/A:1014755123184.

[171] Graham JF, McCague C, Norton PR. Topography and nanomechanical properties of tribochemical films derived from zinc dialkyl and diaryl dithiophosphates. Tribol Lett 1999;6:149–57. https://doi.org/10.1023/A:1019124026402.

[172] Ye J, Kano M, Yasuda Y. Evaluation of local mechanical properties in depth in MoDTC/ZDDP and ZDDP tribochemical reacted films using nanoindentation. Tribol Lett 2002;13:41–7. https://doi.org/10.1023/A:1016559807453.

[173] Dorgham A, Wang C, Morina A, Neville A. 3D tribo-nanoprinting using triboreactive materials. Nanotechnology 2019;30. https://doi.org/10.1088/1361-6528/aaf70c.

[174] Dorgham A, Parsaeian P, Azam A, Wang C, Morina A, Neville A. Single-asperity study of the reaction kinetics of P-based triboreactive films. Tribol Int 2019;133:288–96. https://doi.org/10.1016/j.triboint.2018.11.029.

[175] Taylor LJ, Spikes HA. Friction-enhancing properties of zddp antiwear additive: Part ii—influence of zddp reaction films on ehd lubrication. Tribol Trans 2003;46:310–4. https://doi.org/10.1080/10402000308982631.

[176] Taylor LJ, Spikes HA. Friction-enhancing properties of zddp antiwear additive: Part i—friction and morphology of zddp reaction films. Tribol Trans 2003;46:303–9. https://doi.org/10.1080/10402000308982630.

[177] Morina A, Neville A, Priest M, Green JH. ZDDP and MoDTC interactions in boundary lubrication-The effect of temperature and ZDDP/MoDTC ratio. Tribol Int 2006;39:1545–57. https://doi.org/10.1016/j.triboint.2006.03.001.

[178] Ye J, Kano M, Yasuda Y. Friction property study of the surface of ZDDP and MoDTC antiwear additive films using AFM/LFM and force curve methods. TriboTest 2002;9:13–21. https://doi.org/10.1002/tt.3020090103.

[179] Mansuy H, Beccat P, Huiban Y, Palermo T, Desbat B. Investigation of interactions between antiwear and dispersant additives and their effect on surface activity of zddp. Tribol Ser 1995;30:423–32.

https://doi.org/10.1016/S0167-8922(08)70648-5.

[180] Zhang J, Yamaguchi E, Spikes H. The Antagonism between succinimide dispersants and a secondary zinc dialkyl dithiophosphate. Tribol Trans 2013;57:57–65. https://doi.org/10.1080/10402004.2013.845275.

[181] Zhang Z, Kasrai M, Bancroft GM, Yamaguchi ES. Study of the interaction of ZDDP and dispersants using X-ray absorption near edge structure spectroscopy - Part 1: Thermal chemical reactions. Tribol Lett 2003;15:377–84. https://doi.org/10.1023/B:TRIL.0000003061.10054.cb.

[182] Ramakumar SS V., Aggarwal N, Rao AM, Sarpal AS, Srivastava SP, Bhatnagar AK. Studies on Additive-Additive Interactions: Effects of Dispersant and Antioxidant Additives on the Synergistic Combination of Overbased Sulphonate and ZDDP. Lubr Sci 1994;7:25–38.

[183] Shiomi M, Tokashiki M, Tomizawa H, Kuribayashi T. Interaction between zinc dialkyldithiophosphate and amine. Lubr Sci 1989;1:131–47. https://doi.org/10.1002/ls.3010010203.

[184] Dawczyk J, Russo J, Spikes H. Ethoxylated Amine Friction Modifiers and ZDDP. Tribol Lett 2019;67:1–15. https://doi.org/10.1007/s11249-019-1221-4.

[185] Nalam PC, Pham A, Castillo RV, Espinosa-Marzal RM. Adsorption Behavior and Nanotribology of Amine-Based Friction Modifiers on Steel Surfaces. J Phys Chem C 2019;123:13672–80. https://doi.org/10.1021/acs.jpcc.9b02097.

[186] Soltanahmadi S, Esfahani EA, Nedelcu I, Morina A, van Eijk MCP, Neville A. Surface Reaction Films from Amine-Based Organic Friction Modifiers and Their Influence on Surface Fatigue and Friction. Tribol Lett 2019;67:1–15. https://doi.org/10.1007/s11249-019-1189-0.

[187] Fujita H, Glovnea RP, Spikes HA. Study of zinc dialkydithiophosphate antiwear film formation and removal processes, part I: Experimental. Tribol Trans 2005;48:558–66. https://doi.org/10.1080/05698190500385211.

[188] Harrison PG, Brown P. External reflection FTIR, 31P MAS NMR and SEM study of the thermal decomposition of zinc(II) bis(O,O'-dialkyldithiophosphates) on 316 stainless steel. Wear 1991;148:123–34. https://doi.org/10.1016/0043-1648(91)90211-C.

[189] Dickert JJ, Rowe CN. The Thermal Decomposition of Metal O, O-Dialkylphosphorodithioates. J Org Chem 1967;32:647–53. https://doi.org/10.1021/jo01278a031.

[190] Gosvami NN, Bares JA, Mangolini F, Konicek AR, Yablon DG, Carpick RW. Mechanisms of antiwear tribofilm growth revealed in situ by single-asperity sliding contacts. Science (80-) 2015;348:102–6. https://doi.org/10.1126/science.1258788.

[191] Tysoe W. On Stress-Induced Tribochemical Reaction Rates. Tribol Lett 2017;65:1–16. https://doi.org/10.1007/s11249-017-0832-x.

[192] He X, Kim SH. Mechanochemistry of Physisorbed Molecules at Tribological Interfaces: Molecular Structure Dependence of Tribochemical Polymerization. Langmuir 2017;33:2717–24. https://doi.org/10.1021/acs.langmuir.6b04028.

[193] Ghanbarzadeh A, Wilson M, Morina A, Dowson D, Neville A. Development of a new mechano-chemical model in boundary lubrication. Tribol Int 2016;93:573–82. https://doi.org/10.1016/j.triboint.2014.12.018.

[194] Konda SSM, Brantley JN, Bielawski CW, Makarov DE. Chemical reactions modulated by mechanical stress: Extended Bell theory. J Chem Phys 2011;135. https://doi.org/10.1063/1.3656367.

[195] Sarpal AS, Christopher J, Mukherjee S, Patel MB, Kapu GS. Study of additive-additive interactions in a lubricant system by NMR, ESCA, and thermal techniques. Lubr Sci 2005;17:319–45. https://doi.org/10.1002/ls.3010170307.

[196] Scherer JR, Bailey GF, Kint S. Simple Optical Geometry for Obtaining Raman Back Scattering. Anal Chem 1971;43:1917–8. https://doi.org/10.1021/ac60307a028.

[197] N8 Equipment D8 Bruker Diffractometer n.d. https://www.n8equipment.org.uk/equipment/detail/d8-discovery-diffractometer-system (accessed December 15, 2020).

[198] Dawczyk J, Ware E, Ardakani M, Russo J, Spikes H. Use of FIB to Study ZDDP Tribofilms. Tribol Lett 2018;66:1–8. https://doi.org/10.1007/s11249-018-1114-y.

[199] Mayer J, Giannuzzi L a, Kamino T, Michael J. TEM Sample Preparation and Damage. MRS Bull 2007;32:400–7.

[200] Shimadzu TGA50 Thermogravimetric Analyzer n.d. https://www.shimadzu.com/an/products/thermal-analysis/thermal-analyzer/tga-50-series/index.html (accessed December 15, 2020).

[201] Leica DM6000 Optical Microscope n.d. https://www.leica-microsystems.com/products/light-microscopes/p/leica-dm6000-b/ (accessed December 15, 2020).

[202] Das S, Cadirov N, Chary S, Kaufman Y, Hogan J, Turner KL, et al. Stick-slip friction of gecko-mimetic flaps on smooth and rough surfaces. J R Soc Interface 2015;12. https://doi.org/10.1098/rsif.2014.1346.

[203] Graham J, Spikes H, Korcek S. The friction reducing properties of molybdenum dialkyldithiocarbamate additives: part i — factors influencing friction reduction. Tribol Trans 2001;44:626–36. https://doi.org/10.1080/10402000108982504.

[204] Hu YZ, Tonder K. Simulation of 3-D random rough surface by 2-D digital filter and fourier analysis. Int J Mach Tools Manuf 1992;32:83–90. https://doi.org/10.1016/0890-6955(92)90064-N.

[205] Sahlin F, Larsson R, Almqvist A, Lugt PM, Marklund P. A mixed lubrication model incorporating measured surface topography. Part 1: Theory of flow factors. Proc Inst Mech Eng Part J J Eng Tribol 2010;224:335–51. https://doi.org/10.1243/13506501JET658.

[206] Tran PD, Tran T V, Orio M, Torelli S, Duc Truong Q, Nayuki K, et al. Coordination polymer structure and revisited hydrogen evolution catalytic mechanism for amorphous molybdenum sulfide. Nat Mater 2016;15:640–7. https://doi.org/10.1038/NMAT4588.

[207] Moulder JF. Handbook of X-ray Photoelectron Spectroscopy: A Reference Book of Standard Spectra for Indentification and Interpretation of XPS Data. Illustrate. Physical Electronic Division, Perkin-Elmer Corporation; 1992.

[208] Sherwood PMA. The use and misuse of curve fitting in the analysis of core X-ray photoelectron spectroscopic data. Surf Interface Anal 2019;51:589–610. https://doi.org/10.1002/sia.6629.

[209] Axis K. background and baseline in Peak Fitting in XPS 2006:1–29.

[210] Merki D, Fierro S, Vrubel H, Hu X. Amorphous molybdenum sulfide films as catalysts for electrochemical hydrogen production in water. Chem Sci 2011;2:1262–7. https://doi.org/10.1039/c1sc00117e.

[211] Tang ML, Grauer DC, Lassalle-Kaiser B, Yachandra VK, Amirav L, Long JR, et al. Structural and electronic study of an amorphous MoS3 hydrogen-generation catalyst on a quantum-controlled photosensitizer. Angew Chemie - Int Ed 2011;50:10203–7. https://doi.org/10.1002/anie.201104412.

[212] Lin T, Liu C, Lin J. Applied Catalysis B : Environmental Facile synthesis of MoS 3 / carbon nanotube nanocomposite with high catalytic activity toward hydrogen evolution reaction. "Applied Catal B, Environ 2013;134–135:75–82. https://doi.org/10.1016/j.apcatb.2013.01.004.

[213] Choi J, Thompson LT. XPS study of as-prepared and reduced molybdenum oxides. Appl Surf Sci 1996;93:143–9.

[214] Ganta D, Sinha S, Haasch RT. 2-D Material Molybdenum Disulfide Analyzed by XPS. Surf Sci Spectra 2014;21:19–27. https://doi.org/10.1116/11.20140401.

[215] Lee CH, Lee S, Lee YK, Jung YC, Ko Y Il, Lee DC, et al. Understanding the origin of formation and active sites for thiomolybdate [Mo3S13]2- Clusters as hydrogen evolution catalyst through the selective control of sulfur atoms. ACS Catal 2018;8:5221–7. https://doi.org/10.1021/acscatal.8b01034.

[216] Tran PD, Tran T V., Orio M, Torelli S, Truong QD, Nayuki K, et al. Coordination polymer structure and revisited hydrogen evolution catalytic mechanism for amorphous molybdenum sulfide. Nat Mater 2016;15:640–6. https://doi.org/10.1038/nmat4588.

[217] Fu W, Yang S, Yang H, Guo B, Huang Z. 2D amorphous MoS 3 nanosheets with porous network structures for scavenging toxic metal ions from synthetic acid mine drainage . J Mater Chem A 2019;7:18799–806. https://doi.org/10.1039/c9ta05861c.

[218] Yue D, Qian X, Zhang Z, Kan M, Ren M, Zhao Y. CdTe/CdS Core/Shell Quantum Dots Cocatalyzed by Sulfur Tolerant [Mo 3 S 13] 2− Nanoclusters for Efficient Visible-Light-Driven Hydrogen Evolution. ACS Sustain Chem Eng 2016;4:6653–8. https://doi.org/10.1021/acssuschemeng.6b01520.

[219] Hellstern TR, Kibsgaard J, Tsai C, Palm DW, King LA, Abild-Pedersen F, et al. Investigating catalyst-support interactions to improve the hydrogen evolution reaction activity of thiomolybdate [Mo3S13]2- Nanoclusters. ACS Catal 2017;7:7126–30. https://doi.org/10.1021/acscatal.7b02133.

[220] Liang KS, deNaufville JP, Jacobson AJ, Chianelli RR, Betts F. Structure of amorphous transition metal sulfides. J Non Cryst Solids 1980;35–36:1249–54. https://doi.org/10.1016/0022-3093(80)90369-5.

[221] Tang ML, Grauer DC, Lassalle-kaiser B, Yachandra VK, Amirav L, Long JR, et al. Structural and Electronic Study of an Amorphous MoS 3 Hydrogen- Generation Catalyst on a Quantum-Controlled Photosensitizer ** Zuschriften 2011:10385–9. https://doi.org/10.1002/ange.201104412.

[222] Yan L, Yue W, Wang C, Wei D, Xu B. Comparing tribological behaviors of sulfur- and phosphorus-free organomolybdenum additive with ZDDP and MoDTC. Tribol Int 2012;53:150–8. https://doi.org/10.1016/j.triboint.2012.04.002.

[223] Hu JQ, Wei XY, Yao JB, Han L, Zong ZM. Evaluation of molybdate ester as a synergist for arylamine antioxidant in lubricants. Tribol Int 2006;39:1469–73. https://doi.org/10.1016/j.triboint.2006.05.013.

[224] Kim YW, Chung K, Kim NS, Hwang DH, Cho WO. Synergistic lubricating effect of several ashless dithiocarbamates with Mo-donor additives. Tribol Int 2007;40:397–404. https://doi.org/10.1016/j.triboint.2005.09.029.

[225] Reddyhoff T, Ku ISY, Holmes AS, Spikes HA. Friction modifier behaviour in lubricated MEMS devices. Tribol Lett 2011;41:239–46. https://doi.org/10.1007/s11249-010-9704-3.

[226] Murase A, Ohmori T. ToF-SIMS analysis of model compounds of friction modifier adsorbed onto friction surfaces of ferrous materials. Surf Interface Anal 2001;31:191–9. https://doi.org/10.1002/sia.969.

[227] Wang Y, Du Y, Deng J, Wang Z. Friction reduction of water based lubricant with highly dispersed functional MoS2 nanosheets. Colloids Surfaces A Physicochem Eng Asp 2019;562:321–8. https://doi.org/10.1016/j.colsurfa.2018.11.047.

[228] Basiev TT, Sobol AA, Voronko YK, Zverev PG. Spontaneous Raman spectroscopy of tungstate and molybdate crystals for Raman lasers. Opt Mater (Amst) 2000;15:205–16. https://doi.org/10.1016/S0925-3467(00)00037-9.

[229] Tian H, Wachs IE, Briand LE. Comparison of UV and visible Raman spectroscopy of bulk metal molybdate and metal vanadate catalysts. J Phys Chem B 2005;109:23491–9. https://doi.org/10.1021/jp053879j.

[230] Fuller MLS, Kasrai M, Bancroft GM, Fyfe K, Tan KH. Solution decomposition of zinc dialkyl dithiophosphate and its effect on antiwear and thermal film formation studied by X-ray absorption spectroscopy. Tribol Int 1998;31:627–44. https://doi.org/10.1016/S0301-679X(98)00084-X.

[231] Aktary M, McDermott MT, Torkelson J. Morphological evolution of films formed from thermooxidative decomposition of ZDDP. Wear 2001;247:172–9. https://doi.org/10.1016/S0043-1648(00)00525-1.

[232] Archard JF. The temperature of rubbing surfaces. Wear 1959;2:438–55. https://doi.org/10.1016/0043-1648(59)90159-0.

[233] Williams J. Engineering Tribology. Second. Cambridge: Cambridge University Press; 2005.

[234] Humeres E, Debacher NA, Marta de M, Franco JD, Schutz A. Mechanisms of acid decomposition of dithiocarbamates. 1. Alkyl dithiocarbamates. J Org Chem 1998;63:1598–603. https://doi.org/10.1021/jo971869b.

[235] Cardwell, T. J. and Desarro DJ. Gas chromatography of some volatile metal diethyldithiocarbamates. Anal Chim Acta 1976;85:415–9.

[236] Kalin M, Vižintin J. Comparison of different theoretical models for flash temperature calculation under fretting conditions. Tribol Int 2001;34:831–9. https://doi.org/10.1016/S0301-679X(01)00083-4.

[237] Kennedy FE, Tian X. Modeling sliding contact temperatures, including effects of surface roughness and convection. J Tribol 2016;138. https://doi.org/10.1115/1.4032841.

[238] Francis HA. Interfacial temperature distribution within a sliding hertzian contact. ASLE Trans 1971;14:41–54. https://doi.org/10.1080/05698197108983226.

[239] Laux KA, Jean-Fulcrand A, Sue HJ, Bremner T, Wong JSS. The influence of surface properties on sliding contact temperature and friction for polyetheretherketone (PEEK). Polymer (Guildf) 2016;103:397–404. https://doi.org/10.1016/j.polymer.2016.09.064.

[240] Kennedy FE, Cullen SC, Leroy JM. Contact temperature and its effects in an oscillatory siding contact. J Tribol 1988;111:63–9.

[241] Nakayama K, Martin JM. Tribochemical reactions at and in the vicinity of a sliding contact. Wear 2006;261:235–40. https://doi.org/10.1016/j.wear.2005.10.012.

[242] Adams HL, Garvey MT, Ramasamy US, Ye Z, Martini A, Tysoe WT. Shear induced mechanochemistry: Pushing molecules around. J Phys Chem C 2015;119:7115–23. https://doi.org/10.1021/jp5121146.

[243] Hänggi P, Talkner P, Borkovec M. Reaction-rate theory: Fifty years after Kramers. Rev Mod Phys 1990;62:251–341. https://doi.org/10.1103/RevModPhys.62.251.

[244] Bell G. Models for the specific adhesion of cells to cells. Science (80-) 1978;200:618–27. https://doi.org/10.1126/science.347575.

[245] Jacobs TDB, Carpick RW. Nanoscale wear as a stress-assisted chemical reaction. Nat Nanotechnol 2013;8:108–12. https://doi.org/10.1038/nnano.2012.255.

[246] Li Y, Lu J, Cui XB, Xu JQ, Li KC, Sun HY, et al. Syntheses, structures and third-order non-linear optical properties of homometal clusters containing molybdenum. J Solid State Chem 2005;178:363–9. https://doi.org/10.1016/j.jssc.2004.11.004.

[247] Mayor-López MJ, Weber J, Hegetschweiler K, Meienberger MD, Joho F, Leoni S, et al. Structure and Reactivity of [Mo3-μ3S-(μS2)2]4+ Complexes. Quantum Chemical Calculations, X-ray Structural Characterization, and Raman Spectroscopic Measurements. Inorg Chem 1998;37:2633–44. https://doi.org/10.1021/ic971214t.

[248] Peeters S, Restuccia P, Loehlé S, Thiebaut B, Righi MC. Characterization of Molybdenum Dithiocarbamates by First-Principles Calculations. J Phys Chem A 2019;123:7007–15. https://doi.org/10.1021/acs.jpca.9b03930.

[249] Peeters S, Restuccia P, Loehlé S, Thiebaut B, Righi MC. Tribochemical Reactions of MoDTC Lubricant Additives with Iron by Quantum Mechanics/Molecular Mechanics Simulations. J Phys Chem C 2020;124:13688–94. https://doi.org/10.1021/acs.jpcc.0c02211.

[250] Martin JM, Pascal H, Donnet C, Le Mogne T, Loubet JL, Epicier T. Superlubricity of MoS2: crystal orientation mechanisms. Surf Coatings Technol 1994;68–69:427–32. https://doi.org/10.1016/0257-8972(94)90197-X.

[251] Vazirisereshk MR, Martini A, Strubbe DA, Baykara MZ. Solid lubrication with MoS2: A review. Lubricants 2019;7. https://doi.org/10.3390/LUBRICANTS7070057.

[252] Haque T, Morina A, Neville A, Kapadia R, Arrowsmith S. Effect of oil additives on the durability of hydrogenated DLC coating under boundary lubrication conditions. Wear 2009;266:147–57. https://doi.org/10.1016/j.wear.2008.06.011.

[253] Haque T, Morina A, Neville A, Kapadia R, Arrowsmith S. Non-ferrous coating/lubricant interactions in tribological contacts: Assessment of tribofilms. Tribol Int 2007;40:1603–12. https://doi.org/10.1016/j.triboint.2007.01.023.

[254] Kosarieh S, Morina A, Lainé E, Flemming J, Neville A. The effect of MoDTC-type friction modifier on the

wear performance of a hydrogenated DLC coating. Wear 2013;302:890–8. https://doi.org/10.1016/j.wear.2012.12.052.

[255] Liu F, Wang T, Wang Q, Meng J, Lu J. Improved frictional behavior of SiC derived carbon coating using MoS3 as a solid lubricant. Tribol Int 2016;94:61–6. https://doi.org/10.1016/j.triboint.2015.08.034.

[256] Jackson SA, Radhakrishnan G, Adams PM. Tribochemistry of MoS 3 Nanoparticle Coatings 2014:543–54. https://doi.org/10.1007/s11249-014-0293-4.

[257] Okubo H, Yonehara M, Sasaki S. In Situ Raman Observations of the Formation of MoDTC-Derived Tribofilms at Steel/Steel Contact Under Boundary Lubrication. Tribol Trans 2018;61:1040–7. https://doi.org/10.1080/10402004.2018.1462421.

[258] Strong KL, Zabinski JS, Vreugdenhil AJ. Thermal chemistry of a high temperature solid lubricant, cesium oxythiomolybdate. Part I. Thermo-oxidative stability of Cs2MoOS3. J Mater Sci 2001;36:5407–13. https://doi.org/10.1023/A:1012465127027.

[259] Fleischauer PD, Lince JR. Comparison of oxidation and oxygen substitution in MoS2 solid film lubricants. Tribol Int 1999;32:627–36. https://doi.org/10.1016/S0301-679X(99)00088-2.

[260] Arif T, Yadav S, Colas G, Singh CV, Filleter T. Understanding the Independent and Interdependent Role of Water and Oxidation on the Tribology of Ultrathin Molybdenum Disulfide (MoS2). Adv Mater Interfaces 2019;6:1–9. https://doi.org/10.1002/admi.201901246.

[261] Pereira G, Munoz-Paniagua D, Lachenwitzer A, Kasrai M, Norton PR, Capehart TW, et al. A variable temperature mechanical analysis of ZDDP-derived antiwear films formed on 52100 steel. Wear 2007;262:461–70. https://doi.org/10.1016/j.wear.2006.06.016.

[262] Guegan J, Southby M, Spikes H. Friction Modifier Additives, Synergies and Antagonisms. Tribol Lett 2019;67:1–12. https://doi.org/10.1007/s11249-019-1198-z.

[263] Yin Z, Kasrai M, Bancroft GM, Fyfe K, Colaianni ML, Tan KH. Application of soft X-ray absorption spectroscopy in chemical characterization of antiwear films generated by ZDDP Part II: The effect of detergents and dispersants. Wear 1997;202:192–201. https://doi.org/10.1016/S0043-1648(96)07273-0.

[264] Griffith WP, Lesniak PJB. Raman studies on species in aqueous solutions Part III Vanadates, Molybdates and Tungstates. J Chem Soc A 1969:1066–71. https://doi.org/10.1039/J19690001066.

[265] Okubo H, Tadokoro C, Sasaki S. *In Situ* Raman-SLIM Monitoring for the Formation Processes of MoDTC and ZDDP Tribofilms at Steel/Steel Contacts under Boundary Lubrication. Tribol Online 2020;15:105–16. https://doi.org/10.2474/trol.15.105.

[266] Okubo H, Tadokoro C, Sumi T, Tanaka N, Sasaki S. Wear acceleration mechanism of diamond-like carbon (DLC) films lubricated with MoDTC solution: Roles of tribofilm formation and structural transformation in wear acceleration of DLC films lubricated with MoDTC solution. Tribol Int 2019;133:271–87. https://doi.org/10.1016/j.triboint.2018.12.029.

[267] Kassim KAM, Tokoroyama T, Murashima M, Umehara N. The wear classification of MoDTC-derived particles on silicon and hydrogenated diamond-like carbon at room temperature. Tribol Int 2020;147:106176. https://doi.org/10.1016/j.triboint.2020.106176.

[268] Lu Y, Huang G, Cheng Y, Wang S, Mi C, Wei S, et al. Tribological and adhesive properties of the tungsten-doped diamond-like carbon film prepared by double lasers deposition. Diam Relat Mater 2019;99:107534. https://doi.org/10.1016/j.diamond.2019.107534.

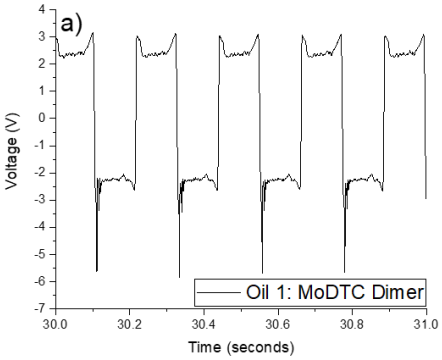
[269] Kržan B, Novotny-Farkas F, Vižintin J. Tribological behavior of tungsten-doped DLC coating under oil lubrication. Tribol Int 2009;42:229–35. https://doi.org/10.1016/j.triboint.2008.06.011.

[270] Zahid R, Masjuki HH, Varman M, Mufti RA, Kalam MA, Gulzar M. Effect of lubricant formulations on the tribological performance of self-mated doped DLC contacts: A review. Tribol Lett 2015. https://doi.org/10.1007/s11249-015-0506-5.

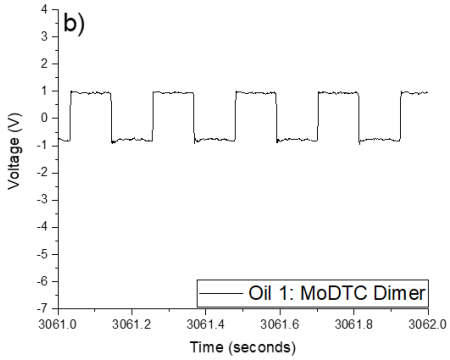
[271] Srinivas V, Thakur RN, Jain AK, Saratchandra Babu M. Tribological Studies of Transmission Oil Dispersed with Molybdenum Disulfide and Tungsten Disulfide Nanoparticles. J Tribol 2017;139:1–6. https://doi.org/10.1115/1.4034766.

[272] Jiang Z, Zhang Y, Yang G, Ma J, Zhang S, Yu L, et al. Tribological Properties of Tungsten Disulfide Nanoparticles Surface-Capped by Oleylamine and Maleic Anhydride Dodecyl Ester as Additive in Diisooctylsebacate. Ind Eng Chem Res 2017;56:1365–75. https://doi.org/10.1021/acs.iecr.6b04074.

Appendix A: TE77 Waveforms for high and low friction sections of the molybdenum additive tests

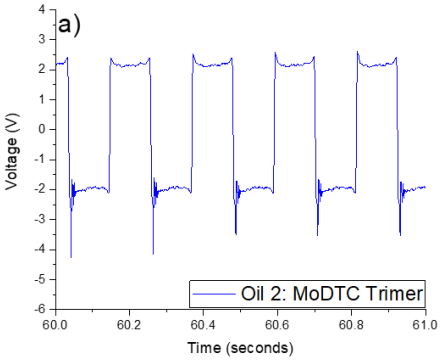


a) Oil 1: MoDTC Dimer, early test

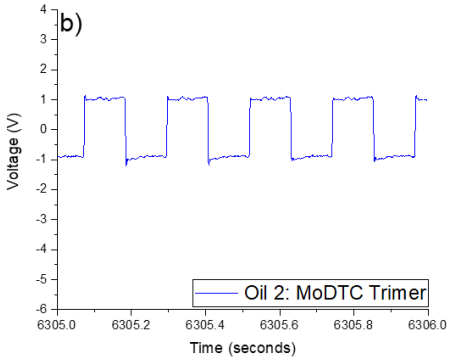


b) Oil 1: MoDTC Dimer, late test

Figure A0.1 TE77 Load Cell response of rough plate 100 N friction test of Oil 1: MoDTC Dimer monoblend

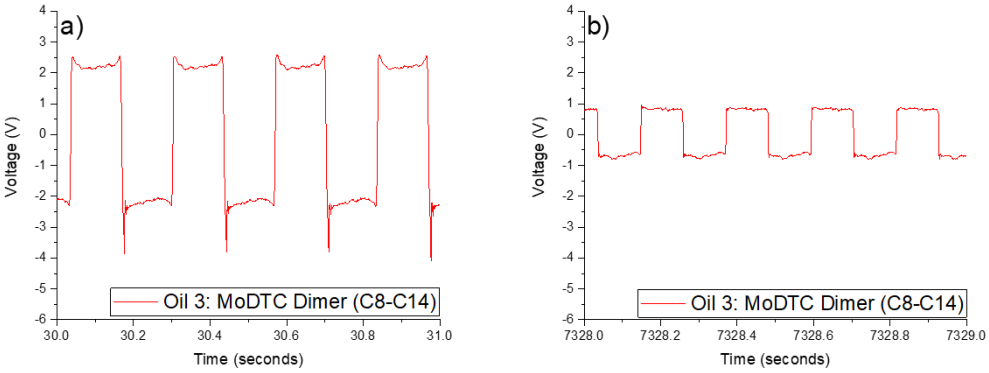


a) Oil 2: MoDTC Trimer, early test



b) Oil 2: MoDTC Trimer, late test

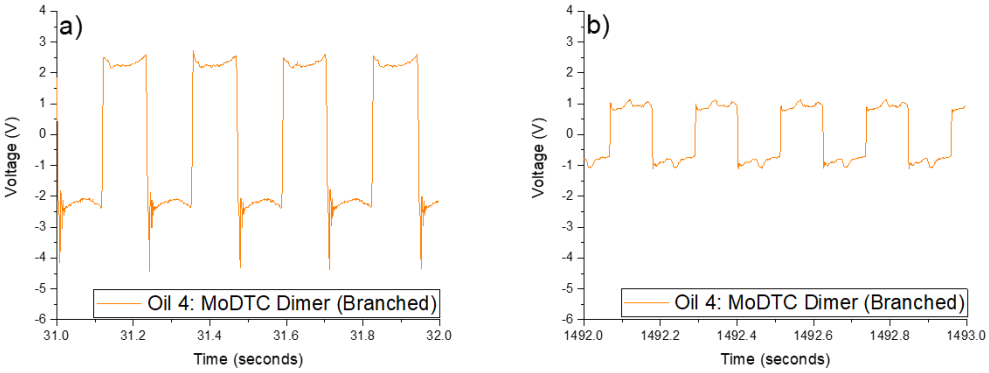
Figure A0.2 TE77 Load Cell response of rough plate 100 N friction test of Oil 2: MoDTC Trimer monoblend



a) Oil 3: MoDTC Dimer (C8-C14), early test

b) Oil 3: MoDTC Dimer (C8-C14), late test

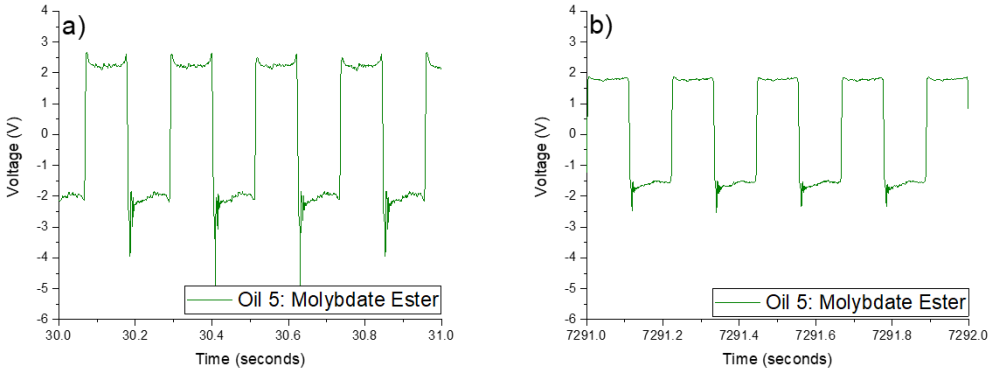
Figure A0.3 TE77 Load Cell response of rough plate 100 N friction test of Oil 3: MoDTC Dimer (C8-C14) monoblend



a) Oil 4: MoDTC Dimer (Branched), early test

b) Oil 4: MoDTC Dimer (Branched), late test

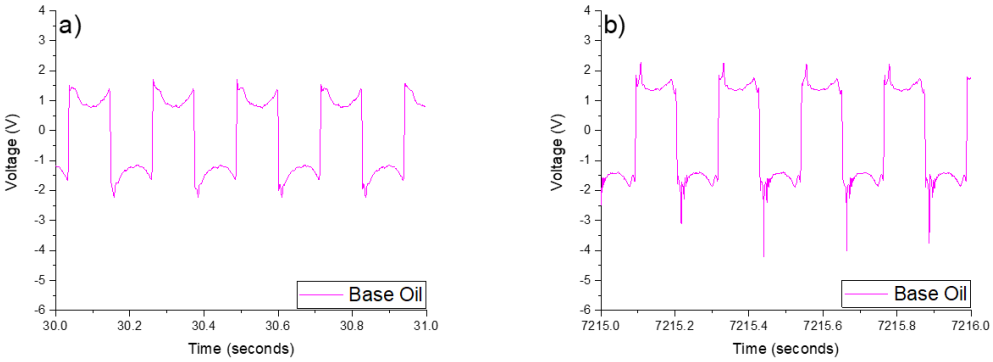
Figure A0.4 TE77 Load Cell response of rough plate 100 N friction test of Oil 3: MoDTC Dimer (Branched) monoblend



a) Oil 5: Molybdate Ester, early test

b) Oil 5: Molybdate Ester, late test

Figure A0.5 TE77 Load Cell response of rough plate 100 N friction test of Oil 5: Molybdate Ester monoblend



a) Base Oil, early test

b) Base Oil, late test

Figure A0.6 TE77 Load Cell response of rough plate 100 N friction test of Polyalpha olefin base oil

Appendix B: Overlaid friction profiles of TE77 friction characterisation tests

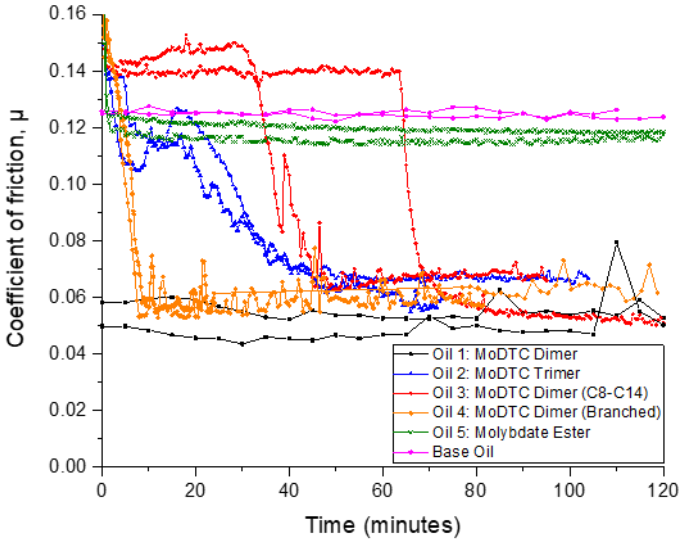


Figure B0.1 Overlaid 100 N friction profiles

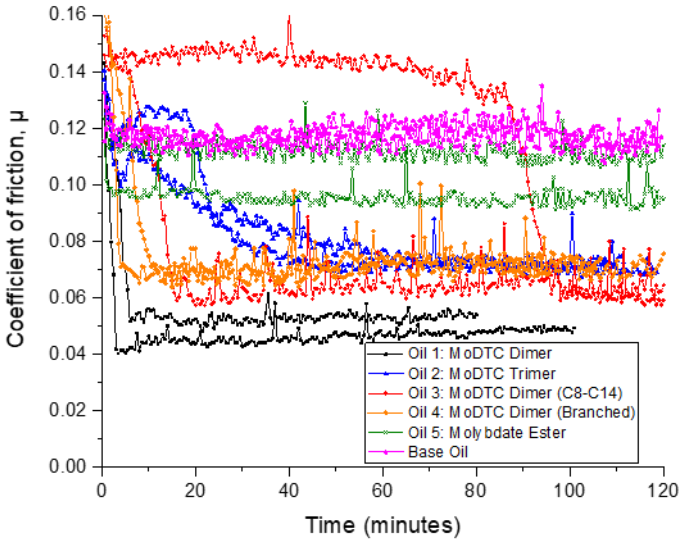


Figure B0.2 Overlaid 25 N friction profiles

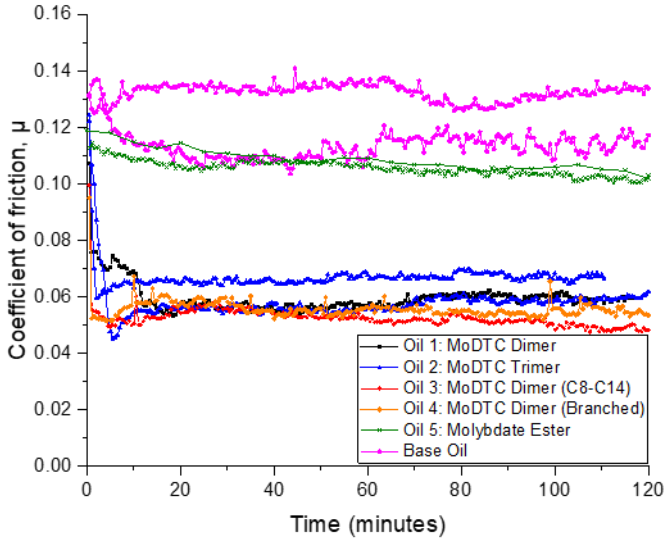


Figure B0.3 300 N smooth plate overlaid friction profiles

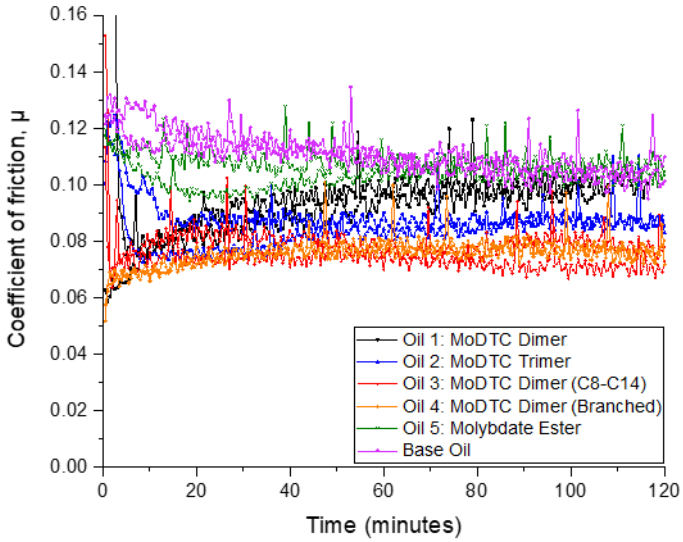


Figure B0.4 Overlaid 25 N smooth plate friction profiles

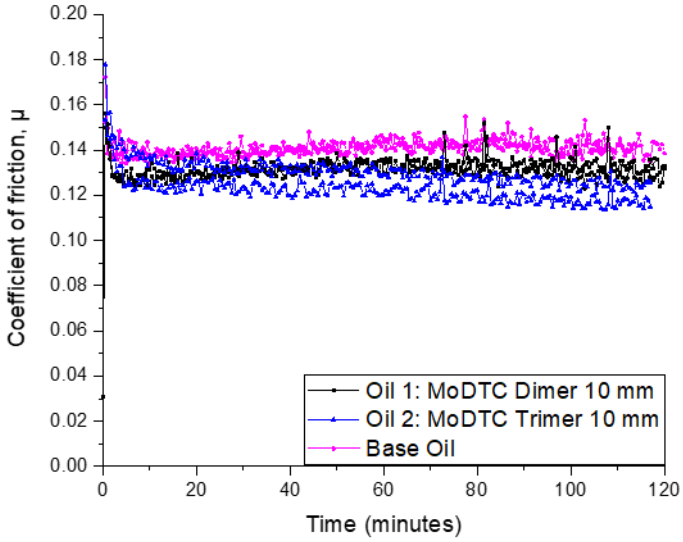


Figure B0.5 Overlaid friction profiles of 10 mm radius pin tests

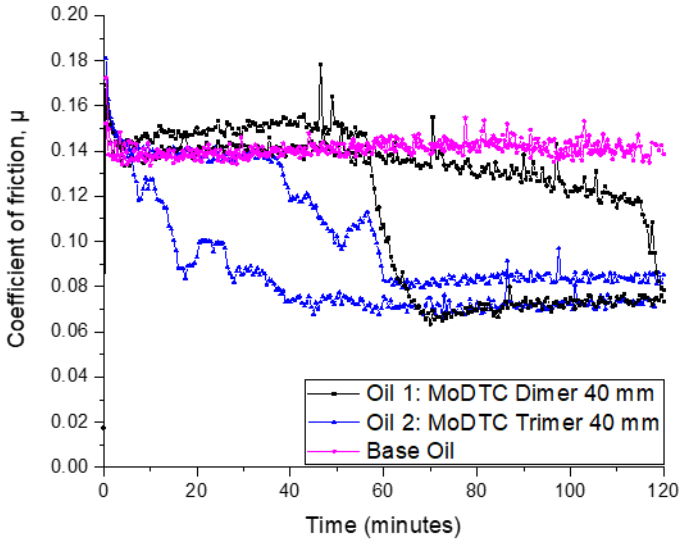


Figure B0.6 Overlaid friction profiles of 40 mm radius pin tests

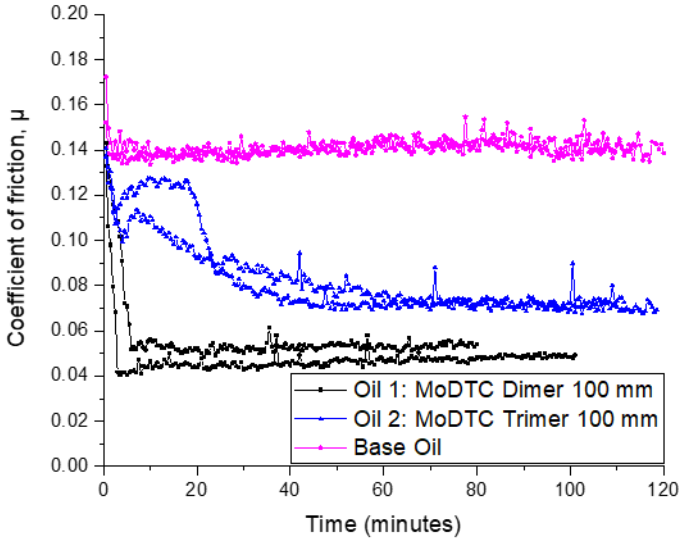


Figure B0.7 Overlaid friction profiles of 100 mm radius pin tests

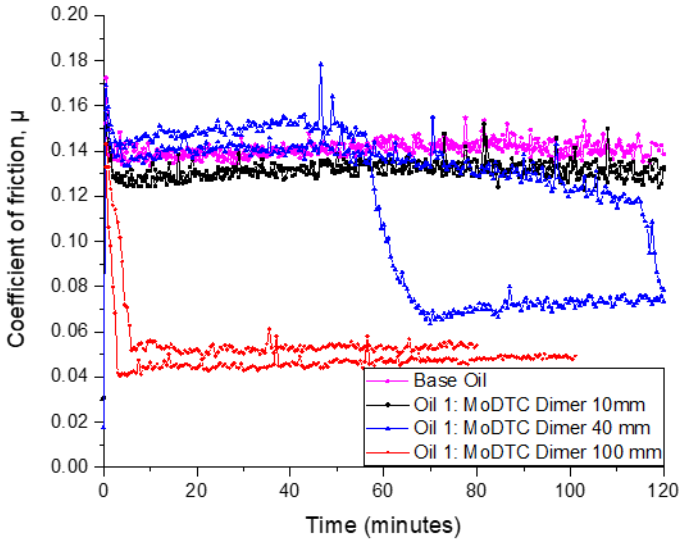


Figure B0.8 Overlaid friction profiles of pin radius testing for Oil 1 (MoDTC Dimer)

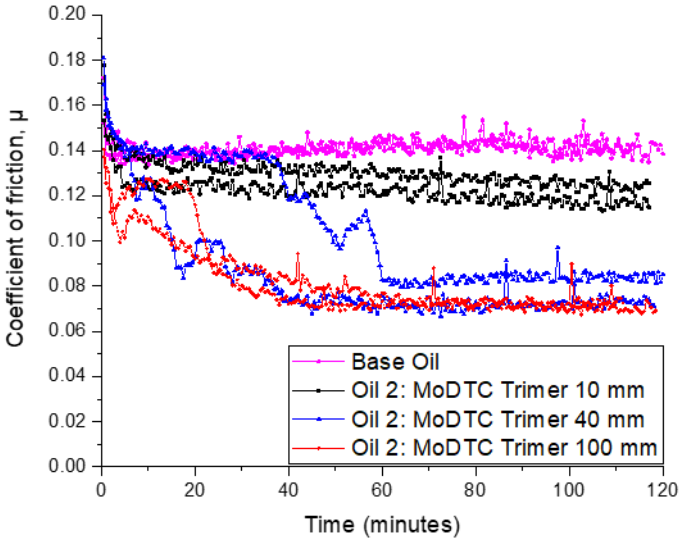


Figure B0.9 Overlaid friction profiles of pin radius testing for Oil 2 (MoDTC Trimer)

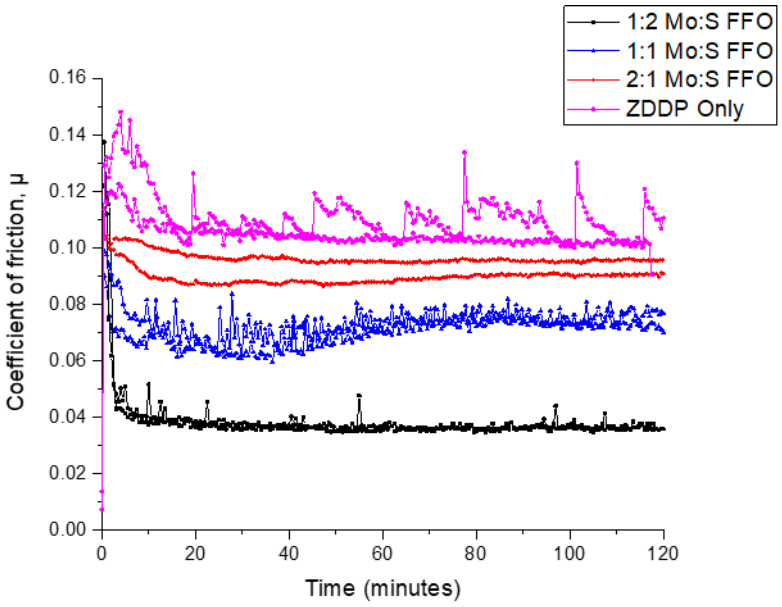


Figure B0.10 Overlaid profiles of molybdate ester FFO Mo:S ratio friction performance at 100°C and 100 N, smooth plate conditions

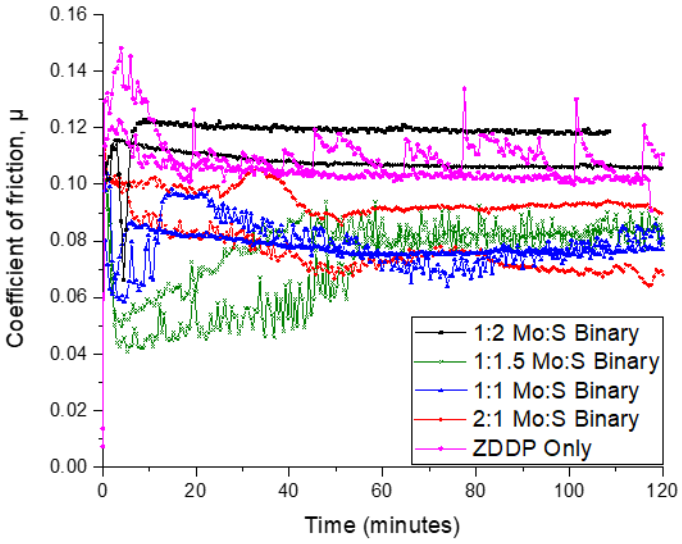


Figure B0.11 Overlaid friction profiles of binary molybdate ester Mo:S ratio oils under smooth plate conditions

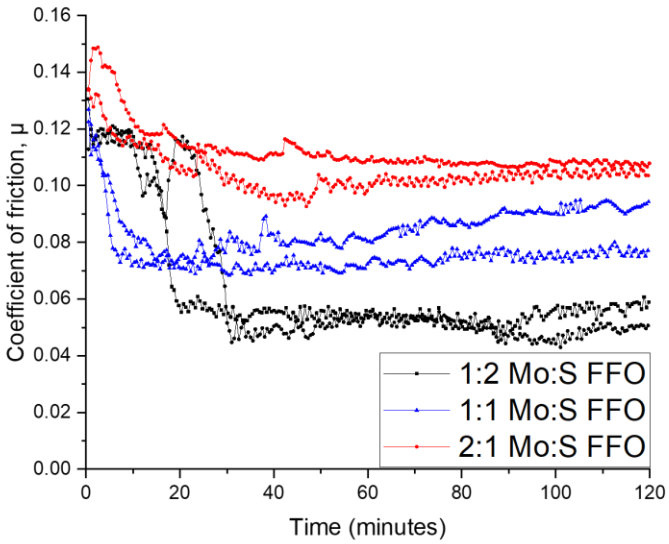


Figure B0.12 Overlaid friction profiles of binary molybdate ester Mo:S ratio oils under rough plate conditions

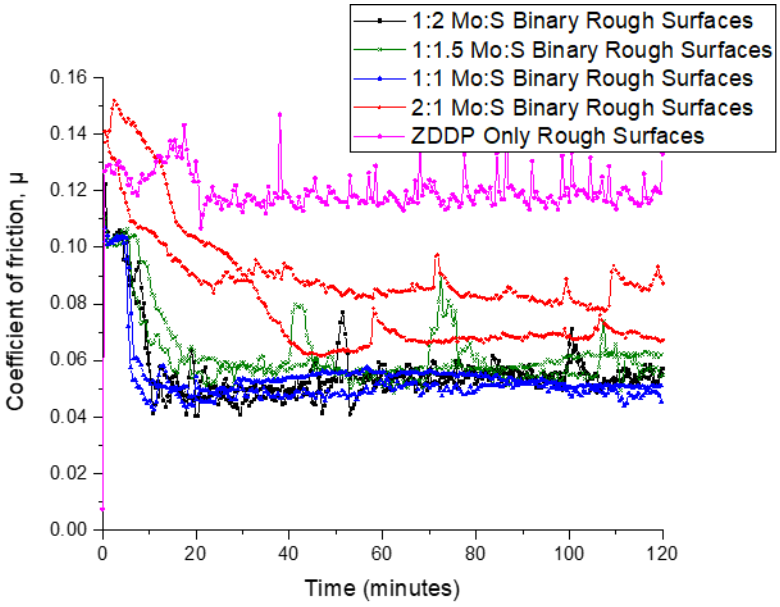


Figure B0.13 Overlaid friction profiles of binary molybdate ester Mo:S ratio oils under rough plate conditions